

MICROEARTHQUAKES, SEISMICITY, AND TECTONICS OF  
THE NORTH-CENTRAL PERSIAN PLATEAU

A THESIS

SUBMITTED BY

ABOLGHASSEM HEDAYATI B.Sc., M.Sc.

FOR THE DEGREE OF  
DOCTOR OF PHILOSOPHY  
OF  
THE UNIVERSITY OF LONDON

DEPARTMENT OF GEOPHYSICS  
IMPERIAL COLLEGE, LONDON

OCTOBER, 1976

It was well said at the  
time of the International  
Geophysical Year (1958)  
that "we know more about  
the face of the moon than  
the interior of the earth".

To my son

BABAK

ABSTRACT

Iran, particularly the North-Central region, is an area of very complex geological structure and young, mostly recent, tectonics. To investigate the relationship of the seismicity, regional structure, and contemporary stress pattern and to assist in the understanding of future activity, a microearthquake survey was undertaken late in 1974. This thesis describes the results of the survey, supported by field observations, interpretation of satellite photographs, and historical and instrumental records of destructive earthquakes.

Because of the relative activity of the Musha-Fasham and the North-Tehran faults, as reported in the literature, attention was concentrated on these two major faults. Located epicentres fell into three groups, two of these being associated with the major fault zone controlling the southern flank of the Alborz Mountains, while the third, which will hereafter be referred to as the Rey-Lineation, forms a lineation striking southeast from Tehran, not previously been reported in the literature.

The survey revealed considerable activity, exceeding 20 shocks/day in places. The slope of the recurrence curve, the so-called b-value, 0.79, compares well with the 0.85 derived from instrumentally recorded events in the region since 1926. Using this b-value, calculations suggest that a Modified-Mercalli intensity of VII can be expected every 12 years, while the reoccurrence time of intensity IX is about 350 years. This compares well with the historical record.

The average value of the ratio of compressional to shear wave velocity was found to be 1.70, showing the crust to be composed of rocks of normal elastic properties, with a Poisson's ratio of about 1/4. For two events, however, lower values of  $V_p/V_s$  were found, 1.46 and 1.60. As these two values occurred consecutively in time and were followed by a magnitude 2.8 microearthquake, it seems likely that they represent a precursory change.

Composite fault plane solutions have been compiled for the P-arrival polarities for each group of microearthquakes. These indicate a combination of left-lateral strike-slip and reverse faulting on the Musha-Fasham Fault, and shallow thrusting on the proposed new fault. Both mechanisms indicate a regional compression direction of about N50E, comparing well with the local structural trend.

From the data, tectonic flux maps were constructed for ten year intervals. These show that, although the activity tends to concentrate within clearly defined zones, within those zones areas occur in which periods of high activity alternate with periods of relative quiet.

Regional strain release, rate of occurrence of microearthquakes, the b-value, and historical records, not only reveal the continuity of activity, but also indicates a high level of seismicity for the region. Of particular interest is the continuous high concentration of activity around 35N and 52.5E since 1926. It is suggested that this highly active zone, which happens to be the end of the newly discovered Rey-Lineation, could be a source of future activity.

CONTENTS

	<u>Page No.</u>
ABSTRACT	3
CONTENTS	4
<u>CHAPTER I</u> INTRODUCTION	
1.1      The aim	7
1.2      The development of seismological studies in tectonics investigations	7
1.3      The use of microearthquake	11
1.4      The use of satellite photographs	12
1.5      A brief description of the forthcoming chapters	12
<u>CHAPTER II</u> REGIONAL GEOLOGY	
2.1      Introduction to the area	14
2.2      Physiography of the region	14
2.3      A brief description of the geology of the region	18
2.4      Tectonics of the region	21
2.5      Some new aspects deduced from ERTS-1 photographs	23
2.5.1    The Musha-Fasham Fault	23
2.5.2    The North-Alborz Border Fault	27
2.5.3    The North-Tehran Fault	27
2.5.4    The Buyin-Zahra Fault	28
2.5.5    The Ardestan Fault	29
2.6      General compressive axis inferred from the ERTS-1 imagery	29
<u>CHAPTER III</u> THE MICROEARTHQUAKE OBSERVATIONS	
3.1      Introduction	34
3.2      Field procedure	39
3.3      Instrumentation	42
3.4      The suitability of Geostores for microearth- quake studies	47
3.5      Replaying the Geostore tape onto chart paper	49
3.6      Data	52
3.7      Seismic activity level of the area	56
3.8      Construction of P-and S-wave travel-time curves	63
3.9      Calculation of short epicentral distances and the Poisson's ratio	64

3.10	The problem of determining the magnitude of local stocks	69
3.11	Determination of the constants A and B for North-Central Iran	72
3.12	Determination of the b-value	78
3.13	Normalized seismicity	84
3.14	Aftershock sequences and b-values	85
3.15	Significant of the b-value	88
3.16	b-value deduced from laboratory experiments	90

#### CHAPTER IV SEISMIC RISK IN THE TEHRAN REGION

4.1	Introduction	93
4.2	Statistical approach to seismic risk	96
4.3	Determination of intensity-magnitude relation	101
4.4	Evaluation of the attenuation coefficients	102
4.5	Determination of risk curve	108
4.6	Significant of the risk curve	116

#### CHAPTER V LOCATING LOCAL EARTHQUAKES AND THE USE OF MICROEARTHQUAKES IN REGIONAL SEISMICITY. APPLICATION OF HISTORICAL RECORDS TO SEISMICITY STUDIES

5.1	Introduction	118
5.2	A method for locating local seismic events	120
5.2.1	Reasons for using FAMG	120
5.3	Velocity structure	124
5.4	Local earthquakes	125
5.5	Significance of the local events and discovery of the Rey-Lineation	140
5.6	Historical events and their role in understanding the seismicity of the area	142

#### CHAPTER VI TEMPORAL VARIATIONS OF $V_p/V_s$ : APPLICATION TO EARTHQUAKE PREDICTIONS: FORSCH DISCONTINUITY

6.1	Introduction	152
6.2	Earthquake prediction	153
6.2.1	Premonitory changes of body wave velocities: Use of microearthquakes	155

	<u>Page No.</u>
6.2.2 Computation of $V_p/V_s$	157
6.3 Decrease in velocity ratio preceding Tehran microearthquakes	160
6.4 Relation between the magnitude and precursor time	164
6.5 Dilatancy, and the energy released by micro-earthquakes	169
6.6 Velocity inversion within the crust of the Tehran region	172
<u>CHAPTER VII</u> GEOLOGICAL STRUCTURE, LARGE EARTHQUAKES AND TECTONICS OF THE TEHRAN REGION	
7.1 Introduction	178
7.2 Large events in the Tehran region	180
7.3 Composite fault plane solution	185
7.3.1 The technique	187
7.3.2 The results	190
7.4 Profile across the Musha-Fasham Fault	200
7.5 Regional strain release, tectonics and seismicity of the Tehran region	208
7.5.1 Method of analysis	210
7.5.2 Strain release maps	212
<u>CHAPTER VIII</u> CONCLUSIONS AND SUGGESTIONS FOR FUTURE RESEARCH	
8.1 Conclusions	222
8.2 Suggestions for future studies	228
ACKNOWLEDGEMENTS	230
LIST OF OTHER CONTRIBUTIONS OF THE AUTHOR	232
REFERENCES	233

## CHAPTER I

## INTRODUCTION

1.1 The Aim

This thesis is concerned to investigate the current seismicity and tectonic structure of North-Central Iran, particularly the Tehran region.

In it, the author concentrates primarily on the results of a microearthquake survey of the region undertaken late in 1974, but also makes use of structural relationships derived from his own analysis of satellite photographs, and the results from historical and instrumental records of major earthquakes.

1.2 The Development of Seismological Studies in Tectonic Investigations

Earthquakes have been known of for many centuries and in most ancient cultures were associated with the wrath of some underground dwelling god.

The first earthquake to arouse widespread interest in the west was that of Lisbon in 1775, which by demolishing the heart of one of Europe's most important centres provoked a great deal of discussion amongst the rationalists of the time, paving the way for much of the scientific progress of the following centuries.

In the latter part of the nineteenth century, with the introduction of recording seismographs it became possible, using timed recordings from several stations, to locate the points of origin of earthquakes.

By about 1904 the world-wide distribution of seismographs was such that major earthquakes were recorded at a large number of stations, and could be moderately well located. Improvement in the sensitivity and frequency response of instruments and greater standardization around the world gradually improved the accuracy of the location and the threshold of detection.

In 1954 B. Gutenberg and C.F. Richter published in their book "The Seismicity of the Earth" a catalogue of all the instrumentally located earthquakes that had occurred world-wide between 1904 and 1952, but even in this, as Ewing and Heezen (1956) showed for the mid-Atlantic ridge, epicenters were in error by as much as a degree or so and are therefore, of little use in tectonic investigations.

From that time on, much effort was put into improving epicentral location on a world-wide scale, encouraged by the need to monitor underground nuclear explosions. The establishment of the World Wide Standard Seismograph Network (WWSSN) in 1962 by the United States Coast and Geodetic Survey (USCGS)\* represented a major step forward, such that it then became possible to locate earthquakes almost anywhere in the world to within 20Km, provided that their body wave magnitudes were greater than about  $4\frac{1}{2}$ .

The plate tectonic hypothesis proposed by McKenzie and Parker (1967), Morgan (1968) and Le Pichon (1968), the new global tectonics of Isack et al., (1968), and the world

---

\* Now known as NOAA (National Oceanic and Atmospheric Administration).



seismicity map of Barazangi and Dorman (1969) were but three of the direct results of the vast improvement in epicentral determination consequent upon the establishment of the WWSSN.

Barazangi and Dorman's map reveals extremely different patterns between oceanic and continental seismicity. Lines of activity at oceanic tectonic boundaries are confined within very narrow and well-defined zones, while in the continental seismic regions the events tend to be dispersed more widely, and mostly without pattern. Figure (1-1) shows an example of the broad distribution of epicenters in part of Central Asia, the Mediterranean Sea and the Persian Plateau, in contrast with the narrow belts along the mid-oceanic ridges.

McKenzie (1972) studied the active tectonics of the Mediterranean region on the basis of all available fault plane solutions in terms of plate tectonics. According to his study the difference between continental and ocean ridge seismicity could be due to the different formation of continental and oceanic plates, or might be because of the presence of numerous faults and fracture zones on the continents which are absent from the ocean ridges.

Although seismicity maps based on the epicentral location of events have been prepared for various parts of the world, they cannot be treated as unbiased information, since they depend on only a very few relatively large magnitude earthquakes, located with an accuracy of 10-20Km, whereas those events with slightly smaller magnitudes are neglected. On the other hand, the number of these larger magnitude earth-

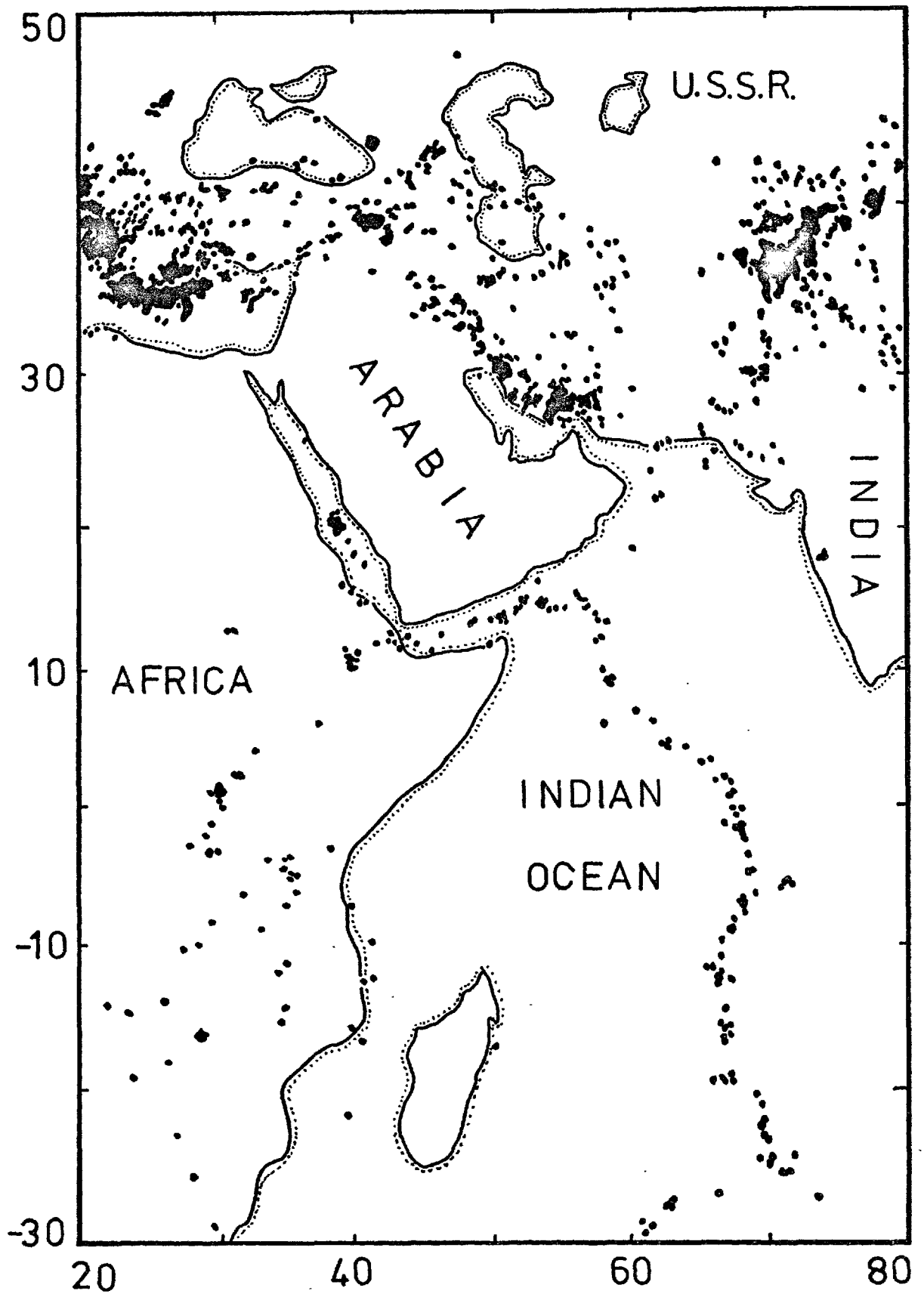


Fig. (1-1). Seismicity map of the Middle East and part of the Indian Ocean (after Barazangi and Dorman, 1969). Note the dispersion of epicenters in the Continental region relative to that of the Oceanic crust.

quakes is so small that it can not reflect the real activity of an area, and does not constitute a statistically representative sample. So one cannot consider those maps as truly representing long-term seismicity.

### 1.3 The Use of Microearthquakes

The above-mentioned diffuse distribution and small number of relatively large magnitude earthquakes implies that, in general, it is not possible to describe the seismic activity and tectonics of a relatively small region, particularly on continents, using only recorded seismic data.

To assess the seismotectonic activity of the Tehran region, considerable use has been made of the results from the microearthquake survey undertaken by the author late in 1974.

According to Asada (1957 and 1958), microearthquakes are classified as local earthquakes which generate seismic waves whose predominant period is not greater than 0.5 second. He observed that microearthquakes can occur in the same region as earthquakes of greater magnitude.

Although a small local earthquake cannot be compared in effects with a large destructive one, nevertheless various authors (e.g. Oliver et al., 1966; Crosson, 1972; Healey et al., 1972; Hadly and Combs, 1974) have shown how because of their much higher rate of occurrence, such earthquakes can be used to derive information about active structures that might otherwise have taken centuries.

Such information can include the exact location of hidden faults, their dip and strikes, differences in rates

of strain accumulation and release on different section of a fault, fault mechanism and stress orientation, and recently the detection of dilatant volumes.

#### 1.4 The Use of Satellite Photographs

Since the launching of the first Earth Resources Technology Satellite (ERTS-1) in 1972, a wealth of high definition, small scale photographs has become available. These are highly suited to the investigation of regional structures and trends, and effectively complement the more traditional aerial photographs.

Mohr (1972, 1973 and 1974) made use of some of these photographs to investigate structural relationships in the African rift system, while Mohajer-Ashjai et al., (1975) used the ERTS-1 photographs from eastern Iran to delineate major structures there.

The author has used the satellite photographs of North-Central Iran to supplement his microearthquake work and investigate structural relationships in the Alborz Mountains.

#### 1.5 A Brief Description of the Forthcoming Chapters

The regional geology of the area and detailed interpretation of satellite photographs of the Tehran region and its vicinity are outlined in chapter II.

Chapter III deals with the use of the portable seismographs and the relevance of the recorded microearthquakes to the regional activity.

In chapter IV the seismic risk curve of the region is discussed and conclusions reached about the frequency with

which the area will be visited by moderate to large magnitude earthquakes. These results are compared with the past activity of the region.

The relation between the located microearthquakes and the level of activity of the region is the main concern of chapter V. It is shown why Shahr-e-Rey, a city about 30Km south of Tehran itself, should have been destroyed frequently in the past.

The applicability of microearthquakes in understanding crustal structure is discussed in chapter VI. To put the concept of earthquake prediction on a more quantitative basis, attention is given to the temporal variation of the ratio of the velocities of compressional and transverse waves.

The tectonics and seismicity of the Tehran region, based on composite fault plane solutions and strain release maps deduced from the instrumental earthquakes which have occurred in the region since 1926, as well as local events recorded in the Tehran survey, are the main interest of chapter VII.

Finally the conclusions reached and remarks for future studies are summarized in chapter VIII.

## CHAPTER II

## REGIONAL GEOLOGY

2.1 Introduction to the Area

The Tehran region here is defined as that part of the Persian Plateau bounded by latitude  $34^{\circ}$  and  $37^{\circ}$  N, and longitude  $49^{\circ}$  and  $55^{\circ}$  E. The north part of the region is bounded by the Alborz Mountain Chain, which runs in a northwest-southeast direction at the west; to the east of the city this trend changes first to approximately east-west, before it becomes northeast-southwest, while to the south of the city of Tehran lies the Dasht-e-Kavir (Desert). Most of the area under investigation is covered by the arid desert of Central Iran, where large fluctuation of temperature occur between summer and winter.

Three and a half million inhabitants live in the capital of Iran. The city is launching great developments such as heavy industries and housing construction, while a well defined seismic belt, the so called "Alpide Belt", crosses its northern part and causes several thousand perceptible shocks per year (Afshar, 1966). Thus, the circumstances make it desirable to have a better understanding of the seismic hazard of the area. Figure (2-1) shows the general physiography of the region.

2.2 Physiography of the Region

The Alborz Mountains which almost cross the whole northern boundary of Iran, continue eastward in a north easterly

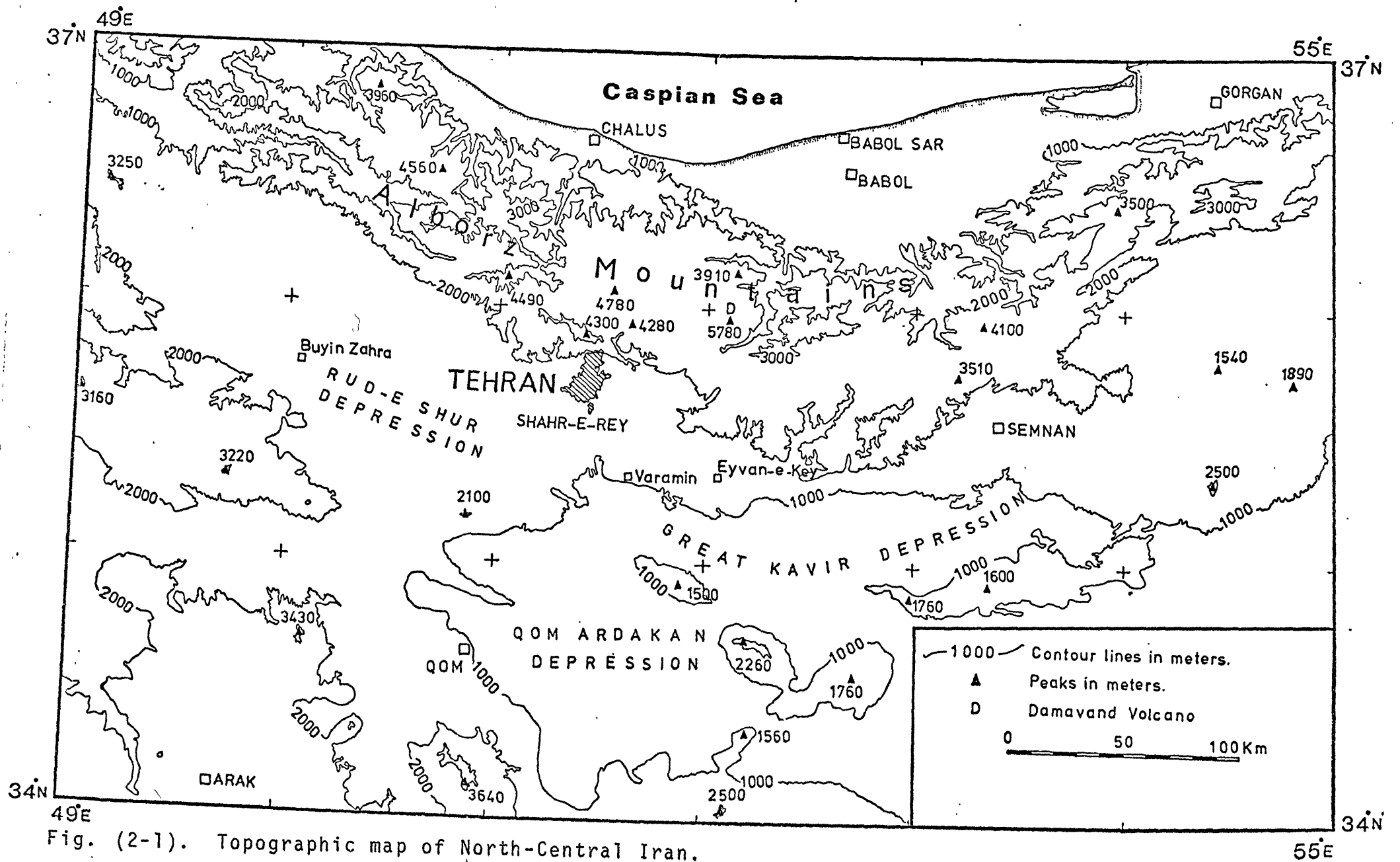


Fig. (2-1). Topographic map of North-Central Iran.

direction from longitude  $53^{\circ}$  E. After changing their strike to the south-east at longitude  $57^{\circ}$ , they continue into Afghanistan and Pakistan and possibly join the Hindu Kush and Pamir Ranges. Westward of longitude  $53^{\circ}$  E the Alborz Mountains strike north-west towards the USSR, where they join the Caucasus.

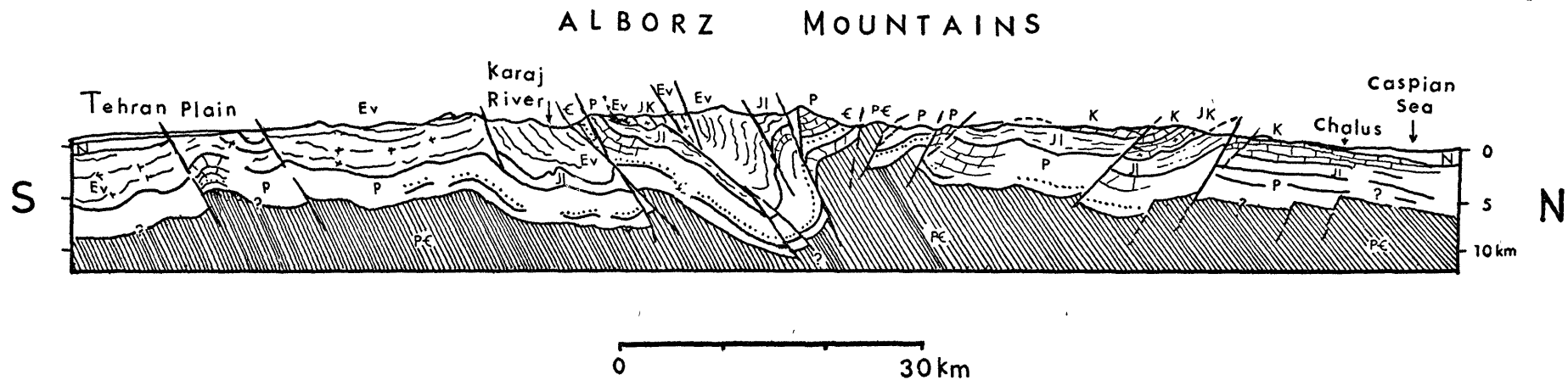
The area under study is separated into two distinct zones, the High Alborz and the Dasht-e-Kavir (Desert). The highest elevation of the Alborz Mountains is the peak of the Quaternary Volcano Damavand, 5780 meters above sea level (National Iranian Oil Company, 1959), while in the Dasht-e-Kavir the elevation does not exceed 1000 meters.

The geological map of Iran shows the age of the southern flank of the Alborz to be as young as the Tertiary (of Palaeogene) whilst the northern part of this Range is as old as Mesozoic-Paleozoic (of Jurassic and Carboniferous respectively).

A sequence of folding and faulting whose orientations follow faithfully the main trend of the Alborz formed the Ranges. According to Stoklin (1968), the Alborz Chain undergoes more deformation on the southern flank than on the northern.

Figure (2-2) shows a north-south cross section through the Alborz Mountains (from Chalus at the Coast of the Caspian Sea in the north to the Tehran Plain in the south). As can be seen, the Range has suffered from extensive folding and faulting, but there is an interesting concentration of tectonic activity between zero and a depth not exceeding 10Km. It seems that the Pre-Cambrian basement behaves as a shield below this depth and that the region has been undisturbed since that





- |    |   |    |   |
|----|---|----|---|
| N  | Neogene   | P  | Paleozoic in general,<br>including Lower-Middle<br>Triassic |
| Ev | Volcanic Eocene                                       | €  | Infracambrian-Cambrian                                      |
| K  | Cretaceous  | PC | Pre-Cambrian basement                                       |
| JK | Jurassic Cretaceous<br>undivided                      |    |   |
| JI | Upper Triassic-Middle<br>Jurassic, mainly continental |    |   |

Fig. (2-2). A north-south cross section through the Alborz Mountains (after Stoklin 1968). Note the concentration of tectonic activity above 10km depth.

period below 10 kilometers depth.

Tchalenko et al., (1974), by accepting that there is a true correlation between geomorphology and tectonic movement, divided the Tehran region into five major zones:

The High Alborz

The Alborz Border folds

The Pediment Zone

The Anti Alborz

The Central and Rud-e-Shur Basin.

These subdivisions are shown on the Figure (2-3).

### 2.3 A Brief Description of the Geology of the Region

The five above-mentioned zones are separated from one another by either a major fault or a topographic change. The Musha-Fasham Fault (named after villages to the east and north of Tehran respectively, which the fault connects) is the border between the High Alborz and the Border Folds; the Alborz Border Folds and the Central Basin are separated by the North-Tehran Fault; the barrier between the Anti Alborz and the Central Basin is the high topography of the Anti Alborz. Similarly, the Pediment Zone is separated by the North-Tehran Fault from the Border Folds, and by the topography from the Central Basin.

According to Stocklin and Nabavi (1971), lithologically the High Alborz consists abundantly of Jurassic-Cretaceous sedimentary sequences. The zone, which underwent folding during the Tertiary, is formed mostly of sandstones and

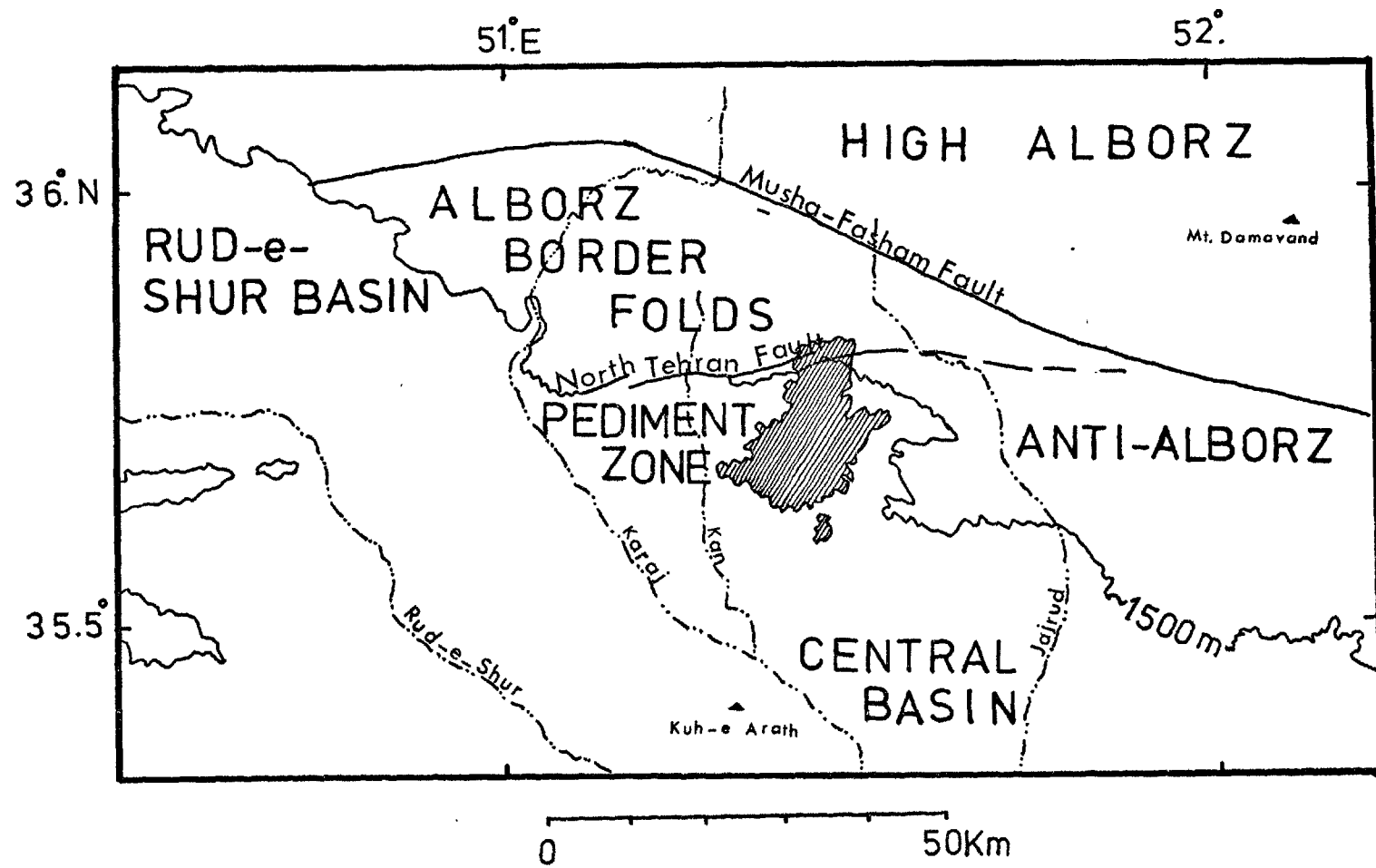


Fig. (2-3). Major topographic zones of the Tehran region (after Tchlenko et al., 1974).

conglomerates (Lower-Middle Jurassic), limestones and marls (Middle-Upper Jurassic Cretaceous), and Cretaceous volcanic rocks in central and western part of its northern flank.

A detailed study by Iwao and Hushmandzadeh (1971) revealed that the area bounded by the Musha-Fasham Fault on the north and the North-Tehran Fault in the south is covered by Eocene volcanic tuffs, and the pyroclastics, known as the Karaj formation. Thick volcanic rocks and tuffaceous sediments are characteristic of this area (Tectonic Map of Iran, 1971).

Tehran is sited on the Quaternary alluvium of the Pediment zone (NIOC, 1959; Tectonic Map of Iran, 1971; Tchalenko et al., 1974). The formation beneath the Quaternary alluvium is thought to be Eocene volcanic tuffs (Karaj Formation).

The Alluvial formation of the Pediment zone has been studied by many geologists. Rieben (1953, 1955, 1966) and later Bassir (1971) have divided the alluvial formation of the Tehran Plain into four groups according to age:

1. The oldest fragment of this formation, the so-called "A" formation, is of Pliocene.
2. The "B" formation of Pleistocene age which is deposited on the eroded surface of the "A" formation.
3. The "C" or the Recent deposition whose age, according to Vita-Finzi (1969), goes back to 50,000 years.
4. The "D", the most Recent formation, responsible for the deposition of gravels and scattered pebbles on

river beds at the present time. The deposition of this formation according to Vita-Finzi (1969) started 6,000 years ago.

The geology of the Anti-Alborz, an isolated topography in the south of the High Alborz, has been studied by Riviere (1936) and Engalenc (1968). The name Anti-Alborz is given to it because of its quite different geological structure from that of the Alborz Border Folds. The geological observations by the above authors revealed the existence of Cretaceous rocks in the area. The zone, which had been folded in early Cretaceous and late Cretaceous-Tertiary times, consists of sandstones and limestones (Triassic-Middle Jurassic) and limestones and evaporites (Middle-Upper Jurassic) but is lacking in volcanic rocks as compared with the Alborz Border Folds (Stocklin and Nabavi, 1971). Bibishahrbanu Mountain, at 2,700 meters height, is the highest of the region and is of Paleozoic age.

The last zone of the Tch<sup>a</sup>lenko division of the Alborz Mountains, the Central and Rud-e-Shur Basin, which are separated from the Pediment zone by topographic change, consists of recent deposits. The intrusion of Kuh-e-Arath (Arath Mountain), 1,500m above sea level, a Neogene volcano, has interrupted the evenness of this Basin.

#### 2.4 Tectonics of the Region

Detailed study of the geology of the Persian Plateau started around the middle of this century. Observations have

been centered in two mountain ranges. The Alborz Mountains in the north and the Zagros Range in the south and west. Geologists of the National Iranian Oil Company started a systematic study of the geology of Iran in 1950. The results of this investigation have been published as the Geological Map of Iran (1:2,500,000 scale). This map shows clearly that Central Iran underwent complex folding and faulting during the Alpidic Orogeny. The survey was taken over by the Geological Survey of Iran (GSI) established in 1959, the results of whose investigations have been published as numerous geological maps for various regions of Iran, such as the Geological Map of Central Alborz (1:100,000 scale), the Tectonic Map of Iran, the Seismicity Map of Iran, etc.

According to Stocklin (1968) the fundamental outcome of the foregoing investigation can be classified as follows:

- a. The Alborz Mountains from stratigraphical and structural viewpoints belong to Central Iran.
- b. Iran was not affected by orogenies during the Pre-Cambrian to Middle-Triassic.
- c. Most of the Persian Plateau, including North-Central Iran, suffered strong folding, faulting, and thrusting during the Alpidic Orogeny in Mesozoic and Tertiary times.
- d. The main trends of the Alpine structural plane is that produced from the Pre-Cambrian Orogeny.
- e. The Lut, a proposed microplate (Takin, 1972; McKenzie, 1972; Nowroozi, 1972) of Eastern Central Iran, remained as a rigid block in Eastern Central Iran, though not as big as the Median mass, which was originally supposed to

cover the whole area between the north and south Iranian ranges.

Mohajer-Ashjai (1975) in a study of Eastern Central Iran, concluded that the rigidity of the Lut Block should be considered dubious.

## 2.5 Some New Aspects Deduced from ERTS-1 Photographs

Since 1972, when the first Earth Resources Technology Satellite (ERTS-1) was launched, satellite photographs have been widely used not only to delineate previously unknown geological features but also to study new aspects of known structures, such as the continuation of a lineament, extension of a fault, or the changing orientation of a trend.

Detailed interpretation of ERTS-1 imagery of the Iranian region has assisted greatly in accurate mapping of the surface faults, trends, changes of orientations, etc., and therefore a better understanding of the tectonics of the Alborz Mountains. A new fault map of the entire Tehran region has been drawn, with the aid of the satellite photographs covering this part of Iran, as well as field observations. The result of this investigation will be discussed later.

### 2.5.1 The Mush<sup>a</sup>-Fasham Fault

Figure (2-4) shows the trace of the faults deduced from various sources, including the field observation, major lineations within the framed region of the ERTS-1 photographs shown in Figure (2-5), the Geological Map of Iran (NIOC, 1957), the Geological Map of Upper Djadjrud and Lar Valleys (Assereto, 1966), the Tectonic map of Iran (Stocklin and Nabavi, 1971),

Fig. (2-4). Tectonic map of the North-Central Iran.

AF : Ardastan Fault

BZF : Buyin-Zahra Fault

CSF : Chah Sorb Fault

GKF : Great Kavir Fault

KBF : Kuh Banan Fault

MFF : Musha-Fasham Fault

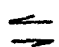
NABF : North Alborz Border Fault

NF : Nayband Fault

NTF : North-Tehran Fault

SF : Sarvestan Fault

ZF : Zagros Fault

 : Sense of relative horizontal movement.



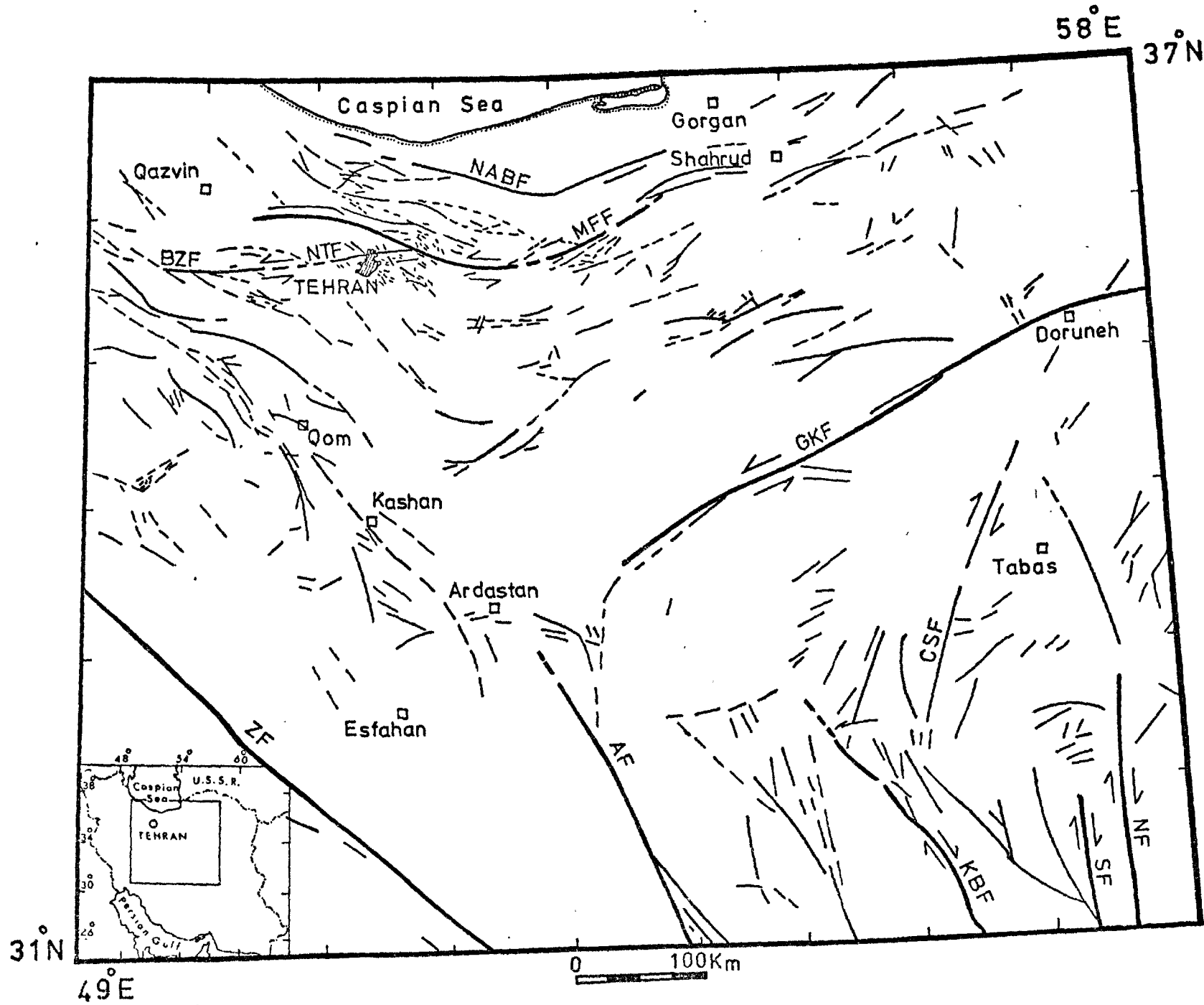


Fig. (2-4).

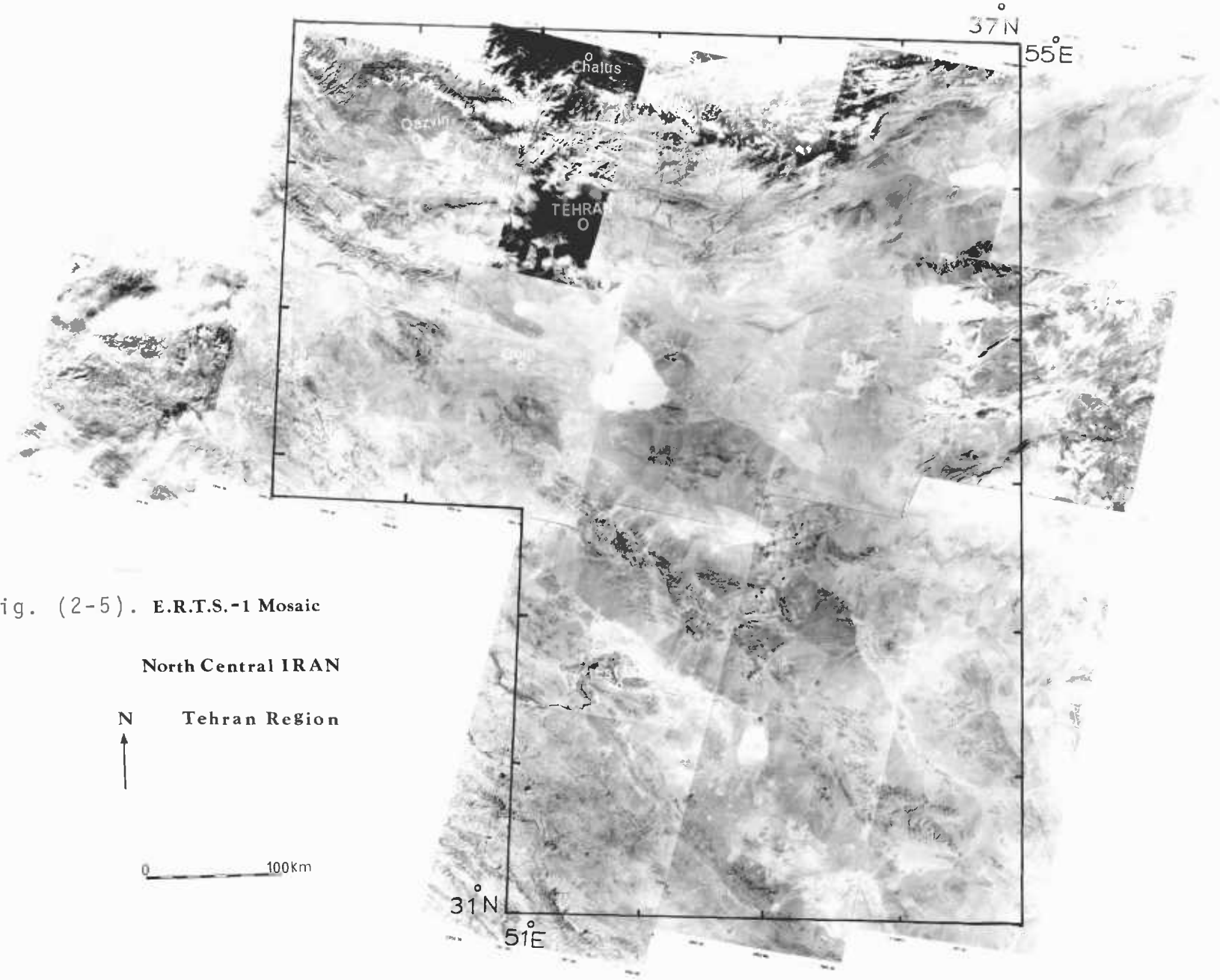


Fig. (2-5). E.R.T.S.-1 Mosaic

North Central IRAN  
Tehran Region

N  
↑

0 100km

Geological Map of the Central Alborz (Assereto, 1972), the Seismicity Map of Iran (Berberian, 1973), and the Seismotectonic Map of North Central Iran (Tchalenko et al., 1974).

The Musha-Fasham Fault, a very clear feature on the ERTS-1 photographs, formerly known as the Shahrud Fault, forms the border between the High Alborz and the Alborz Border Folds. It runs continuously from a few Km south of the Qazvin in the west, following gently the Alborz Mountains trend all the way down to Shahrud, a city about 300Km north east of Tehran in the east. The entire length of the fault is thought to be more than 900Km (Wellman, 1966).

By examining the air-photo mosaic of Iran, Afghanistan, and Pakistan, Wellman (1966) observed many horizontal drainage displacements on this fault. In some cases the offsets amounted to 50 meters. According to him, the fault has no recognisable vertical movement, and on his map it is marked as a sinistral strike-slip type.

Nowroozi (1972) in his study of the seismotectonics of the Persian Plateau and its vicinity, based on relocation of all earthquakes occurring between 1950 and 1965, assigned a left-lateral direction of motion to the Musha-Fasham Fault (the Shahrud Fault).

Tchlenko et al., (1974) based on an expedition on 50Km of the Musha-Fasham Fault, considered the fault to have principally reverse movement. According to their observation the dip direction of the entire length of this fault is northwards, with the dip angle varying from  $35^{\circ}$  to  $70^{\circ}$ . Tectonic movement on this fault commenced in the Jurassic, and the total

movement since then amounts to four kilometers. After a long quiescent period, activity recommenced on this fault during the Pliocene, and continues to the present day.

### 2.5.2 The North-Alborz Border Fault

This fault, which forms the northern border of the Alborz Mountains, extends across almost half of northern Iran, following the curvature of the Caspian Sea coast from about 10Km south of Chalus to about 40Km south-west of Gorgan. The entire length of this fault exceeds 300Km. The general trend of the fault, which follows the trend of the Alborz Mountains, is ESE-WNW west of  $53^{\circ}$ E longitude, thereafter bending northwards and running in an ENE-WSW direction.

The geological Map of Iran (NIOC, 1957) proposed a thrust mechanism on the entire length of the fault, whilst the Tectonic Map of Iran (1971) accepted a thrust mechanism east of  $53^{\circ}$ E but a strike-slip movement (of undefined sense) west of that latitude. The left-lateral movement on the parallel Musha-Fahsam Fault (after Wellman, 1966; Nowroozi, 1972) suggests that the sense of strike-slip movement to the North Alborz Border Fault is also left-lateral.

The Kopet-Dagh, a NW-SE running fault on the frontier joining Iran and USSR in the east might truncate this fault at its northeast end.

### 2.5.3 The North-Tehran Fault

The North-Tehran Fault is the closest tectonic feature to the north of Tehran. This fault, which is the frontier

between the Pediment zone and the Alborz Border Folds, runs WSW-ENE in the west and becomes E-W to the north of Tehran. On the ERTS-1 imagery, the surface trace of the fault can be followed from about 60Km south east of Karaj city in the west to near Musha, where it meets the Musha-Fasham Fault. In the west, the fault could be extended to near the Buyin-Zahra Fault, where the great Buyin-Zahra earthquake of September 1, 1962, with an average magnitude  $7\frac{1}{4}$ , occurred (Ambraseys, 1963; Tehran University Report, 1962).

Close inspection of the area of the fault revealed that there is no indication of disturbance of the "D" formation on the alluvial deposits of the Pediment zone. It can be concluded that the most recent movement of the North-Tehran Fault should have taken place before the deposition of the "D" formation, not less than 6,000 years ago (Vita-Finzi, 1968).

#### 2.5.4 The Buyin-Zahra Fault

The fault which inherited its name from a village called Buyin-Zahra immediately to the north, extends from the south of Eshtehard in the west in an E-W direction as far as to the south of Buyin-Zahra, where its trend changes to ESE-WNW (Figure 2-4). The satellite photographs show a remarkably well defined left-lateral movement on this fault (Figure 2-5).

Berberian (1971), from a study of the joints on this fault, confirmed the sinistral movement of the Buyin-Zahra fault.

The fault, which is responsible for the 1962 earthquake, produced vertical as well as horizontal displacements. Field

observations by Ambraseys (1963) showed that the displacements measured between zero and 76cm in the vertical sense and up to 51cm in a left-lateral sense.

#### 2.5.5 The Ardestan Fault

A very clear lineament on the ERTS-1 imagery striking N155°S is recognizable on the mosaic of North-Central Iran. This fault, which is shown on the Tectonic Map of Iran (1971), runs for more than 400Km south of Ardestan to beyond the Shahr-e-Babak. The fault, which is classified as strike-slip (with no sense of movement) on the Tectonic Map of Iran, is marked as a right-lateral fault by Wellman (1966). The fault bifurcates half way along its length, one branch cutting across the Gavkhuni Depression, while the other passes near the city of Shar-e-Babak. It disappears about 100Km to the south east of the city under the Quaternary deposits. A series of en echelon patterns parallel to the trend of this fault extends northwards about 15Km to the west of Qom.

#### 2.6 General Compressive Axis Inferred from the ERTS-1 Imagery

Detailed study of the satellite photographs of North-Central Iran, particularly the Tehran region, has resulted in some new observations of the tectonic movements which were unknown before launching of the ERTS-1.

An attempt is now made to construct the general direction of the compressive stress acting on the region.

Pertinent data including name, general trend, sense of movement, and literature sources of the main faults of the region

is given in table (2-1). Figure (2-6) shows the azimuthal distribution of the major faults in North-Central Iran. The diagram is indicative of dominant wrench movements striking WSW-ENE, WNW-ESE, and N-S. This pattern suggests a  $N35^{\circ}-45^{\circ}E$  compression, which shows excellent agreement with that of the general direction of NE movement from the Arabian Plate (Nowroozi, 1972) and the opening of the Red Sea (McKenzie, 1972).

Regarding the compressive axis deduced from the circular diagram of Figure (2-6) and the general trend of the axes of folding of the Alborz and Zagros Ranges, it seems that an overall NE direction of crustal shortening can be assigned to the movement of the major faults of the region. It is quite clear from Figure (2-6) that it is not possible to accept the Musha-Fasham Fault as a pure thrust (Tchalenko et al., 1974), and that, as Wellman suggested, at least a strong component of strike-slip movement must exist on this, the main fault of the Alborz Mountains.

Table 2.1

Summarizing the trends and direction of motion  
of the main faults of the North-Central Iran.

Name of the fault	General trend	Sense of movement	Reference
Musha-Fasham	ESE-WNW	T	NIOC (1957)
	and	T	GSI (1971)
	ENE-WSW	T	Tchalenko (1974)
		LL	Wellmwn (1966)
		LL	Nowroozi (1972)
North-Tehran		LL	CFPS (this study)
	WSW-ENE	T	NIOC (1957)
	to	SS*	GSI (1971)
Buyin-Zahra	E-W	LL	ERTS-1 (this study)
	WSW-ENE	SS	GSI (1971)
	to	LL	Ambraseys (1963)
	E-W	N	Ambraseys (1963)



Table 2.1 (contd)

Name of the fault	General trend	Sense of movement	Reference
Buyin-Zahra		LL	Berberian (1971)
		LL	ERTS-1 (this study)
Great Kavir	E-W	LL	Wellman (1966)
	and	N	Tchalenko (1973)
	ENE-WSW	LL, and R	Mohajer-Ashjai (1975)
Kuh Banan	NW-SE	RL	Huchride et al., (1962)
		RL	Wellman (1966)
Nayband	N-S	RL	Wellman (1966)
		N	Stocklin (1965)
		RL	Mohajer-Ashjai (1975)

T : Thrust Fault  
 RL : Right-Lateral Fault  
 LL\* : Left-Lateral Fault  
 SS : Strike-slip Fault (of undefined sense)  
 N : Normal Fault  
 SS : Strike-slip Fault  
 R : Reverse Fault  
 GSI : Geological Survey of Iran  
 NIOC: National Iranian Oil Company  
 ERTS: Earth Resources Technology Satellite  
 CFPS: Composite Fault Plane Solution ( will be discussed later)

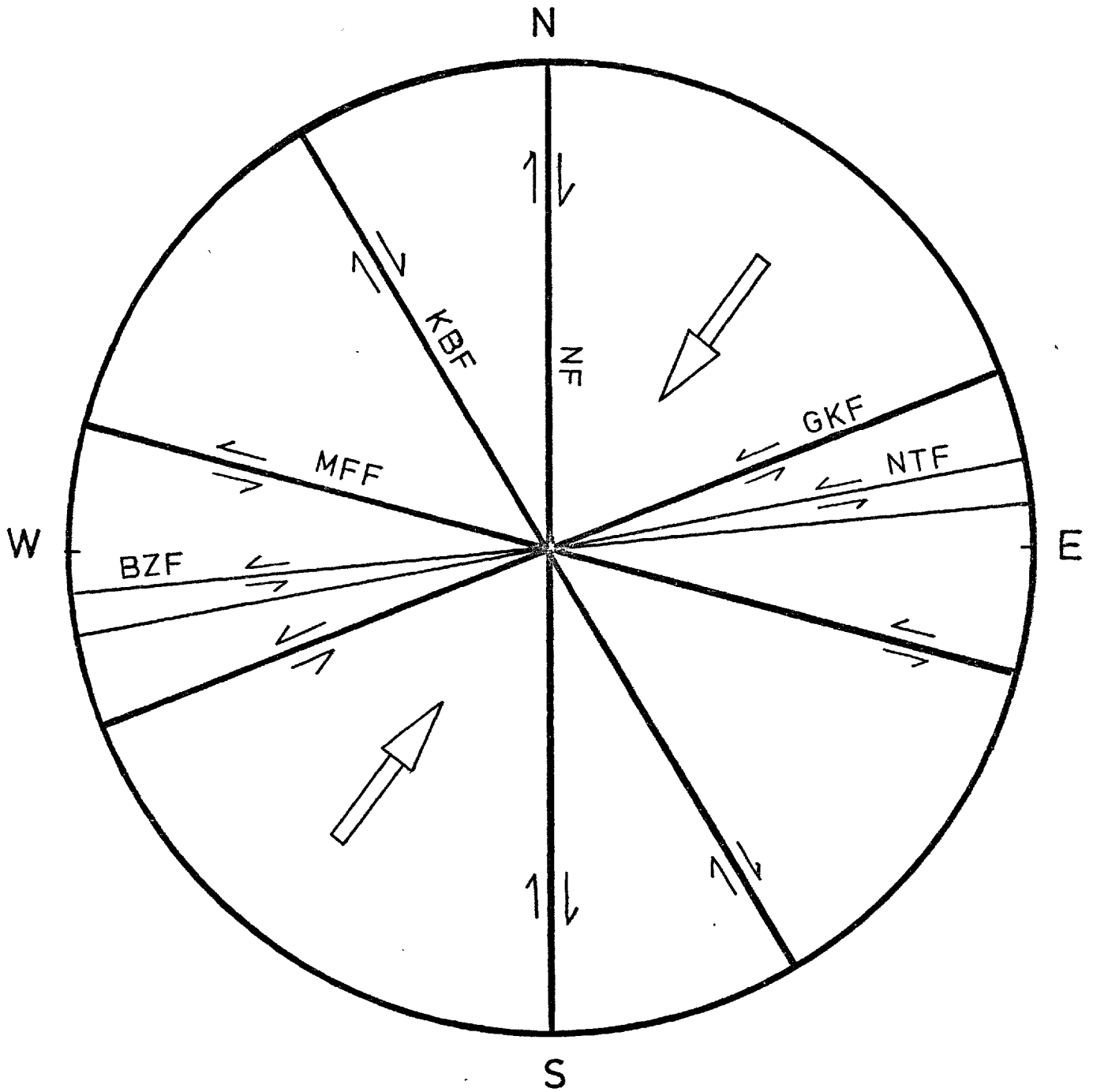


Fig. (2-6). Azimuthal distribution of the major faults, in North-Central Iran. Note the consistency of the general compressive axis with respect to the known direction of motion of major faults. Fault names are as Figure (2-4).

## CHAPTER III

## THE MICROEARTHQUAKE OBSERVATIONS

3.1 Introduction

Throughout history the Tehran region has been a tectonically active part of the Persian Plateau, and many destructive earthquakes have occurred within it (Ambraseys, 1966, 1968, 1974; Nabavi, 1972). Shahr-e-Rey, a city in its immediate vicinity (about 30km south), has suffered many destructive earthquakes since ancient times.

These large earthquakes and the numerous smaller events which have been felt from time to time have provoked much speculation about the seismicity of the region. However, as in many other seismically active continental areas, instrumentally located earthquakes turn out to be few in number and geographically scattered.

Asada, who made a study of the microearthquakes occurring in the Matsushiro district of Japan (Asada, 1957, 1958) appears to have been the first to recognize that these small earthquakes are genetically related to the larger ones, i.e. that they originate from the same active faults. A similar conclusion was reached by Eaton et al., (1970), in a study of the after-shock sequence of the 1966 Parkfield-Cholame earthquake, who showed conclusively the association of the epicenters with the Parkfield-Cholame fault, while Healy et al. (1972) found that microearthquakes indicated clearly in which parts of the San-Andreas Fault creep was occurring and in which parts strain was building up.

In the same study of the Matsushiro microearthquakes, Asada (1958) observed that a linear relation existed between magnitude and the logarithm of the frequency of occurrence of earthquakes throughout the magnitude range from -1 to +5. Evernden (1970), in a study of regional and world seismicity, using local data and epicentres located by the USCGS, showed that the range extended at least up to magnitude 8 earthquakes. Thus the relation developed by Richter (1954) between magnitude and frequency of occurrence:

$$\text{Log}_{10} N = a - bm$$

where  $N$  is the number of shocks of magnitude  $m$  and over per unit of time and  $a$  and  $b$  are constants, applies equally well to microearthquakes as to major events.

It follows that many of the techniques that have been developed for studying the seismicity, structure and tectonics of continental areas using large earthquakes can equally well be applied to microearthquakes, with the great advantage that useful information can be obtained in a matter of weeks or months as against the tens of years or even centuries of study that would be necessary if only instrumentally recorded events were to be used.

Thus the above relation can be used in the statistical prediction of earthquake occurrence, and it can also be used to obtain values for  $b$ , which is an important parameter related to the seismicity of an area. For large earthquakes,  $b$  normally has a value lying between 0.4 and 1.8 (Allen et al., 1965) for both regional seismicity and aftershock sequences.

Figure (3-1) shows an example of a so-called recurrence curve (plot of Log N against m) which was obtained by Evernden (1970) for southern Iran (within a 1000Km radius of Shiraz). The b-value in this particular case is 1.46, which is the sort of value to be expected from a tectonically active zone.

These several observations underline the fact that microearthquakes are part of the continuous spectrum of seismic activity and that their study represents an equally valid means for studying the tectonics of a region as study of larger events. Many of the relationships which have been developed in the study of major earthquakes apply equally to microearthquakes, for example, anomalous changes in the  $V_p/V_s$  ratio and their relation to future earthquakes. On the other hand, the more frequent occurrence of microearthquakes enables techniques to be developed which could not be applied to the study of major earthquakes, such as the recently introduced composite fault plane solution technique.

One way of deducing the nature of the movement on, and the mechanism of, currently active faults is by studying the P-wave radiation pattern of earthquakes occurring on them, recorded at a number of azimuthally well distributed sites. This conventional way of determining the mechanism of faulting is referred to as a fault plane solution. In the case of microearthquakes, the number of local seismograph stations is usually too small, and their azimuthal distribution inadequate, for a fault plane solution to be possible. However, on the assumption that they originate from the same fault, and that the fault plane mechanism is the same in all cases, it is

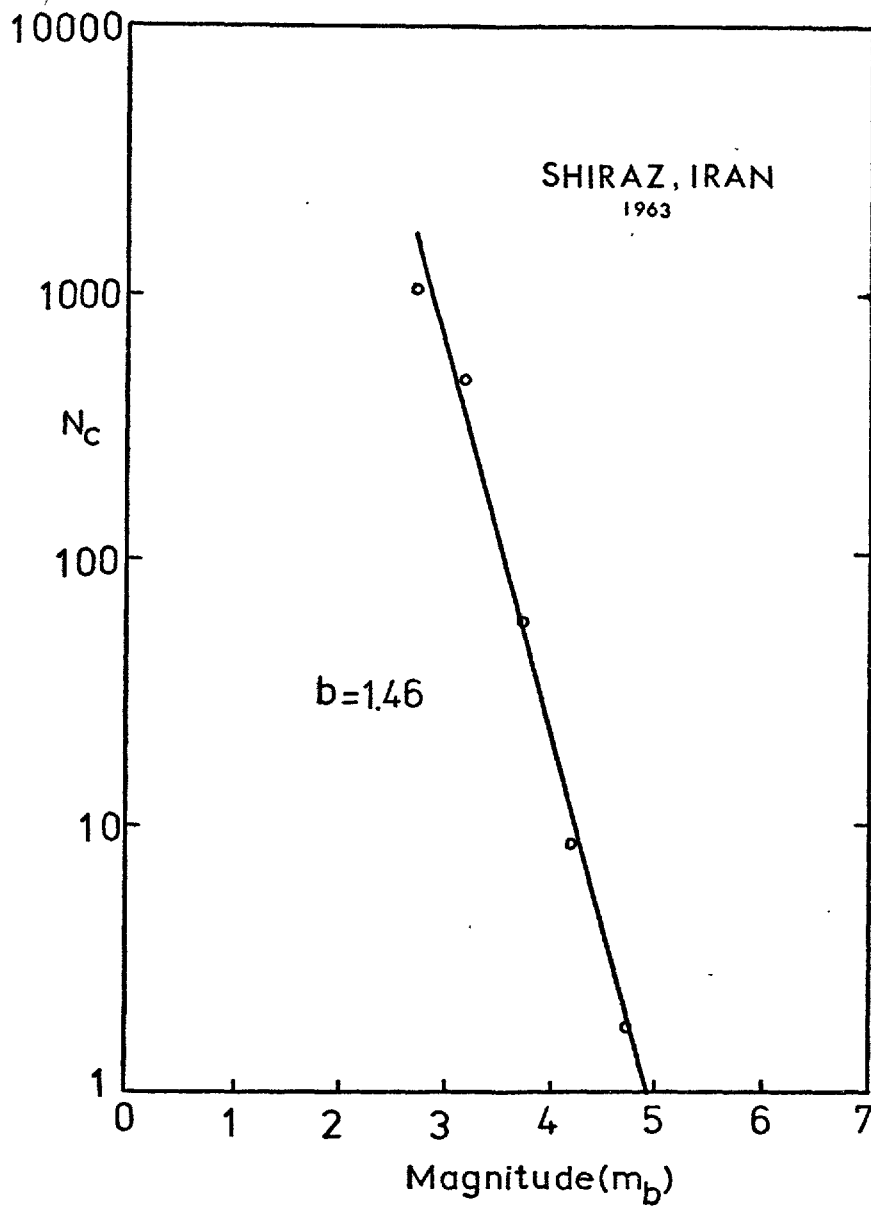


Fig. (3-1). An example of recurrence curve showing the regional seismicity of Shiraz, Iran (after Evernden, 1970).

possible to combine the radiation pattern of the P-arrivals of a number of microearthquakes recorded by a local network to obtain the mechanism solution. The process is known as a composite fault plane solution. Further improvement of the azimuthal distribution can be obtained by moving the recording stations around, as was done in the present case.

Composite fault plane solutions have been widely used in various parts of the world by many investigators (e.g. Scholz et al., 1969; Hadley and Combs, 1974; Trimble and Smith, 1975; Hedayati and Hedayati et al., 1976). Although there must always be some uncertainty about the matter, various comparisons made of composite and conventional fault plane solutions applied to the same fault systems support the assumption that the same mechanism is involved in both cases. Thus Trimble and Smith (1975) found that the composite fault plane solution derived from a study of the microearthquakes of the Hebgen Lake-Yellowstone Park region led to the same strain field as that obtained from a conventional fault plane solution.

Prediction of earthquakes has been a long-standing objective of seismologists. Semenov (1969) observed that changes occurred in the ratio of compressional to transverse wave velocity ( $V_p/V_s$ ) prior to a moderate sized earthquake in the Garm region of the Central Asia. The effect, if universally present, has obvious applications in earthquake prediction and has since been looked for in other parts of the world as well as in the laboratory (Gupta, 1972).

It has been suggested by many seismologists (e.g., Scholz et al., 1973; Aggarwal et al., 1973; Kisslinger, 1974;

Kelleher and Savino, 1975) that the precursory changes in seismic body wave velocity ratio occur before small to moderate as well as major earthquakes, and that the amount of the anomalous change of the velocity ratio correlates with the magnitude of the forthcoming earthquake. Also, it is concluded that the duration of the precursor time is longer for larger earthquakes.

Microearthquakes recorded in the Tehran region have been examined for evidence of precursory velocity changes on the short time-scale involved. The results are discussed in chapter VI.

Seismic risk in earthquake prone areas is of great concern to engineers. Cornell (1968) introduced a method for evaluating the seismic risk at an engineering site as a function of average return period (the elapsed time between two successive earthquakes). An attempt has been made to apply the technique to the Tehran region.

### 3.2 Field Procedure

The Tehran expedition extended from early November to early December 1974. The instruments used were two Geostore tape recorders and one Sprengnether smoked drum seismograph which will be described later.

To make the best use of a microearthquake survey it is most important to site the seismographs properly. Generally, the seismographs are installed either near fault traces, if there are any, or close to an area which has been active in the past. In the case of the Tehran region, a survey of the historical record show<sup>ed</sup> that the earthquakes were scattered, and gave no clear indication as to where to site the instruments. Knowing the relative activity of the Musha-Fasham and the North-



Tehran Faults from the literature, it was decided to install the seismometers along these faults, and also near the city of Shahr-e-Rey, which has been destroyed by earthquakes many times in the past.

Installations were made in a tripartite array in the north, west, and southern parts of Tehran. Having defined the general area of interest, in relation to the known activity of the area or proximity to a fault scarp, the next question to be decided is where to locate the seismometers. There are two requirements, first, they have to be protected from the wind and be distant from cultural noise, and second they have to rest on hard bedrock. In this expedition, all the seismometers were installed in natural caves, on the Mesozoic bedrock west and northwest of Tehran, and on the Tertiary formation south of the city.

To obtain a visual record of the background noise it was necessary to operate the Sprengnether at each site at least for 24 hours and then replace it by a Geostore. The survey was started by installing the Sprengnether at Soleqan (SO), Figure (3-2). It was found that the background noise at this station was too high, and therefore the instrument was moved to the next station, Kan (KA), in which the noise level appeared to be reasonable for installation of the first Geostore. In this manner, the first tripartite array was formed on the north of Tehran consisting of Kan (KA), Lashgarak (LA) and Shemshak (SH) stations. The same procedure was followed for the three other Geostore stations, none of which was occupied by a Geostore without having first been occupied by the Sprengnether.

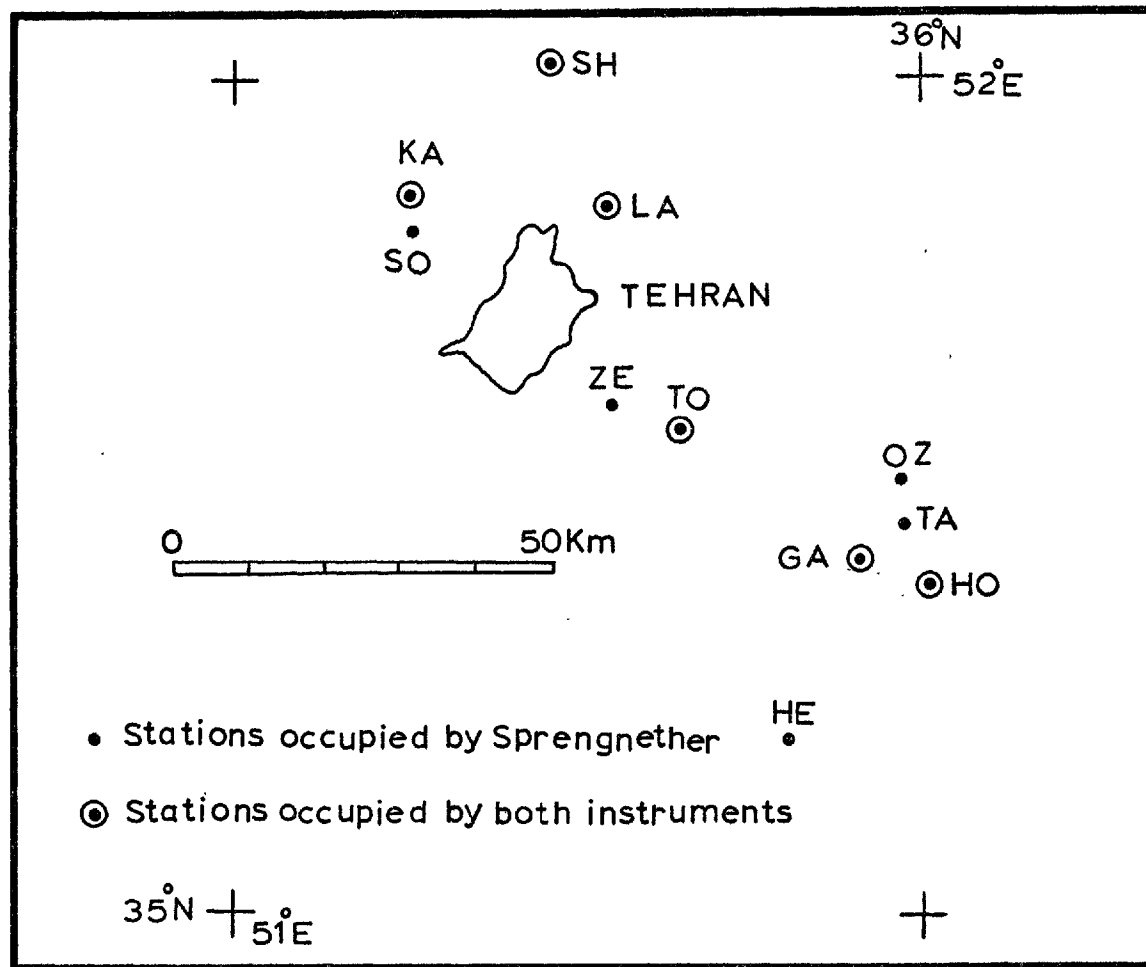


Fig. (3-2). Sketch map of the position of the recording stations. GA: Gandab; HE: Hessarsanbak; HO: Hosseinabad; KA: Kan; LA: Lashgarak; OZ: Ozdar; SH: Shemshak; SO: Soleqan; TA: Tangeh; TO: Tochal; ZE: Zendan.

A total of eleven recording sites was occupied, some for only one day, one for as long as two weeks.

### 3.3 Instrumentation

The objectives of the microearthquake survey, conducted late in 1974, were to describe the microearthquake distribution, to determine the contemporary stress pattern from the composite fault plane solutions, and to find a way of assessing the future activity. Figure (3-3) shows the location of seismographic stations on a geological map of the region. Pertinent data such as location, latitude, longitude, elevation, type of instrument, and duration of recording are given in table (3-1).

Three short-period vertical component seismographs were used. These were a Sprengnether MEQ 800 smoked drum seismograph with a Willmore 1Hz geophone, and two Racal Geostore fourteen-channel magnetic tape recorders, each with a Geo Space Hs10 2Hz geophone. The Sprengnether is the property of the Geophysics Department of Imperial College and the two Geostores were borrowed from the U.K. Natural Environment Research Council's pool of seismic equipment. Geostore equipment had not previously been used for microearthquake studies, and one of the purposes of the survey was to investigate their suitability for such work.

The gain of the seismograph is expressed in db, which is a function of the ratio of input and output voltages of the amplifier, i.e. its voltage gain. The latter is related to the db gain of the seismograph (N) by:

Fig. (3-3). Location of seismograph stations on a geological map of the Tehran region (after Tchalenko et al. 1974). All the stations are installed on bedrock, even though it is not evident from the map. Station names are as Figure (3-2).

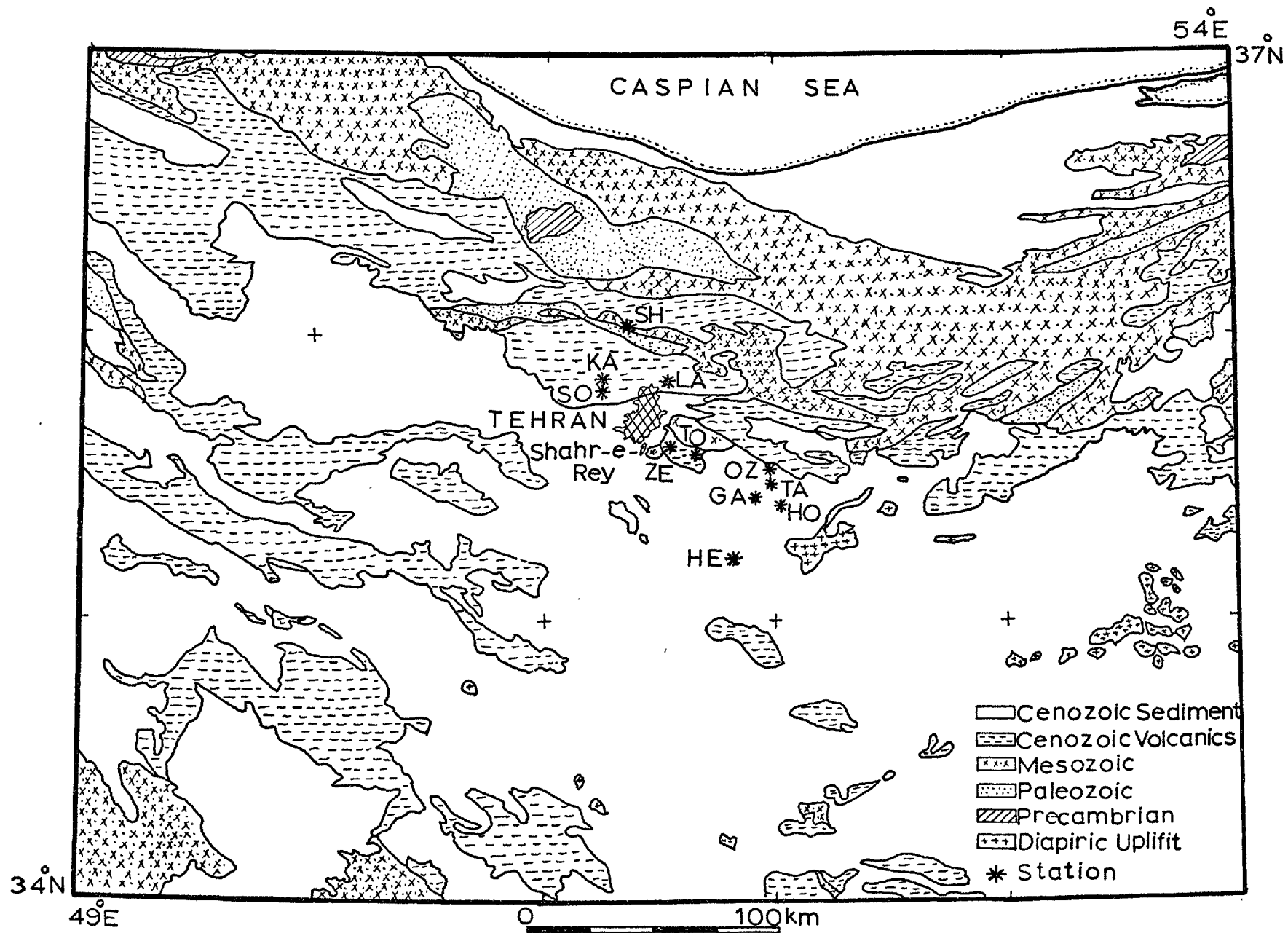


Fig. (3-3).

TABLE 3-1

NETWORK STATION DATA

STATION		LATITUDE (N)		LONGITUDE (E)		ELEVATION(m)	NO. OF DAYS	
		Deg.	Min.	Deg.	Min.		MEQ 800	Geostore
SOLEQAN	(SO)	35	49.48	51	15.56	1780	1	-
KAN	(KA)	35	51.15	51	15.60	1760	1	8
LASHGARAK	(LA)	35	51.60	51	32.70	1850	1	4
SHEMESHAK	(SH)	36	00.33	51	27.16	3300	1	6
ZENDZN	(ZE)	35	36.10	51	33.60	1350	3	-
GANDAB	(GA)	35	25.79	51	55.77	1190	2	13
HOSSEIN- ABAD	(HO)	35	24.50	52	01.69	1190	1	3
TANGEH	(TA)	35	29.33	51	58.70	1550	1	-
OZDAR	(OZ)	35	31.48	51	59.20	1780	2	-
TOCAHL	(TO)	35	34.57	51	39.62	1500	3	8
HESSAR- SANBAK	(HE)	35	12.81	51	50.09	1050	6	-

44

$$N_{(db)} = 20 \text{ Log}_{10} V_2/V_1.$$

Thus, the Sprengnether's seismometer was set between 90 and 102db, depending on the background noise, which corresponds to a voltage gain of between 32,000 and 126,000. Figure (3-4) shows the combined system response for the Geostores and the Sprengnether.

The Geostores were operated at full gain (82db), which appeared not to overload them, whereas it was found best to operate the Sprengnether at rather less than its maximum gain of 120db.

The recording speeds used were 60 mm per minute for the Sprengnether, giving a twenty-four hour record, and 15/320 inches per second for the Geostores, giving a 340 hour record.

The Geostores were powered by a twelve-volt car battery, giving them an unattended run of about seven days, while the Sprengnether was driven from four internal rechargeable twelve-volt lead-acid batteries, providing enough power to operate the instrument for more than a week. Each instrument site was checked at least once a day.

Each seismograph has its own internal crystal clock. That in the Sprengnether puts minute and hour marks onto the smoked paper; the Geostore clock records days, hours, minutes, and seconds onto one of the channels.

Inter-station time control was achieved by means of synchronisation, firstly of the Sprengnether to G.M.T., then of the Sprengnether to each Geostore. It was found at the end of the survey that there was no more than a quarter of a second discrepancy between the three clocks.

Fig. (3-4). Response curves for the Sprengnether MEQ 800 (A) and Geostore (B) seismograph systems.

Curves (A):

- I: Low and high frequency filters out
- II: Low frequency filter = 5, High frequency filter out
- III: Low frequency filter = 10, High frequency filter out
- IV: High frequency filter = 5, Low frequency filter out
- V: High frequency filter = 10, Low frequency filter out
- VI: High frequency filter = 30, Low frequency filter out



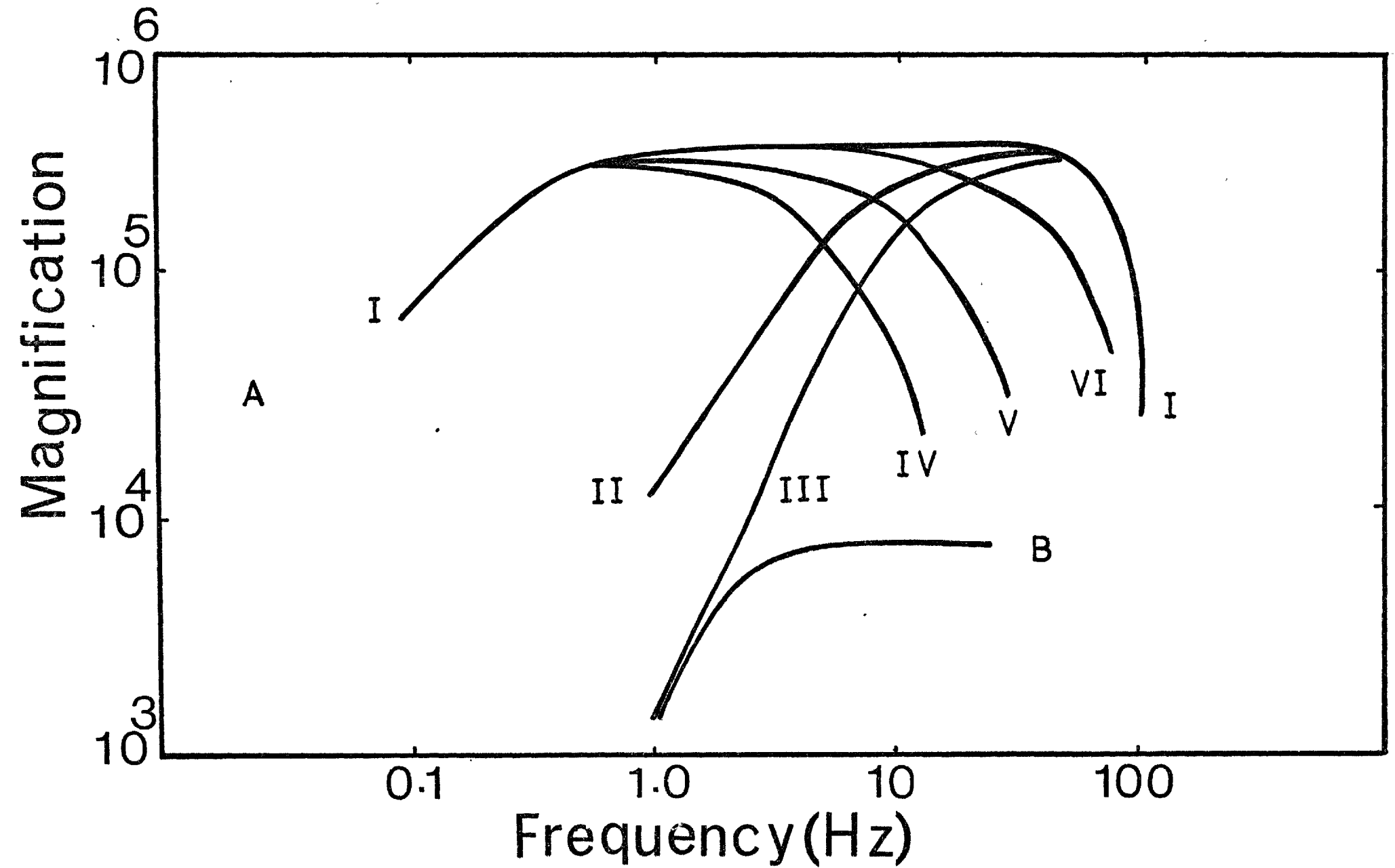


Fig. (3-4).

### 3.4 The Suitability of Geostores for Microearthquake Studies

One of the purposes of the Tehran expedition was to investigate the suitability of the Geostore tape recorder system for recording microearthquakes, principally in comparison with the Sprengnether.

Originally, the Geostores were designed for refraction seismic applications, in which a number of geophones are connected to a central recorder, normally by cable, though telemetering is possible. The Geostore is equipped with fourteen channels, of which two are used for flutter control and one for the internal digital clock. Of the remaining eleven, one is usually used for an external time mark and the rest are for the geophones.

In microearthquake investigations, such as this, the optimum station separation is of the order of 10Km. This is too great to enable stations to be connected by cable to a central recording system without resort to telemetering, which was not possible in the present case. As, at most, only three seismometers can usefully be employed at each recording station (one vertical and two horizontal), not more than three of the ten available seismometer channels could be used. Thus the recording system cannot be used to its full capability. However the Tehran field trip exposed more serious weaknesses, which can be summarized as follows.

- a. The bulk of the recording system is large in volume and weight. Each tape recorder, including pre-amplifier, cable and geophone, weighs more than 45 kg, while the Sprengnether as a whole weighs less than 23 kg.

- b. A car battery is required to run the system, and this makes the Geostore less convenient in the field, especially in regions difficult of access, as in the present case. By contrast, the Sprengnether is equipped with four internal rechargeable batteries whose weight is about 3kg, which is included in the overall weight of 23 kg.
- c. The maximum gain is about 82db, which makes the instrument less reliable for monitoring very small events, say less than half a unit in magnitude, than the Sprengnether, which has a maximum gain of 120db, adjustable in 6db steps from 60db.
- d. It is impossible to obtain a visual assessment of the background noise. The accompanying Field Test Box is not sensitive enough, and without a knowledge of the background noise level it is impossible to set the gain to an optimum value.

Nevertheless there are also some advantages such as:

- a. Using a recording speed of 15/320 inches per second, and a 50 AH 12 volt car battery, the system can run unattended for about one week, which should not normally be done, but might occasionally be necessary.
- b. The greatest advantage of the Geostores is the flexibility of magnetic tape recording, which allows an accurate interpretation of the events and the avoidance of the "white-out" problem (merging of successive oscillation of the stylus, producing a white patch) which can affect smoked paper records

during periods of high activity.

Slight improvement of the system sensitivity, both of the tape recorder and the Field Test Box, and reduction of its volume and weight, would make it a more useful instrument for microearthquake surveys. Even so, experience suggests that Geostore equipment on its own is not satisfactory for such work. It is necessary to supplement it with a visual recorder, such as the Sprengnether, for monitoring the background noise level at each recording station prior to setting up the Geostore.

### 3.5 Replaying the Geostore Tape onto Chart Paper

In the Tehran field work the Geostores were used at maximum gain (82db), which turned out to have led to the recording of an excessive amount of cultural noise. The frequency associated with this background noise was about 20 Hz, which was easily removed by use of a low pass filter, on playback. The setting of the low pass filter should be chosen in accordance with the playback speed. Figures (3-5) and (3-6) show block diagrams of recording and replay systems.

It is not possible to trace the events by watching them on an oscilloscope, and to be on the safe side it is necessary to play back the whole tape onto chart paper. To do this without using an inordinate quantity of paper, a suitable combination of tape playback and chart recorder speed should be chosen. The best combination was found to be  $1 \frac{7}{8}$  inches (about 47 mm) per second of tape playback

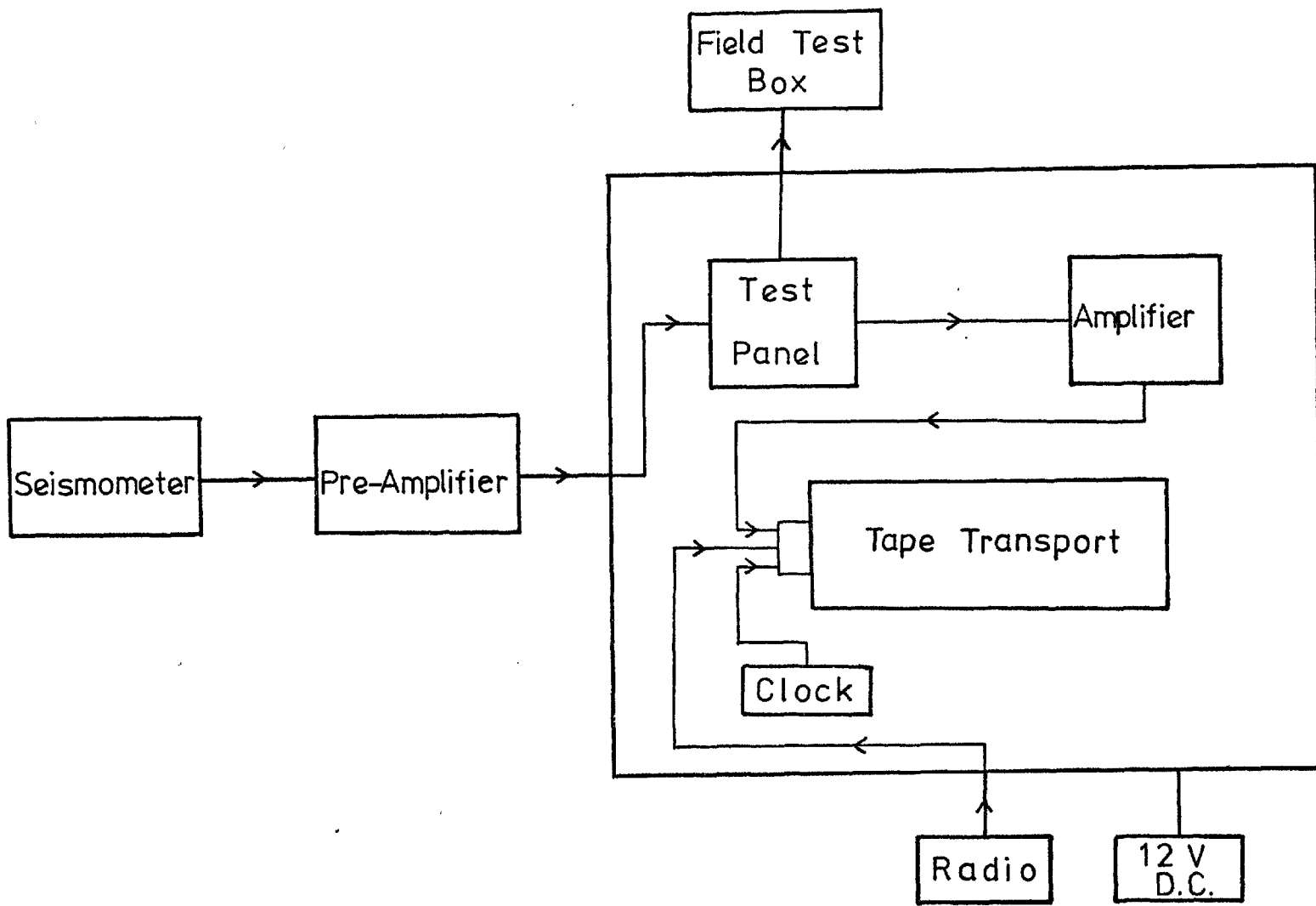


Fig. (3-5). Block diagram of the Geostores field recording system.

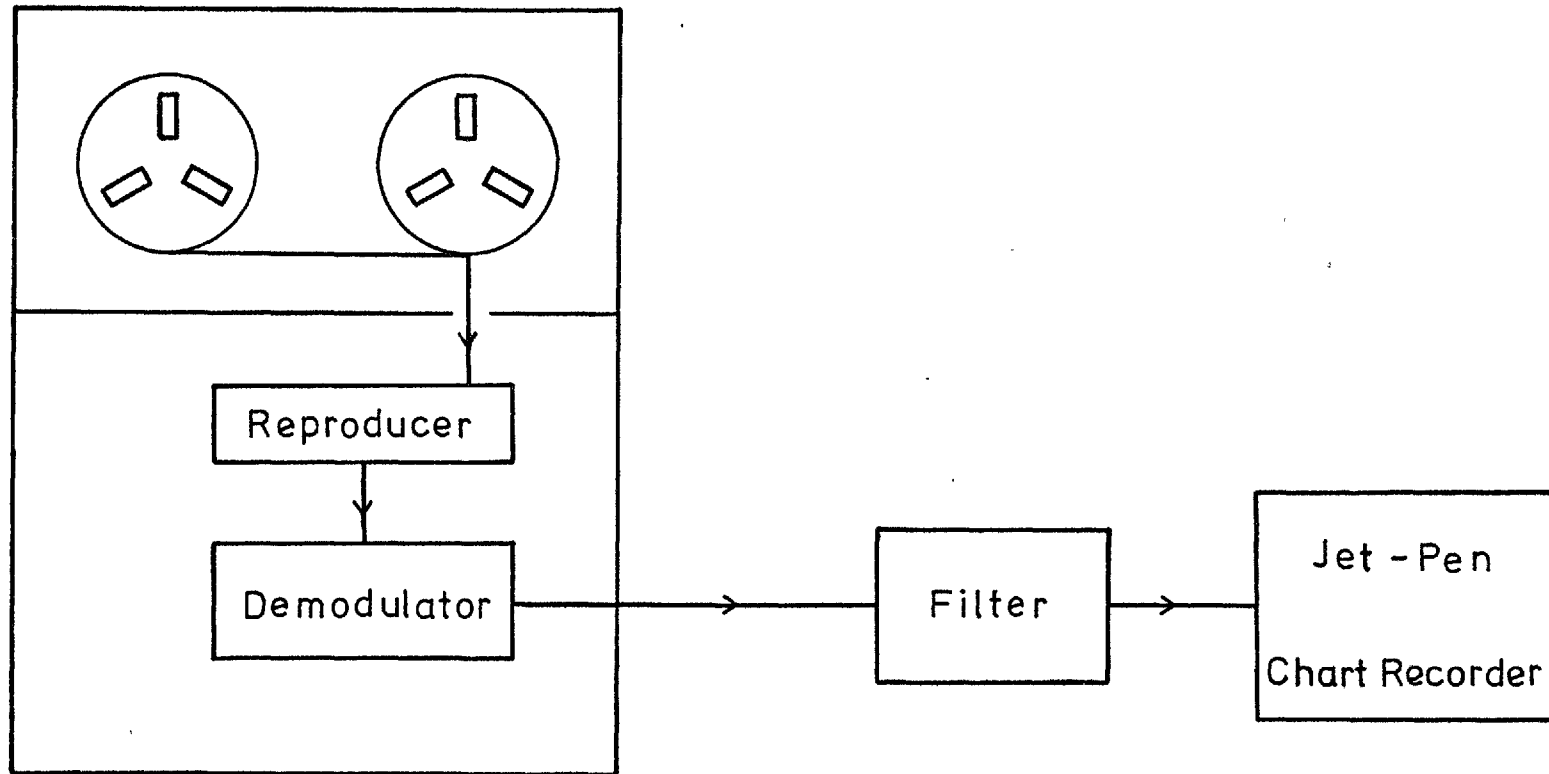


Fig. (3-6). Block diagram of the replay system.

and 2.5 mm per second of chart paper when searching for events, while the combination of 15/64 inches (about 6 mm) per second of tape playback and 25 mm per second chart paper speed gives excellent reproduction of the wave forms and arrival times of events. Figures (3-7) and (3-7a) illustrate records using these two combinations.

The low-pass filter should be set at 400 Hz for the first combination and 100 Hz for the second, (these correspond to 10 Hz and 20 Hz respectively at the original recording speed of 15/64 inches per second). It is important to reset the filter for each combination or else the wanted events will be filtered out.

### 3.6 Data

In reading the seismograms, intervals with a high noise level were omitted. This eliminated only a small fraction of events recorded in most cases, but provided a more homogeneous set of data for comparison between stations. Inter-station comparison was utilized whenever possible.

Microearthquakes are characterised as seismic waves having a predominant period of less than half a second, a sharp onset, frequency changes during the event, distinct S-phases (in most cases) and a steadily decaying coda. In some cases, even with the help of the above criteria, it is not easy to distinguish a very small nearby earthquake from noise. Therefore, doubtful events were omitted from the final analysis. Figures (3-7a) and (3-8) show seismograms of local events recorded by a tape recorder (after playing back onto

Fig. (3-7). An example of a played back record using a tape playback speed of  $1 \frac{7}{8}$  inches (about 47 mm) per second and a chart speed of 2.5 mm per second, for looking for events.

Fig. (3-7a). Reproduction of seismic waves recorded by the Geostore using a tape playback speed of  $\frac{15}{64}$  (about 6 mm) per second and a chart speed of 25 mm per second (page 54).

Fig. (3-8). An example of smoked paper seismograms recorded at Hessarsanbak (south of Tehran), showing typical character of the microearthquakes. Note the change of background noise level between day and night, and the effect on some of the events of the limited amplitude of the stylus deflection (page 55).



First Combination

Station : TOCHAL

Gain : 82db

Date : 08 Dec., 1974

Time : 01 41 11.8

Fig. (3-7).

Second Combination

Station: TOCHAL

Gain : 82db

Date : 08 Dec., 1974

Time : 0141 11,8

10 Sec.

Second Combination

Station: GANDAB

Gain : 82db

Date : 08 Dec., 1974

Time : 0141 11,9

10 Sec.

Fig. (3-7a).

Z Dec 7 1974 Gain: 90 HESSAR SANONK

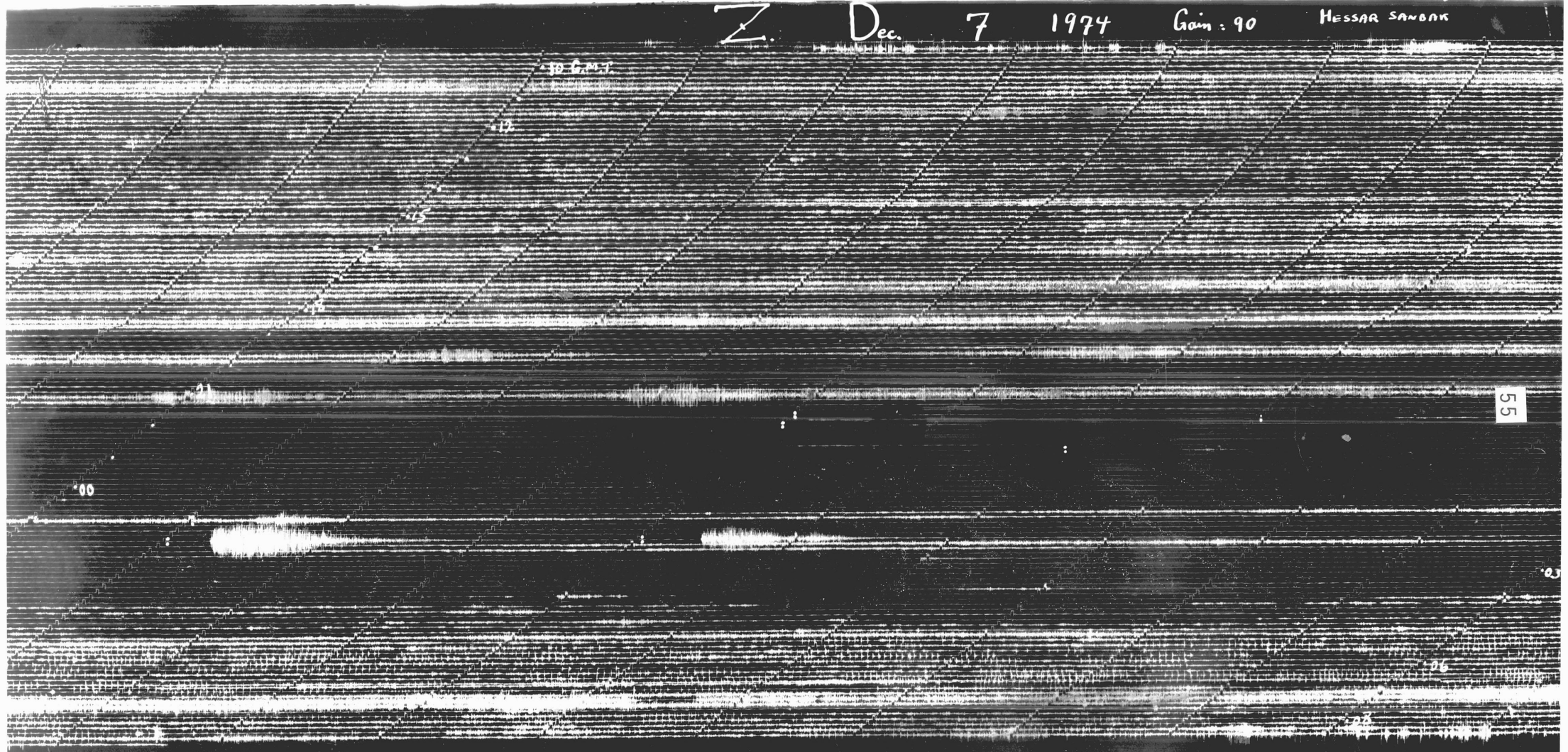


Fig. (3-8).

60Sec

chart paper), and by the Sprengnether, in the Tehran region.

To reduce the interpretation errors to a minimum, the arrival times of P- and S-phases were read with high precision, better than 0.1 second for the Geostore seismograms and better than 0.25 second for the smoked paper, by using a magnifying lens. Only those events were retained for precise location by the computer for which four or more P- and S-readings could be identified without ambiguity.

The number of microearthquakes recorded during any twenty-four hour period varied from a few to several tens, and the total effective recording time (all three stations working) was 336 hours.

### 3.7 Seismic Activity Level of the Area

Figure (3-9) shows the number of events recorded by the Sprengnether seismograph each day at the various recording stations. It is assumed that there is little day-to-day variation in overall seismic activity in the area, and that the observed variation is an indication of the variation of activity from station to station. This assumption is supported by the fact that the day-to-day variation at those stations at which the seismograph was operated for more than one day is generally less than the differences between the various stations.

Thus, the actual recording of activity in the Tehran region was started by installing the first seismograph on the western part of the North-Tehran Fault near the village of Solegan. It became evident later that only about five percent of the located microearthquakes are associated with this fault.

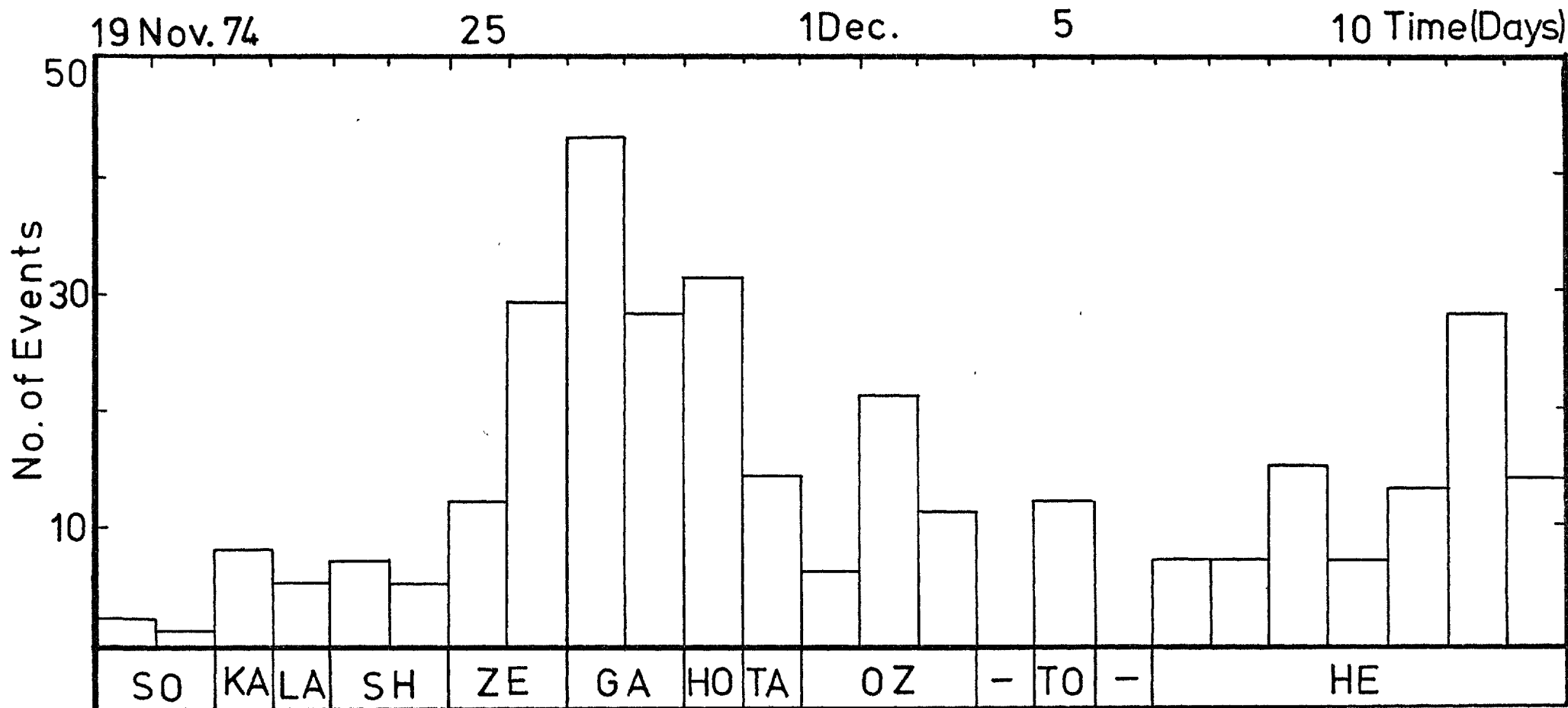


Fig. (3-9). Histogram showing the regional variation of activity from station to station as recorded by the Sprengnether seismograph.

Moreover, the microearthquakes recorded in this part of the region have S-P intervals between 10 and 15 seconds, corresponding to epicentral distances of 80 to 120 Km. On the basis of the S-P observations, the instruments were moved to the east and south sides of Tehran, where activity was higher and S-P intervals shorter, showing that the events were much closer. The average rate of activity for this particular region is identified as 21.4 shocks per day. The individual activity of each recording station is shown in Figure (3-10). The numerical values at each circle shows the normalized percentage of activity at a particular station.

The above discussion revealed that the areas to the east and south of Tehran are responsible for most of the activity of the region. This could be concluded from the S-P frequency distribution. Figure (3-11) shows the frequency distribution of microearthquakes versus epicentral distances in terms of S-P time interval. The figure shows clearly that more than 70 percent of the events originated from sources not more than 60 Km (S-P less than 7.5 seconds) away from the recording stations. Considering the inter-station distances, which vary from 15 to 40 Km it can be concluded that the area of highest rate of occurrence is the same as shown by Figure (3-10), namely southeast of Tehran itself.

Table (3-2) summarizes sites, dates of recording, number of shocks in various S-P intervals, effective recording time, and rate of occurrence.

Fig. (3-10). Normalized rate of occurrence of micro-earthquakes (numerals in the circle) per day. Station names are as Figure (3-2).

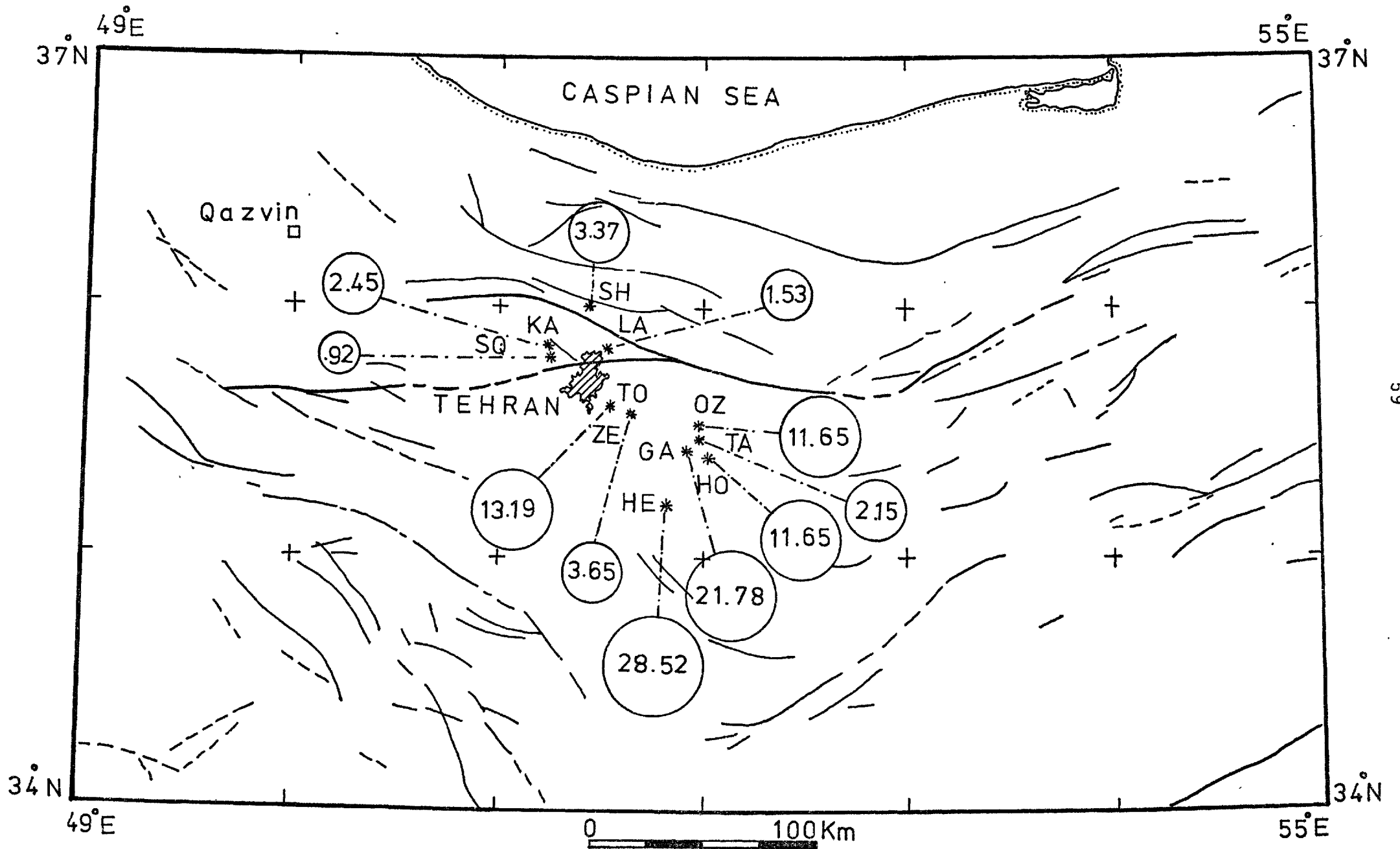


Fig. (3-10).



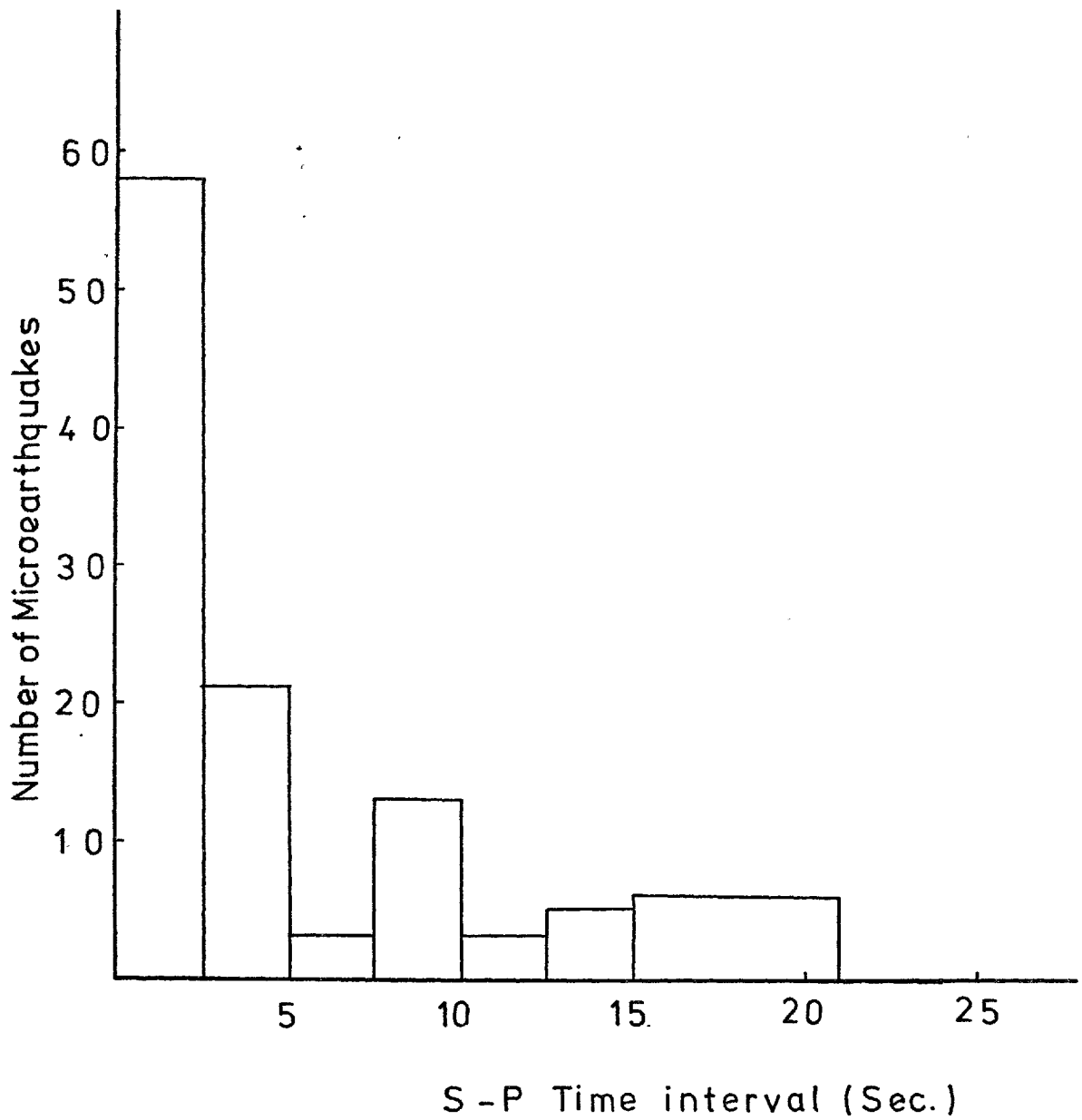


Fig. (3-11). Frequency of microearthquakes against distance from the seismograph stations. Distances are shown as S-P time intervals.

TABLE 3-2

SUMMARY OF OBSERVED ACTIVITY

Date	No. of Events		S-P Time Intervals, in Seconds, Less than or Equal to:							No. of no S Reading	Cumulative No. of Events	Effective Recording Time (Hour)	No. of Shocks Per Day	Site
	Read	Counted	2.5	5.0	7.5	10.0	12.5	15.0	21.0					
19 11 74	2	-	-	-	-	-	1	1	-	-	2	9	5.33	SO
20 11 74	1	-	-	-	-	-	-	-	1	-	1	6	4.00	SO
21 11 74	8	-	-	3	-	2	1	2	-	-	8	15	12.80	KA
22 11 74	5	-	-	2	-	-	-	-	-	3	5	16	7.50	LA
23 11 74	7	-	-	-	1	3	1	-	1	1	7	23	7.30	SH
24 11 74	3	-	-	-	1	-	-	-	2	-	3	5	14.40	SH
24 11 74	2	-	-	-	-	-	-	1	-	1	2	15	3.20	ZE
25 11 74	9	3	-	-	-	-	-	-	-	9	12	24	12.00	ZE
26 11 74	17	12	-	4	-	1	-	-	-	12	29	24	29.00	ZE
27 11 74	25	18	5	-	-	-	-	-	2	18	43	22	46.90	GA
28 11 74	11	17	3	-	-	-	-	1	1	6	28	12	56.00	GA
29 11 74	18	13	1	1	-	-	-	-	-	16	31	12	62.00	HO
30 11 74	7	-	5	-	-	-	-	-	-	2	7	6	28.00	HO

..... contd ..

TABLE 3-2 (Contd.)

SUMMARY OF OBSERVED ACTIVITY

Date	No. of Events		S-P Time Intervals, in Seconds, Less than or Equal to:							No. of no S Reading	Cumulative No. of Events	Effective Recording Time (Hour)	No. of Shocks Per Day	Site
	Read	Counted	2.5	5.0	7.5	10.0	12.5	15.0	21.0					
30 11 74	4	3	1	-	-	-	-	-	-	3	7	4	42.00	TA
01 12 74	5	1	4	-	-	1	-	-	-	-	6	11	13.09	OZ
02 12 74	21	-	10	4	-	1	-	-	-	6	21	22	22.90	OZ
03 12 74	8	3	-	3	-	-	-	-	1	4	11	12	22.00	OZ
05 12 74	6	6	3	-	-	-	-	-	-	3	12	14	20.57	TO
07 12 74	7	-	-	-	-	1	-	-	1	5	7	12	14.00	HE
08 12 74	7	-	2	1	-	3	-	-	1	-	7	21	8.00	HE
09 12 74	7	8	2	1	1	-	-	-	-	3	15	23	15.60	HE
10 12 74	3	4	2	1	-	-	-	-	-	-	7	8	21.00	HE
11 12 74	14	-	6	-	-	-	-	-	-	7	13	17	18.35	HE
12 12 74	28	-	13	-	-	-	-	-	-	15	28	24	28.00	HE
13 12 74	5	9	1	1	-	1	-	-	1	1	14	9	37.33	HE

### 3.8 Construction of P-and S-Wave Travel-Time Curves

For a long time the author has been aware of the need for a travel-time curve for local earthquakes in the Tehran region. The microearthquakes recorded in this survey provided the opportunity for constructing the P-and S-wave time-distance curves of local and shallow depth (up to 22 Km) events for the region.

Standard travel-time curves are normally presented for different hypocentral depths and seismic phases (e.g. Jeffreys and Bullen, 1940; Arnold et al., 1968). It is not possible to use such time-distance charts to interpret microearthquakes, firstly, because they are not available for the short epicentral distances (less than 200 Km) involved in microearthquakes studies, and secondly because of the large effect of crustal inhomogeneities on local shocks, much of whose ray paths lie within the crust. Therefore, each observatory has to establish its own curves using its own local network.

Local travel-time curves (mainly P-and S-phases in microearthquakes studies), produced in this way, can be used for phase identification as well as for epicentral location, particularly when an earthquake is recorded by only one three-component recording station. Normally, it is not possible to make any sort of epicentral determination for events recorded in such fashion, but travel-time curves enable good estimates to be made of epicentral distances, using the S-P time interval. This information can be combined with azimuthal calculations (from the relative magnitude of the P-wave arrivals on two horizontal components) to give an approximate epicentral location.

To construct such transit-time curves, it is necessary to establish a local network of at least three stations. Such an extended effort is efficient and practicable in a region as active as the Tehran area, where microearthquakes are frequent enough (at an average rate of more than 20 per day) to yield results in a limited time.

The technique used in the present study is described in chapter V. In brief, the coordinates and origin time of each event have to be calculated, which can be done if the arrival times of P- and at least one S-phase at three recording stations are known. Figure (3-12) shows a plot of the epicentral distances of earthquakes recorded at three stations versus arrival times of P- and S-waves. It can be seen that there is a linear relation between arrival times of P- and S-phases at short epicentral distances, less than 200 Km. These curves can be used as a good tool for the interpretation and location of future earthquakes in the area.

### 3.9 Calculation of Short Epicentral Distances and the Poisson's Ratio

In general S-P time intervals have to be used in conjunction with the S- and P-travel time curves in order to determine the epicentral distance. However, reference to travel time curves is not necessary for short epicentral distances, where, the travel time curve being a straight line, the epicentral distance can be determined from the S-P time interval using a simple algebraic expression:

$$\Delta = K(t_S - t_P)$$

where K is a function of P- and S-wave velocities (equal to

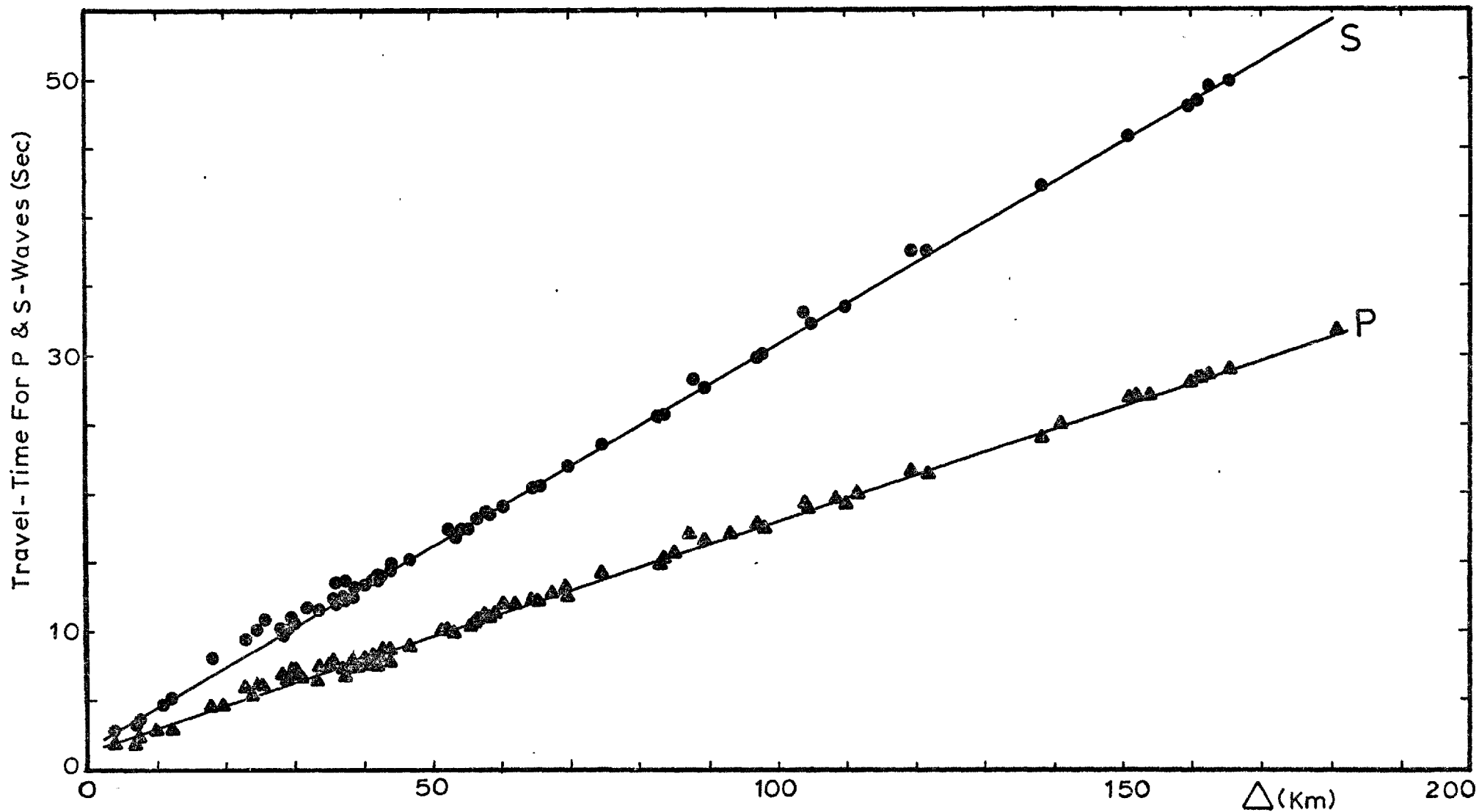


Fig. (3-12). Travel-time curves of P-and S-waves for the Tehran region. Note the close grouping of the data points about the fitted lines.

$V_p \cdot V_S / V_p - V_S$  km/sec). It is assumed, of course, that for short epicentral distances  $V_p$  and  $V_S$  are constant at any particular depth. The slope of the straight line passing through the plots of epicentral distances (see chapter V) versus S-P time-interval, Figure (3-13), gives the numerical value for K. Using a least-square technique, this value is found to be  $7.80 \pm 0.05$  km/sec for the Tehran region. In a study of micro-earthquakes in the Rift Zone of East African Rykounov et al. (1972) found that  $K = 7.8 \pm 0.4$  km/sec, which is similar at least, within the uncertainty limits, to the value found here.

Although, S-wave arrivals are of less reliable quality, many events show good impulsive S-phases. S-P ( $t_S - t_p$ ) are plotted against P-0 ( $t_p - t_0$ )\* in Figure (3-14) for a number of events for which S-phases could be reliably picked. The linear relationship indicates the constancy of  $V_p/V_S$  and the slope of the straight line fitted to the data by a regression method gives an apparent velocity ratio of P-and S-waves of  $1.703 \pm 0.007$ . Using the relation:

$$\sigma = \frac{(V_p/V_S)^2 - 2}{2((V_p/V_S)^2 - 1)}$$

which can be derived from basic elastic theory, the value of  $\sigma$  is found to be  $0.240 \pm 0.003$ , which lies within the range normally found for crustal rocks. The small scatter of the points in Figure (3-14) suggests considerable crustal homogeneity and mechanical stability.

---

\* 0: Stands for origin time.

Fig. (3-13). Epicentral distances (km) versus S-P time-interval (sec). The slope of the line gives the value of K in the relation  $\Delta = K (t_S - t_p)$ .



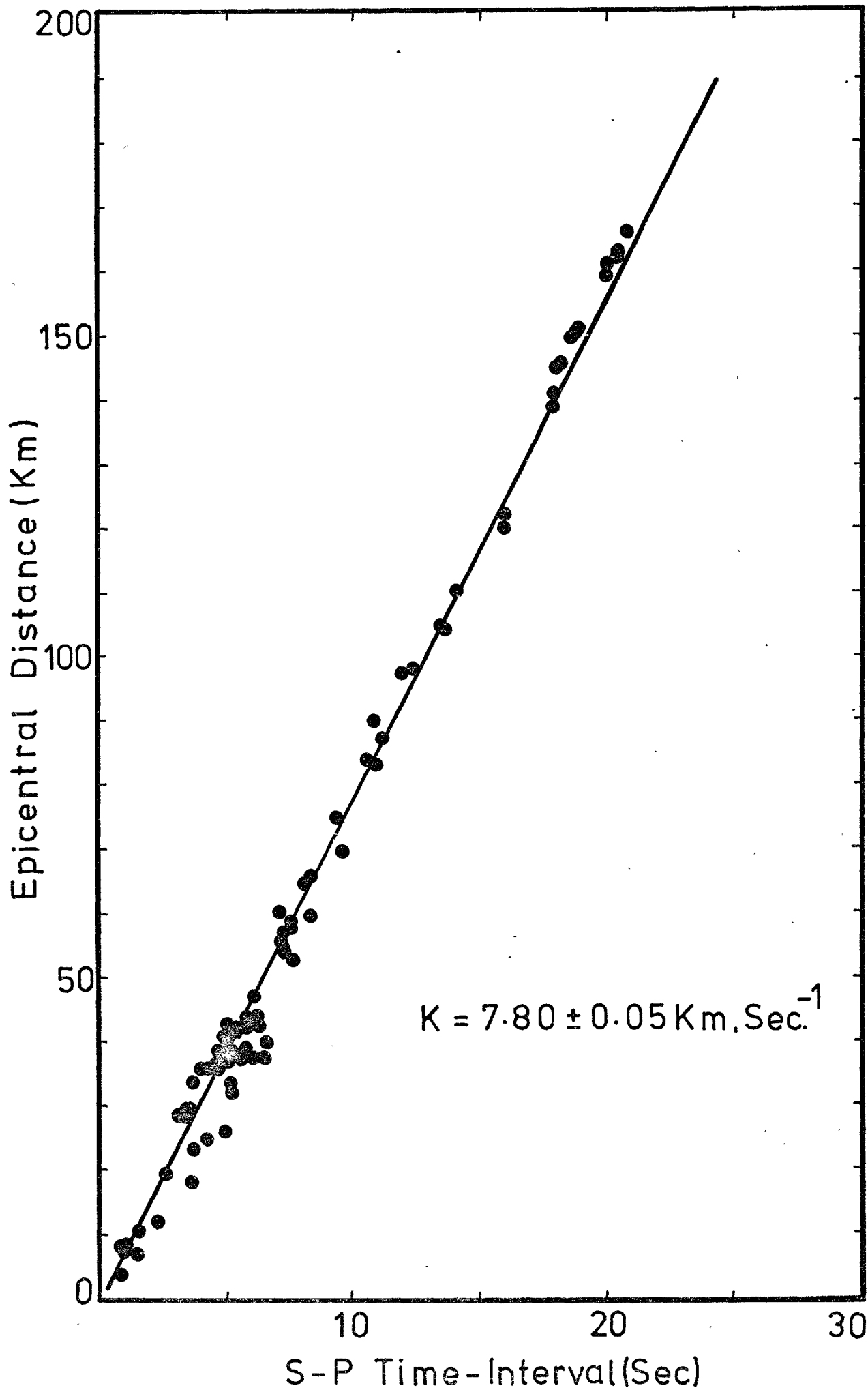
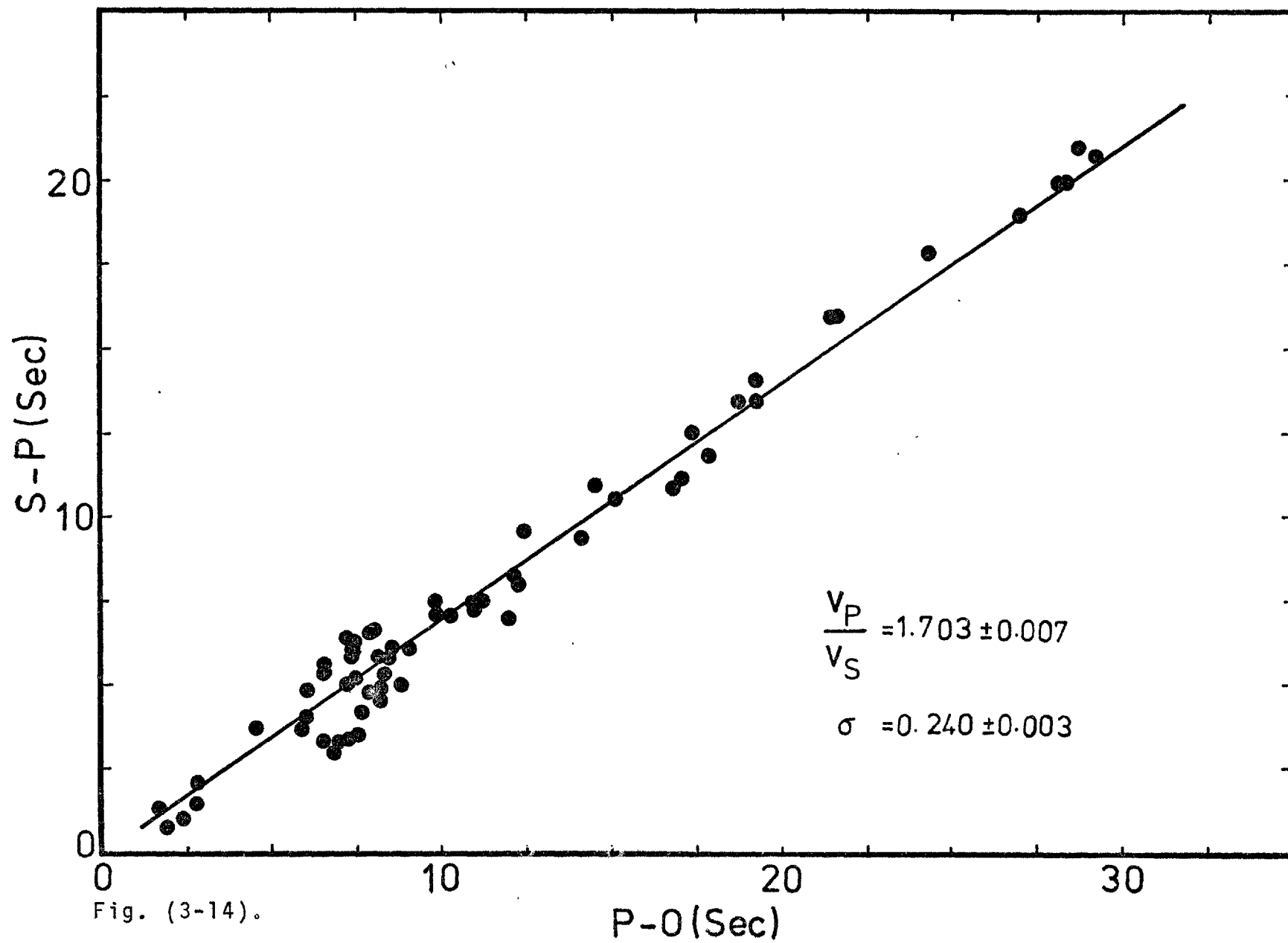


Fig. (3-13).

Fig. (3-14). S-P arrival times versus P-arrivals. The slope of the line gives the velocity ratio of P-and S-waves,  $V_P/V_S$ .



### 3.10 The Problem of Determining the Magnitudes of Local Shocks

Various relations are in common use for determining the magnitude of an earthquake, mostly derived from the original Richter (1935) relation for the magnitude of a local earthquake:

$$M_L = \text{Log}_{10} A$$

where A is the maximum amplitude in microns that a standard (Wood-Anderson) seismograph would have recorded at an epicentral distance of 100 Km. In this case the maximum amplitude might be associated with either body or surface waves. Relations have since been developed based on the specific use of body waves only. Magnitudes calculated in this way are generally referred to as body wave magnitudes ( $m_b$ ).

In practice, this expression is suitable only for local earthquakes, and even so, modifications have to be made to take care of factors to do with the particular seismograph being used (not normally a Wood-Anderson), the nature of the installation, and local geology. Further difficulties arise in the case of local networks of highly sensitive vertical component seismographs, such as were used in the Tehran area, due to lateral variation in attenuation caused by differences in elastic properties of the crust (Eaton et al., 1970).

In the present case an additional difficulty arose from the fact that the stylus deflection of the Sprengnether seismograph had to be limited to  $\pm 25$  mm in order to avoid excessive interference between adjacent traces on the drum, and thus for many of the larger events it was not possible to estimate the maximum trace amplitude.

In view of the uncertain nature of using the amplitude data for determining the magnitude (particularly when there are different instruments with different responses, as in the present study) and to overcome the above mentioned difficulties, the magnitudes of the microearthquakes recorded in the Tehran region were calculated using the method developed by Tsumura (1967). This depends on the relationship that exists between magnitude and signal duration (coda length), and first requires the measurement of coda lengths for a number of earthquakes whose magnitude have been determined by conventional methods.

The method has been used successfully by many seismologists (e.g. Unger, 1969; Lee et al., 1972; Crosson, 1972; Singh and Sanford, 1972; Mohajer-ashjai, 1975; Hedayati et al., 1976). It has the advantage of being simple and easy to apply to visual records. Furthermore, the problem of saturation is completely eliminated.

Tsumura's method evolved from a study of the microearthquakes recorded at the Wakayama network in Japan. From the relationship between coda length and magnitude of microearthquakes, Tsumura concluded that to within  $\pm 0.3$  units around the mean value, for epicentral distances of less than 200 Km and depths of less than 60 Km the two are linked by a simple logarithmic expression:

$$m = A + B \text{Log}_{10} (F-P)$$

where  $m$  is the local magnitude,  $(F-P)$  is the signal duration of the event in seconds (the coda length), and  $A$  and  $B$  are constants.

Tsumra (1967) also showed that the validity of this expression can be extended to 1000Km by including a small range term. The relation then becomes:

$$m = A + B \text{Log}_{10} (F-P) + C (\Delta)$$

in which C is a constant and  $\Delta$  the epicentral distance. The value of C is of order of 0.001 for  $\Delta$  measured in Km.

Although all possible care should of course be taken in reading (F-P), the logarithmic dependence does mean that the effect of reading error will be lessened in the magnitude determination.

One disadvantage of the method is that the constant A depends upon the instrument being used and upon the local geology, so that a calibration has to be made for each separate microearthquake survey. Thus, applying the method to the Puget Sound region of Washington, Crosson (1972) obtained the relation:

$$m = -2.46 + 2.82 \text{Log}_{10} (F-P).$$

However, for Central California, Lee et al. (1972) found that:

$$m = -0.87 + 2.0 \text{Log}_{10} (F-P) + 0.0035\Delta.$$

Other recently published results include:

$$m = -1.9 + 2.0 \text{Log}_{10} (F-P)$$

for the Elsinore Fault zone in Southern California (Langenkamp and Combs 1974),

$$m = -2.53 + 2.85 \text{Log}_{10} (F-P) + 0.0014\Delta$$

for the Wakayama region of Japan (Tsumura, 1967), and

$$m = -3.53 + 3.32 \text{ Log}_{10} (F-P)$$

for the earthquakes of the Eastern Central Iran (Mohajer-Ashjai, 1975).

A magnitude one earthquake at a distance of 10Km would produce coda lengths of 16.86, 7.94, 28.18, 16.77, and 23.14 seconds respectively in the above cases. As stated before, variables such as local geology, source and amplitude of background noise, frequency response of the system, and methods of reading records, are the main causes of this wide variation. Therefore, a calibration has to be made for each separate survey.

Table (3-3) summarises the values of A and B determined from the above studies in the various regions.

### 3.11 Determination of the Constants A and B for North-Central Iran

An attempt has been made to determine the constants A and B in the expression connecting magnitude and coda length

$$m = A + B \text{ Log}_{10} (F-P).$$

for the North-Central Iran (Tehran region). To do this, the signal duration of the local earthquakes recorded in the region has to be measured. Assigning coda lengths is somewhat subjective, and may exhibit large variations depending on the noise level, the criteria for assignment, and the personal judgement of the seismogram reader.

The assignment of the coda length reading in this study is based on the time interval from the initial P-arrival until,

TABLE 3-3

Summary of the Values of A and B in the Magnitude Coda Length Relation,  
 $m = A + B \text{ Log } (F - P)$ , for various parts of the world.

Investigator	Year	Region Studied	A	B
Bisztricsany	1958	Eastern Europe	-2.92	2.25
Solovev	1965	Sakhalin, USSR	-	2.25
Tsumura	1967	Hunshu, Japan	-2.36	2.85
Crosson	1972	Puget Sound Washington	-2.46	2.82
Lee et al.	1972	Central California	-0.87	2.00
Real and Teng	1974	Southern California	-1.01	1.84
Langenkamp and Combs	1974	Elsimore fault zone, Southern California	-1.90	2.00
Mohajer-Ashjai	1975	Eastern Iran	-3.53	3.32
Hedayati	1975	North Central Iran (Tehran Region)	-1.70	2.91



in the best judgement of the interpreter (the author), the signal returns to the noise level present before the arrival of the P-waves.

Owing to the sensitivity of the value of A to the instruments used, and regional geology, it is necessary, for calibration, to have a number of earthquakes during the survey whose magnitude could be determined by a more conventional approach. As no such events occurred during the 1974 expedition, an indirect approach had to be adopted, using earthquakes recorded in the Tehran area on smoked drum seismographs of the Geophysical Institute of Tehran University similar to the one used in the present study. The data used are sixteen shocks whose magnitudes had been determined in the conventional way by the U.S. Coast and Geodetic Survey. Table (3-4) gives the pertinent facts about these events, such as date, time, magnitude, and coda-length.

Results of plotting magnitude against the logarithm of signal duration are shown in Figure (3-15). A least squares fit to these points gives the following expression for the body wave magnitude ( $m_b$ ):

$$m_b = 0.565 + 2.131 \text{ Log}_{10} (F-P)$$

From the relationship between the signal duration and magnitude of earthquakes obtained above, it can be concluded that even if the discrepancies in picking the coda-length is of the order of  $\pm 5$  seconds, the magnitude may be determined with an accuracy of better than  $\pm 0.2$  units of magnitude.

TABLE 3-4

Summary of the USCGS Data used for Determination  
of A and B in the Relation  $m = A + B \text{ Log } (F - P)$   
for the Tehran Region.

Date	Time	USCGS Magnitude		Coda Length (Seconds)
		m(b)	m(L)	
17 12 61	14 33 19	5.0	4.4	110
13 10 62	10 23 42	5.5	5.1	255
28 05 63	10 32 47.3	4.3	3.4	60
21 12 63	04 50 39	4.5	3.7	95
03 11 64	17 36 09.5	5.3	4.8	135
03 10 66	17 05 10.4	4.9	4.2	86
23 06 67	13 15 10	4.4	3.5	67
10 12 67	10 52 52.1	5.0	4.4	90
26 04 68	02 58 22.1	5.3	4.8	180
12 05 68	16 49 50.4	4.7	3.9	75
29 07 68	16 03 42	4.8	4.1	65
01 11 70	15 45 07.3	3.0	1.66	16
08 08 72	00 44 55.2	4.7	3.9	67
17 09 73	04 06 03.7	4.8	4.1	125
27 10 73	14 22 45.8	4.3	3.4	78
30 10 73	15 59 30.0	3.7	2.6	36

Fig. (3-15). Magnitude of earthquakes occurring in the Tehran region, as determined by the USCGS, versus the logarithms of their coda-lengths. Dashed and dot-dashed lines show Tsumura's and Crosson's curves, for comparison.

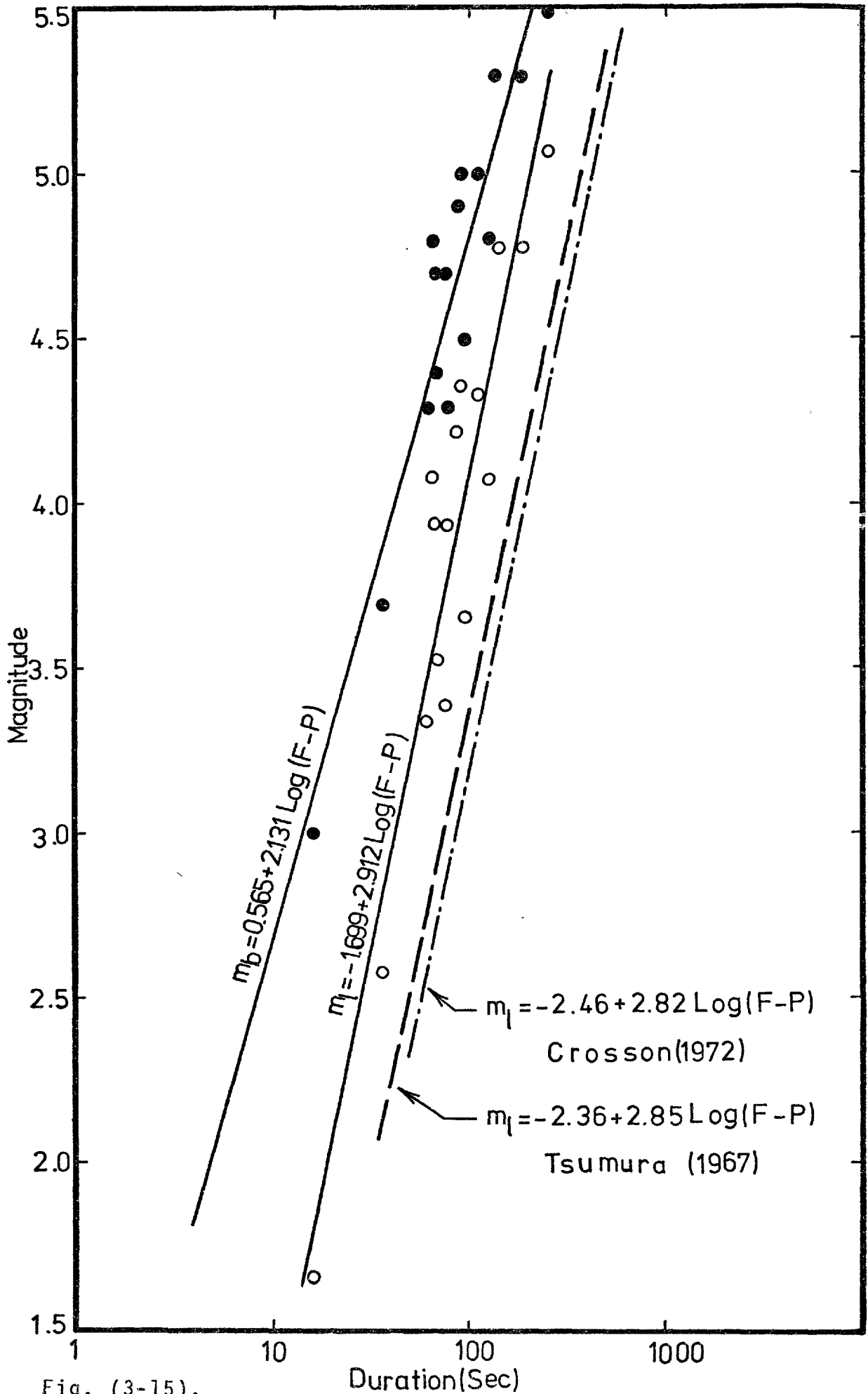


Fig. (3-15).

Duration(Sec)

To evaluate the relation between the local magnitude and the signal duration, the USCGS magnitudes were converted to local magnitudes ( $m_L$ ) using the Gutenberg and Richter (1954) expression:

$$m_b = 1.7 + 0.8 m_L - 0.01 m_L^2$$

and the results plotted in Figure (3-15). By fitting a straight line to these points by a regression method, the following expression for  $m_L$  in terms of coda length was obtained:

$$m_L = -1.70 + 2.91 \text{ Log}_{10} (F-P)$$

Even though the determination of A and B is based on a limited number of observations, the results agree well with those obtained for other regions, especially by Tsumura (1967) and Crosson (1972), and differ greatly only from Mohajer-Ashjai (1975), who is the only other author to have published results from Iran.

In Figure (3-15) Tsumura's and Crosson's curves for  $m_L$  are shown by dashed and dot-dashed lines respectively, for comparison. The displacement of the three curves would be expected, because of the differences in the instruments used and different criteria in picking (F-P) intervals.

In order to determine the magnitude of the events recorded during the 1974 survey, as many station as possible were used for each event, usually three. The difference between the three magnitude determinations were always found to be insignificant.

Even without the exact value of A, it is possible to determine the slope of the recurrence curve for the events

recorded, as this is not influenced by additive errors in the magnitude determination.

### 3.12 Determination of the b-value

Using the above determined constants, A and B,  $m_L$  and  $m_b$  have been calculated for the 198 best recorded earthquakes from the 1974 survey. These values have been used to plot the so-called "recurrence" curves (Figure 3-16). As no sufficiently large earthquake occurred during the course of the survey for its magnitude to be determined independently, the constant A could not be determined directly, and therefore the abscissa scales are probably in error by a constant amount, but this will not affect the slope of the linear part of each curve. The plots in Figure (3-16) show the cumulative number of events above a specific magnitude versus the magnitude. The following expressions, which were both obtained by least squares fitting the linear portion of the recurrence curves, show the relation between the cumulative number of events and  $m_L$  and  $m_b$ :

$$\text{Log } N = 3.039 - 0.635 m_L$$

$$\text{Log } N = 4.374 - 0.787 m_b^*$$

The deviation of the points from the straight lines in Figure (3-16), suggests that magnitude 1.5 - 2.0 is the approximate detection threshold for the earthquakes of this study. Moreover, the relatively good fit of the data points

---

\* Since the calculation was performed, more data have become available, by courtesy of Dames and Moore Inc., consisting of instrumental records from the year 1926 to the present time, which lead to a b-value of 0.852, almost identical with those values found from both the USCGS records and the microearthquakes.

Fig. (3-16). Cumulative number of recorded microearthquakes versus magnitude (the recurrence curve) for the Tehran region. Solid and hollow circles signify the local and body wave magnitudes respectively, which are determined from their total (F-P) signal durations. Solid lines are least-squares fits to the linear parts of the curves.

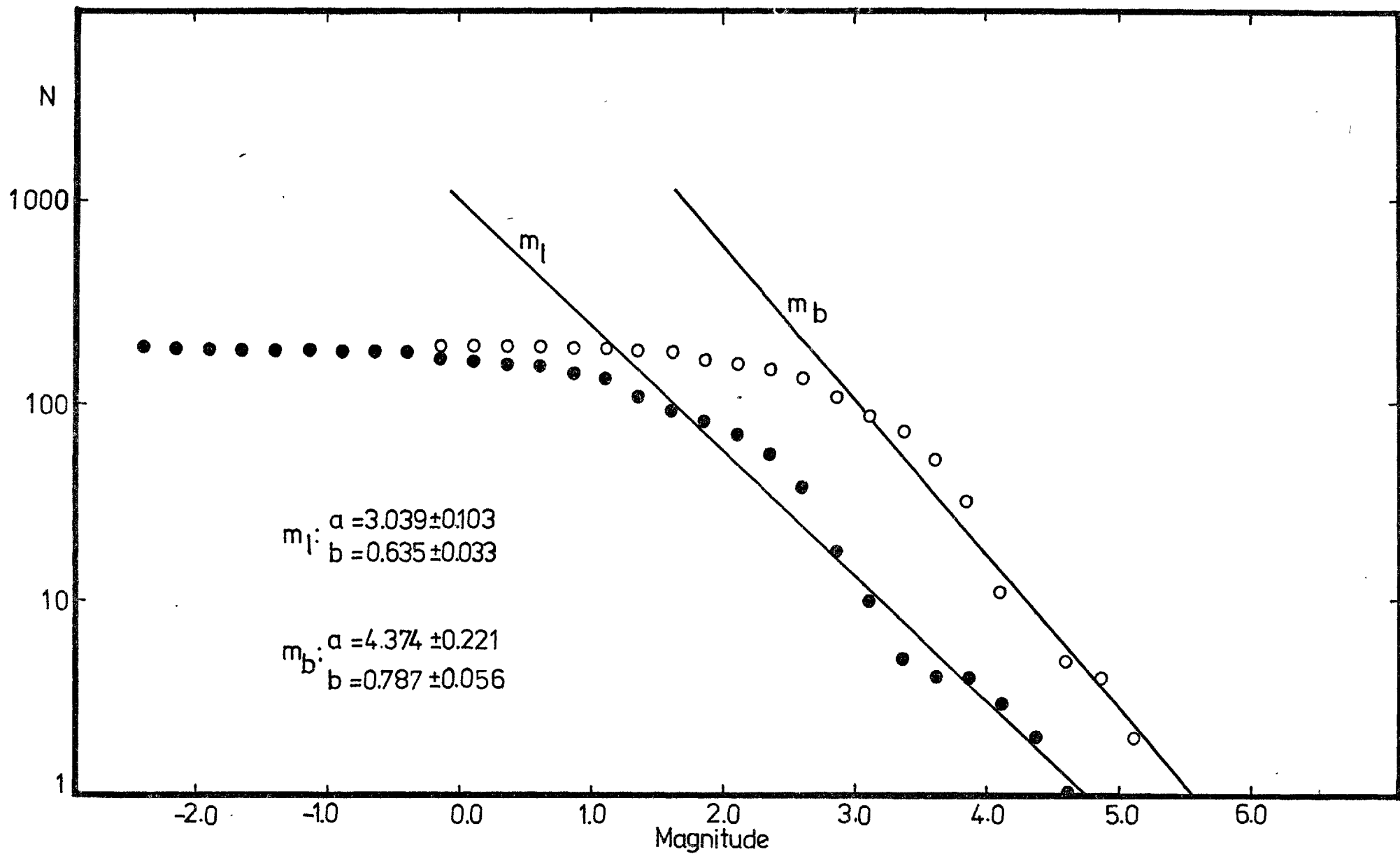


Fig. (3-16).



to straight lines for magnitudes above threshold gives additional support to the validity of the method for estimating the magnitudes of local events using signal duration.

As a check on the validity of the above results, the recurrence curve has been drawn also for the thirty events published by the USCGS for the Tehran region between 1961 and 1973 (table 3-5). The relation between the cumulative number of the events and body magnitude is found to be:

$$\text{Log } N = 5.135 - 0.856 m_b$$

Figure (3-17) shows the least square regression fit to the linear section of the USCGS data. Thus, the two determinations of body wave magnitude recurrence slope (b-value) agree well, at least within the calculated limits of uncertainty. Such values show good agreement with those given by Kaila et al., (1974) in their seismotectonic zoning maps of south-west Asia. Figure (3-18) shows the b-value contours of the Tehran region (after Kaila et al., 1974). Thus, the b-value obtained from the approximately one month of observation involved in the present study is almost identical to the value obtained from the approximately thirteen years of USCGS data. It should be noted that some investigators (e.g. Singh and Sanford, 1972, Udias and Rice, 1975) consider that reliable results cannot be obtained from such a short period of time. However, if these results are accepted as giving a true picture of the activity of region, it can be concluded that the area, as Kaila et al. (1974) suggested, should be distinguished as an active part of the Persian Plateau, in which the strain is normally

TABLE 3-5

Summary of the USCGS Data used for Determination  
of b-value, in the Relation  $\log N = a - bm$ , for  
the Tehran Region.

Date	Origin Time	Latitude (N) (Degree)	Longitude (E) (Degree)	Depth (Km)	Mag.
17 12 61	14 33 19	38.31	51.0	47	5.0
01 09 62	20 27 37	35.6	49.9	31	4½
02 09 62	07 12 03	35.6	49.4	31	4½
04 09 62	13 30 13	35.6	49.4	N*	5½
11 15 09	11 15 09	36.0	49.9	33	4½
12 09 62	02 15 45	35.7	49.0	--	4½
29 09 62	19 23 22	36.0	53.3	--	4½
13 10 62	10 23 42	36.0	50.0	--	5.5
02 12 62	22 21 31	35.6	50.0	--	5.0
28 05 63	10 32 47.3	35.4	49.8	33	4.3
21 12 63	04 50 39	33.8	51.5	51	4.5
03 11 64	17 36 09.5	36.0	50.6	33	5.3
03 10 66	17 05 10.4	35.7	53.2	35	4.9
23 06 67	13 15 10	35.7	49.5	52	4.4
25 08 67	12 26 48.7	35.4	49.1	43	4.8

..... contd ..

TABLE 3-5 (Contd.)

Summary of the USCGS Data used for Determination of b-value, in the Relation  $\log N = a - bm$ , for the Tehran Region.

Date	Origin Time	Latitude (N) (Degree)	Longitude (E) (Degree)	Depth (Km)	Mag.
10 12 67	10 52 52.1	36.0	53.6	51	5.0
26 04 68	02 58 22.1	35.1	50.2	21	5.3
12 05 68	16 49 50.4	36.3	53.4	33	4.7
29 07 68	16 03 42	36.5	53.7	14	4.8
02 08 68	03 59 23	36.6	49.1	10	4.4
10 12 69	11 00 00.2	35.2	49.2	--	3.8
27 06 70	07 57 53.3	35.2	50.7	14	4.9
03 10 70	06 57 02.0	36.1	51.4	68	4.1
31 03 71	21 50 10.3	34.6	50.3	31	4.4
30 04 71	09 06 16.5	34.6	50.3	42	4.7
09 09 71	02 54 36.7	36.2	52.7	27	5.2
08 09 72	00 44 55.2	36.3	52.6	47	4.7
13 07 73	10 05 24.7	38.5	49.5	N*	4.4
17 09 73	04 06 03.7	36.5	51.1	47	4.8
10 05 74	13 47 02.7	33.5	53.5	65	4.4

\* N: Stands for Normal Depth (within crust, but insufficient data available for precise determination).

Fig. (3-17). Recurrence curve derived from the data given by the USCGS for earthquakes occurring between 1961 and 1973. Note the similarity between the slope of this curve (the b-value) and that of Figure (3-16).

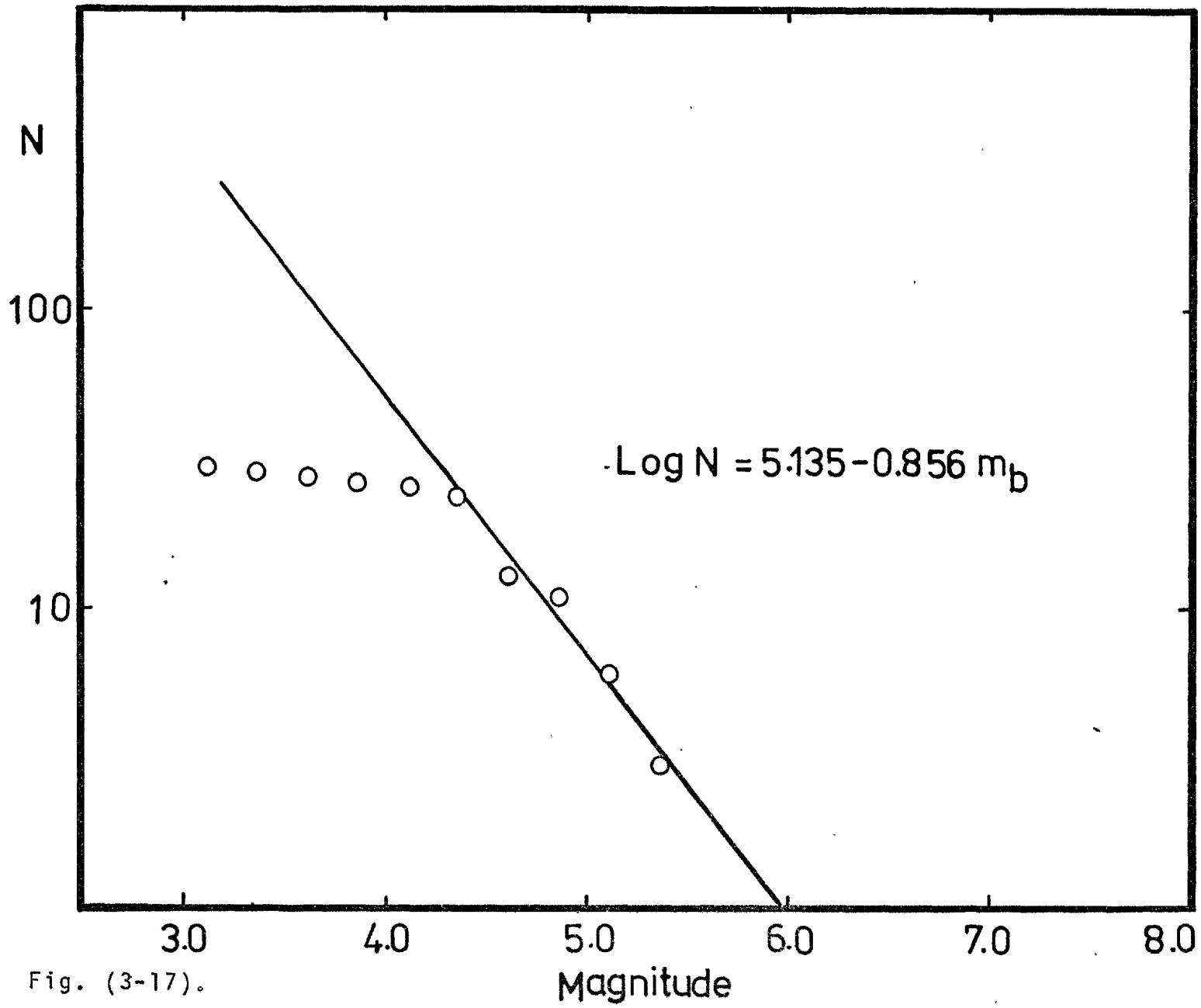


Fig. (3-17).

released by frequent moderate sized events.

### 3.13 Normalized Seismicity

Assuming Figure (3-16) to represent the seismicity of the Tehran region, it is of interest to compare this with other seismic areas. For this, the seismicity has to be normalized with respect to time and area. Following Allen et al. (1965), the cumulative number of events is normalized to a unit area of  $1000\text{Km}^2$  and a time unit of one year. The area covered by the Tehran array is taken as approximately  $400\text{Km}$  by  $180\text{Km}$  or  $72,000$  square kilometers and the observation period was approximately one month, or  $1/12$  year. Thus to obtain the normalized cumulative number of events,  $(N_n)$ ,  $N$  has to be divided by 72 and multiplied by 12, i.e.,

$$N_n = N/6$$

whence

$$\text{Log}_{10} N_n = 2.261 - 0.635 m_L$$

Similarly, for the body magnitude,

$$\text{Log}_{10} N_n = 3.596 - 0.787 m_b$$

Thus the recurrence rate at magnitude 4.0 is found to be  $0.53$  events per year per  $1000$  square kilometers for the Tehran region. Evernden (1970) gives a normalized value for California of  $0.15$  at the Mendocino Escarpment,  $0.20$  on the North San-Andreas Fault,  $0.2$  in southern California and  $0.8$  in the Imperial valley, while for Eastern-Central Iran,

Mohajer-Ashjai (1975) gives a value of 0.33. Consequently, the Tehran region can be characterized as being seismically active on a broad regional basis, a result borne out by historical activity studied by Ambraseys (1966, 1968, 1974) and Nabavi (1972).

### 3.14 Aftershock Sequences and b-values

The inclusion of the aftershock sequences in micro-earthquakes studies has been questioned by some seismologists. Crampin (1969), using the USCGS-located aftershocks of the Dasht-e-Bayaz earthquake in East-Central Iran (magnitude 7.2, Ambraseys and Tchlenko, 1969), showed the activity of the area to be characterized by a relatively high b-value of between 1.0 and 1.2. The quantitative seismicity maps of south west Asia, based on b-value contours (see Figure 3-18), the strain release map of Niazi and Basford (1968), and seismic studies by Bayer et al. (1969) which describes the area as one of the major seismic zones of Iran (Figure 3-19), give similar values for East-Central Iran. Suyehiro (1966) obtained a b-value of 0.76. using aftershocks of Central Japanese earthquakes, which agrees well with that of the ordinary activity of the region. He obtained a similar result after the great Chilean earthquake of 1960.

However, in a study of the microearthquake activity on the Dasht-e-Bayaz Fault in the summer of 1973, five years after the main shock, Mohajer-Ashjai (1975) obtained b-values of 0.45 ( $m_L$ ) and 0.57 ( $m_b$ ). These values are quite different from those obtained by Crampin, which suggests that the state

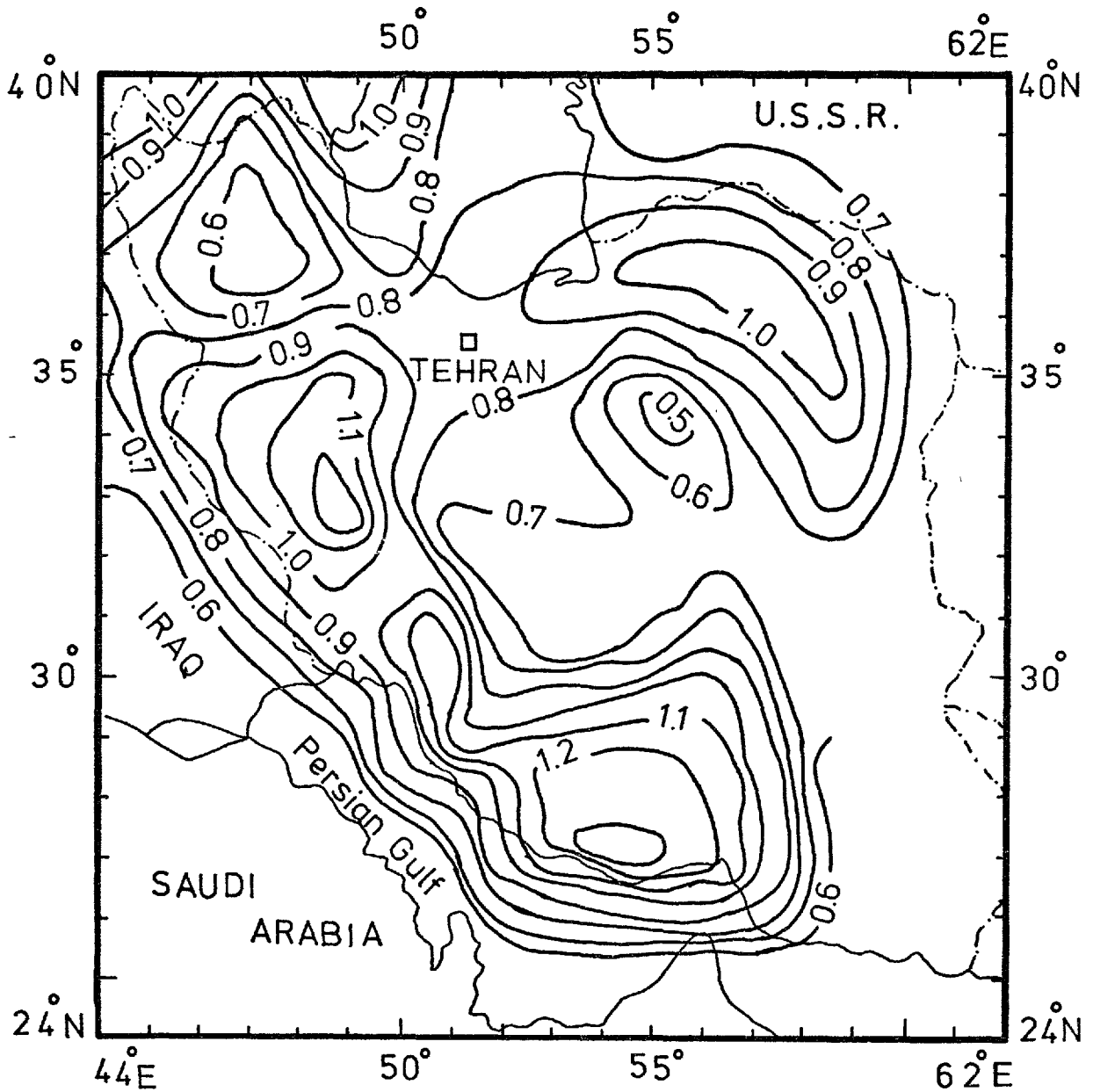


Fig. (3-18). The b-value contours of Iran (after Kaila et al. 1974). Numerals on each curve shows the appropriate b-value. Similarity between the b-values found from the Tehran region microearthquake study and that of this figure is noticeable.



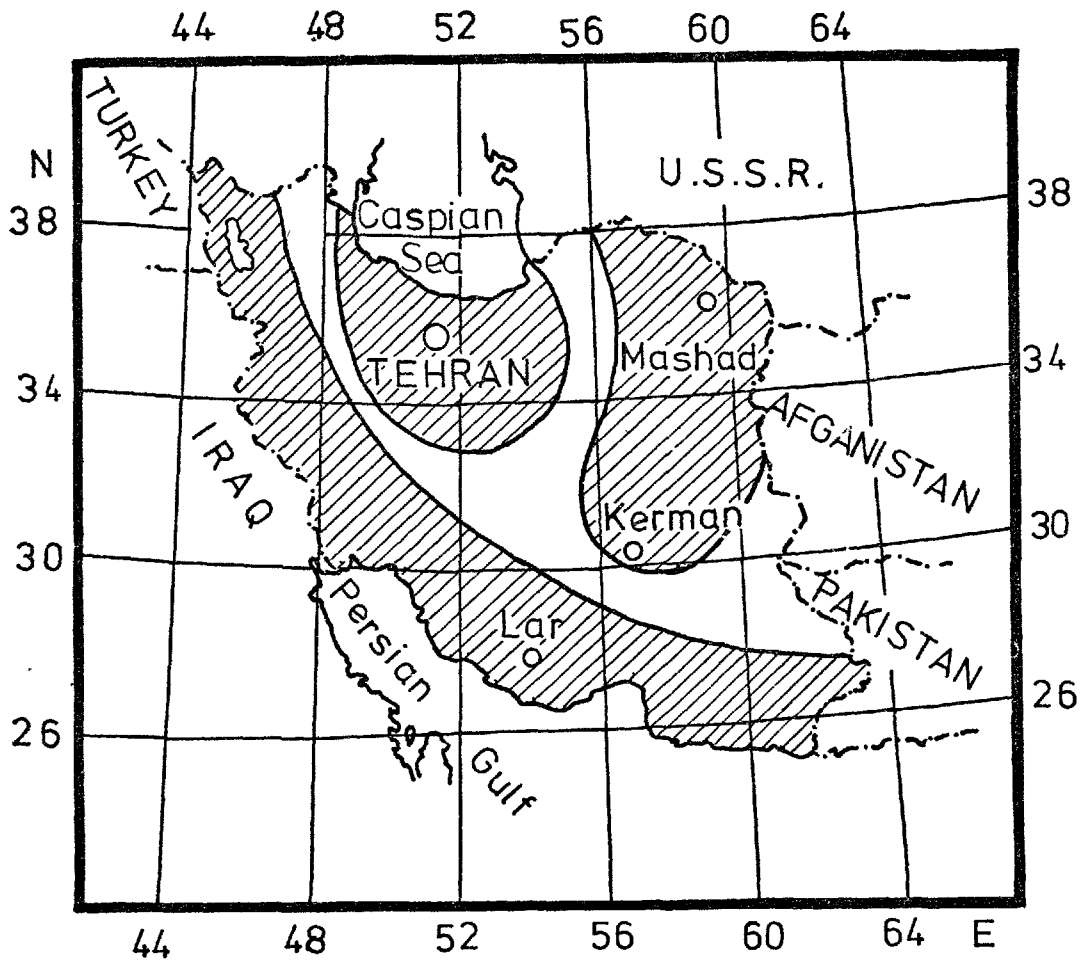


Fig. (3-19). Major seismic zones of Iran (after Bayer et al., 1969).

of the seismicity immediately after the earthquake was entirely different from what it was five years later, when the micro-earthquakes could not be considered to be aftershocks (Shelien and Toksoz, 1970) of the original event. Considering the concentration of stress at the ends of the fault break (Chinnery 1966; and Rybiki, 1973), where the seismographs were installed, the low values obtained by Mohajer-Ashjai are perhaps surprising. However, they might be the consequence of the period of abnormally high concentration of activity at the ends of the fault, immediately following the main shock, to which Crampin's b-value applies. Whatever the explanation, it appears in this particular case that the b-value obtained from the aftershock sequence does not represent the steady-state seismicity of the region.

### 3.15 Significance of the b-value

The best approach to the problem of delineating seismicity is to plot the curves of earthquake magnitude against frequency of occurrence, the so called recurrence curve. The level of activity reflected by various curves can be compared, indeed, if a sufficient number of such recurrence curves is established. Having done this, it is possible to draw the b-value contours and estimate the activity level of various part of the world, such as was done by Kaila et al., (1974).

Gutenberg and Richter (1954) determined a b-value of 0.88 for the southern California region, and about one decade later from the much larger amount of data, Allen et al. (1965) obtained a comparable value of 0.86, reflecting the stability of seismic activity of the area. Calculated b-values for

various part of the world range from 0.4 for Australia, a stable shield area, to 1.8 for the East Pacific margin, a zone of active mountain building. Thus the b-value might be accepted as a measure of tectonic activity.

Allen et al., (1965), in a study of the seismicity of Southern California, found that the recurrence curves throughout the area have closely similar slopes, which may reflect the mechanical homogeneity of the region. This conclusion might be extended to the result of the Tehran region, in which the calculated b-value from two completely different sets of data show closely comparable values.

Gutenberg and Richter (1954) pointed out that the extrapolation of recurrence curves must somehow terminate at the upper end, in as much as earthquakes larger than magnitude 9 simply do not seem to occur. Studies by many seismologists suggest that the curve may be linear up to magnitude  $7\frac{1}{2}$  or 8 in some areas. At the lower end of the curve special studies using ultra-sensitive seismometers indicate that the recurrence curves may be linear down to a magnitude well below zero (Asada, 1957 and 1958; Sanford and Holmes, 1962).

The recurrence curve for the Tehran region (Figure 3-16) shows the lower limit of the curve to be around 1.5 - 2.0, while USCGS data place the upper end around magnitude 6. It seems, from a statistical viewpoint, that the upper limit of magnitude 6 is reasonable, since the region has fortunately not been visited very often by very large sized earthquakes.

It is well accepted that determination of the b-value is one of the most reliable ways of determining the level of

activity of an area. Other methods are less reliable and may even be grossly misleading. For example,

- a. Determination of the "relative activity" of faults on the basis of geological evidence, such as Quaternary displacement, is difficult and not so accurate, partly because not necessarily all faults have surface traces. Also, proximity to relatively active faults is by no means the only factor contributing to seismic hazard because, even under similar geological conditions, it may be that shaking during a destructive earthquake is more intensive at points more distant from a fault than at points closer to it, especially for long period vibrations.
- b. Using aftershocks of major earthquakes as an indicator of seismicity, since these do not reflect the true activity of an area because they are temporary and die away according to the inverse law  $n(t) = A.t^{-p^*}$ , leaving the area under steady-state seismicity.

### 3.16 b-value Deduced from Laboratory Experiments

It is widely accepted that earthquakes are the result of fractures in the earth's crust and that, therefore, the characteristics of the brittle rocks of the crust have a close bearing on the occurrence of earthquakes.

Irregularities such as fractures, faults, and changes

---

\* In this relation  $n(t)$  is the frequency of aftershock at time  $t$  after the main event and  $A$  and  $p$  are constants (Utsu, 1961).

of physical properties of rocks in the earth's crust are evident. Therefore it is reasonable to consider the crust as a heterogeneous medium. Laboratory experiments on natural rock specimens by Mogi (1962a) showed a conclusive relation between the magnitude distribution of microfractures in the laboratory specimens and the magnitude distribution of tectonic earthquakes. He concluded that the number of events (fractures) satisfies the Ishimoto-Iida empirical formula:

$$n(a) da = K a^{-p} da$$

where  $n(a)$ , the amplitude frequency, is the rate at which events of amplitude  $a$  to  $a+da$  occur,  $a$  is the maximum trace amplitude, and  $K$  and  $p$  are constants.  $p$ , the slope of the line fitting a plot of the above relation, ranges between 1.5 and 2.5. Suzuki, (1959), showed that the constant  $p$  in the Ishimoto-Iida relationship is related to the  $b$ -value of the Gutenberg-Richter instrumental magnitude by:

$$p = b + 1.$$

Similarly, Scholz (1968a and b) studied the cracking of rocks during uniaxial deformation tests by analysing the propagation of elastic waves similar to those of natural earthquakes. He showed that as stress increases, the cracking accelerates steadily until, shortly before failure, a rapid increase occurs, leading to the formation of a fault. Moreover, he showed that seismic waves detected from a compressional test, satisfy the recurrence curve of Gutenberg and Richter:

$$\text{Log}_{10} N = a - bm.$$

These investigations leave no doubt about the similarity of the formation of fractures in rocks during compressional tests and during natural earthquakes. In these experiments, different b-values have been found under different conditions, and as a result it is shown that the slope of the recurrence curves depend fundamentally on the stress applied. The fact that there is, thus, agreement between the distribution of earthquake occurrence and that of the occurrence of brittle fracture in rock samples suggests that the heterogeneity of the earth's crust might be less important in controlling the occurrence of earthquakes than uniformity of applied stress. Similarly, the extensively documented variations of the b-value for earthquake occurrence, seemingly a characteristic of the seismicity within a region, might reflect variations in the state of stress of different regions.

However, the low b-value in Eastern-Central Iran should be indicative of either very coherent material forming the region or an extremely low rate of increase of stress, neither of which reflect the activity of the region discussed earlier.

## CHAPTER IV

## SEISMIC RISK IN THE TEHRAN REGION

4.1 Introduction

During the last few decades our understanding of the causes and effects of ground movements has developed significantly. By precise study and analysis of the results of destructive earthquakes, seismologists have learned how forces exerted by earthquakes act upon man-made structures. These forces are due to a dynamic readjustment of the internal stresses in parts of the earth's crust which have been subjected to stress and strain for many years. The effects of this readjustment show as fault breaks, landslides, and uplifts.

As a result of the experience gained by seismologists and engineers since the beginning of this century, a corpus of knowledge has been created whereby structural designs can be modified to take account of the seismic hazard of an area, and thus increase the ability of structures to resist these natural destructive forces.

A well known seismic belt, the Alpide, crosses the Persian Plateau. As a result, many earthquakes occur every year, causing considerable damage to property and life. The destruction resulting from them requires the taking of precautionary measures such as estimation of the seismic risk at the site of an engineering project. This estimation depends on a specific formulation of the problem i.e. what kind of a project and what site it is intended to protect. Of course, the formulation of this problem for various types

of construction is out of the scope of this thesis, though it is important to appreciate the factors involved. The final goal of this and similar preceding work (e.g. Cornell, 1968; Howell, 1973; Cornell, 1973; Caputo et al., 1974) is to illustrate the possible methods of estimating the risk and to outline the data requirements and the method of processing it.

As a start, it is usual to divide an area into zones according to their seismic activity. This way of approaching seismic zoning is over-simplified; it presents boundaries which have no physical meaning, and it does not reflect the statistical nature of the risk. In most cases, attention has been directed towards predicting the occurrence of earthquakes of a certain magnitude in a specified zone. This alone, however, cannot define seismic risk; the destructive effect of an earthquake of given magnitude depends also on local geological factors.

The purpose of this chapter is to describe a quantitative approach to the study of earthquake risk, based on a statistical analysis of seismic data, and to apply the method to the data obtained in the Tehran area.

In recent years a number of quantitative approaches have been developed to earthquake regionalization. To assess the relative activity in various parts of a region, St. Amand (1956) proposed two measures of seismic activity based upon physical quantities, "specific seismicity" and "tectonic flux". The former depends on the sum of the energy released by all earthquakes occurring per unit of area and time, while the



latter specifies the amount of strain release per unit of time and area by all the events. This approach has been questioned by Richter (1959) who, in a study of the regional seismicity of the U.S.A., concluded that separation into regions on the basis of surface geology alone is impossible, and that even when surface geology is supplemented by geophysical data it does not provide a unique guide without the use of earthquake statistics, including both historical and contemporary instrumental observations.

To improve the estimation of the time interval to be expected between events producing a given ground acceleration (the so called return period) Milne and Davenport (1969) studied the distribution of earthquake risk in Canada, using peak acceleration as the basic parameter. In a discussion of regional seismic hazard in the United States, Howell (1973) suggested four points for evaluating hazards from earthquakes. Thus, an ideal measure of seismic risk should:

- a. Provide a realistic assessment of the degree of danger.
- b. Be based on the measurement of physical quantities, such as strain and energy released by earthquakes.
- c. Be easily understandable by everyone who needs to use it.
- d. Have a flexible scale, so as to be able to deal with the developing earthquake information.

The present study represent a quantitative approach based on a statistical description of the maximum intensity

that might be expected at a given point in a given time interval. Several indexes may be used as a measure of these earthquake intensities, such as amplitude, magnitude, or peak acceleration. As is well known, all these measures can be related to one another by a simple conversion.

#### 4.2 Statistical Approach to Seismic Risk

The results of regional seismicity studies can be used in three different applications:

1. To indicate the distribution of currently active tectonic structures, using epicentral locations.
2. For evaluating the level of activity or frequency of occurrence of earthquakes in a particular region.
3. For engineering purposes, giving the maximum intensity to be considered in the design of a new construction.

The third application, which is the main concern of this study, must take into account the character of the ground and its effect on expected intensity.

If the earthquakes in a particular region occur randomly in time, then their time-distribution can be described by the well-known Poisson distribution. Properties of a Poisson distribution include:

- a. The probability that  $n$  random events occur between times  $t$  and  $t+T$  depends on  $n$  and  $T$  but not on  $t$ , i.e. the conditions under which the earthquakes occur do not change with time.

- b. The probability that  $n$  random events occur between times  $t$  and  $t+T$  does not depend on the number of events that occurred before time  $t$ , i.e. the occurrence of random events in one time interval does not affect the probability of random occurrence in any other time interval.

The question of whether or not the time distribution of earthquakes follows a Poisson distribution has long been a matter of contention. Thus, Knopoff (1964) made an analysis of more than 5,000 southern California earthquakes of magnitude 3 and greater and concluded that there was some kind of inter-relation between the smaller events, and that they did not follow a Poisson distribution.

Lomnitz (1966), after dividing an active region into a number of smaller areas and assuming that each area produce earthquakes randomly in time, showed that the Poisson distribution did apply in this case. He concluded that the deviation of the time distribution from a Poisson distribution when the region was considered as a whole might be attributed to spatial inhomogeneity. In the same paper Lomnitz drew attention to the fact that the results of an investigation by Ben-Menahem showed that a Poisson distribution can be fitted to the occurrence of world-wide events of magnitude seven and over.

Shelien and Toksoz (1970) examined the possibility of a Poisson distribution for the 35,000 earthquakes recorded by the U.S. Coast and Geodetic Survey between 1961 and 1968.

Their results showed that if all earthquakes, including aftershocks, are considered, it is not possible to describe their distribution as Poissonian. The reason is that aftershock sequences are triggered by the main shock. Their occurrence time depends on the magnitude, depth, and particularly the epicentral location of the main shock, and they die out obeying an inverse law (Crampin, 1969; Utsu, 1961; and also see chapter three).

To evaluate the applicability of the Poisson distribution to microearthquake sequences, Udias and Rice (1975) used more than 4,500 small nearby events recorded between 1968 and 1971 within 25km of the San-Andreas Fault. The magnitude of the events used ranged up to about 4. The grouping effect of epicenters (Figure 4-1), which might be indicative of inter-relation between the events, is thought to be the main reason for departure of the distribution from a Poissonian. They concluded that the four years of data used might not be long enough for such statistical analysis.

Gardner and Knopoff (1974) put an end to the question of the Poisson distribution of earthquake sequences by showing that, provided that all aftershocks have been removed, the time distribution of earthquakes obeys the expression:

$$P(n,a) = \frac{a^n}{n!} \exp(-a) \quad (\text{after Udias and Rice, 1975})$$

the Poisson distribution, where

$a$  = Constant rate of occurrence of independent events

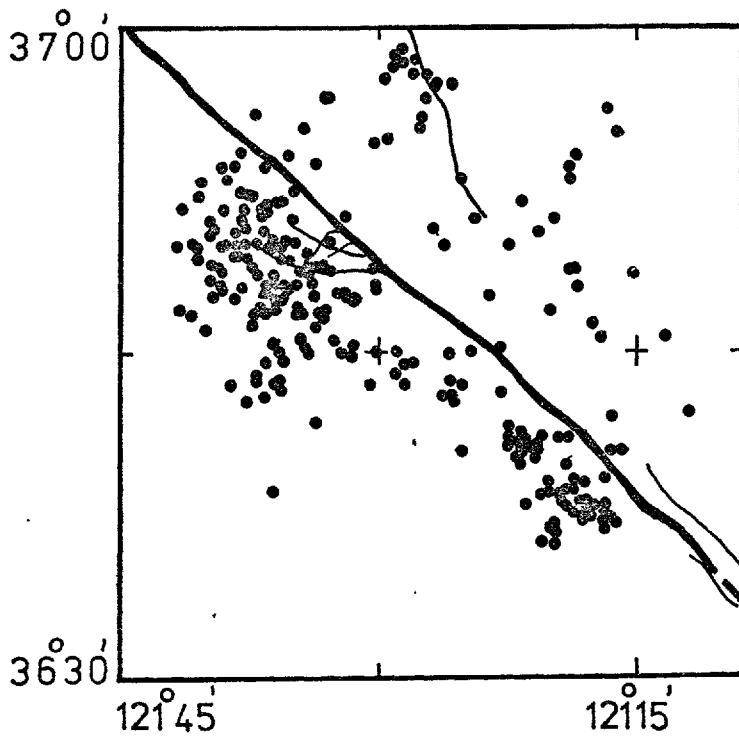


Fig. (4-1). Epicenters of microearthquakes occurring within 25 km of the San-Andreas Fault. Note the clustering of events, showing the inter-relation between the earthquakes (after Udias and Rice, 1975).

$n$  = Number of events occurring in a particular time interval.

$P$  = The probability that within the time interval  $n$  events will occur.

To this end, to distinguish between aftershocks and main events, they used the relations:

$$\text{Log } T = a_1 M + b_1$$

$$\text{Log } L = a_2 M + b_2$$

between the time and distance separating two successive events. In the above relation,  $T$  is the time between the two events,  $M$  is the magnitude of the first shock,  $a_1$ ,  $a_2$ ,  $b_1$ , and  $b_2$  are constants, and  $L$  is the distance between the epicenters. Events will be treated as independent if either or both,  $T$  and  $L$  exceed the respective values given by the above expressions. Inserting appropriate values for the constants, this technique, the so called "window", shows for example that an event which occurs beyond 40km and 155 days after a magnitude 5 earthquake in southern California is not an aftershock.

Seismological observations for the area of interest are needed to define both the mean rate of occurrence of events of significant magnitude and also the slope of the frequency versus magnitude relation, both of which are used to determine the characteristics of the Poisson distribution. Regarding the latter, it is necessary to exclude the aftershock sequences, but this seems not to be significant in the present context because, although large earthquakes are often

followed by aftershocks, for an engineering site only the damaging effect of the main shock is important.

#### 4.3 Determination of Intensity-Magnitude Relation

In discussing seismic hazard we are concerned with expected intensities, or ground movement. However, observed intensities do not form a satisfactory basis for any prediction system since intensity is a notoriously difficult quantity to estimate by direct observation. Magnitude provides a much more reliable value on which to base a system. All that is needed is to convert the magnitude to intensity as a function of hypocentral distance. To this end it is necessary to include terms allowing for the ground condition, since seismic waves like any other waves suffer from attenuation in propagation.

As a starting point in converting magnitude to intensity, Gutenberg and Richter (1956) obtained the following relation between the magnitude and intensity of Californian earthquakes:

$$M = 1 + \frac{2}{3} I_{\max}$$

where  $I_{\max}$  is the intensity at the epicenter. The usefulness of this relation was extended by Howell (1973) who, on the basis of the energy released, showed that the decay of intensity, in the United States, with respect to the epicentral distance is given by:

$$I = I_{\max} 10^{-\alpha\Delta}$$

in which  $\Delta$  is epicentral distance and  $\alpha$  is a constant of the order of  $10^{-3}$ . It seems, however, that Cornell (1968) was the first to consider the effect of focal distance in the distribution of intensity. He used the following relation:

$$I = C_1 + C_2 M - C_3 \ln R \quad (4-1)$$

in which  $C_1$ ,  $C_2$ , and  $C_3$  are the so-called attenuation coefficients,  $M$  is magnitude,  $R$  focal distance, and  $\ln$  denote the natural logarithm. To evaluate the relation between magnitude and intensity in the present case, Cornell's method has been followed, derivation of the coefficients being discussed in the following section.

#### 4.4 Evaluation of the Attenuation Coefficients

The most satisfactory procedure for calculating the coefficients is by employing a least-squares technique, since they are not, strictly speaking, constant, because of local variations in attenuation. As a result, in general:

$$I - C_1 - C_2 M + C_3 \ln R \neq 0$$

Putting the right hand side equal to  $e$ , then the best values for  $C_1$ ,  $C_2$ , and  $C_3$  are such that  $\sum e^2$  for all observation points is a minimum. To find the condition for a minimum, the partial coefficients with respect to  $C_1$ ,  $C_2$ , and  $C_3$  are set equal to zero:



$$\frac{\partial \Sigma e_i^2}{\partial C_1} = 0$$

$$\frac{\partial \Sigma e_i^2}{\partial C_2} = 0$$

$$\frac{\partial \Sigma e_i^2}{\partial C_3} = 0 \quad i = 1, \dots, n$$

which implies

$$\Sigma (I_i - C_1 - C_2 M_i + C_3 \ln R_i) = 0$$

$$\Sigma (I_i - C_1 - C_2 M_i + C_3 \ln R_i) M_i = 0$$

$$\Sigma (I_i - C_1 - C_2 M_i + C_3 \ln R_i) \ln R_i = 0$$

Hence

$$\Sigma I_i - n C_1 - C_2 \Sigma M_i + C_3 \Sigma \ln R_i = 0$$

$$\Sigma I_i M_i - C_1 \Sigma M_i - C_2 \Sigma M_i^2 + C_3 \Sigma \ln R_i M_i = 0$$

$$\Sigma I_i \ln R_i - C_1 \Sigma \ln R_i - C_2 \Sigma \ln R_i M_i + C_3 \Sigma (\ln R_i)^2 = 0$$

These, the so-called "normal equations", can be solved simultaneously for the most probable values of  $C_1$ ,  $C_2$ , and  $C_3$ :

$$C_1 = \frac{1}{n} (\Sigma I_i - C_2 \Sigma M_i + C_3 \Sigma \ln R_i)$$

$$C_2 = \frac{C_3 \times B + A}{D}$$

$$C_3 = \frac{A \times B + D \times E}{D \times G - H^2}$$

where

$$A = \sum M_i \sum I_i - n \sum I_i M_i$$

$$B = \sum M_i \sum \ln R_i - n \sum \ln R_i M_i$$

$$D = (\sum M_i)^2 - n \sum M_i^2$$

$$E = n \sum I_i \ln R_i - \sum \ln R_i \sum I_i$$

$$G = (\sum \ln R_i)^2 - n \sum (\ln R_i)^2$$

and

$$H = \sum M_i \sum \ln R_i - n \sum M_i \ln R_i.$$

To determine the attenuation coefficients, published macroearthquake observations of the recent major earthquakes, Buyin-Zahra, 1962 (Abdalian, 1962), Macou, 1968 (Nabavi, 1969), and Dasht-e-Bayaz, 1968 (Sobuti et al., 1969) from the area of interest have been used.

It is possible to solve the three simultaneous equations of (4-1) to compute  $C_1$ ,  $C_2$ , and  $C_3$ . To obtain more reliable results, the isoseismal contours, Figures (4-2) to (4-4), of the above mentioned earthquakes are considered. Employing a computer program, written by the author, based on the least-squares technique discussed in a previous section, the values

$$C_1 = 7.59$$

$$C_2 = 1.10$$

$$C_3 = 1.75$$

are obtained, which may be compared with values of 8.16, 1.45, and 2.46 found by Esteva and Rosenblueth (1964) for firm ground in southern California.

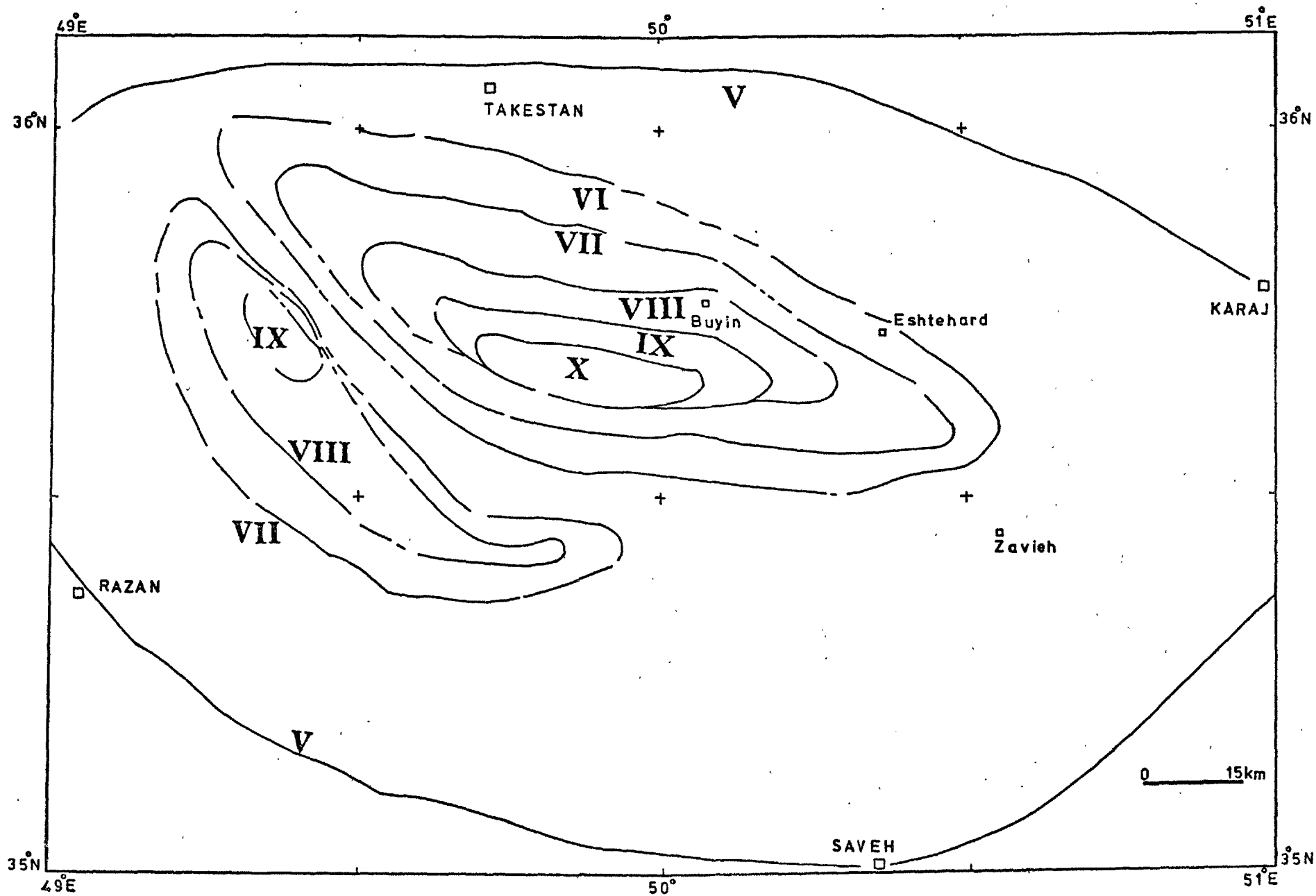


Fig. (4-2). Isoseismal contours of the Buyin-Zahra earthquake of 1962 (after Abdalian, 1962).

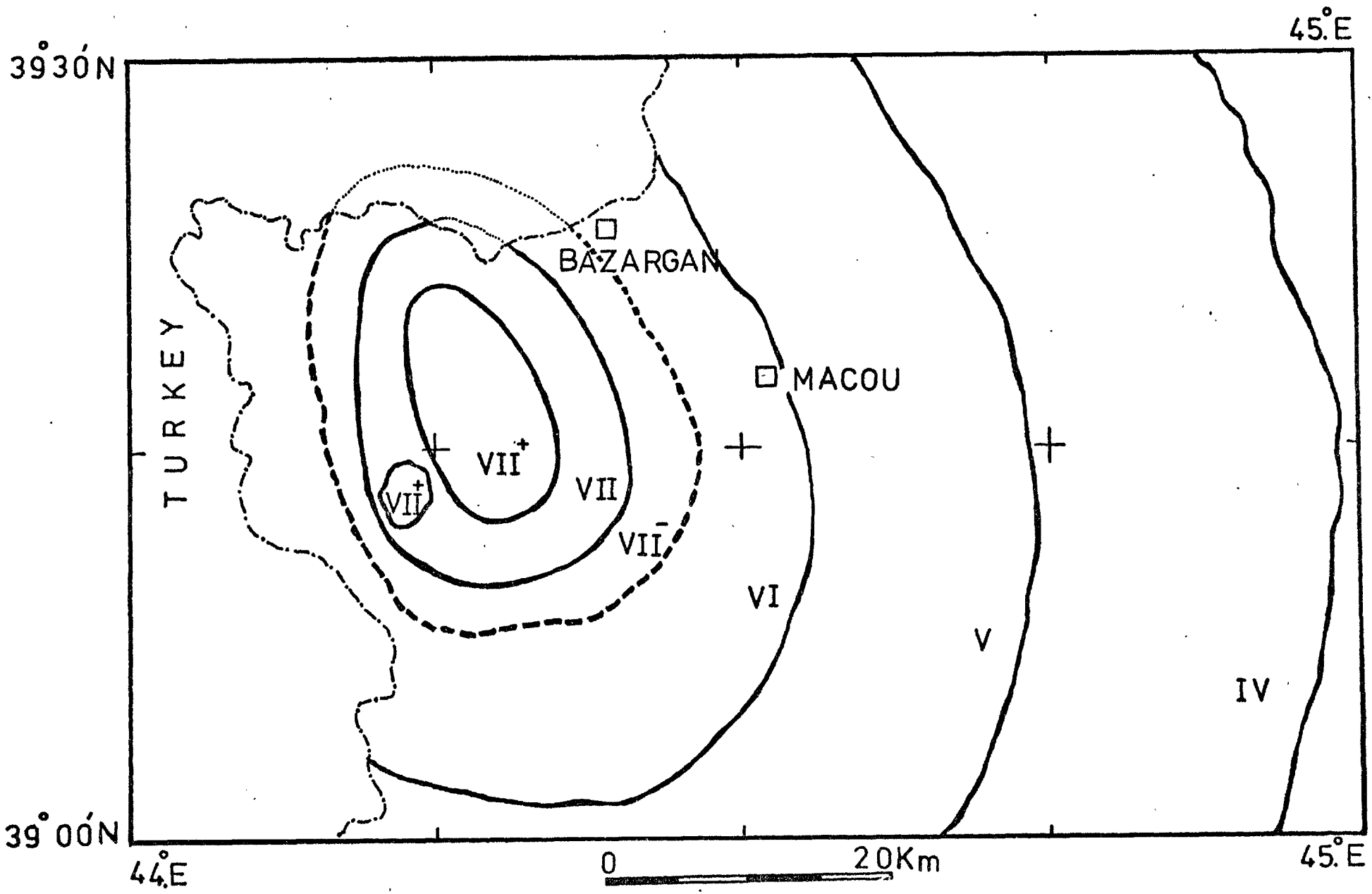


Fig. (4-3). Isoseismal contours of the Macou earthquake of 1968 (after Nabavi, 1969).

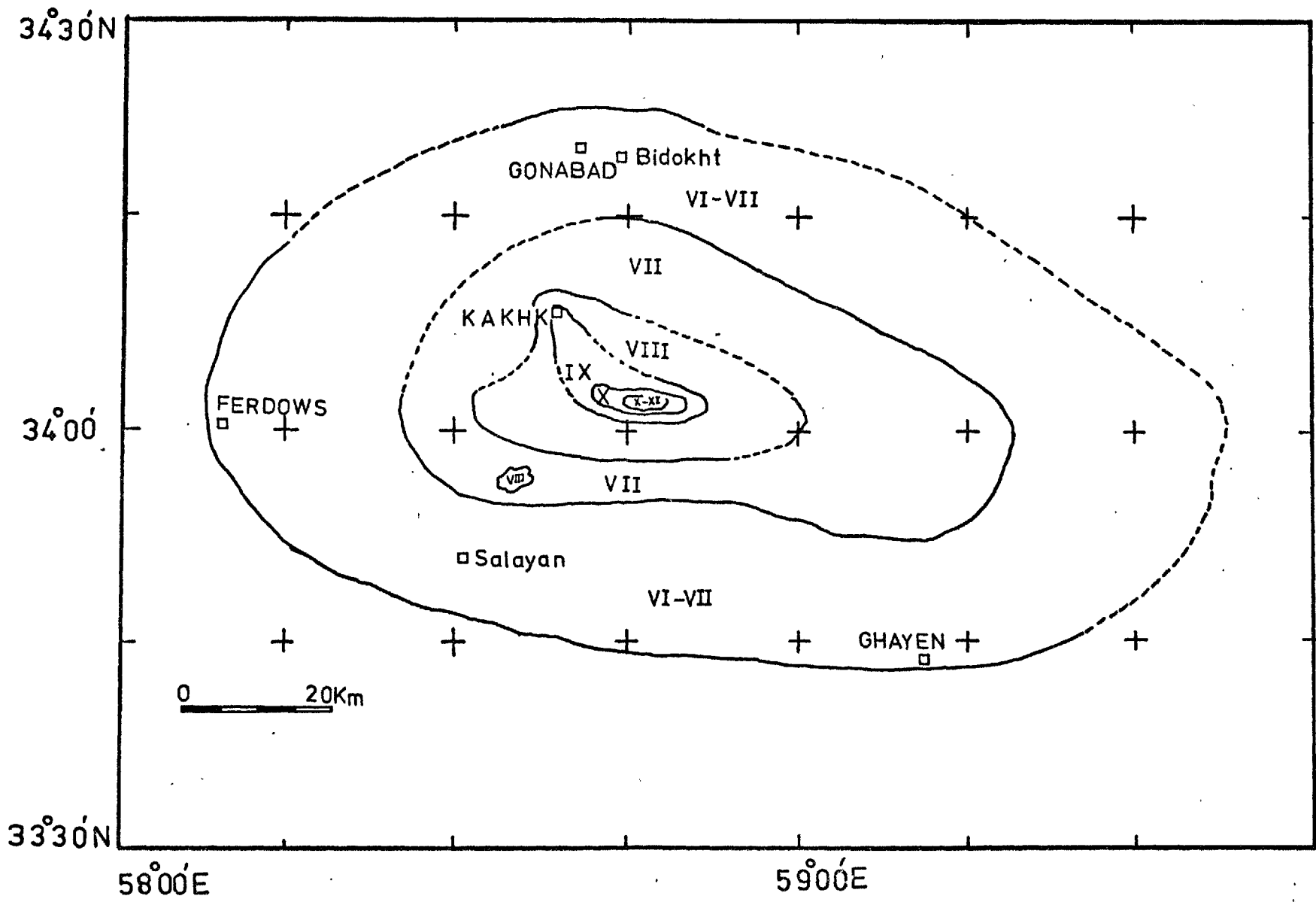


Fig. (4-4). Isoseismal contours of the Dasht-e-Bayaz earthquake of 1968 (after Sobuti et al. 1969).

#### 4.5 Determination of the Risk Curve

Seismologists are often consulted by those planning to build heavy constructions as to the safety of a given site with respect to the occurrence of earthquakes. Usually the first question refers to the location of the faults relative to the position of the construction site. As discussed earlier (see also chapter three), in a region such as Tehran the differences between two locations depends less on their distance from faults than on the character of the ground. Assuming uniform distribution of events, any given point is sooner or later certain to be affected by earthquakes, at least either by a large distant event or a small nearby one. In either case, "INTENSITY" will be higher, other things being equal, on unconsolidated ground than on firm rock. In chapter two it was shown that the city of Tehran is built on the former.

Strong shaking is especially likely when seismic waves emerge from basement rocks into an alluvial area. Such danger spots can be easily identified from the seismic history of the region and should be avoided as sites for important engineering constructions, or strong precautions should be taken before construction.

Considering the unconsolidated Alluvial Formation of the Pediment zone, Rud-e-Shur and Central Basin (see chapter two) on which the city lies, and the proximity of the North-Tehran and Musha-Fasham Faults, risk in the Tehran region is particularly high. However, even close to major faults, investigation will generally identify individual small areas

of unfractured rocks, which might be used as construction sites, with comparatively low risk.

Assuming a Poisson distribution, Cornell (1968) introduced two measures for determining seismic risk using available earthquake data and the average level of activity in the region of a future construction site. The first measure determines the effects at the site of the seismic activity along a nearby fault, while the second deals with damage caused by the earthquakes occurring within a particular region in terms of the maximum expected intensity.

One difficulty in using the first measure is that the geology of an engineering site is often inadequately known; faults do not always reach the surface, and in any case the dispersion of epicenters about the faults is generally not very well known. The second measure does not depend on these factors, but does require the necessary data for plotting a recurrence curve, i.e. information about recurrence rates as a function of magnitude (see chapter three). This gives the maximum intensity to be expected within the area of a proposed construction site. Using the second measure, an attempt has been made to determine the relationship between the ground motion, intensity, and average return period for the Tehran region.

The average return period,  $T_i$ , of an event and its intensity,  $I$ , are related by:

$$I = \frac{C_2}{a} \ln(sCGT_i) \quad (\text{after Cornell, 1968}) \quad (4-2)$$

in which

$a = b \ln 10$ , where  $b$  is the slope of the  
recurrence curve

$$C = \exp\left[a\left(\frac{C_1}{C_2} + m_0\right)\right]$$

$m_0$  = Significant magnitude\*

$$G = \frac{2\pi}{(k-1)d^{(k-1)}}\left[1 - \left(\frac{r_0}{d}\right)^{-(k-1)}\right]$$

$$k = a\frac{C_3}{C_2} - 1$$

$s$  = The average number of earthquakes of  $M \geq m_0$   
per year per unit area

$d$  and  $r_0$  = Hypocentral distances

Figure (4-5) illustrates a site surrounded by an area of epicentral location (after Cornell, 1968).

The data needed are seismological observations for the area under study, to define both the mean rate of occurrence of events of significant magnitude and the slope of the frequency versus magnitude relation; and geographical distribution of epicenters. The technique on which this study is based provides the method for investigating the individual influence of the potential earthquake sources, moderate or larger and of uncertain distances from the site, and of the

---

\*  $m_0$ , the so-called threshold magnitude is understood to be the magnitude which will cause significant damage to a structure. Significant damage in this context is taken to mean that damage for which remedial action is necessary. The threshold magnitude is commonly taken to be five.



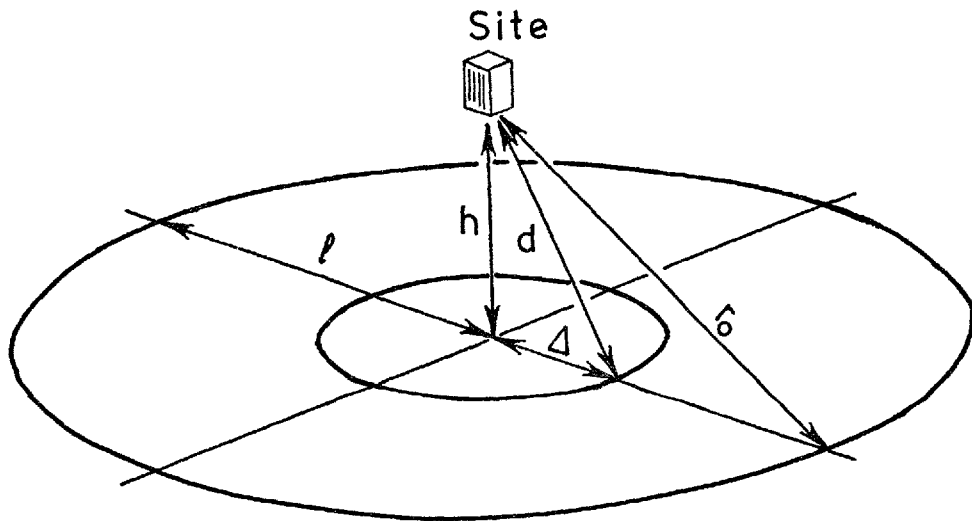


Fig. (4-5). Illustration of a site surrounded by an area of epicentral locations.  $r_0$  and  $d$  are hypocentral distances,  $\Delta$  and  $l$  epicentral distances, and  $h$  is depth of focus (after Cornell, 1968).

uncertain number of events in any time interval, and so on into a distribution function of maximum intensity.

Although the b-value obtained from the 1974 survey agrees well with that determined from the USCGS teleseismic data, the latter has been used in the present case because it is more representative, being based on data covering the period 1961-1973 (see chapter three). Using the values obtained earlier for the attenuation constants, the b-value deduced from the USCGS data, the risk curve is calculated by the following procedure.

As stated earlier, the threshold magnitude in the present case is chosen to be five. Taking the average b-value as 0.8 (see chapter three), and the constant a as 5.15, the relation:

$$\text{Log}_{10} N = a - bm$$

becomes  $\text{Log}_{10} N = 5.15 - 0.8 m$

Thus, for events of magnitude 5 (significant magnitude),  $N = 14$ . Calculating the numerical values for coefficients a, s, k, C, and G and introducing them in equation (4.2), the risk curve for the region can be expressed as:

$$I = 0.59 \ln (12724 T_i)$$

in which I is the expected Modified Mercalli intensity of the ground movement, and  $T_i$  the time interval in years. This relation, which is plotted in Figure (4-6), shows that in the Tehran region ground movement of Modified Mercalli

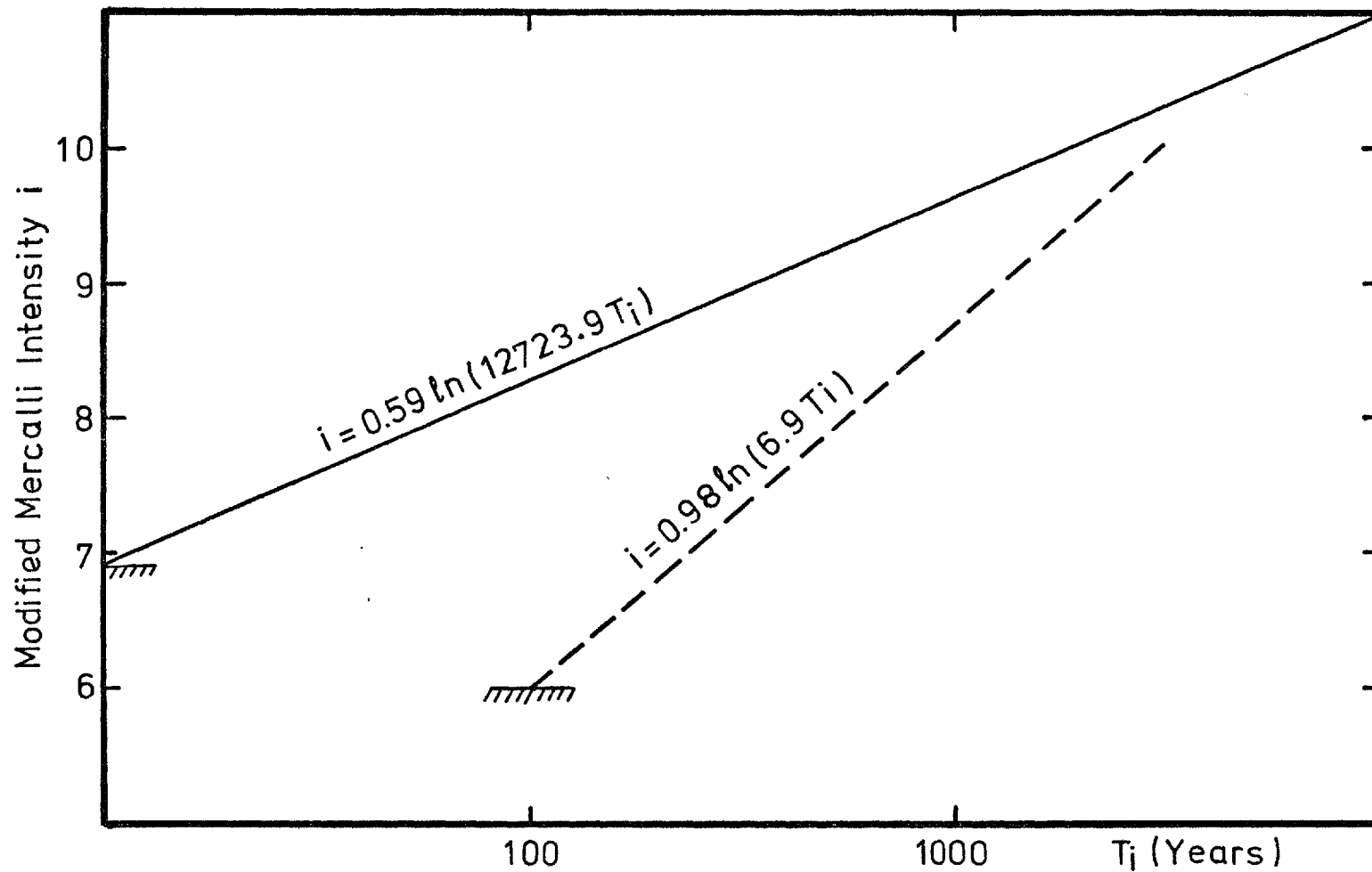


Fig. (4-6). Modified-Mercalli intensity  $I$  versus time  $T_i$  (years) showing the risk curve for the Tehran region. Dashed line represent the same curve for Turkey (after Cornell, 1968).

intensity 7, can be expected within 12 years, and M.M. intensity 9 within about 350 years.

This curve should not, of course, be taken completely literally, and certainly makes no prediction as to when and where the expected magnitude earthquake will occur, but shows only that within a given interval of time the area will very probably be visited by ground movement of the particular intensity.

The dashed curve in Figure (4-6) represents the risk curve for Turkey, assuming all the earthquakes of threshold magnitude ( $m=5$ ) occur along the 650Km of the major fault system of the region (Cornell, 1968), and is shown for comparison. The curve indicates that the region may be visited by an earthquake producing a maximum intensity of 6 (M.M.) within 100 years, which it seems does not reflect the activity of the region. The difference between these two curves may be explained as follows.

1. Less seismic activity ( $b = 0.644$ ) of the Turkish region.
2. The assumption that the events are confined to the fault system and not distributed randomly in space.
3. The use of the attenuation coefficient for southern California, which might not be appropriate for Turkey.

Return period intervals resulting from the risk curve drawn for the Tehran region agree well with those given in a return period map of south west Asia presented by Kaila et al., (1974). Figure 4-7 (after Kaila et al., 1974) shows

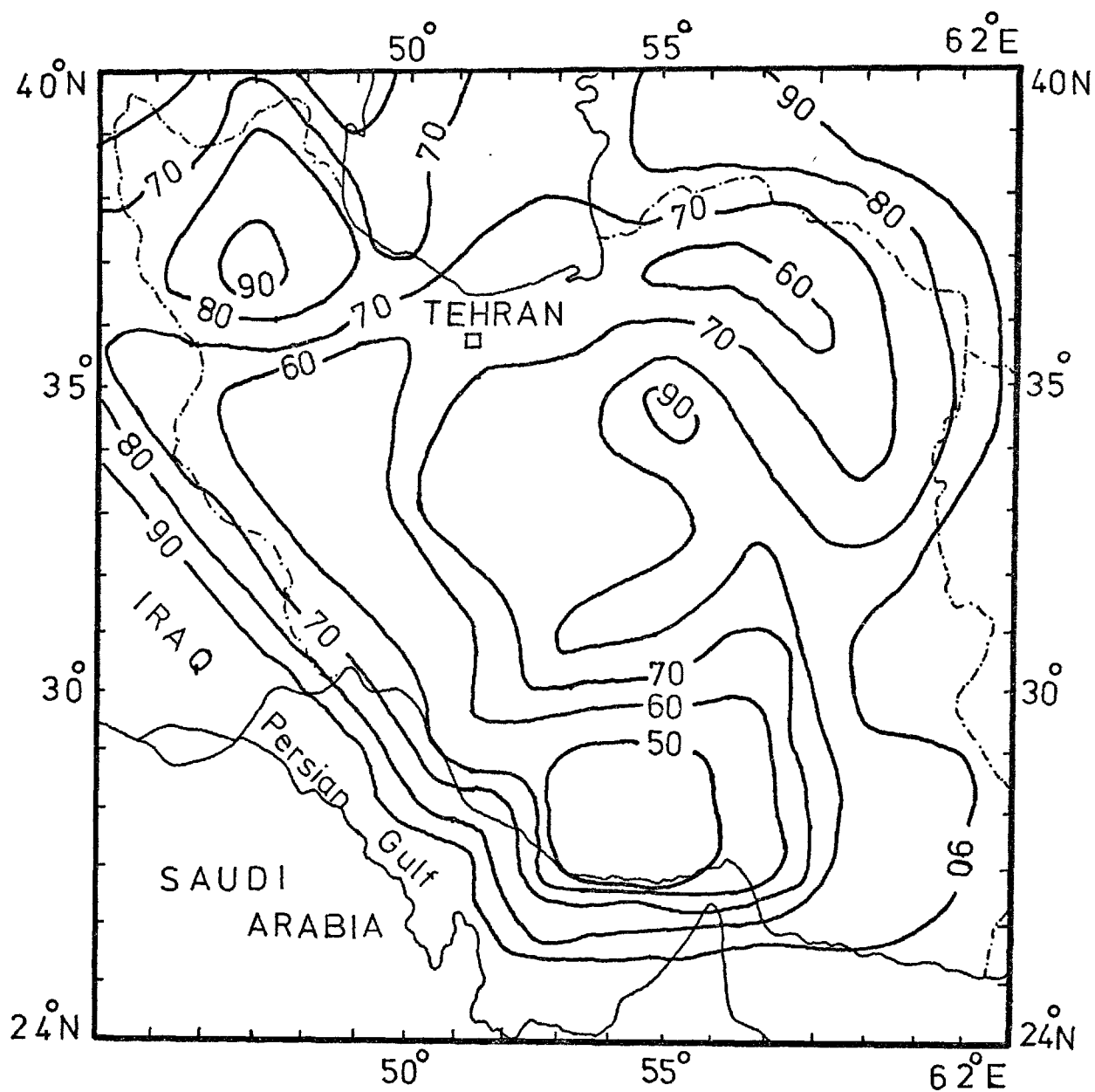


Fig. (4-7). Return period contour map of Iran (after Kaila et al., 1974). Numerals on contour lines represent the average return period (years) of an earthquake of magnitude 6 and over. The smaller the return value, the greater the risk.

that the area in this study is expected to suffer an earthquake of magnitude 6 each 60 or 70 years, which is much as would be expected from the risk curve presented here. Furthermore, its agreement with the historical compilation of Ambraseys (1966, 1968, and 1974), which shows destructive earthquakes to have occurred in the Tehran region every few hundred years, is striking.

#### 4.6 Significance of the Risk Curve

In studying the seismic hazard from earthquakes at any site or location, it is the usual practice to estimate the likelihood of the future occurrence from the history of the past activity, and any engineering analysis of the expected ground movement must be estimated from the historical events. The available data are usually of the form of:

- a. A list of earthquakes, giving quantitative information, such as epicentral parameters, and size, either as magnitude or maximum intensity.
- b. Isoseismal maps, based on qualitative information.

A disadvantage of the latter is that isoseismal lines are usually drawn to connect all points where a particular value of intensity was observed, and are influenced by local factors as well as by the magnitude of the earthquake itself, and thus have a limited bearing on future seismic activity. Such curves (Moazami-Gudarzi et al., 1972 a and b) show only the distribution of recorded intensity. They give no information about the time-distribution of events, and how

much time might elapse before the occurrence of a moderate or large magnitude earthquake. Furthermore, dividing an area by means of isoseismal lines into different zones implies discontinuity of intensity across the contour lines, and for construction projects it is not easy to decide which intensity to use in estimating the seismic risk, bearing in mind that the design should not, for economic reasons, be unnecessarily resistant.

The quantitative method presented here, for determining seismic risk, has the flexibility of being able to take into account the risk from various potential sources of earthquakes. The technique is particularly appropriate when no information about the area is available other than historical seismicity. It has the advantage of easy application, the constants are easily updated as new information becomes available, and it shows how the risk decays when the resistance of a design is increased. Perhaps one of the important aspects of the "seismic risk curve" is its feature of predicting the seismic intensities to be expected at a given site as a function of time.

## CHAPTER V

LOCATING LOCAL EARTHQUAKES AND THE USE OF MICROEARTHQUAKES  
IN REGIONAL SEISMICITY. APPLICATION OF HISTORICAL  
RECORDS TO SEISMICITY STUDIES.5.1 Introduction

The fundamental approach in the Tehran region micro-earthquake study was the determination of precise hypocenters of nearby events so that the active seismic structures could be identified and mapped. The area studied included the North-Tehran and the Musha-Fasham Faults, and around Shahr-e-Rey to the south of the city.

Since the development by the U.S. Coast and Geodetic Survey in the late 1950's of computer methods for determining earthquakes hypocenters, various methods have been used for locating nearby earthquakes, many of which have utilized a non-linear iterative least-squares process. Most methods use at least two seismic phases. Thus Flinn (1960) used direct P-and S-waves in a program developed for use by the Australian National University Network, while Nordquist (1962) used both direct and reflected P-waves for determining the source parameters and origin times of Californian earthquakes. An improvement introduced by England and Gunst (1966) was to obtain a crude solution using only a limited number (5) stations and then to include all stations in the final, more precise determination. This effects a considerable saving in computer time. Another development (Eaton, 1969) was the introduction of a crustal model, involving a uniform half-space overlain by a layer of



constant velocity, which results in an improved hypocentral determination.

These non-linear techniques calculate the four hypocentral parameters, origin time ( $T_0$ ), latitude ( $\phi$ ), longitude ( $\lambda$ ), and depth of focus ( $Z$ ) independently. This four parameter approach has been found (James et al., 1969) to give solutions that depend, perhaps not surprisingly, on the number of observing stations and on the initial approximation to the hypocenter. They concluded that different numbers of seismographic stations, particularly in a small local network, will give different, often quite considerably different, hypocentral parameters for the same events.

One of the problems arising in the development of iterative least-squares programs is the interdependence of the four computed variables, especially origin time and depth of focus. In an attempt to deal with this, James et al., (1969), developed a three parameter least-squares method which calculates the origin time independently by using the S-P time intervals. They used the relation:

$$T_0 = T_P - \frac{K(T_S - T_P)}{V_P}$$

in which  $T_P$  is the arrival time of P,  $K$  the S-P velocity, and  $T_S - T_P$  the time interval between P- and S-wave arrivals, to calculate origin time, leaving the least-squares program to calculate the other hypocentral parameters. This three-parameter technique might compute a better location for earthquakes provided that for each event an S-wave onset time is also interpreted, which is not always the case.

Other investigators including Nordquist (1962) and Bolt (1960) have discussed the problems involved in locating the events recorded by local networks, using least-squares techniques. They have stated conditions to be met if a more reliable solution is to be obtained. These conditions include that an event should be recorded by a large number of seismographic stations installed with a good azimuthal distribution surrounding the epicenter.

## 5.2 A Method for Locating Local Seismic Events

To avoid the inconsistencies due to the limitation of the least-squares procedure, attempts have been made to develop more stable techniques and more reliable solutions.

In an area of uniform structure the computed epicentral location will not depart widely from the true one, though in an area of complex structure in which the seismic waves have to travel through various media, the travel-time residuals cannot be treated as a negligible part of the entire transit-time.

A method for locating nearby earthquakes occurring within a small local network, taking the restrictions mentioned above into account, has been developed by Crampin and Willmore (1973), the so called FAMG program. The method, using travel-times developed from geometric ray paths Figure (5-1) taking into account the crustal velocity structure of the area, has been used for locating the microearthquakes recorded in the present study.

### 5.2.1 Reasons for using FAMG

It had always been assumed that the shield areas of the

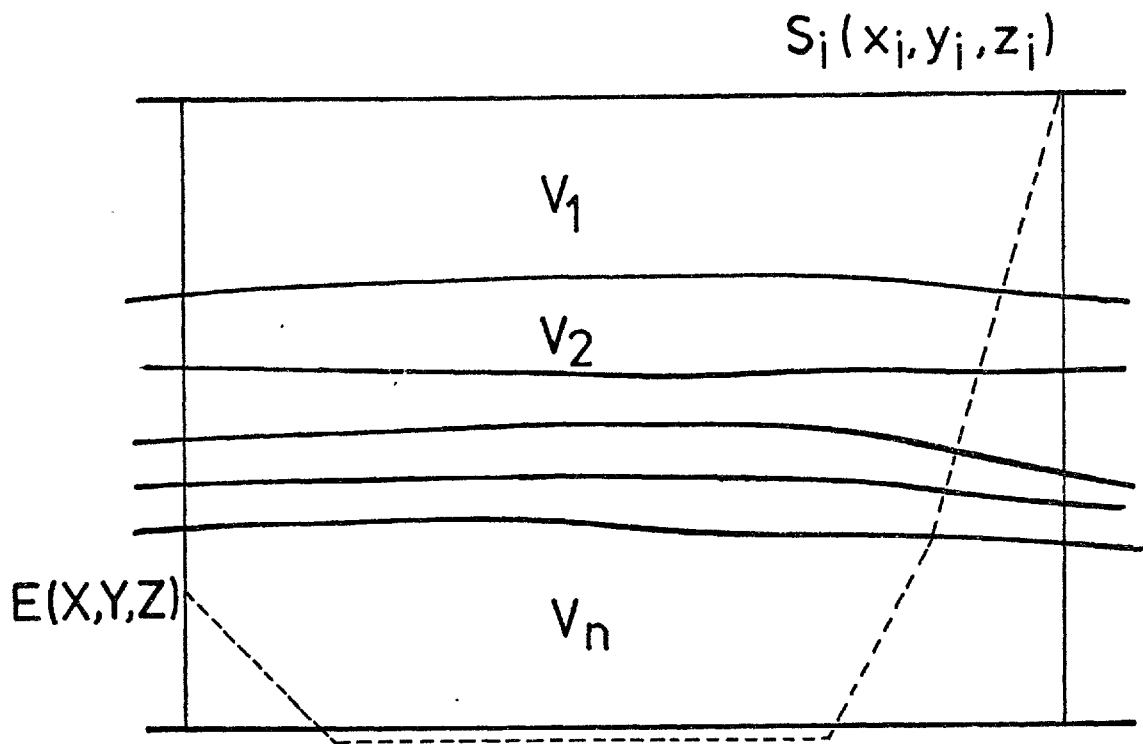


Fig. (5-1). Simplified ray path from epicenter,  $E(X, Y, Z)$ , after passing various layers to station,  $S_i(x_i, y_i, z_i)$ .

world were uniform and simple structures (Steinhart and Meyer, 1961), until Steinhart (1964) carried out an extensive study of the crust and upper mantle in the Lake Superior region of the Canadian shield. The result was published as travel time curves and showed, surprisingly, that the geological structure of the region was not uniform and simple. It was found that the velocity in the upper part of the crust exceeded  $6.5 \text{ Km Sec}^{-1}$  and the apparent velocities of  $P_n$  were in excess of  $9 \text{ Km Sec}^{-1}$  to the east of the lake.

According to Berry and West (1966) the inconsistency of the result might be due to the relatively large inter-station distances and difference between the crustal models in the east and west. To overcome the inconsistencies, they introduced a method for determining the travel-time from shot point to station involving the so-called "time-term".

The theoretical travel-time  $t$  of a wave propagating as a head wave travelling from the shot-point to the station (Figure 5-2), can be written approximately as:

$$t = \frac{\Delta}{V_n} + \int_0^{Z_1} \frac{(V_n^2 - V(Z_1)^2)^{\frac{1}{2}}}{V_n V(Z_1)} dZ_1 + \int_0^{Z_2} \frac{(V_n^2 - V(Z_2)^2)^{\frac{1}{2}}}{V_n V(Z_2)} dZ_2$$

(after Berry and West, 1966)

in which:

$\Delta$  = epicentral distance

$V(Z)$  = the velocity at depth  $Z$

$V(n)$  = the velocity at the base refractor

$Z$  = the depth to the refractor, measured  
in a direction perpendicular to its  
surface.

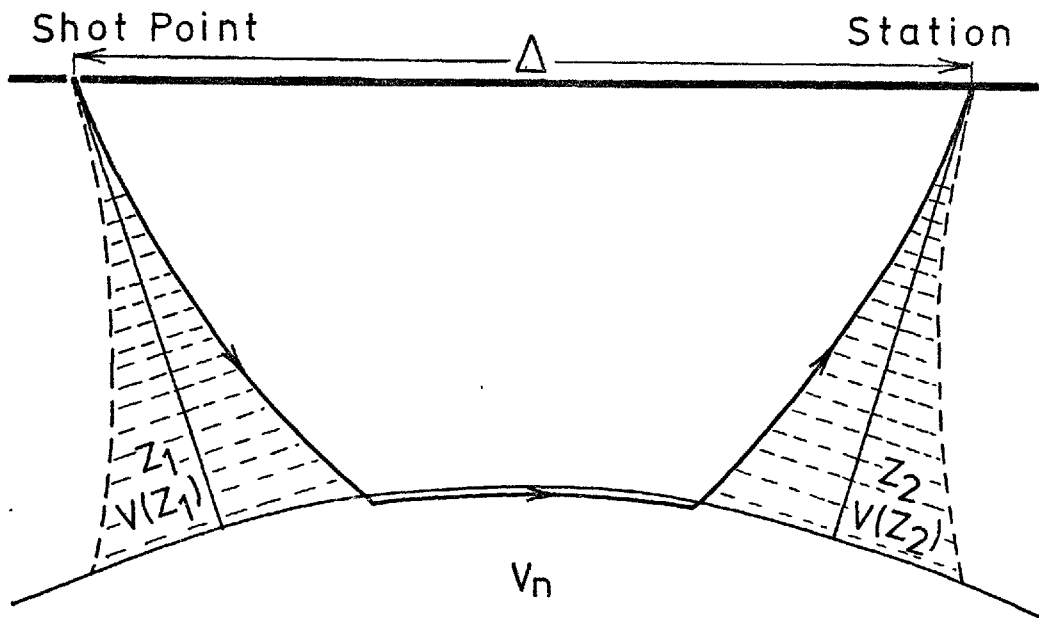


Fig. (5-2). Ray path travelling from shot point to recording station at  $\Delta$  epicentral distance from the shot point.  $Z_1$  and  $Z_2$  are the depth to the refractor measured in a direction perpendicular to the surface of the refractor.  $V(Z)$  and  $V_n$  are the velocity at depth  $Z$  and at the base refractor respectively (after Barry and West, 1966).

The second and third terms on the right-hand side of the above equation are called shot time-term and station time-term respectively.

Assuming that:

- a. The velocity varies only with depth (perpendicular to the reflector surface).
- b. Velocity of the base refractor is constant.
- c. Slope and curvature of the refracting surface are negligible.

it can be seen that the travel-time  $t$  depends only on the velocity structures beneath shot-point and station.

Crampin (1970) is the only other author who has applied the time-term to provide information on local variations in structure. His method for computing the hypocentral parameters of local earthquakes recorded within a small array is based on the derivation of travel-time equations (see above) from the geometric ray paths in a known geological structure, using the time-terms at each point, in which each station has its own delay time, to obtain information on local geological conditions.

The program, called FAMG (Crampin and Willmore, 1973), is a trial-and-error procedure which computes the hypocentral parameters of events recorded by a low density seismic network for a succession of predetermined hypocentral depths in a three layered crust, calculating the other parameters by a least-squares iterative technique. That depth is chosen as correct which yields the smallest root mean square (RMS) residual.

### 5.3 Velocity Structure

The determination of focal positions with the necessary

degree of precision requires accurate knowledge of crustal velocities in the area under study. No such model was available for the Tehran region at the start of this survey.

To evaluate the effect of the velocity structure of the three layered crust on hypocentral determinations, the crustal velocity models employed by Crampin (1969) and Mohajer-Ashjai (1975), in Eastern Central Iran were used (table 5-1).

Figure (5-3) shows the effect of applying the models to the set of readings obtained from the recorded events in the Tehran region. The discontinuities in the plots show the variation of the RMS residuals versus depths with respect to the velocity structure used. Figure (5-3 A and B) show the result of using the velocity structures used by Mohajer-Ashjai (1975) in Eastern Central Iran and shows that the residuals sometimes exceeded 0.8. Figure (5-3 C) is a structural velocity model modified by the author and used throughout the present study. A comparison of these curves clearly illustrates that, within the limits of the present knowledge about crustal velocities in the Tehran region, the third model is the best for locating the microearthquakes. However, a detailed knowledge of the crustal velocity structure is essential to minimize the number of discontinuities and reduce the chance of oscillations in the hypocentral locations.

#### 5.4 Local Earthquakes

As is true for most parts of Iran, the area studied is strongly folded and faulted, though there is no way of knowing from the geological map anything about the present level of activity.

Table 5.1  
 Crustal velocity used to locate  
 microearthquakes of Tehran region

Investigator	Region studied	Depth (Km)	P-Velocity (Km/Sec)	S-Velocity (Km/Sec)
Crampin (1969)	Eastern Iran	3	5.0	2.89
		27	6.0	3.46
			8.1	4.5
Mohajer-Ashjai (1975) Model A	Eastern Iran	1.3	3.5	2.0
		15.00	5.75	3.30
		31.30	6.70	3.90
		Mantle	8.0	4.70
Mohajer-Ashjai (1975) Model B	Eastern Iran	3.00	5.00	2.89
		15.00	6.00	3.50
		27.00	6.70	3.90
		Mantle	8.0	4.70
Hedayati (1975) Model C	North Central Iran (Tehran region)	2.00	3.45	2.00
		17.00	5.85	3.40
		31.00	6.70	3.90
		Mantle	8.0	4.70



Fig. (5-3). Variation of RMS residuals (km) versus depths with respect to the velocity structure used. A and B are the crustal velocities used by Mohajer-Ashjai (1975) in Eastern Central Iran and C is the modified structural velocity used for locating the microearthquakes recorded in the Tehran survey.

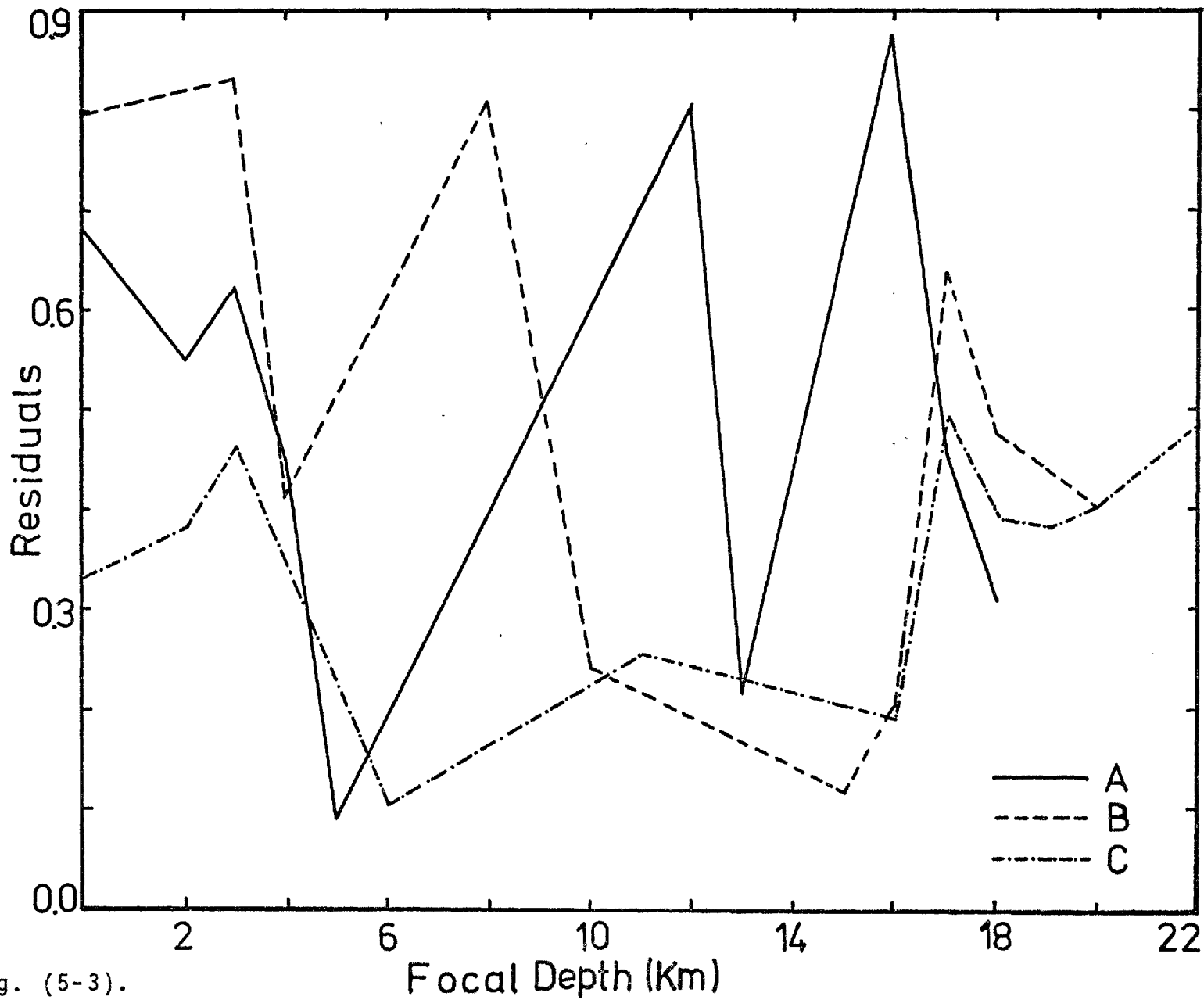


Fig. (5-3).

Since instrumental records have become available, many earthquakes have occurred in the region. It can be seen from Figure (5-4) that the majority of these events have occurred on the northern flank of the Alborz Mountains, although there is also a strong concentration of activity to the west of the city of Tehran, where the 1972 Buyin-Zahra earthquake, of average magnitude  $7\frac{1}{4}$ , occurred (Ambraseys, 1963). In Figure (5-4) the solid circles show the relocated epicenters from 1913 to 1949 (after Nabavi, 1972), while the open ones represent the earthquake locations from 1950 to 1965 (after Nowroozi, 1972). Open triangles represent epicentres located either by U.S. Coast and Geodetic Survey or by the International Seismological Centre (ISC) up to the present time. Table (5-2) summarizes all recorded events within the Tehran region.

It is particularly noticeable that the two major faults of the southern boundary of the Alborz-Mountains, the North-Tehran and the Musha-Fasham Faults, (denoted by NTF and MFF respectively on Figure 5-4) have been comparatively quiet, seismically, so far this century.

It can also be seen that there have been events scattered over much of the area studied, many of them not associated with obvious surface faults. The inconsistency of the distribution pattern of earthquakes with respect to known faults might be indicative of the lack of an appropriate structural velocity model when they were located.

Using all the instrumentally located epicenters from 1917 to 1971 for North-Central Iran, Tchalenko (1974) concluded that the region can be divided into several seismotectonic

Fig. (5-4). Seismicity map of the Tehran region. Solid and open circles show the relocated events from 1913 to 1949 (after Nabavi, 1972) and from 1950 to 1965 (after Nowroozi, 1972) respectively. Open triangles represent all other earthquakes located either by the USCGS or the ISC up to the present time. Solid triangles are indicative of the location of microearthquakes recorded in Tehran survey. The dot-dashed line is the proposed Rey Lineation and the area enclosed by the two arcs of circles represents the zone responsible for the earthquakes recorded at two stations only.

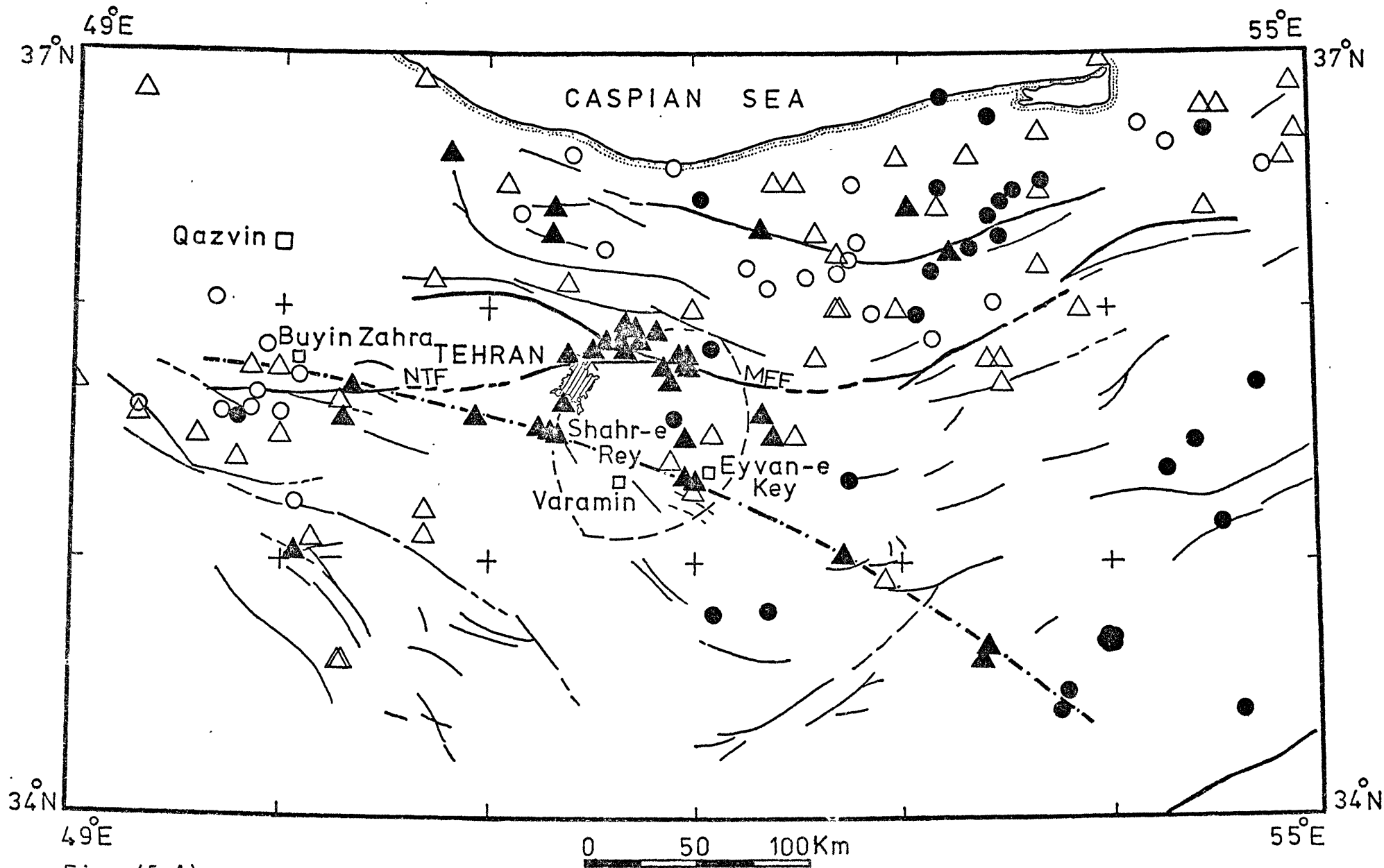


Fig. (5-4).

Table 5.2

Instrumental earthquakes occurring within  
the Tehran region since 1926

Date			Origin Time			Latitude	Longitude	Depth	Mag.
D	M	Y	H	M	S	(N)	(E)	(Km)	
22	07	26	03	54	54	34.7	54.0	--	6.5
22	07	26	08	37	30	34.7	54.0	--	5.25
22	07	26	20	33	08	34.7	54.0	--	4.75
23	07	26	20	17	46	34.7	54.0	--	5.75-6.
23	07	26	22	40	18	34.7	54.0	--	5.75-6.
27	07	26	11	33	12	34.7	54.0	33	4.75
22	07	27	03	55	14.4	34.5	53.80	33	4.0*
23	07	27	20	18	01.6	34.42	54.64	33	4.0*
23	07	27	22	40	37.0	34.42	53.76	33	4.0*
27	07	27	20	41	57.2	35.37	54.30	33	4.0*
29	07	27	11	33	20.9	35.49	54.49	33	4.0*
28	04	28	13	16	48.6	35.71	54.74	33	5.
02	10	30	15	33	09.7	35.86	52.08	33	4.0
07	10	30	20	53	03.0	35.58	51.90	33	5.0
20	05	32	19	16	17.0	36.25	53.36	33	5.25-5.5
05	03	35	10	26	40.5	36.15	53.16	33	5.25-5.5
11	04	35	23	14	48.4	36.47	53.56	33	4.0*
11	04	35	23	59	19.5	36.48	53.21	33	4.75
12	04	35	00	11	26.1	36.84	53.22	33	5.25-5.5
12	04	35	00	34	42.2	35.98	53.09	33	5.25
12	04	35	01	06	42.9	36.51	53.71	33	5.25

contd/ .....

Table 5.2 (contd)

Date			Origin Time			Latitude	Longitude	Depth	Mag.
D	M	Y	H	M	S	(N)	(E)	(Km)	
12	04	35	12	44	35.6	36.37	53.45	33	5.75
12	04	35	22	31	57.2	36.44	53.51	33	5.25-5.5
15	04	35	23	04	49.4	36.77	53.46	33	4.25-4.5
07	04	37	18	31	03.3	34.81	52.37	33	5.5
06	04	39	04	08	07.8	35.15	54.56	33	5.25
25	09	40	19	31	25.0	36.44	52.04	33	5.25
11	05	45	20	17	35.3	35.34	52.75	33	4.75
22	04	51	06	32	41	34.8	52.1	--	5.0
13	11	51	14	01	55.8	35.89	53.17	69	4.8
09	10	52	19	12	19.1	36.65	54.33	00	5.0
02	09	53	01	45	33	35.7	53.5	--	4.0*
02	09	54	22	44	00	35.3	52.0	--	4.5
16	03	57	00	43	48.2	34.94	52.93	46	5.5
06	05	57	15	06	48.7	36.23	51.56	00	5.5
02	07	57	00	42	23.0	36.14	52.90	10	7.4
02	07	57	01	16	51.3	36.08	52.37	00	4.5
02	07	57	04	56	03.5	35.98	52.67	00	4.5
02	07	57	05	09	49.4	36.57	51.90	262	4.0*
02	07	57	14	22	40.3	36.16	52.26	60	4.5
04	07	57	22	43	47	36	53	--	4.25
07	07	57	18	12	50	36.0	52.7	--	4.25
09	07	57	09	09	11	36.0	52.7	--	4.25
08	10	57	11	47	24	36.4	54.5	--	4.0*

contd/ .....

Table 5.2 (contd)

Date			Origin Time			Latitude	Longitude	Depth	Mag.
D	M	Y	H	M	S	(N)	(E)	(Km)	
25	10	57	08	24	20	36.4	53.2	--	4.25
16	01	58	02	04	29.2	36.13	52.55	45	4.8
17	06	58	16	55	00.2	36.21	52.76	00	4.5
25	06	58	01	14	01.7	36.27	52.80	04	5.3
02	11	58	07	14	34.9	36.61	51.42	63	4.8
08	03	59	14	48	59.8	36.49	52.78	110	5.0
01	05	59	08	24	02.1	36.38	51.16	33	5.9
05	09	61	14	09	52.8	36.74	54.18	26	4.0
10	06	62	21	12		36.5	52.5	--	4.0*
23	07	62	02	57		36.6	53.0	--	4.0*
01	09	62	19	20	39.0	35.59	49.85	21	7.3
01	09	62	20	27	40.9	35.86	49.93	40	4.3
02	09	62	07	12	03.9	35.59	49.33	48	4.5
02	09	62	13	21	35.1	36.03	49.64	105	4.3
03	09	62	01	01	58.3	35.68	49.89	37	4.0*
03	09	62	02	08	26	35.75	50.0	--	4.0*
04	09	62	13	30	13.9	35.58	49.71	43	5.3
06	09	62	07	30	35	36	52	--	4.0
07	09	62	06	32	20	35.5	50	--	4.0*
11	09	62	11	15	02.2	35.58	49.81	00	4.5
12	09	62	02	15	45	35.7	49	--	4.5
29	09	62	19	23	21.7	36.03	53.49	00	4.5
13	10	62	10	33	38.0	35.47	50.09	32	5.5

contd/ .....



Table 5.2 (contd)

Date			Origin Time			Latitude	Longitude	Depth	Mag.
D	M	Y	H	M	S	(N)	(E)	(Km)	
17	11	62	21	39		35.5	52.1	--	4.0*
02	12	62	22	21	31.1	35.23	50.06	53	5.0
02	12	62	23	36	34.6	35.58	50.00	24	4.3
08	12	62	09	02	53.9	36.56	54.80	25	5.0
28	05	63	10	32	47.3	35.4	49.8	33	4.3
05	07	63	04	40		36.5	52.4	--	4.0*
05	07	63	23	49	34	35.8	51.5	--	4.0*
15	05	64	01	56	08.0	35.76	49.86	29	4.0*
03	11	64	17	36	06.3	35.86	50.39	18	5.1
01	12	64	08	21	53.3	36.8	54.57	33	4.3
03	10	66	17	05	08	35.00	53.44	14	4.9
08	11	66	03	14	12.8	36.10	50.74	41	4.8
03	02	67	11	17	38	36.7	53.7	37	4.0*
16	02	67	11	55	19.8	35.7	51.9	16	4.0*
23	06	67	13	15	08	35.5	49.6	38	4.4
06	08	67	20	40	13.3	36.9	54.94	33	4.5
25	08	67	12	26	50.5	35.58	49.33	55	4.7
02	09	67	08	02	09	46.71	54.95	36	4.0*
10	11	67	02	50	52	36.0	53.89	05	4.9
10	12	67	10	52	50	36.19	53.69	19	4.9
26	04	68	02	58	23.8	35.09	50.16	32	5.2
19	05	68	16	49	50	36.61	53.35	22	4.6
29	07	68	16	03	42.1	36.5	53.7	14	4.8

contd/ .....

Table 5.2 (contd)

Date			Origin Time			Latitude	Longitude	Depth	Mag.
D	M	Y	H	M	S	(N)	(E)	(Km)	
02	08	68	03	59	27.1	36.85	49.33	39	4.7
12	12	68	18	54	47	35.80	53.49	27	4.9
26	01	69	02	25	55.8	36.8	54.5	48	4.8
09	04	69	01	04	48.8	37.0	54.0	45	4.0*
12	05	69	12	22	45.3	35.5	52.5	29	4.0*
27	06	70	07	57	53.3	35.2	50.7	14	4.9
03	10	70	06	57	02.0	36.1	51.4	68	4.1
16	03	71	05	28	11.6	36.6	54.9	54	4.0*
31	03	71	21	50	10.3	34.6	50.3	31	4.4
30	04	71	09	06	16.5	34.6	50.3	42	4.7
09	09	71	02	54	36.7	36.2	52.7	27	5.2
08	09	72	00	44	55.2	36.3	52.6	47	4.7
17	09	73	04	06	03	36.5	51.1	--	4.8
27	10	73	14	22	45	35.8	52.6	--	4.3
30	10	73	15	59	30	36.9	50.7	--	3.7

\* Assigned magnitude (will be discussed later).

localities which undergo active and quiet periods of either 3 to 12 or 50 years.

It should be said here that the city of Shahr-e-Rey (about 30 Km) south of Tehran has been destroyed on several occasions in historical times, (Ambraseys, 1961, 1966, 1968, 1974; Nabavi, 1972), though no fault appears on the surface which can obviously be held responsible.

One of the main objectives of the detailed seismic monitoring of the Tehran region was to outline the earthquake distributions and their relation to the regional tectonics by means of precise location of the events.

Epicentral locations were obtained for thirty seven of the events recorded well at three stations in the 1974 survey, ranging in magnitude from around zero to 4. The crustal model and technique described in the previous section were used for all epicentral locations. Table (5-3) lists all the calculated solutions, including the RMS residuals and the number of readings used.

In Figure (5-4) the solid triangles show the epicenters of all located microearthquakes recorded in the Tehran region. Since seismograms have been interpreted to better than 0.25 second (see chapter III), it is believed that errors in the epicentral locations are less than  $\pm 2$  Km.

Control of depth is one of the important concerns of any location program. Since FAMG calculates the hypocenter by fixing the depth at predetermined intervals, it is believed that the accuracy in depth calculation is better than one kilometer.

Figure (5-5) is a histogram of the computed depths of all located events, along with the structural velocity model

Table 5.3

## Summary of Microearthquakes Located in the Tehran Region during the Present Work

No.	Date			Origin Time			Latitude (N)			Longitude (E)			Depth (Km)	Residual	No. of Readings
	D	M	Y	H	M	S	Deg.	Min.	Sec.	Deg.	Min.	Sec.			
1	24	11	74	03	17	01.04	35	02	24.41	50	04	00.39	22	0.487	5
2	24	11	74	18	11	55.94	35	41	28.27	50	21	49.06	2	0.294	5
3	26	11	74	04	34	38.44	35	52	24.78	51	40	25.26	0	0.206	6
4	26	11	74	08	59	52.55	35	51	26.18	51	40	30.70	0	0.346	6
5	26	11	74	11	46	39.19	35	54	58.36	51	50	12.33	18	0.392	6
6	26	11	74	19	24	23.07	35	56	11.53	51	41	35.42	0	0.229	5
7	26	11	74	19	24	57.55	35	52	57.64	51	44	53.24	18	0.225	5
8	27	11	74	16	53	33.61	35	34	37.40	50	14	16.54	11	0.258	5
9	27	11	74	18	40	07.92	36	18	57.71	51	20	15.34	18	0.025	4
10	28	11	74	06	09	18.62	35	51	20.54	51	31	43.56	0	0.088	4
11	28	11	74	06	19	43.25	36	18	48.15	52	20	35.68	17	0.492	6
12	01	12	74	14	49	39.57	35	29	29.76	51	58	19.47	6	0.108	6
13	01	12	74	17	33	05.03	35	19	29.58	52	01	51.86	20	0.212	5

Table 5.3 (contd)

No.	Date			Origin Time			Latitude (N)			Longitude (E)			Depth (Km)	Residual	No. of Readings
	D	M	Y	H	M	S	Deg.	Min.	Sec.	Deg.	Min.	Sec.			
14	01	12	74	21	12	30.66	35	31	49.71	51	16	26.08	18	0.346	6
15	02	12	74	00	16	14.99	35	35	14.06	50	57	32.98	17	0.389	4
16	02	12	74	00	28	53.77	35	36	22.17	52	24	07.21	18	0.118	6
17	02	12	74	00	32	37.96	35	21	02.24	51	58	15.37	19	0.326	6
18	02	12	74	05	35	11.92	35	36	15.19	52	20	46.22	18	0.239	6
19	02	12	74	06	53	21.89	36	25	06.30	53	03	28.22	19	0.329	5
20	02	12	74	11	21	49.72	35	39	10.06	51	21	55.02	18	0.154	6
21	02	12	74	12	46	25.99	36	14	17.31	53	15	57.57	19	0.373	5
22	02	12	74	14	31	45.11	35	46	29.95	51	54	35.01	18	0.168	6
23	03	12	74	01	27	10.59	34	38	00.04	53	24	20.00	18	0.216	5
24	03	12	74	01	56	18.16	35	48	13.08	51	58	26.84	18	0.244	5
25	03	12	74	02	31	55.66	34	40	17.61	53	25	14.42	18	0.196	5
26	03	12	74	02	47	33.37	35	02	27.18	52	43	04.61	18	0.277	5
27	07	12	74	16	17	16.75	36	38	03.01	50	50	24.61	2	0.109	5

contd/ .....

Table 5.3 (contd)

No.	Date			Origin Time			Latitude (N)			Longitude (E)			Depth (Km)	Residual	No. of Readings
	D	M	Y	H	M	S	Deg.	Min.	Sec.	Deg.	Min.	Sec.			
28	07	12	74	21	53	48.29	35	54	07.68	51	35	25.89	19	0.009	4
29	07	12	74	22	56	32.82	35	47	47.22	51	58	00.54	2	0.193	5
30	08	12	74	01	01	11.73	35	48	37.53	51	58	48.27	3	0.379	5
31	08	12	74	01	41	05.36	35	45	59.88	51	56	56.93	2	0.380	5
32	08	12	74	01	44	10.81	35	49	54.87	51	56	57.02	3	0.463	4
33	08	12	74	02	25	31.82	36	25	30.98	51	21	12.37	2	0.249	5
34	09	12	74	10	26	33.77	35	56	27.56	51	43	31.27	20	0.403	5
35	09	12	74	11	00	31.04	35	49	55.53	51	23	51.99	19	0.189	4
36	12	12	74	13	03	25.95	35	32	40.46	51	19	56.54	18	0.228	6
37	12	12	74	13	03	53.32	35	31	50.39	51	20	59.31	16	0.198	5

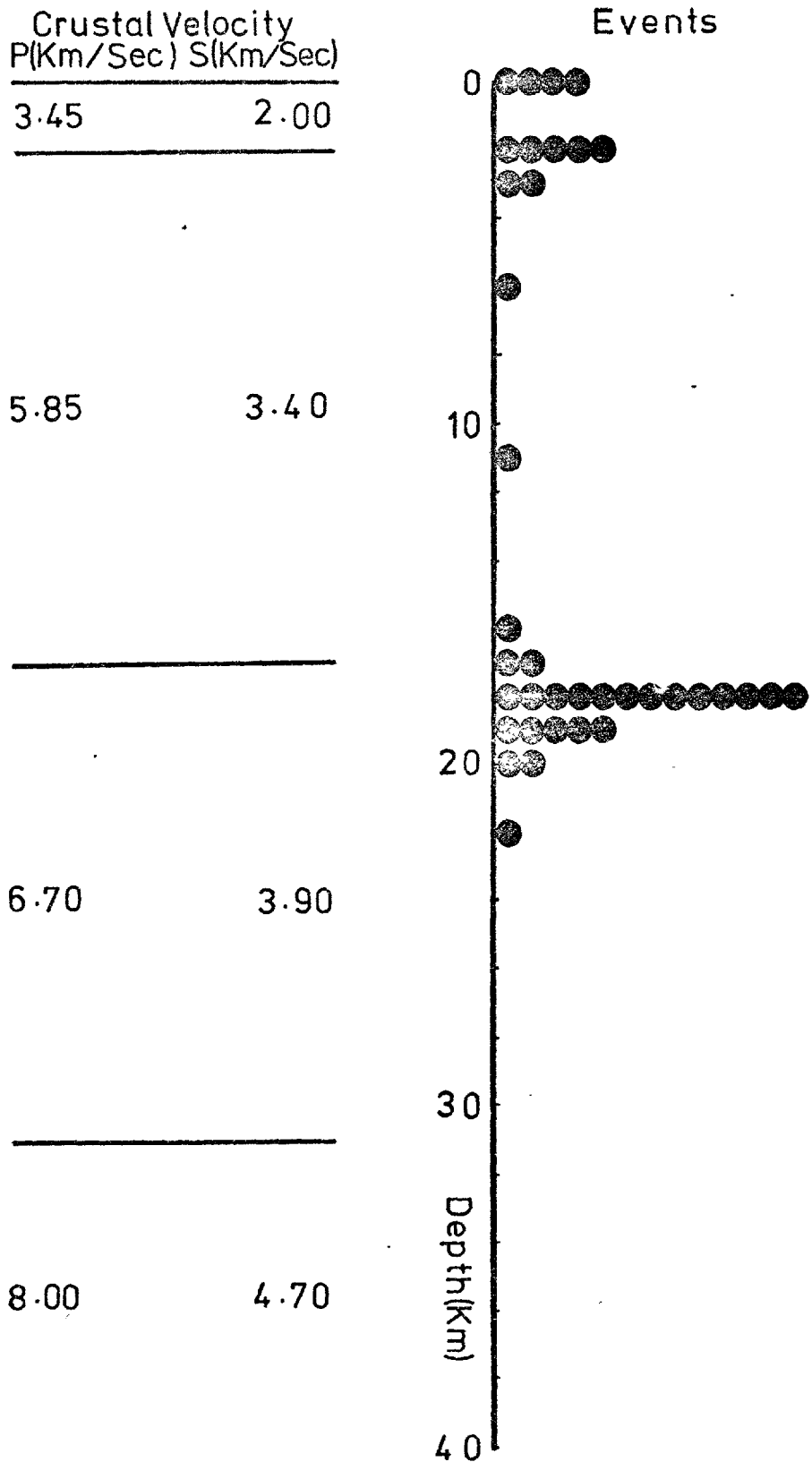


Fig. (5-5). Histogram of the computed depths of all the local events along with the structural velocity model used in the location. Note the concentration of hypocenters at depths 2-3 and 18-19 km.

used. This shows that there is a very pronounced grouping of hypocenters at depths of between 2 and 3 Km and between 17 and 19 Km, the upper and lower boundaries of layers in the crustal model used. The significance of these two depths of clustering will be discussed in chapter VII.

#### 5.5 Significance of the Local Events and Discovery of the Rey Lineation

Close inspection of Figure (5-4) reveals that the majority of epicenters fall on the southern flank of the Alborz Mountains, and are almost certainly associated with the Musha-Fasham Fault. This, as was mentioned above, is quite at odds with the distribution of the larger events, most of whose epicenters fall on the northern flank of the Alborz Mountains. The noticeable lack of microearthquake activity on the North-Tehran Fault may be due to less activity of the fault itself, or simply a question of insufficient instrumental sensitivity. It seems that the latter of these alternative is less likely, since none of the epicenters of the larger events is associated with this fault. This might mean that the fault is creeping, though more likely that it is just quiet.

The observed imbalance of activity on the Musha-Fasham Fault, which must be a real effect, implies either that the stress is being (and has been for most of this century) relieved by a large number of very small earthquakes, or that the activity on the southern flank of the Alborz Mountains has been very low and is only just beginning to increase (again?). Energy considerations, regarding the logarithmic relation between



magnitude and energy released, makes the former of these alternatives less likely, and it must be considered a real possibility that the faults on the southern flank of the Alborz Mountains, just north of Tehran, are increasing in activity.

Most of the remaining epicenters found by the present study fall on a pronounced lineation (enhanced by the positions of some of the epicenters of the larger events) which stretches from near Buyin-Zahra, east of the Shahr-e-Rey, then south east to beyond Eyvan-e-Key and Varamin for about two hundred kilometers. This newly discovered lineation (shown as a dashed-dot line on Figure (5-4)), to be called hereafter the "Rey Lineation", seems to have isolated sections of faults associated with it at various places, but nothing continuous over its entire length. The Rey Lineation might well be responsible for the recorded destruction of Shahr-e-Rey, and constitute a severe threat to the metropolitan complex of the area. The significance of this lineation will be discussed further in chapter VII.

The located microearthquakes show a pronounced clustering, particularly on the Musha-Fasham Fault (see Figure 5-4), which indicates strong interrelation between them. According to the elastic rebound theory, (Reid, 1910), each event would disturb the strain field and thus tend to trigger another nearby event. Udias and Rice (1975) studied the microearthquake activity, ranging in magnitude from zero to four, of the San-Andreas Fault during 1968-1971. They, also, have shown conclusively the interdependence of microearthquakes on this fault (see Figure 4-1). If this is the case, microearthquakes could be used as an indicator of future activity, and might be used in prediction.

Proper epicentral location requires an event to be recorded by at least three stations. Because of the reconnaissance nature of the Tehran survey, stations were moved regularly in order to obtain a more even azimuthal distribution, and often an event was recorded by only two stations. Using the numerical value of K determined in chapter III (7.80), approximate locations for thirteen events recorded at two stations were obtained using the relation:

$$\Delta = K(t_s - t_p)$$

Six of these shocks were recorded in Tochal and Gandab, three in Hosseinabad and Gandab, and the remainder at Ozdar and Hosseinabad. Figure (5-6) shows that many of these micro-earthquakes (those in the rectangular box), which have occurred within 25 to 60 Kilometers of the recording stations, are associated with the newly discovered Rey Lineation. The zone enclosed by the broken line in Figure (5-4), found by graphical methods using the S-P time interval, represents the area responsible for the earthquakes.

#### 5.6 Historical Events and their Role in Understanding the Seismicity of the Area

Despite the great advances in instrumental seismology made this century, instrumental data exist for only sixty years, and to draw far-ranging conclusions about the seismicity of a region within such a short time interval could easily give grossly misleading results. However, historical records of seismic activity, though not of great quantitative accuracy can,

Fig. (5-6). Distances from either H0 or T0 plotted against distances from either OZ or GA (in terms of S-P time intervals). The close grouping of the events recorded at GA and T0 and H0 and OZ (enclosed by the box) implies that the events originated from the same area. This area is shown as the zone enclosed by broken line in Figure (5-4).

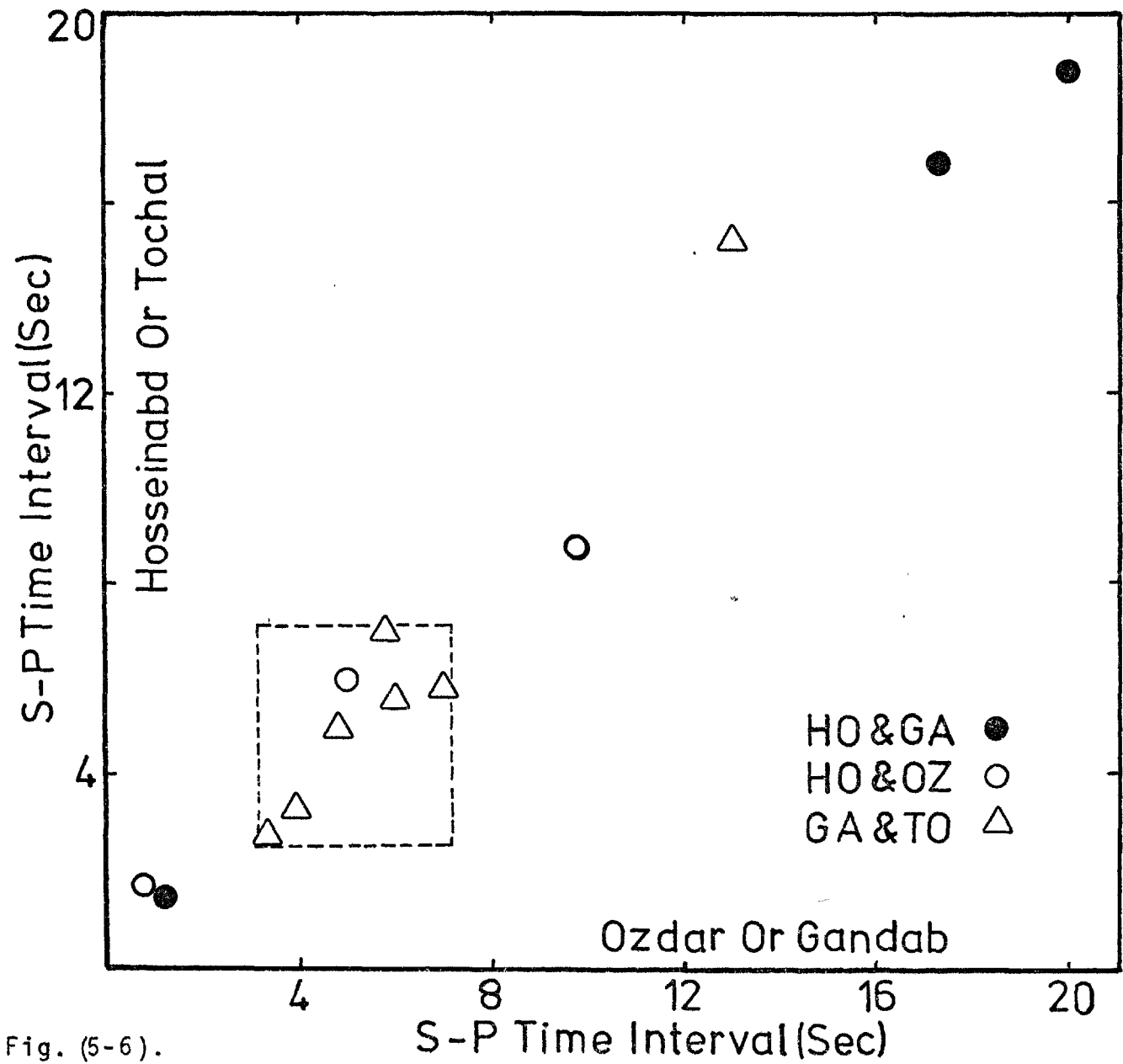


Fig. (5-6).

if used cautiously, add much to the understanding of present day activity.

Good evidence to support the high activity of the Tehran region (21.4 earthquakes per day, Hedayati et al., 1975) inferred from the microearthquake survey, is provided from the well documented historical earthquakes of the area under investigation. For this particular region, recorded history goes back as far as 280 AD, and contains valuable information regarding earthquakes in earlier times.

Historical events from 280 to 1900 AD are listed in table (5-4), and the instrumentally located epicenters from 1900 up to the present time are shown in table (5-2). The data are from Ambraseys (1961, 1966, 1968, 1971, 1974), Nabavi (1972), Nowroozi (1971), the USCGS, ISC, and the Iranian press.

The distribution of earthquakes which occurred in the Tehran region over the period 280-1974 is shown in Figure (5-7). It can easily be seen that the historical events (represented by the shaded surface) follow faithfully the tectonic boundaries, particularly at the southern flank of the Alborz Mountains, where most of the located events of the 1974 microearthquake survey are clustered.

Figure (5-8) shows the time distribution of destructive earthquakes from 800 to 1974 AD. It can be concluded from this figure that for the interval 800 AD to 1000 AD the region was highly active, after which it became comparatively quiet until the 18th century, when activity increased to its present high level.

The results of the present microearthquake survey show that the Tehran region is as highly active now as it has been

Table 5.4  
Historical Earthquakes of the Tehran Region

Date	Location	Remarks
280-312 AD	Shahr-e-Rey	A destructive earthquake.
802 AD	Semnan and Damghan	About 70 villages were destroyed.
846 January	Shahr-e-Rey	Damaging earthquake at Shahr-e-Rey, many houses destroyed.
855 AD	Shahr-e-Rey	A violent earthquake followed by a number of aftershocks about forty days. It cost many lives and destruction of many houses.
856 AD	Qom	A violent shock, 45000 people were killed at Qom.
856, Dec.3-30	Damghan Shahr-e-Rey Qom and Kashan	The earliest earthquake in North-Central Iran. Near Qom 45000 people were buried under the ruins.
863 AD	Qazvin and Tabriz	An earthquake.
864 AD Jan.15-Feb.12	Shahr-e-Rey	A violent earthquake destroyed many houses and the inhabitants run away to the country.
893 AD	Tabaristan and Shahr-e-Rey	A strong earthquake.
898 Jan. 28	Shahr-e-Rey	An earthquake at Shahr-e-Rey and in the region between Gilan and Gorgan.

contd/ .....

Table 5.4 (contd)

Date	Location	Remarks
812, Aug.18- 913, Aug.6	Dinawar	At Dinawar (WNW of Hamedan) an earthquake shattered a mountain from which steams of water gushed out and submerged many villages.
956 AD	Hamedan	A destructive earthquake occurred in Hamedan.
956, Apr.27	Hamedan	An earthquake occurred at Hamedan (Iran) cost many lives and property.
957 AD	Shahr-e-Rey and Taleqan	A number of great earthquakes occurred at Shahr-e-Rey and Taleqan (near Qazvin), which ploughed the ground.
957, Apr.4- 958, Mar.24	Shahr-e-Rey	An earthquake occurred in Shahr-e-Rey and its vicinity, lasted for forty days. At Shahr-e-Rey 450 settlements sunk into the ground. The ground was open and water and smoke rushed out.
958, Mar.25- 959, Mar.13	Qom and Halvan	An earthquake in Qom and Halvan (33.95N, 56.22E) and extended to Kaman in Turkey, Bagdad and Jebble in Syria.
959 AD	Qazvin and Gilan	Damaging earthquake in Qazvin and Taleqan-Rud village.
1007 AD	Dinavar	A great earthquake which killed 16000 people in Dinavar.
1067 AD	Qazvin	Damaging earthquake destroyed the walls of Qazvin and ruined one third of the town.
1119, Dec.10	Qazvin	The city was destroyed by an earthquake.
1120, Nov.29	Qazvin	An earthquake shook Qazvin again.
1166, Oct.28	Qazvin	An earthquake caused some damage in Qazvin.

contd/ .....

Table 5.4 (contd)


Date	Location	Remarks
1208, Jul.16	Neishabur	A shock occurred in Neishabur and lasted for ten days.
1280 AD	Neishabur	An earthquake destroyed Neishabur.
1324 AD	Hamedan	An earthquake occurred in Hamedan.
1389, Jan.30- Feb. 27	Neishabur	An earthquake perished many persons in Neishabur.
1400 AD	Koutoum	This town (37.13N, 50.15E) was damaged by a local earthquake.
1403 AD	Hamedan	An earthquake occurred in Hamedan.
1485, Aug.14	Tamidjan	The city (37.10N, 50.16E) practically destroyed.
1549 AD	Qazvin	The province of Qazvin were destroyed by earthquake and 3000 persons were buried.
1554 AD	Kashan	The city was visited by an earthquake.
1639 AD	Qazvin	A violent earthquake shook Qazvin, 12000 lives were lost.
1664 AD	Damavand	A destructive earthquake occurred in Damavand and vicinity. Numerous people were killed and all the buildings were destroyed.
1667, Mar.6- 1668, Feb.22	Lahijan	The city was shaken by a severe earthquake.
1677 AD	Lahijan	Many public buildings destroyed near Lahijan (37.17N, 50.00E).
1709, Mar.13-	Rasht	An earthquake shook Rasht.
1710, Mar.1		

contd/ .....



Table 5.4 (contd)

Date	Location	Remarks
1713, Jan.28- 1714, Jan.16	Rasht	The city of Rasht was shaken again.
1755, Jan.7	Kashan	More than 300 houses were destroyed and 40000 people were killed.
1794 AD	Kashan	An earthquake occurred in Kashan.
1808 AD	Gilan	An earthquake occurred in south east of Gilan and felt in Tehran and Rasht.
1815, June	Damavand	A strong shock occurred in Damavand.
1820 AD	Mazandaran	Strong shock in Mesha-Sar and Babol.
1823 AD	Mazandaran	Many people were killed in the cities of Mazandaran.
1830, May 9	Damavand	About 500 people were killed in east Damavand because of an earthquake. Rock fall and damage in Lavasan.
1844, Apr.25	Rasht	No damage is reported for this earthquake.
1844 AD	Kashan	About 1500 people were killed as the cause of an earthquake.
1851 AD	Shahrud	A strong earthquake.
1852, Oct.1	Gilan	A destructive shock in Bandar-e-Pahlavi and Rasht. No damage was reported
1862, Oct.1	Gilan	Three violent shocks felt at Rasht and Bandar-e-Pahlavi.
1868 AD	Tehran	A strong shock occurred and was felt at Tehran, Firuzkuh, Qom and Kashan.
1872, June	Hamedan	An earthquake.
1872, June	Hamedan	The city was destroyed by an earthquake.
1893, Nov.21	Kashan	$\frac{2}{3}$ of the town was destroyed because of a severe earthquake.

Fig. (5-7). Distribution of the historical earthquakes occurring in the Tehran region, listed in table (5-4), between the years 280 A.D. and 1900, shown as shaded surface (after Ambraseys, 1966). Circles and triangles are as Figure (5-4). , represent a city. D: Damavand; F: Fasham; G: Gorgan; K: Kashan; L. Lavasan; Q: Qom; Qa: Qazvin; S: Shahrud; Sh: Shahr-e-Rey; T: Tehran; Ta: Taleqan.

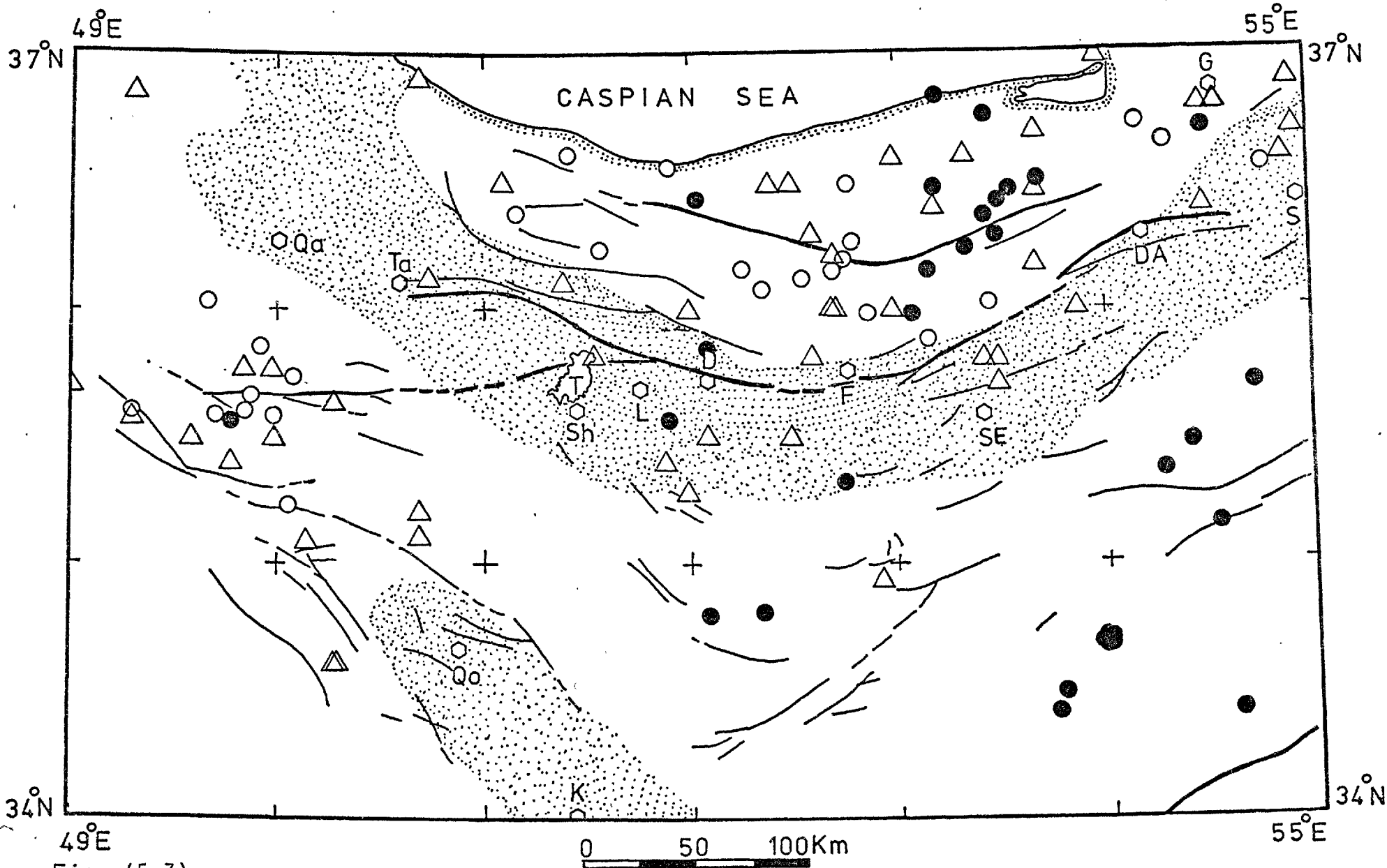


Fig. (5-7).

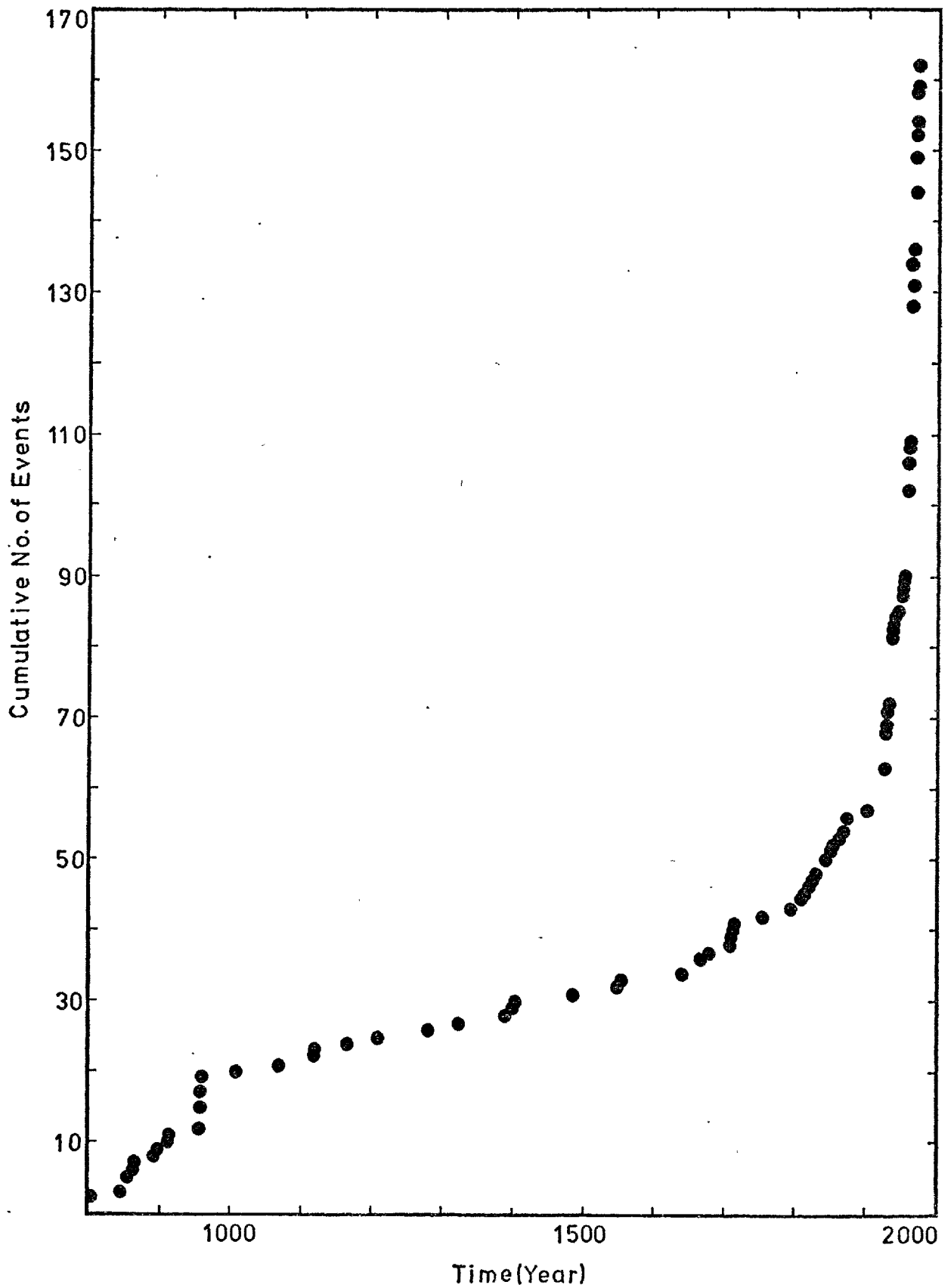


Fig. (5-8). Time distribution of earthquakes occurring in the Tehran region between the years 800 and 1974. Note the active period from 800-1000 and relatively quiet period up to 18th century when high activity commenced again.

in the historical past, and confirms the validity of using microearthquake data to assess regional seismicity.

## CHAPTER VI

TEMPORAL VARIATIONS IN  $V_P/V_S$ : APPLICATION TO  
EARTHQUAKE PREDICTION: FORSCH DISCONTINUITY6.1 Introduction

One of the major aspects of the microearthquake survey in the Tehran region was to investigate the relationship of the seismicity, regional tectonics, and crustal structure.

All previous studies dealing with the seismotectonics of the Tehran region are based on historical activity (e.g. Tchalenko et al., 1974). Many seismologists (e.g. Barazangi and Dorman, 1969; McKenzie, 1972) have shown how dispersed are the epicentral locations in the continental areas in comparison with those on oceanic ridges. This diffuse distribution of historical epicenters makes it difficult to draw definite conclusions about continental tectonics (see Figure 5-4).

Recording a large number of small nearby earthquakes, which are certainly related to the tectonic processes within the earth, provides information with greater resolution in both time and space, and therefore a better understanding of the current activity and structure of the region under investigation.

Thus, information obtained by recording microearthquakes is a valuable supplement to that from larger events, and provides a means of accelerating the effort of seismologists towards understanding the earth's tectonic processes. Microearthquakes, which are in fact indicative of the present regional activity and exhibit the nature of crustal evolution,

are used as another step towards predicting the future activity of the area.

In this chapter an attempt has been made to infer indirectly the crustal velocity structure of the region, using microearthquakes.

## 6.2 Earthquake Prediction

For many years seismologists have been aware that foreshocks often precede strong earthquakes. Recently, numerous investigators have examined regional seismic activity for short and long intervals before moderate and large earthquakes to look for any changes in seismic characteristics. In some instances these studies, considering historical events, have shown that in the areas concerned major shocks are preceded by periods of relative quiet, while in other areas increasing activity presages the main shock.

Fedotov et al., (1969), based on the seismicity changes preceeding the great earthquakes of the southern Kuriles on November 6, 1958, and October 13, 1963, concluded that the seismic activity level increases about 5 to 20 years before the main shock.

Mogi (1969a) in a detailed study of four great Japanese earthquakes suggested that in a period as long as some 20 years before a great event, the area within about 100 Km radius of the future epicenter becomes abnormally seismically quiet while the surrounding regions become increasingly active. According to him, the phenomenon, the so called "doughnut pattern" of seismic activity, dies out just before the main shock, and the

area close to the epicenter becomes active.

Borovik et al., (1971) in studying the seismic history of the Priбайkalia area of Russia found that for at least  $7\frac{1}{2}$  years before the magnitude  $6\frac{3}{4}$  earthquake of 29 August, 1959 in central Baikal, a relatively quiet zone developed prior to the main shock. They termed this quiet area the "preparation region", and observed that the preparation region was seismically quiet while the surrounding area was active prior to the main shock.

Sadovsky et al., (1972) studied the processes prior to large earthquakes in central Asia. They concluded that, if over a period of 5 to 10 years the activity of an area decreased or was stable, the possibility of occurrence of a destructive shock in the next five years is low. In contrast, if the activity increased during the 5 to 10 years period, it could be an indication of future activity.

Kelleher and Savino (1975) confirmed the doughnut pattern originally noticed by Mogi (1969a) for the pattern of distribution of seismicity before large strike-slip and thrust mechanism earthquakes in various parts of the world.

All the conclusions discussed above are indicative of various changes in the activity of, or surrounding, the epicentral area, which might be of use in predicting future activity. Nevertheless, it should be borne in mind that seismic preconditions can only be used as long-term indicators of the future activity in an area provided the region concerned has suffered from moderate to strong earthquakes in the past sufficiently often to allow the accumulation of data on several cycles of activity.



It seems, however, that microearthquakes could be of great help, since within a short interval of time it is possible to record many small nearby events, containing a great deal of information on the current level of tectonic activity of an area. Thus they can be used as a passive tool to examine the change of seismicity patterns before large earthquakes.

#### 6.2.1 Premonitory Changes of Body Wave Velocities: Use of Microearthquakes

Predicting earthquakes, a long standing and elusive desire of seismologists, seems to be on the verge of becoming a practical proposition, due to the progress made in the application of microearthquakes, and the recent achievements in the earth and materials sciences in laboratory experiments.

It is probable that before all great crustal earthquakes various seismic preconditions such as mentioned in (6.2) as well as in the ratio of seismic body wave velocities ( $V_p/V_s$ ), magnetic field, tilt, strain, electric field, and patterns of microearthquakes happen.

From the work that has been done in various parts of the world, it seems that the most practical way of approaching the final goal of predicting events is to use premonitory changes in the velocity ratio ( $V_p/V_s$ ). Because it may take a long time to observe other phenomena, microearthquakes offer a very convenient way of establishing these changes.

Evidence for a decrease in the compressional to transverse wave velocity ratio prior to moderate size earthquakes in the

Garm region were first observed by seismologists of the USSR. Semenov (1969) showed that the velocity ratio ( $V_p/V_s$ ) decreased and subsequently returned to normal before earthquakes of magnitude 4 to 5 in the Garm region. Thus, applying the method to the Matsushiro earthquake swarm in Japan, Ohtake (1973) not only noticed decreases in  $V_p/V_s$ , but also obtained correlations between anomalous changes in  $V_p/V_s$  and the seismicity during the swarm. Similarly, for the eastern United States, Aggarwal et al. (1973) found large changes in the velocity ratio of compressional to shear waves before small and moderate earthquakes. They showed that the premonitory effect occurs at a characteristic time before earthquakes, which increases with the subsequent earthquake's magnitude. Other recently published results include observation of a similar effect prior to the earthquake of 16 October, 1970 in the Akita Prefecture of Japan (Hasegawa et al., 1975) and the observation of the same phenomenon before the Blue Mountain Lake earthquake, New York, which enabled Aggarwal et al. (1975) to predict a small earthquake in the region on August 3, 1975.

Nur (1972) on the basis of fracture studies on various rock specimens showed that they undergo an inelastic volumetric increase preceding failure, which is produced by the formation and propagation of cracks within the rocks, while Gupta (1972) reported small decreases in the P- and S-velocities before failure, in laboratory experiments. However, Sholz et al. (1973) demonstrated from rocks deformed in the laboratory that microfractures occur in rock samples in the same manner as fractures in tectonic shocks. If one could accept that rock

deformation is a miniature model of the earth's crust, the instability of  $V_p/V_s$  thus seems commonly applicable at least to some types of tectonic earthquakes.

By contrast, McEvelly and Johnson (1973) are the only authors to have reported negative results on the decrease of the velocity ratio of P-and S-waves, as will be discussed later.

Figure (6-1) shows the decrease of  $V_p/V_s$  and its return to its normal value prior to a moderate earthquake in Nagano Prefecture, Japan, as an example of this kind of work (after Ohtake, 1973).

#### 6.2.2 Computation of $V_p/V_s$

For the 326 microearthquakes recorded in the Tehran survey, the arrival times of P-and S-waves (when possible) at each seismograph station were read with a precision of better than 0.1 second for the Geostore and better than 0.25 seconds for the Sprengnether, using a magnifying lens. Those earthquakes were selected for the  $V_p/V_s$  study where the onset of the P-and S-waves were impulsive. Thus the problem of phase identification which usually arises could be neglected for the events used here.

The technique used was to plot the time differences between S-and P-arrivals ( $t_s - t_p$ ) as a function of the P-wave travel-time ( $t_p - t_0$ ), as shown in Figure (6-2), using only those events which were recorded by at least two stations. Assuming a homogeneous velocity structure, these points should lie on a straight line, from the slope (S) of which a value can be obtained for  $V_p/V_s$ , as follows.

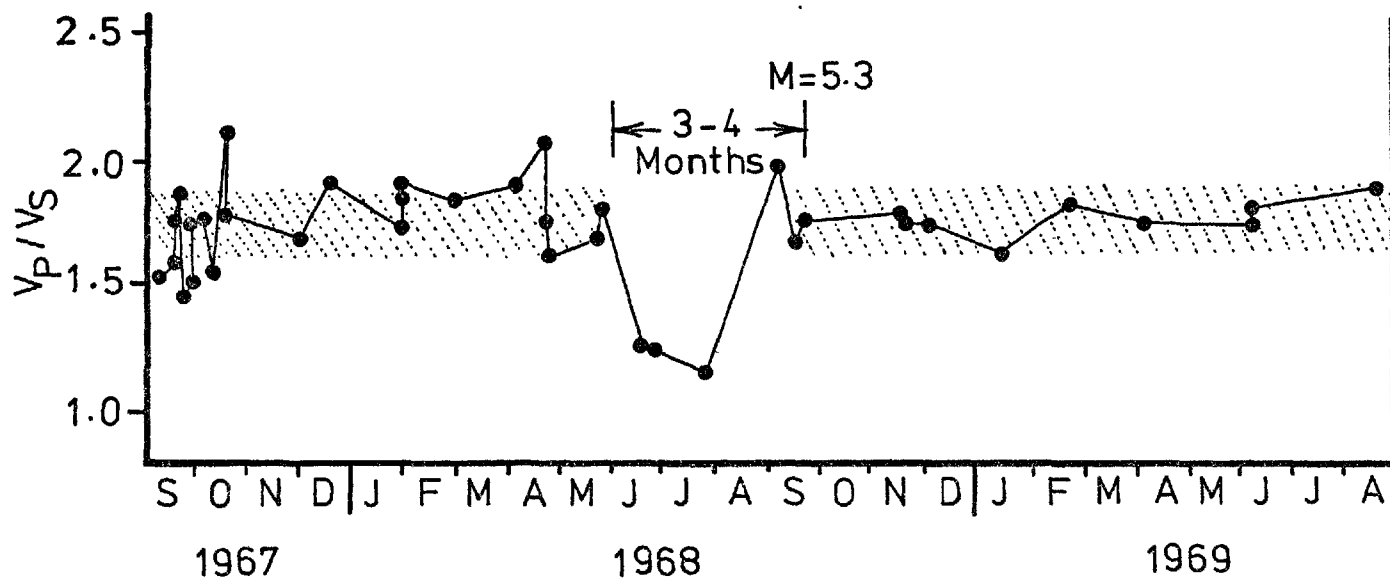


Fig. (6-1). Velocity ratio  $V_p/V_s$ , versus time. Note the decrease of  $V_p/V_s$  and its return to its normal value prior to the earthquake (after Ohtake, 1973).

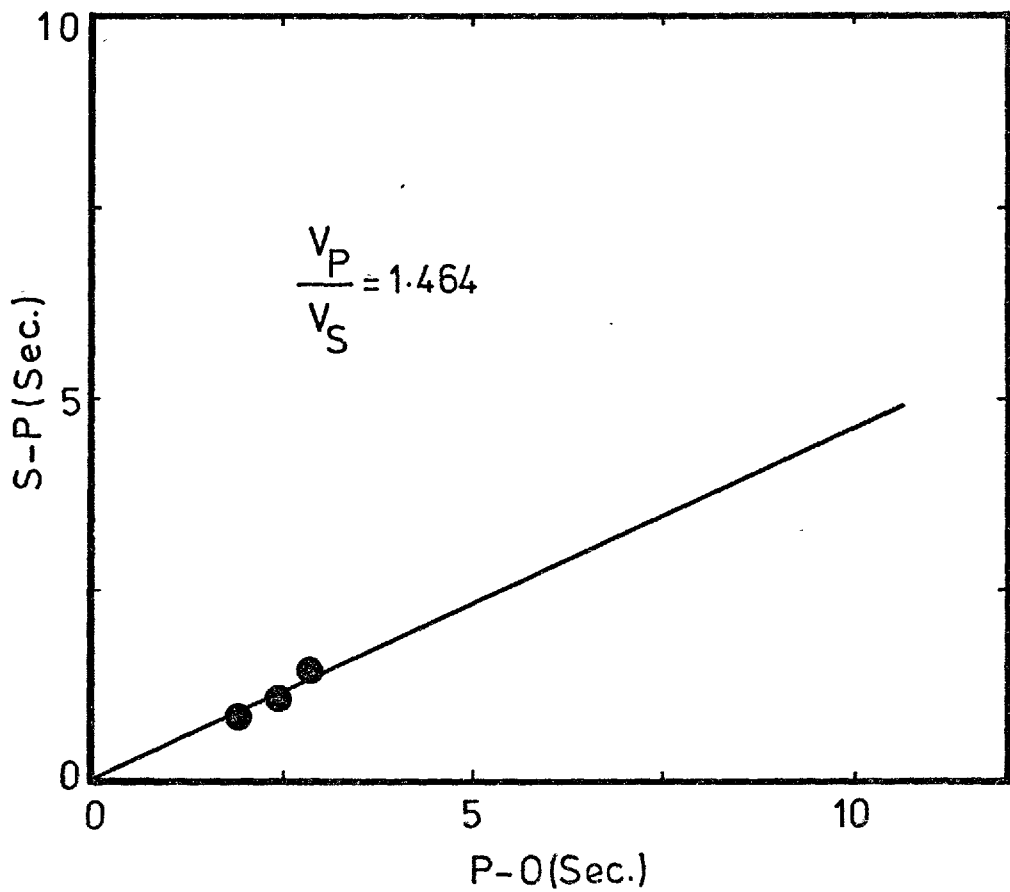
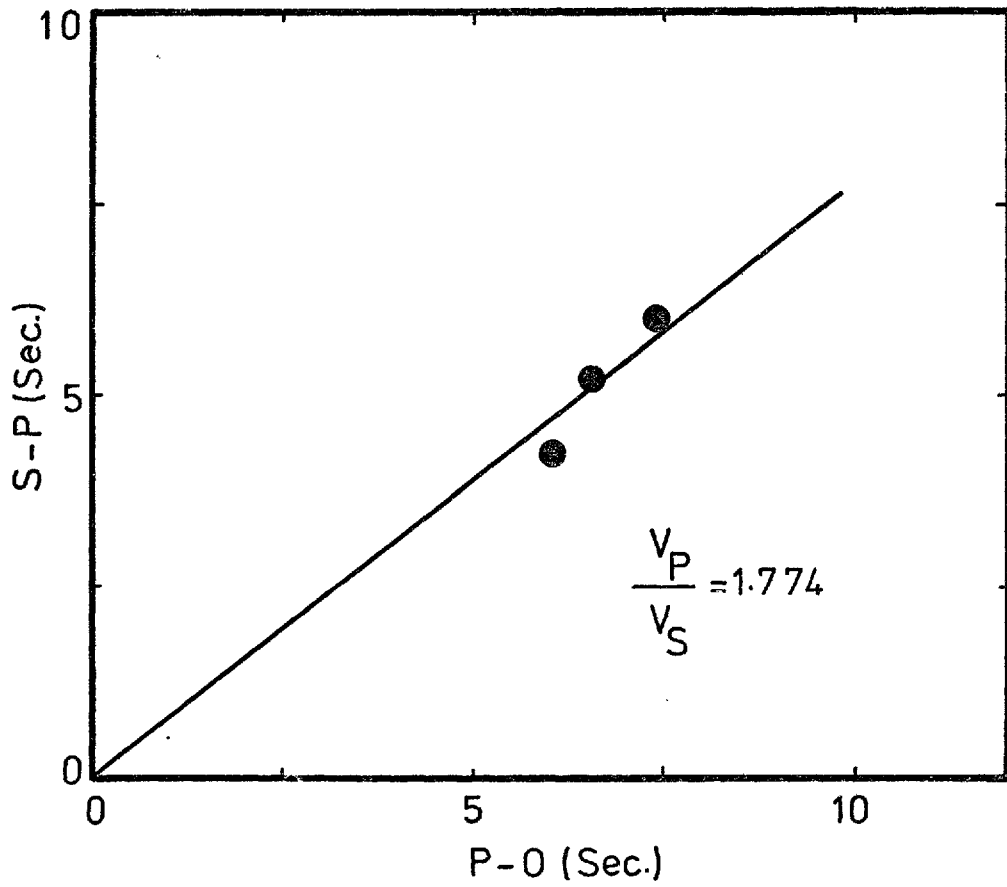


Fig. (6-2). S-P time interval versus P-0 arrival time. The slope of the line is  $(V_P/V_S)-1$ .

Let 
$$S = \frac{t_S - t_P}{t_P - t_0}$$

Now if  $\Delta$  is the epicentral distance of a particular earthquake,

$$t_S - t_0 = \frac{\Delta}{V_S}$$

and 
$$t_P - t_0 = \frac{\Delta}{V_P}$$

whence 
$$\frac{t_S - t_0}{t_P - t_0} = \frac{V_P}{V_S}$$

and 
$$\frac{t_S - t_P}{t_P - t_0} = \frac{V_P}{V_S} - 1$$

i.e. 
$$\frac{V_P}{V_S} = 1 + S$$

In the present study,  $S$  was found by fitting a straight line to the data points, using a least-squares regression method.

### 6.3 Decrease in Velocity Ratio Preceding Tehran Microearthquakes

Figure (6-3) shows the individual calculations of  $V_P/V_S$  as a function of time before the three largest earthquakes recorded in the present study, of magnitudes 2.4, 2.8, and 2.1 and occurring on December 2, 3 and 13 respectively. The occurrence times of these events are indicated by arrows. The prominent features of Figure (6-3) are the sudden decreases of  $V_P/V_S$  followed by a gradual increase to its normal value. The decreases of  $V_P/V_S$  are about 14 percent from its average value of 1.73 (see also chapter three). Table (6-1) summarizes the results of similar studies by other investigators elsewhere.

Fig. (6-3). The ratio of the velocities of longitudinal and transverse waves versus time. Note the decrease of  $V_p/V_s$  and its return to its normal value before an earthquake.

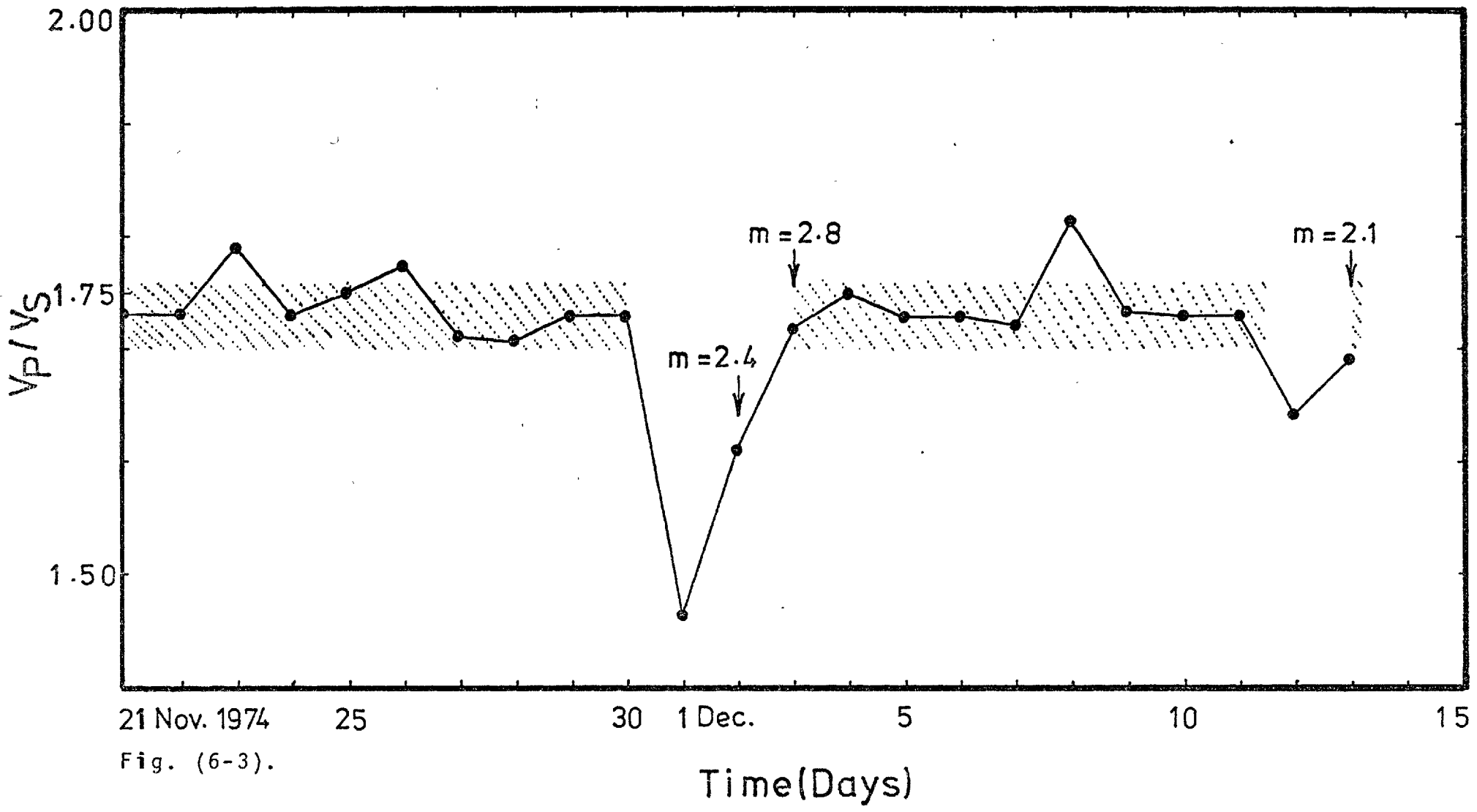


Fig. (6-3).



Table 6.1

Comparison of premonitory changes from the present study with those  
of findings of other regions

Investigator	Region studied	Average velocity ratio	Percentage of decrease
Semenov (1969)	Garm region USSR	1.77	6
Aggarwal et al., (1973)	Blue Mountain Lake New York	1.75	13
Whitcomb et al., (1973)	San Fernando California	1.75	10
Brown (1973)	Chugoku-Kinki Japan	--	9
Ohtake (1973)	North Nagano Japan	--	30
Kisslinger and Engdahl (1974)	Aleutian Islands	--	5
Hedayati (1975)	Tehran region	1.73	14

It is perhaps surprising that drops in the velocity ratio as large as 14 percent should occur in a relatively short time prior to small and moderate sized earthquakes. This time is particularly short when compared with that necessary for the strain accumulation in the earth responsible for earthquakes, but nevertheless it is long when compared with the propagation time of the seismic waves. It seems that the effect of phenomena such as pore pressure changes, crack formation, and fluid flow might be responsible for this short time interval.

Semenov (1969) showed that the variation of the velocity ratio ( $V_p/V_s$ ) before earthquakes in the Garm region was related to the magnitude of the events. Figure (6-3) shows clearly that not only do the decreases occur before the small to moderate microearthquakes in the Tehran region, but also that the size of each fall is related to the magnitude of the succeeding earthquake.

The direct relationship between the size of earthquakes and the duration of the velocity-ratio precursor times, shown by Semenov (1969), Aggarwal et al., (1972), Whitcomb et al., (1973), Ohtake, (1973), Hasegawa et al., (1974), and Aggarwal et al., (1975), seems to be a pronounced effect of "dilatancy" in the region studied, and might be interpreted as the effect of the velocity variation between unsaturated and saturated states of the rocks in the dilatant volume. Dilatancy is the name given to the increase in volume resulting from a change in shape due to the formation and propagation of fractures caused by the build-up of tectonic stress.

#### 6.4 Relation between the Magnitude and Precursor Time

If it is true that there is a relation between the magnitude of an earthquake and the total potential energy stored in the crust and upper mantle rocks surrounding the epicentral region, then there should be a relation between magnitude and the dilatant volume. It might be expected that the time taken to accumulate sufficient energy to bring the epicentral region up to rupture level will be related to the size of the resulting earthquake. This time allows the fluid to flow into the fractures formed and re-saturate the rocks in the dilatant volume. Consequently, a larger pre-seismic time period implies a larger dilatant volume, which eventually will result in an earthquake of larger magnitude.

However, Tsubukawa (1969) seems to be the first to propose an empirical relation between the logarithm of the pre-seismic time period and the magnitude of the forthcoming event. He studied all the destructive earthquakes occurring in Japan during the present century, and showed the relation to be of the form:

$$\text{Log}_{10} t = AM - B$$

in which  $t$  is the pre-seismic time interval in days,  $M$  is magnitude, and  $A$  and  $B$  are constants. The coefficients  $A$  and  $B$  vary from region to region. Thus for Japan they are found to be 0.79 and 1.88, respectively, while for the events occurring during the Blue Mountain Lake, New York, earthquake swarm of 1971, Scholz et al., (1973), obtained the values 0.685 and 1.57.

Assuming the above relation to be the true one between the precursor time and magnitude, attempts have been made to evaluate the constants A and B for the Tehran region.

Accepting the time interval between the last normal value of  $V_p/V_s$  before the fall and its return to its normal value as the precursor time (see Figure 6-3) the following result was obtained:

$$\text{Log}_{10} t = 0.7 M - 1.4$$

This is very close to the result obtained by Whitcomb et al., (1973), for the events preceding the San Fernando earthquakes:

$$\text{Log}_{10} t = 0.68 M - 1.31$$

Other recently published results include

$$\text{Log}_{10} t = 0.76 M - 1.83$$

for Japanese earthquakes (Rikitake, 1975).

Extrapolating the above equations to higher magnitudes, they yield precursor times ranging from 5 to 13 years for a magnitude 7 earthquake and 23 to 84 years for magnitude 8. Variables such as pore pressure, fracture formation, range of rock velocities between the saturated and unsaturated states, fluid flow in the surrounding area, particularly the dilatant volume, and local structure, account for the wide variation in the estimate of precursory times. Also, it might be suggested that for a particular size of event, different earthquake mechanisms will affect different anomalous volumes. The

period of anomalous velocity and the magnitude of the subsequent events found in this study seem to be in good accord with those observed elsewhere, particularly with the results of Whitcomb et al., (1973), and Scholz et al., (1973), who also used microearthquakes.

Figure (6-4) illustrates the pre-seismic duration  $t$  as a function of magnitude  $M$  obtained from existing data from various parts of the world. It is interesting to note the close fitting of pre-seismic duration for the same magnitude, which suggests that the same mechanism operates in the various regions. The open triangles represent the results of the present study. The best-fitting line obtained by means of a least-squares regression, gives the magnitude-precondition time dependence as:

$$\text{Log}_{10} t = 0.73 M - 1.51.$$

The anomalous period of 10 and 56 years, for magnitude 7 and 8 respectively, found from the above relation seems to be in good accordance with that expected from the linear relation between magnitude and the logarithm of pre-seismic time duration obtained by other investigators (see above).

Results from natural earthquakes and explosions, as well as laboratory tests (e.g., Nur and Simmons, 1969) confirm that the decrease in the ratio  $V_p/V_s$  associated with the phenomenon known as "dilatancy" is mostly brought about by a reduction in  $V_p$ . During the decrease, both  $V_p$  and  $V_s$  drop, but the reduction of  $V_p$  is more significant because of a sudden decrease in the bulk modulus of the rock. When the dilatant fractures

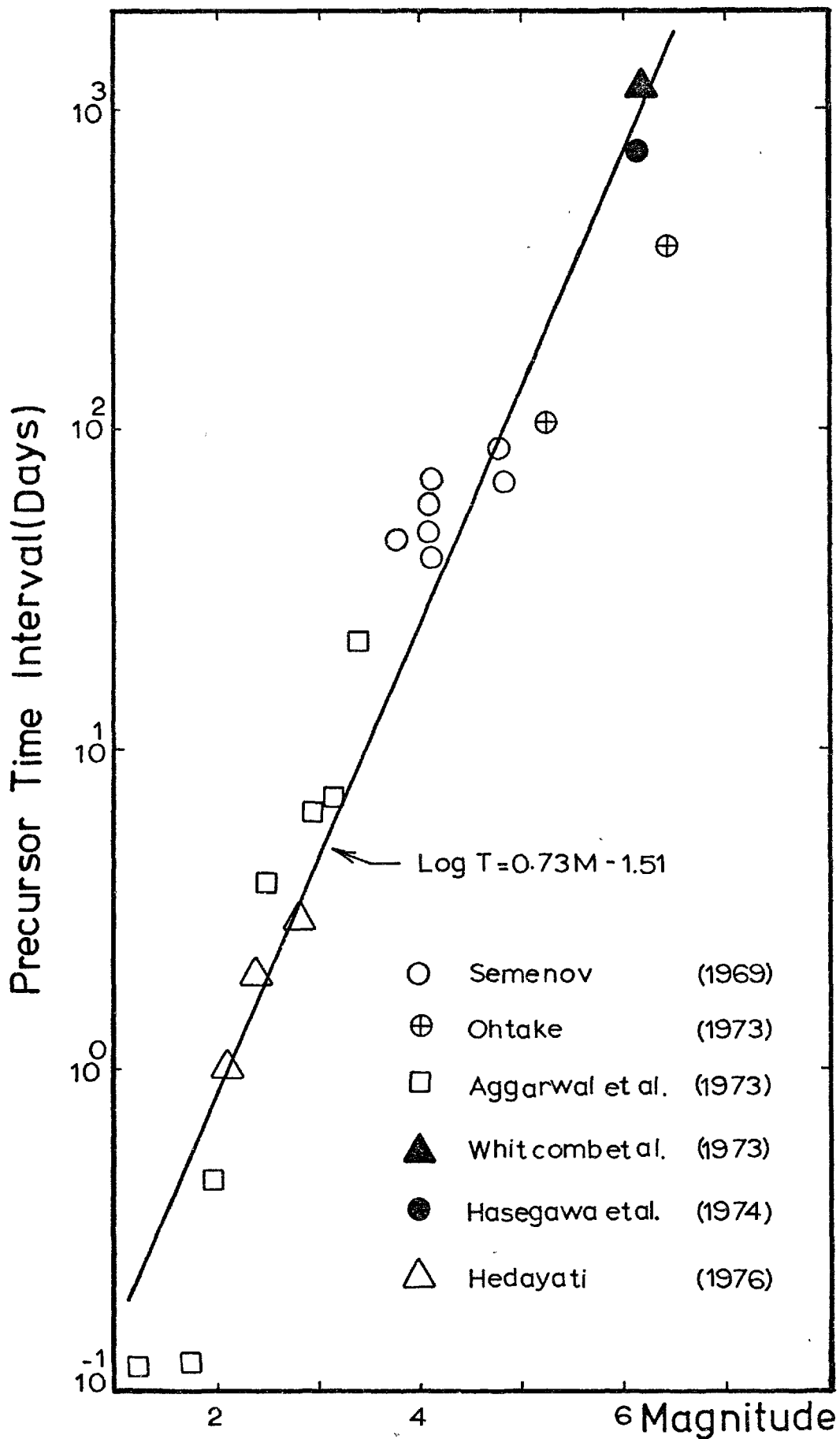


Fig. (6-4). Precursor time intervals versus magnitude, from existing data for various parts of the world.

eventually become filled with water under ambient pressure, the effect on the P-wave velocity will be small, whereas the S-wave velocity decreases remarkably. Therefore,  $V_p/V_s$  increases due to resaturation, the rock weakens (decreasing the internal friction), and an earthquake follows. According to Nur (1972) an increase of pore pressure in saturated rock causes a marked decrease in  $V_s$  and a small decrease in  $V_p$ , thus raising the ratio of  $V_p/V_s$ . On this basis, the high values of  $V_p/V_s$  (see Figure 6-3) found in the Tehran region might be due to an abnormally high pore pressure.

The results obtained in this study are in agreement with other works discussed above. By contrast, McEvelly and Johnson (1973), in a study of the records of more than 60 explosions in California, found no significant changes in the ratio of compressional to shear wave velocities. This negative result, which is mostly thought to be due to the location of events associated with the strike-slip type of fault, might be explained by their occurrence in a highly disturbed and anisotropic crustal structure beneath the epicenters, or could be indicative of a very shallow focal depth, for which premonitory changes have not been found significant in other parts either (Aggarwal et al., 1975). Also, the unvarying  $V_p/V_s$  values for this region could be indicative of some permanent fractures in the region, and therefore permanent dilatancy.

It seems, however, that the instability of  $V_p/V_s$  is a very promising technique for foreseeing the future activity of a region. The discovery of this variation of seismic body

wave velocities from the microearthquake survey in the Tehran region, strengthens the potential ability of the dilatancy effect to predict at least a certain class of earthquake.

Investigations of other phenomena associated with dilatancy, such as changes in ground elevation (see Figure 6-5 after Tsubukawa, 1964), ground tilt, electrical conductivity, etc., might reveal other precursory changes which could be used in long-term prediction.

#### 6.5 Dilatancy, and the Energy Released by Microearthquakes

Although it is true that the frequency of occurrence of earthquakes increases with decreasing magnitude (see chapter three), the energy dissipation of the individual shocks calculated from any given empirical formula converting magnitude to energy, decreases more rapidly. Consequently, most of the energy released in any region is derived from only a few shocks of higher magnitude.

The energy of all the earthquakes recorded during the Tehran survey has been calculated from the empirical relation given by Gutenberg and Richter (1954),  $\text{Log}_{10} E = 11.4 + 1.5 M$ , and is shown plotted cumulatively beneath the dilatancy curve in Figure (6-6). In support of the dilatancy idea, any drop and return to normal of the velocity ratio  $V_p/V_s$  (except on 7 December, when the events increased in number rather than magnitude) is accompanied by a release of a large amount of energy through the occurrence of small nearby earthquakes. If the accumulated energy released is converted back to magnitude, it gives an earthquake of equivalent magnitude about  $m_L = 3$  to 3.5. Therefore, the idea that small earthquakes can play an



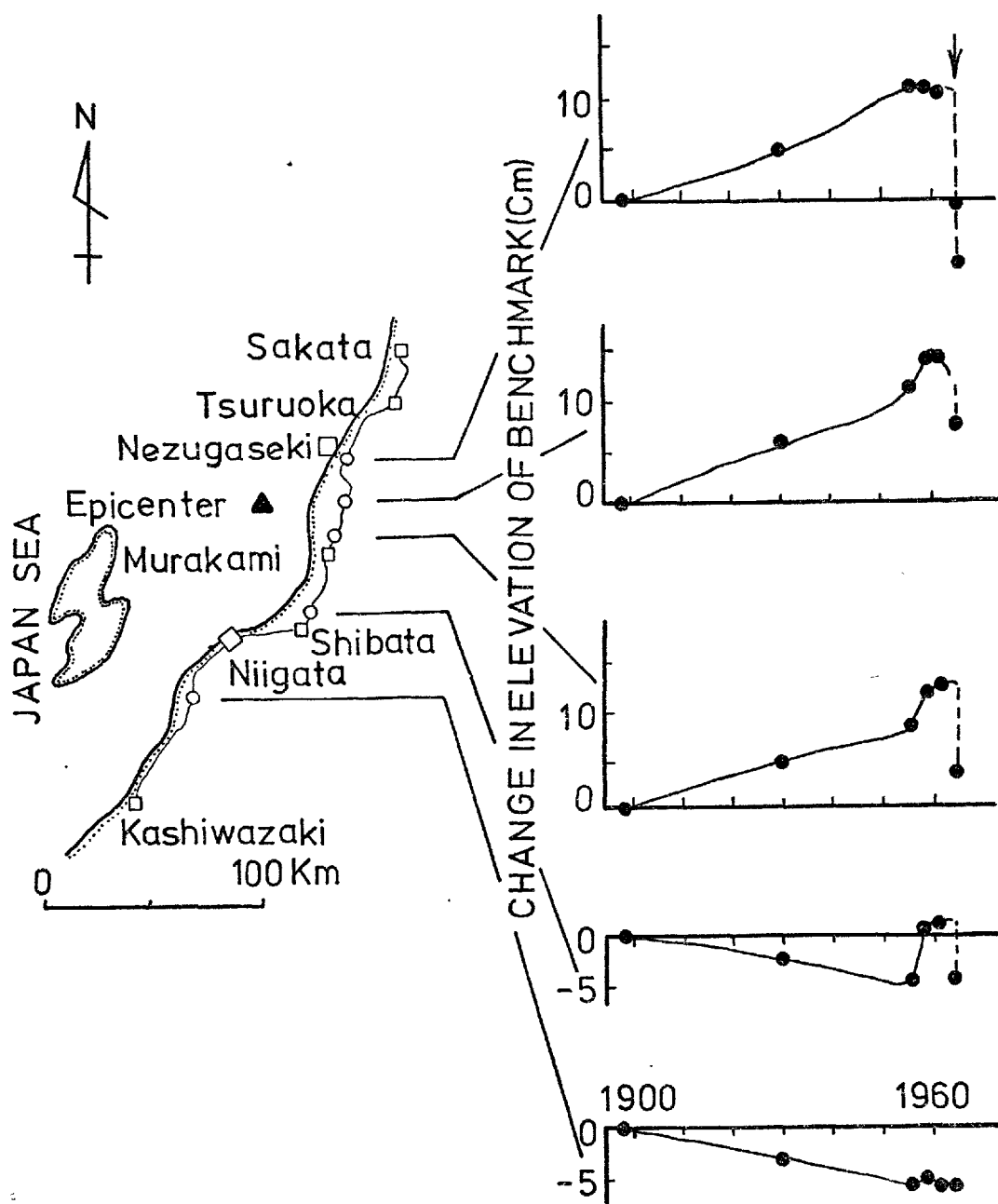


Fig. (6-5). Data from levelling at five locations near the epicenter of a 1964 earthquake in Japan. Arrow shows an abnormal rise in elevation of benchmarks before the occurrence of the shock (after Tsubokawa, 1964).

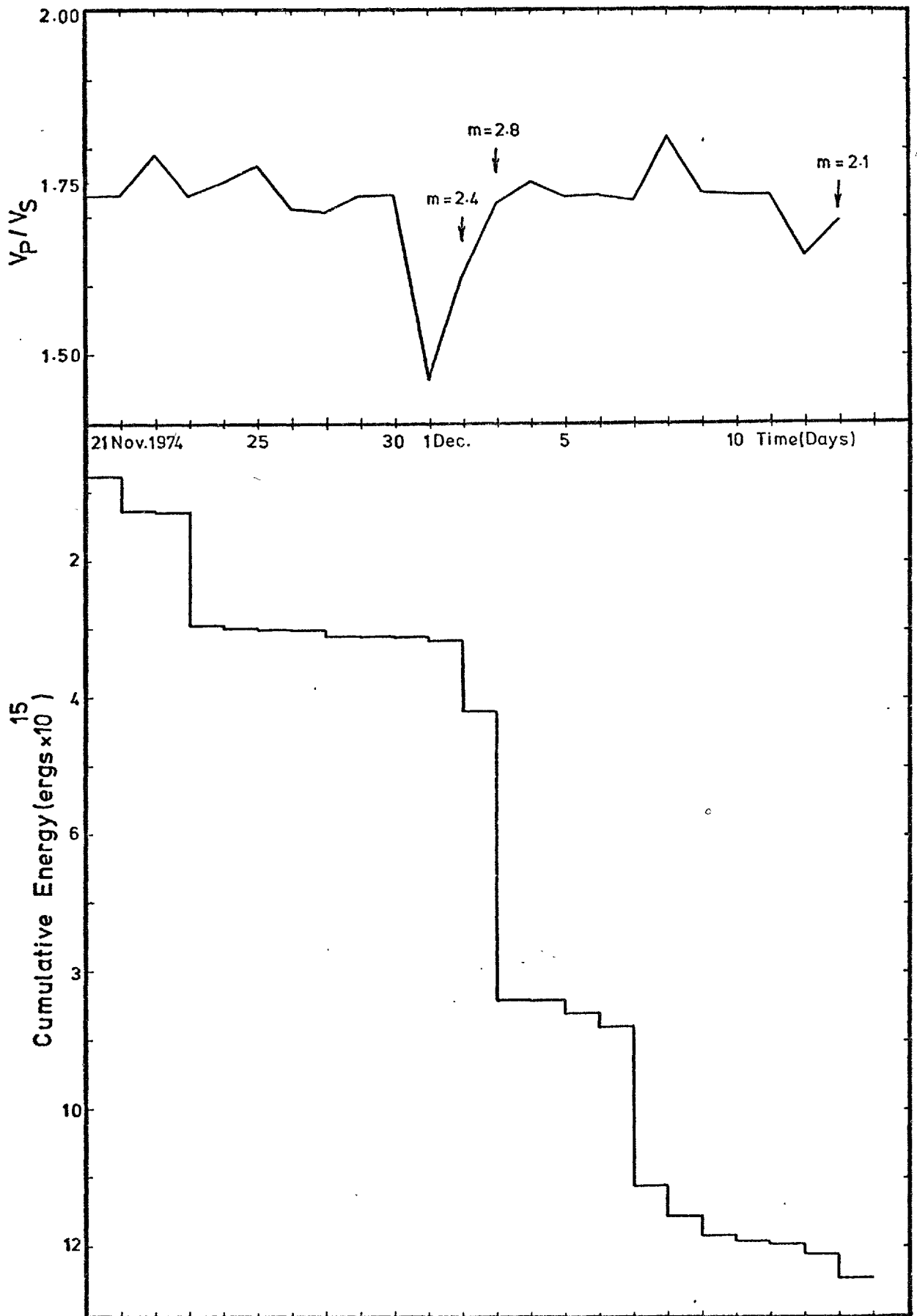


Fig. (6-6). Cumulative energy release versus time, with the dilatancy ( $V_p/V_s$ ) curve for comparison (for Tehran region).

important role, that of the so called "safety valve", by releasing a large amount of energy to reduce the harmfulness of destructive shocks, cannot be valid. The logarithmic relation connecting energy and magnitude implies that the major energy release will occur only in major earthquakes. Incidentally, it should be pointed out that microearthquakes are indicative of regional strain accumulation and show that the area is seismically active. However, although small local events whose frequency of occurrence is high relative to that of destructive ones might release enough strain to postpone a major event, nevertheless, when major strain is built up it can only be completely relieved by means of a big shock.

#### 6.6 Velocity Inversion within the Crust of the Tehran Region

Although the concept of velocity inversion in the crust was first invoked by Gutenberg (1950) on the basis of observations of earthquakes and explosions in southern California, the current interest in this question developed only from 1966. From a detailed study of the earth's crust, using artificial seismic waves, Muller and Landisman (1966) showed that the velocity decreases at a depth of about 6km and then abruptly increases at a depth of 10km, known as the Forsch discontinuity (Figure 6-7).

Berry (1972) provided evidence supporting the presence of velocity inversion in the crust. As an explanation of the low velocity layer he speculatively suggests that the presence of free water may be responsible.

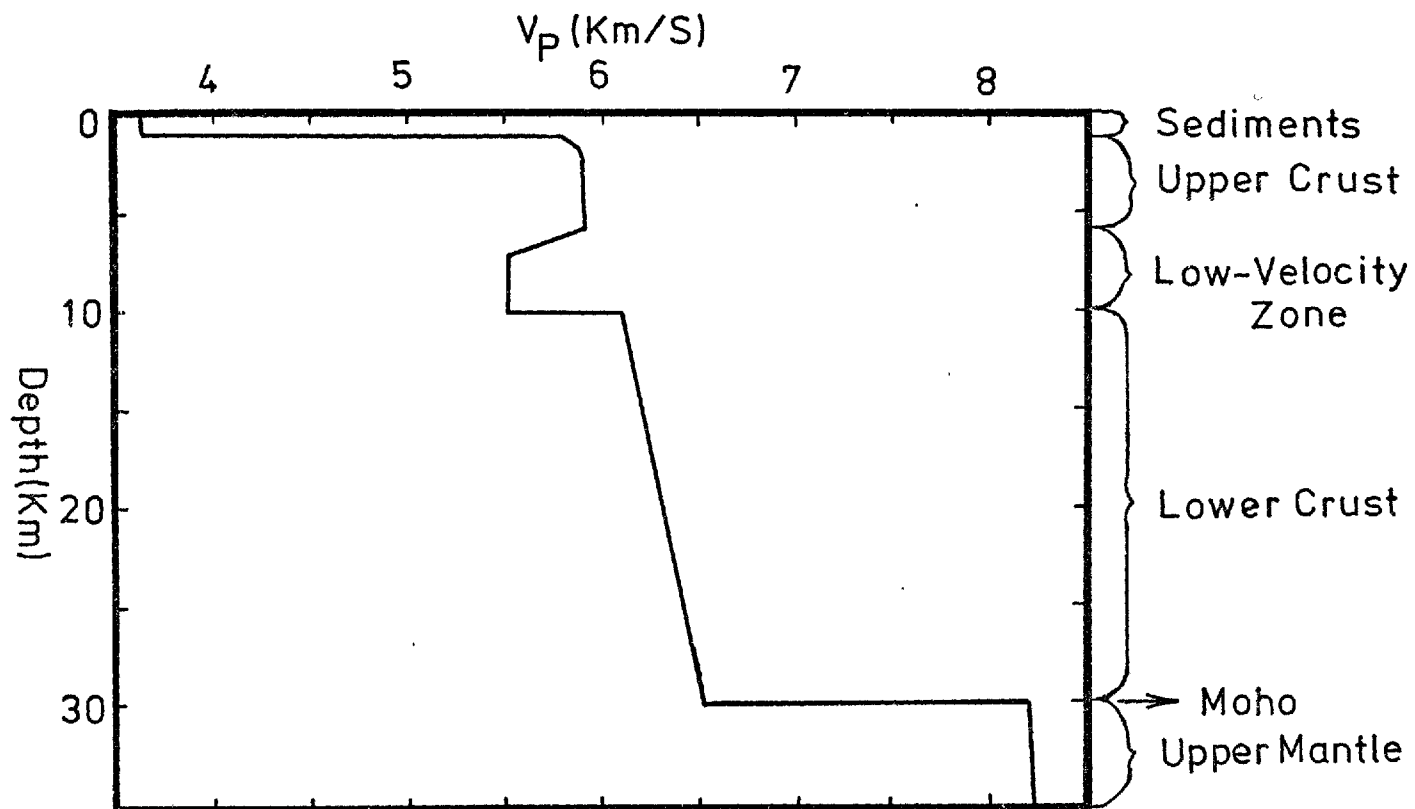


Fig. (6-7). P-wave velocity versus depth, showing the decrease of  $V_p$  at depth 6 km and the increase at depth 10 km, the Forsch Discontinuity (after Muller and Landisman, 1966).

Kosniskaya et al., (1972) observed the low velocity layer within the crust, but suggested that the boundaries cannot be represented in terms of the sharp laterally continuous discontinuities shown in Figure (6-7).

Fuchs and Muller (1971) compared synthetic seismograms with an observed one, obtained from refraction studies of the earth's crust and upper mantle, and showed not only the existence of velocity reversals in the upper crust, but also discovered a new discontinuity beneath the Mohorovicic at a depth of 35km, where the velocity drops to  $8\text{km}\cdot\text{Sec}^{-1}$ .

Following Gutenberg (1950), natural earthquakes have been used in the present study to investigate the existence of this particular feature in the crust of the Tehran region. The velocities at various depths (see chapter five) have been determined by measuring the slopes of the lines found by fitting a straight line, using a least-squares technique, to the plots of the arrival times versus epicentral distances. Figure (6-8) shows an example for determining the velocity at depth 18km. Figure (6-9) illustrates the plot of these velocities against depth. It is shown that a velocity reversal does exist in the region studied. The velocity decreases at a depth of 6km and then abruptly increases at the Forsch discontinuity, at a depth of 11km.

Rather high velocity at depths zero and 2km may be attributed to the existence of volcanic rocks, covering the Alborz Mountains, in which the seismic waves propagate faster than in the sediments. The relatively low value of the compressional wave velocity at depth 6km, compared with values

Fig. (6-8). P-0 time interval (sec) versus epicentral distance (km). Solid line is the least-squares fit to the data points. The reciprocal of the slope of the line is the velocity at 18 km depth.

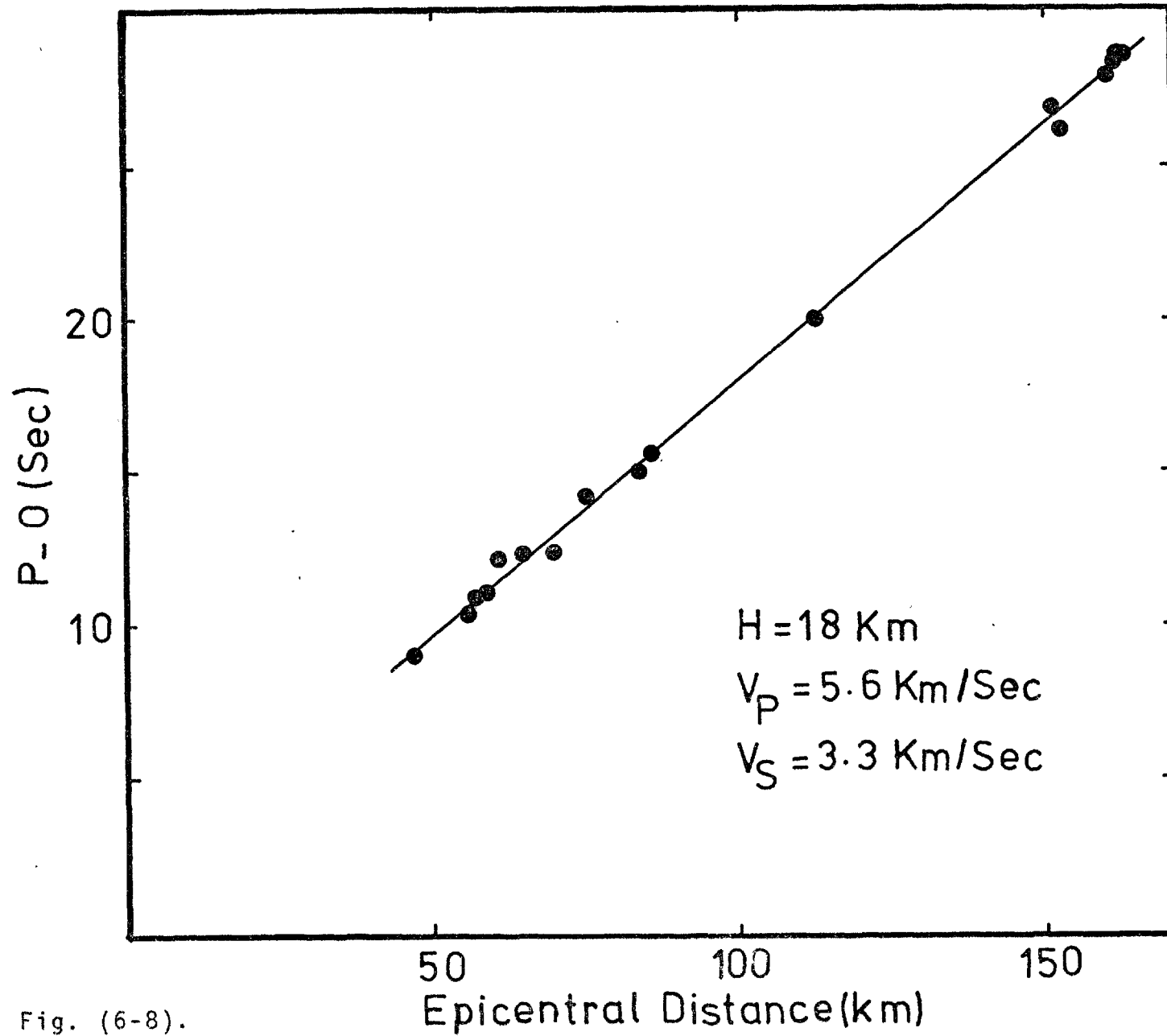


Fig. (6-8).

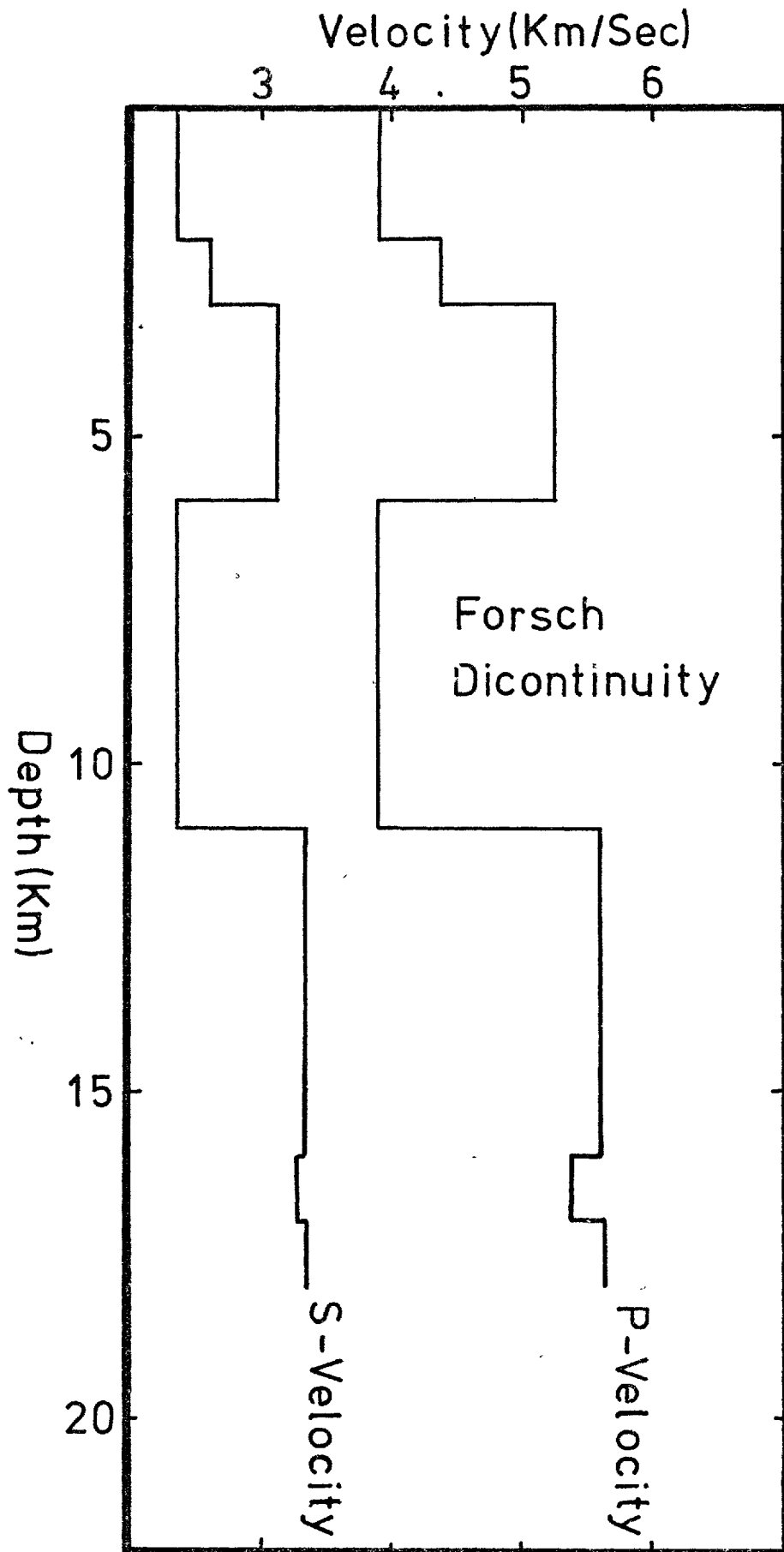


Fig. (6-9). P-and S-waves velocity versus depth. Note the decrease of velocities at depth 6 km and increase at 11 km.



elsewhere, might be indicative of the seismic waves travelling through a dilatant zone, which decreases the velocity more than normal at the Forsch discontinuity. It is interesting to note that the minimum value for the velocity ratio  $V_p/V_s$ , 1.46, occurs at this particular depth.

It seems from the results of microearthquake studies and explosion seismology, both of which have contributed greatly towards the solution of the problems related to the earth's crust, that the simple idea of subdivision of the continental crust into two layers (granite and basalt), separated by the so called Conrad discontinuity, is not valid.

## CHAPTER VII

GEOLOGICAL STRUCTURE, LARGE EARTHQUAKES AND  
TECTONICS OF THE TEHRAN REGION7.1 Introduction

Iran, particularly the Tehran region, with its very complex geological structure and young, mostly recent, tectonics seems at first sight to be an ideal place for studying the relationship between earthquake activity and the structural framework. However, the last devastating earthquakes that occurred in the region showed that it is by no means easy to relate the seismic activity to the known geological features.

During the 20th century, earthquake activity in Iran as a whole, and especially in the Tehran region, seems to have increased in frequency as well as in magnitude. Considering the Alborz Mountains to form an east-west range across northern Iran south of the Caspian Sea, constituting the northern part of the Alpine-Himalayan Orogen, the region might be designated as one of the most active areas in the world.

On the north, the Alborz Mountains face the Caspian Sea Depression, while the Dasht-e-Kavir (Desert) of Central Iran forms the southern boundary of the range. The range has a long tectonic history continuing up to the Mesozoic and Tertiary (Stocklin 1968, 1974 and National Iranian Oil

Company, 1959). The southern margin of the Mountains consist of a heavily tectonised area, and major faults, such as the Musha-Fasham and the North-Tehran Faults, form the boundary between the Alborz and the Dasht-e-Kavir. Despite the presence of the tectonically active central part of the Alborz Mountains in between, tectonic activity decreases steadily towards the Caspian Sea Depression in the north (Gansser, 1969).

The Alborz Belt as a whole is the result of two great orogenies, the Pre-Cambrian and the Alpine, of Mesozoic-Tertiary age (Stocklin, 1974). The orogeny in the Alborz Range is closely related to the metamorphism which resulted from the consolidation of the Pre-Cambrian basement during the northern extension of the Arabian Shield between the Infra-Cambrian and Triassic.

According to Stocklin (1974) the last tectonic movement affecting north central Iran took place in the late Pliocene or early Pleistocene, resulting in folding, faulting and further elevation of the Alborz. Volcanic activity is a characteristic tectonic feature from Post-Eocene to Quaternary. The extinct Quaternary volcano, Mount Damavand, the highest peak of western Asia, is situated in the central Alborz Mountains, near the point where the WNW strike of the Range changes rather sharply to ENE direction.

Considering the above-mentioned complicated structural features of the Tehran region, the occurrence of frequent, large magnitude earthquakes is to be expected. With the present knowledge of the geology of the area, epicentral

locations can be related to the geological structure in a broad sense. In the following section, an attempt will be made to relate the surface indications of seismic activity to known geological features.

## 7.2 Large Events in the Tehran Region

Within the last 50 years there has been a notable increase in the seismic activity of the area, and it seems that recently earthquakes of larger magnitude have occurred more frequently. Eight areas which have suffered the effects of big earthquakes are, Mobarakabad (1930), the Central Alborz (1935), Garmsar (1945), Torud (1953), Buyin-Zahra (1962) and Babol Kenar (1971). These areas are shown in Figure (7-1).

### (a) The Mobarakabad Earthquake of October 1930

Mobarakabad, a village some 60 Km east of Tehran, was shaken by an earthquake on 22 October, 1930. According to the International Seismological Summary (ISS) the epicenter was situated at  $35.8^{\circ}\text{N}$ ,  $52.1^{\circ}\text{E}$ , and the average magnitude was estimated to be 5 (table 7-1). It cost three lives and caused some damage to property. In spite of its relatively low magnitude, the earthquake should be considered important, since it is evidence for the reactivation of the Musha-Fasham Fault, which is so near to the city of Tehran itself.

### (b) The Alborz Earthquakes of March and April 1935

The first earthquake occurred on 5 March, 1935. Its location determined by the ISS was  $36.2^{\circ}\text{N}$ ,  $53.0^{\circ}\text{E}$ , and its magnitude around 6 (table 7-1). This event, which was

Fig. (7-1). Map showing the instrumentally recorded destructive earthquakes of the Tehran region. BZF: Buyin-Zahra Fault; NABF: North Alborz Boundary Fault; NTF: North-Tehran Fault; MFF: Musha-Fasham Fault; GKF: Great Kavir Fault.

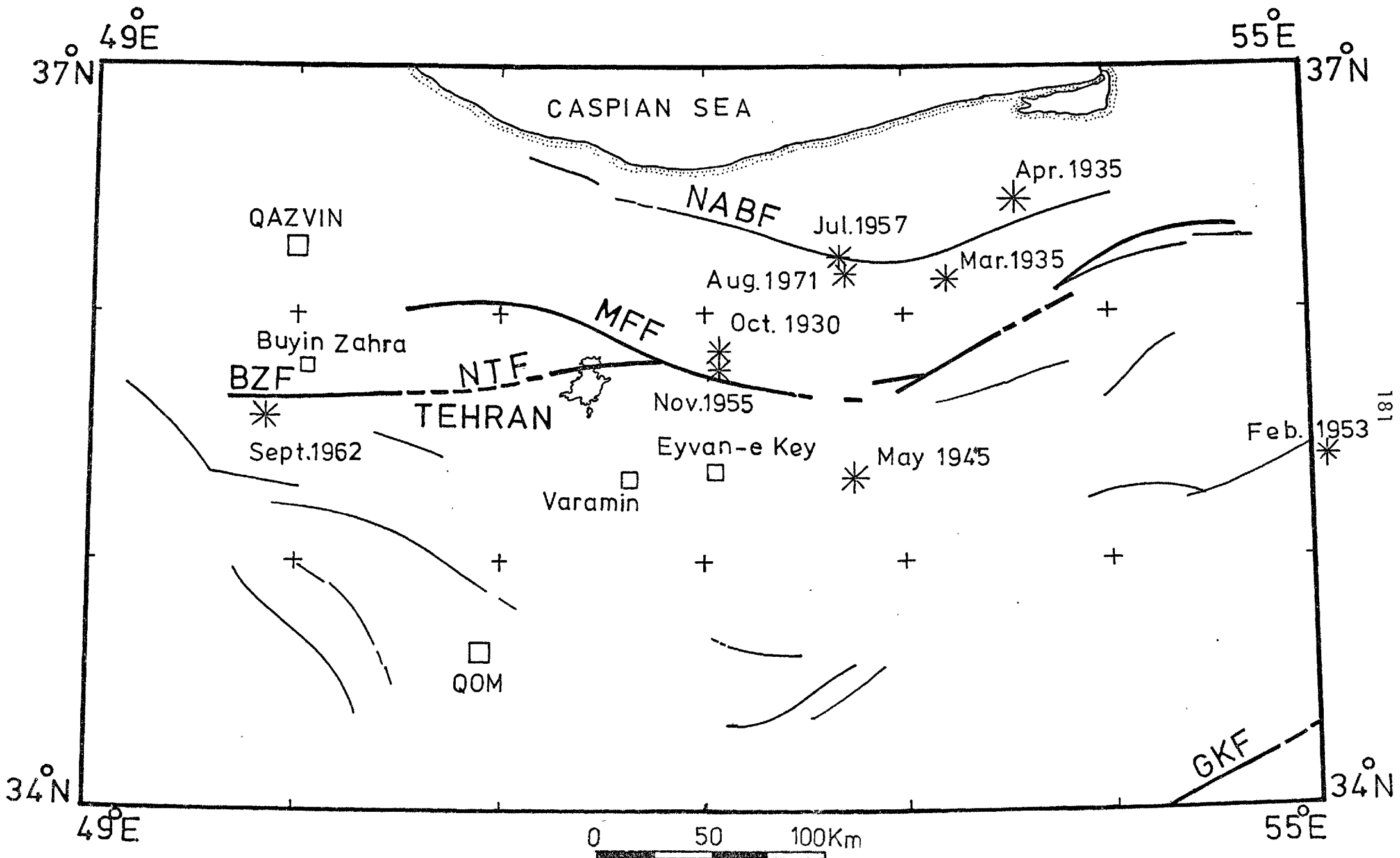


Fig. (7-1).

followed by a more severe one on 11 April, 1935 at  $36.3^{\circ}\text{N}$ ,  $53.5^{\circ}\text{E}$  with a magnitude of  $6\frac{3}{4}$  (table 7-1), caused heavy damage and the death of more than 550 persons. The affected area is some 200 Km northeast of Tehran.

(c) The Garmsar Earthquake of May 1945

The epicentral location of the Garmsar earthquake which occurred on 11 May, 1945 is given as  $34.8^{\circ}\text{N}$ ,  $52.1^{\circ}\text{E}$ , and it was of magnitude 5 (table 7-1). The shock destroyed many houses in Garmsar and the surrounding area, but no loss of life. The epicenter of this earthquake is about 150 Km south east of the city of Tehran.

(d) The Torud Earthquake of February 1953

This earthquake, which occurred in the Kavir, was given the name of Torud, from the nearest town, and was located by ISS at  $35.8^{\circ}\text{N}$ ,  $55^{\circ}\text{E}$ , having magnitude about 6.5 (table 7-1). Over 900 people were killed and the survivors suffered much property damage. The epicenter was located some 300 Km east of Tehran.

(e) The Musha Earthquake of November 1955

A small earthquake occurred on 24 November, 1955, near Musha village, and damaged most of the houses. According to the Institute of Geophysics of Tehran University (1966) the epicentre was located at  $35.8^{\circ}\text{N}$ ,  $52.1^{\circ}\text{E}$ , about 60 Km north-east of Tehran. This earthquake, and preceding Mobarakabad event of 1930, are suggestive of the reactivation of the Musha-Fasham Fault, and probably its branches also.

(f) Sang-e-Chal earthquake of July 1957

This shock, which destroyed Sang-e-Chal and its surrounding villages, took place on 2 July, 1957. The epicentral location was determined as  $36.1^{\circ}\text{N}$ ,  $52.7^{\circ}\text{E}$ , and the focal depth was 10 Km. The estimated magnitude was 7.4. The epicentral region of this event covered an inaccessible area of the Alborz Mountains. The total number of fatalities, according to the Persian Press, exceeded 1000.

(g) The Great Buyin-Zahra Earthquake of September 1962

The region which was devastated by the Buyin-Zahra earthquake of September 1, 1962 had been quiet at least from the beginning of the present century. The earthquake, which had an average magnitude of  $7\frac{1}{4}$  and was located by ISS at  $35.58^{\circ}\text{N}$ ,  $49.88^{\circ}\text{E}$ , destroyed the epicentral region and cost more than 12,000 lives (Ambraseys, 1963). It seems that after the nine months for which the aftershock activity lasted, the seismic activity migrated towards Tehran and the southern Alborz (Tchalenko 1974).

(h) The Babol Kenar Earthquake of August 1971

This earthquake, which was felt over most of north central Iran, was located some 150 Km north-east of Tehran. The instrumental location given by the USCGS was  $36.2^{\circ}\text{N}$ ,  $52.7^{\circ}\text{E}$ , with a focal depth of 27 Km. The average magnitude was 5.2 (table 7-1) and it caused much loss of property and the loss of one life (Tchalenko, 1974).



Table 7.1

## Instrumentally destructive earthquakes of Tehran region

Earthquake	Date			Origin Time			Location		Magnitude	Depth (Km)
	D	M	Y	H	M	S	Lat(N)	Long(E)		
Mobarakabad	02	10	1930	15	33	09.7	35.86	52.08	$5\frac{1}{4}$ - $5\frac{1}{2}$	33
Alborz	05	03	1935	10	26	40.5	36.15	53.35	$5\frac{1}{2}$ - $5\frac{3}{4}$	33
Alborz	11	04	1935	23	14	48.4	36.47	53.56	$6\frac{1}{2}$ - $6\frac{3}{4}$	33
Garmsar	11	05	1945	20	17	35.3	35.34	52.75	$4\frac{3}{4}$	33
Torud	12	02	1953	08	15	29.9	35.40	55.08	6.5	00
Musha	24	11	1955	--	--	--	35.8	52.1	--	--
Sang-e-Chal	02	07	1957	00	42	23.0	36.14	52.70	7.4	10
Buyin-Zahra	01	09	1962	19	20	39.0	35.59	49.85	$7\frac{1}{4}$	21
Babol Kenar	09	08	1971	02	54	36.7	36.2	52.7	5.2	27

It would appear from Figure (7-1) that very few of these recent destructive earthquakes are directly associated with the main surficial structure of the region. However, this may be due to poor epicentral location, resulting from the poor distribution of seismograph stations in Iran, particularly in the region under investigation, and to the lack of a satisfactory value for crustal velocity. The location of the earthquakes in this region depends principally on distant stations, and as a consequence the depth control on the hypocentral parameter is poor and unlikely to be reliable to better than 50 Km (McKenzie, 1972).

Because of these difficulties, and because it is only since the establishment in the 1950's of high density seismic networks that epicentral locations have been reliable enough for conclusions to be drawn about the tectonic activity of a region, conclusions drawn from earlier data should be considered suspect.

In the Tehran region in particular, because of the small number of large magnitude earthquakes that have occurred since 1950, it seems that microearthquakes offer the only reliable means of discovering the mechanism of current tectonic activity.

### 7.3 Composite Fault Plane Solution

An important application of observational seismology is in the determination of the mechanism of earthquakes, which in turn provides information about regional tectonics. Studies of the radiation patterns of P-wave first motions initiated

by Byerly (1926, 1928) were one of the first steps in the development of what is now known as the fault plane solution technique for determining the focal mechanism of earthquakes, using seismograms.

Byerly's ideas were later extended to other phases of the arrival waves in an attempt to resolve the ambiguities inherent in the use of P-waves alone. Thus Adams (1958), used S-wave data to evaluate the mechanism of the August 5, 1949 earthquake in the Adens region of Central Ecuador, and the August 6, 1949 earthquake in the Tonga Islands region.

In some cases where P-wave data is lacking, or inadequate for obtaining a satisfactory solution, it may be possible to use indirect phases, for example reflected waves such as pP, particularly for earthquakes of intermediate depth. Hedayati and Hirasawa (1966) showed, in a study of the Hindu Kush earthquake of January 28, 1964, that the use of pP, in combination with P, led to the same stress field as was obtained independently using S only. Other phases have also been used, such as surface waves (Aki, 1966; Filson and McEvelly, 1967), but the P-wave radiation pattern still seems to be the most reliable for investigating fault plane movement, particularly for shallow earthquakes (e.g. Stauder, 1960; Sutton and Berg, 1958; Niazi, 1969).

A recent development of the fault plane solution, uses the radiation pattern from a number of microearthquakes occurring on the same fault and recorded at a small number of stations, rather than the pattern from one large earthquake recorded at a large number of stations. This is known

as a composite fault plane solution\*. The technique requires for its validity that earthquakes originating from the same area have identical mechanisms. The necessary distribution of the points on the focal sphere projection can be obtained provided that earthquakes are distributed along a section of fault which is long in comparison with the recording array dimension. Thus, to fulfil the requirement that the mechanism of all the earthquakes be the same, it is necessary to have a small array, unless the fault happens to be entirely homogeneous over long distances. If the earthquakes are coming from a source which is a point in relation to the size of the recording array, then the seismographs must be moved regularly in order to ensure good azimuthal distribution on the focal sphere projection (Hedayati and Hedayati et al. 1976). If these conditions are met, the composite fault plane solution will give the same result as a conventional fault plane solution obtained from the recording of a single event at many stations.

### 7.3.1 The Technique

The number of microearthquakes and their distribution in the Tehran region stimulated an attempt to construct composite fault plane solutions for groups of events which were well recorded and located. The technique has been successfully used by other investigators (e.g. Scholz et al. 1969; Seeber et al. 1970; Crosson, 1972; Hedayati and Hedayati et al.

---

\*The derivation of fault plane solution is a complicated geometrical matter and will not be explained here. The reader might care to refer to Honda (1962).

1976). The method consists of projecting back the polarity of the P-arrivals of each event at each station to the focal sphere, assuming that the mechanisms of a number of small nearby earthquakes are the same. To do this, it is necessary to calculate the take-off angle, the angle at which a ray travelling to a given point leaves the hypocenter, which in turn requires a knowledge of the velocity structure in the hypocentral region.

In the present case, because of short epicentral distances and shallow depths of the events, it has been assumed that the velocity structure can be adequately represented by a continuous model consisting of a linear increase in the velocity with depth (Crosson, 1972). The expression used,

$$V = 3.46 + 0.113 H$$

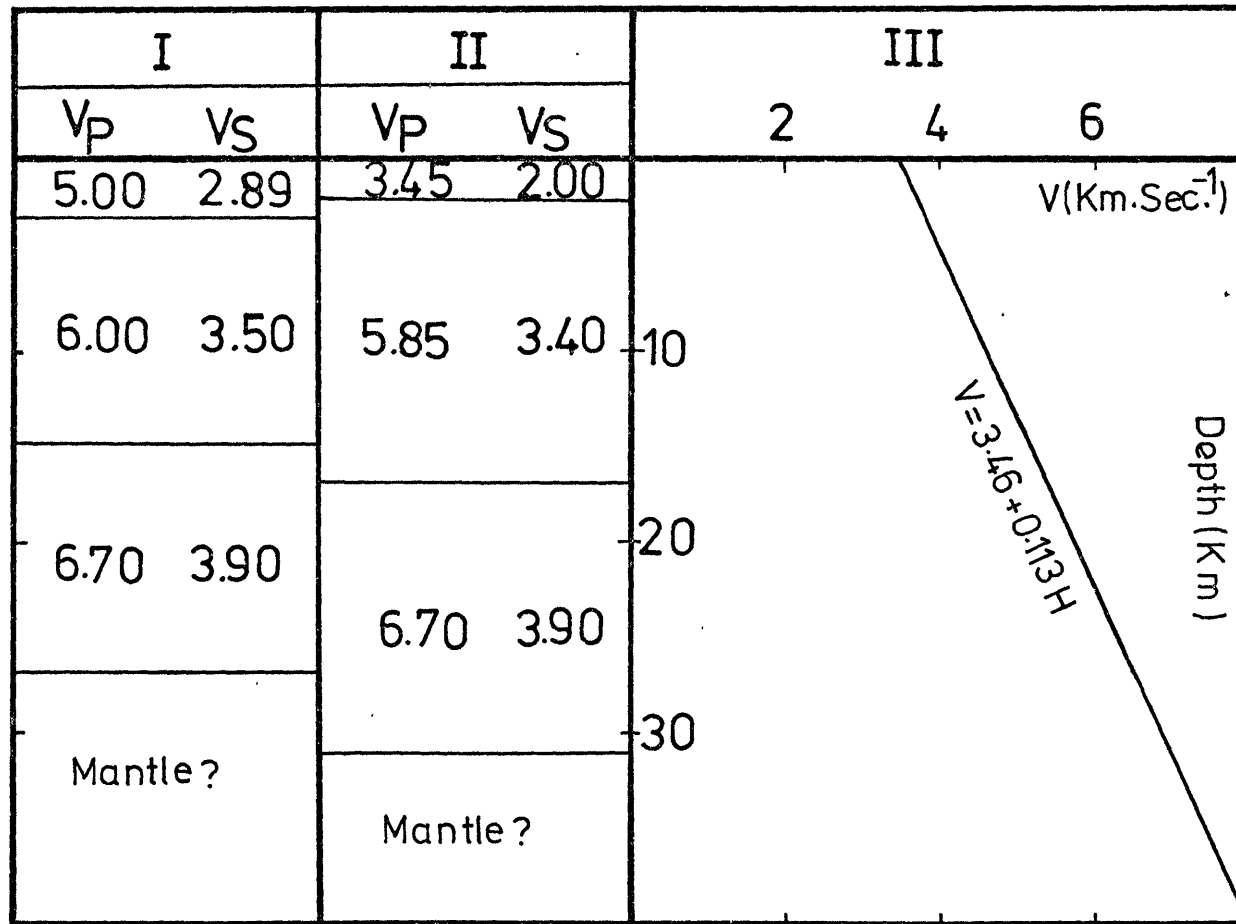
was derived from the least-squares fit to the velocity versus depth structure found from the hypocentral determinations. In this relation, which is plotted in Figure (7-2),  $V$  is velocity and  $H$  the depth.

In a study of microearthquakes in the Puget Sound region, and their relation to tectonic movement, Crosson (1972) used the relation:

$$\tan \theta = \frac{D^2 - 2HV/a - H^2}{2D(H + V/a)}$$

where  $\theta$  = take-off angle

Fig. (7-2). Linear relation between the velocity and depth derived from the least-squares fit to the layered velocity structure versus depth. CFPS: Composite fault plane solution.



I: After Mohajer Ashjai (1975)

II: Used in this study for locating events

III: Linear approximation to II used in CFPS

Fig. (7-2).

D = epicentral distance

V = velocity

H = focal depth

a = coefficient of linear velocity relation

This relation is based on the assumption of a linear variation of velocity with depth, and has formed the basis of a computer program, written by the author, which has been used throughout this study for calculation of take-off angles. Composite fault plane solutions were made for the three groups of events recorded by the 1974 survey. These three groups are associated with the activity of the Musha-Fasham Fault and the newly discovered Rey-Lineation.

All projections are made to the lower half of the focal sphere and plotted on a Wulff-Net stereographic projection. Figures (7-3), (7-4 a and b), and (7-5) show the radiation patterns of the detected P-waves. In these figures, compressions and dilatations are symbolized by solid and hollow circles respectively. The triangles show emergent onsets for rays originating close to one of the nodal planes.

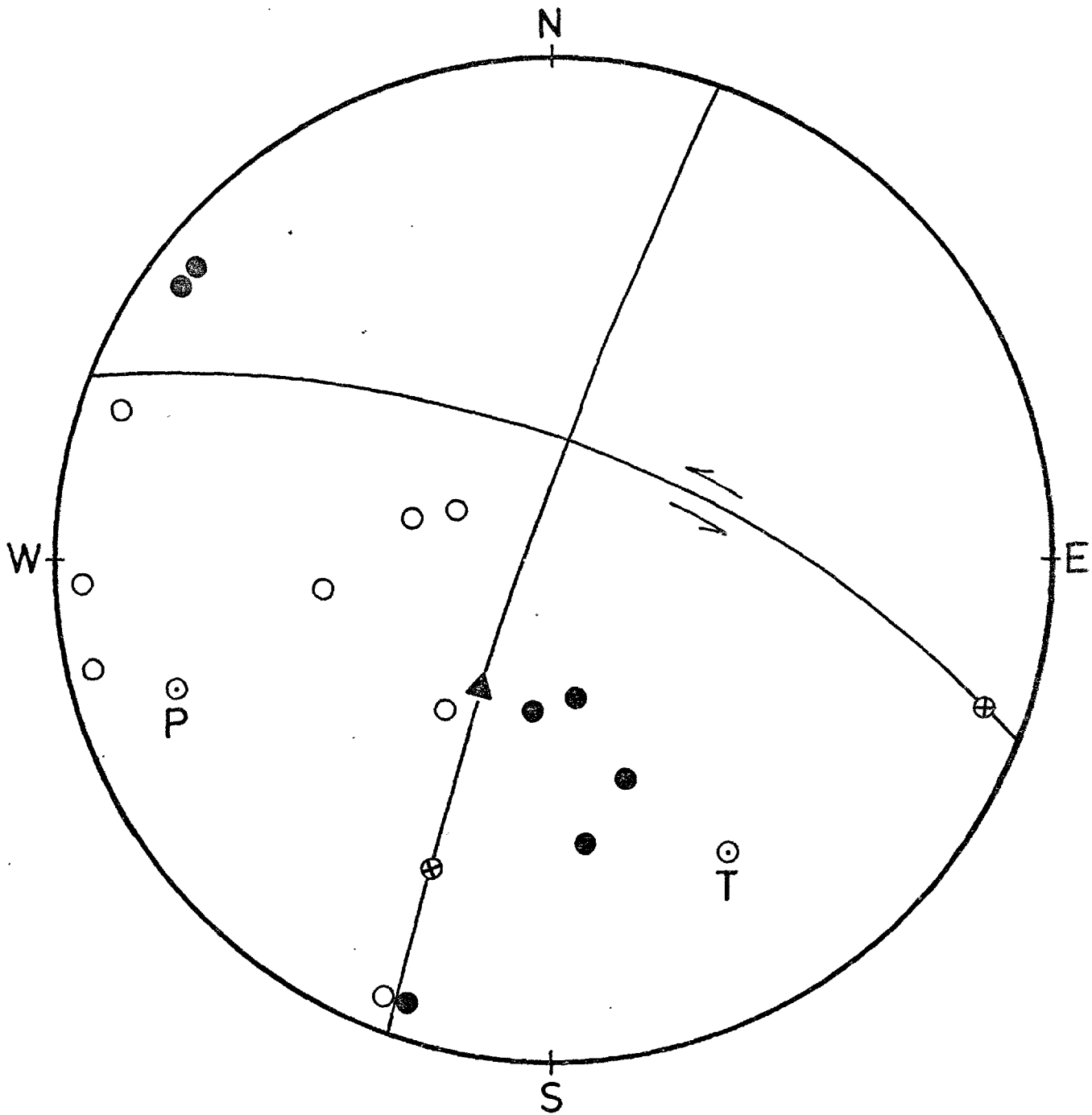
### 7.3.2 The Results

Owing to the preliminary nature of the 1974 survey, using only vertical seismometers, only P-wave first motions were consistently available. The polarity data were carefully interpreted when the seismograms were read. All the trace polarities were initially verified carefully against the background noise.



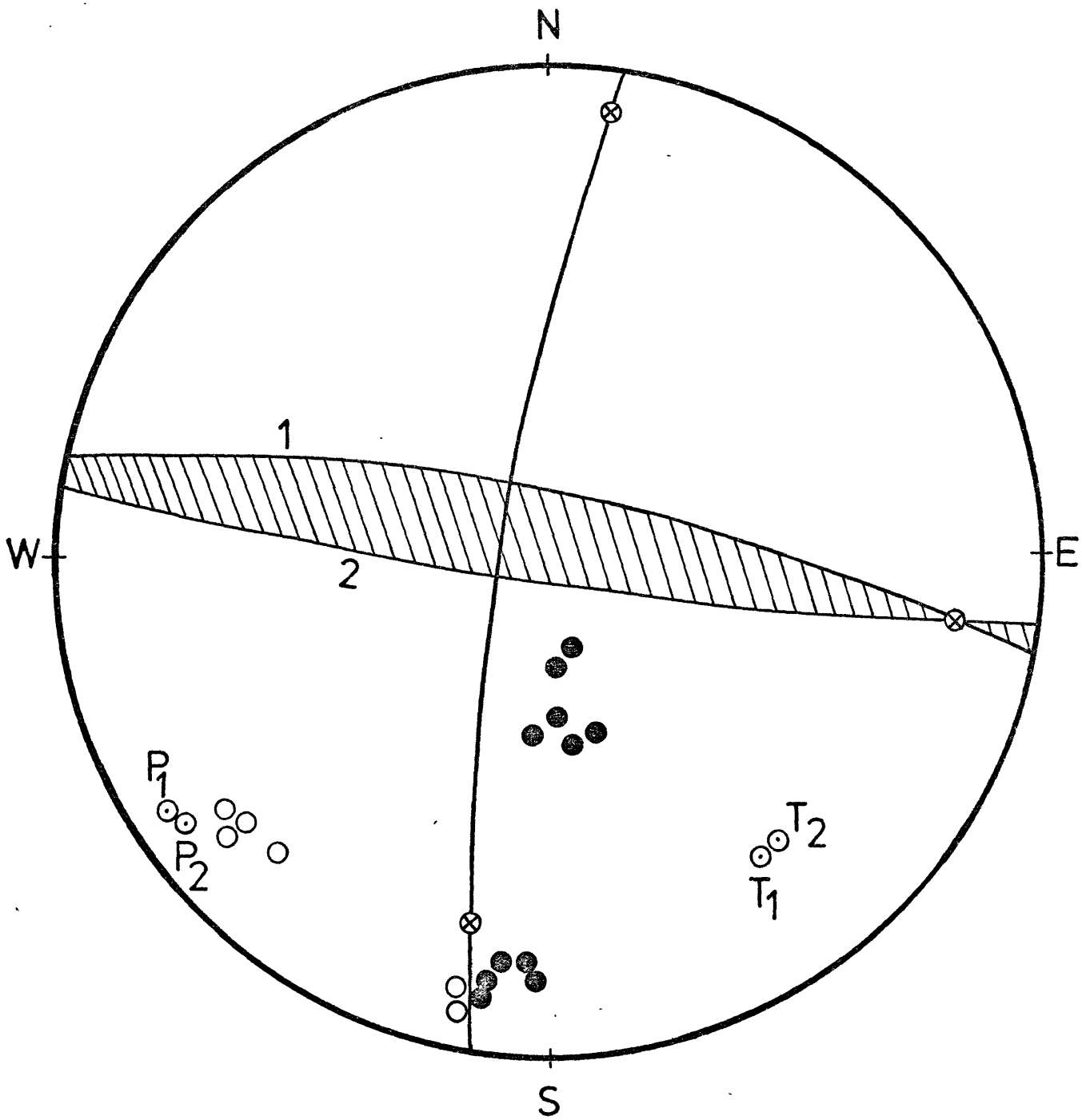
Sixteen first motion polarities of the P-arrivals from the easterly group (group one) consisting of seven microearthquake on the Musha-Fasham Fault (see chapter five) are plotted in figure (7-3). The resulting composite fault plane solution shows the nodal planes striking at  $N 21^{\circ} E$  and  $N 111^{\circ} E$ , with dip directions of  $N 72^{\circ} W$  and  $N 21^{\circ} E$  and dipping  $84^{\circ} NW$  and  $64^{\circ} NE$  respectively. The strike of the fault where the epicenters cluster is  $N 113^{\circ} E$ , and the dip about  $70^{\circ} NE$  (Tchalenko et al., 1974). Therefore, the second plane, because of its close agreement with the surface fault trace, is identified as the fault plane. In this case, the mechanism is left-lateral strike-slip, with some degree of thrust movement. The principal axes of compression and tension indicated by this solution are  $N 65^{\circ} E$  and  $N 155^{\circ} E$  plunging  $14^{\circ} SW$  and  $21^{\circ} SE$  respectively.

Figures (7-4 a and b) show the polarity distribution of sixteen detected P-wave first motions from the six microearthquakes further east on the Musha-Fasham Fault (group two). One of the nodal planes, whose strike is  $N 09^{\circ} E$  and dip  $80^{\circ} NW$ , is well defined, but two possibilities exist for the second nodal plane. The first, Figure (7-4 a), has a strike of  $N 99^{\circ} E$  and near-vertical (within fifteen degrees either way) dip. The second, Figure (7-4 b), has a strike of  $N 30^{\circ} E$  (also within fifteen degrees) and dip  $10^{\circ} NE$ . The first combination of nodal planes indicates a strike-slip mechanism very similar to that obtained from the first group on the Musha-Fasham Fault, the second indicates high angle reverse or thrust faulting, depending upon which plane is chosen to represent



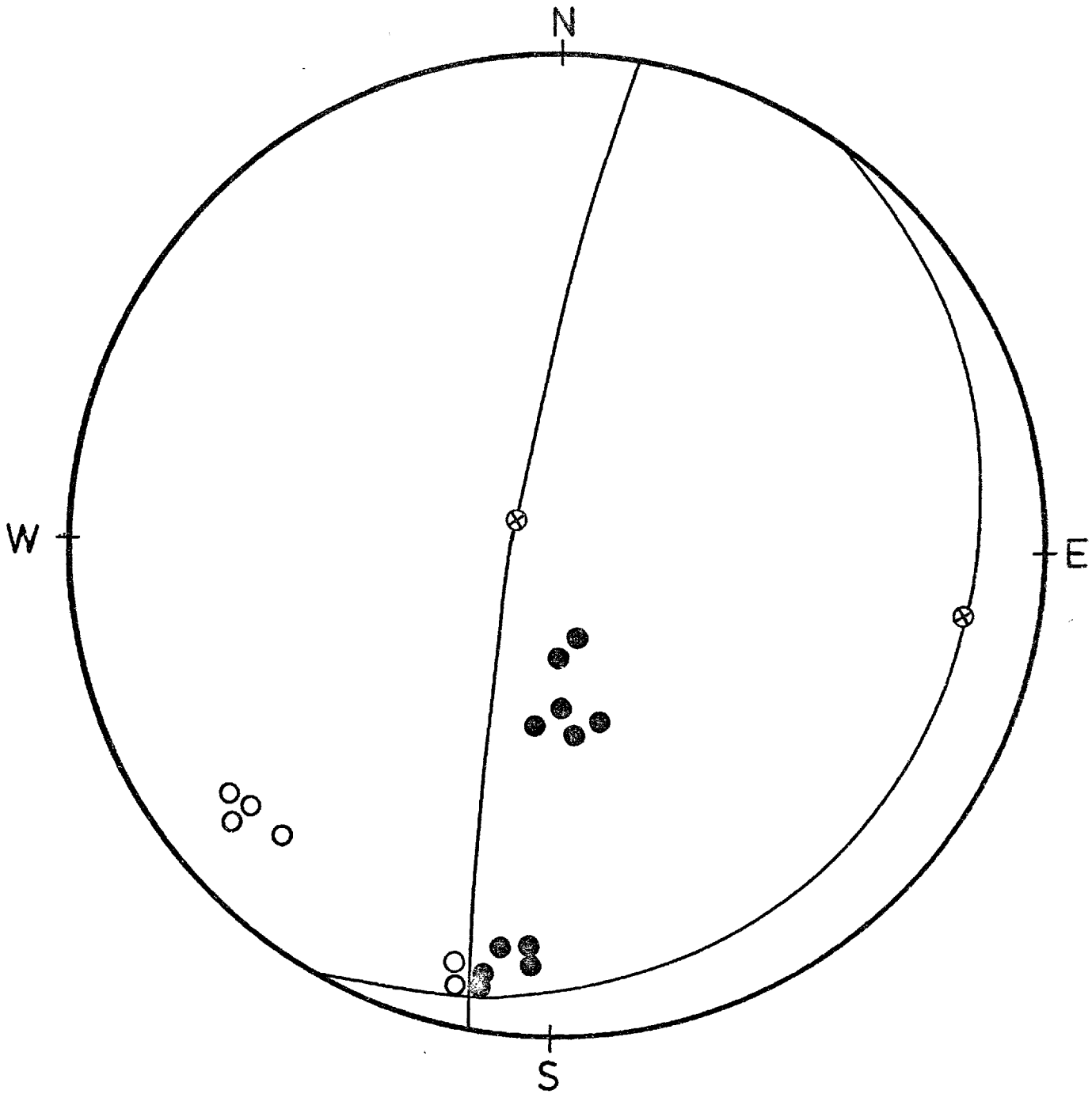
- Compression
- Dilatation
- ▲ Emergent
- Pole of nodal plane
- ⊙ Stress axes

Fig. (7-3). Composite fault plane solution from the easterly group of earthquakes associated with the Musha-Fasham Fault (group one).



- Compression
- Dilatation
- ⊗ Pole of nodal plane
- ⊙ Stress axes

Fig. (7-4a). Composite fault plane solution of group two of the earthquakes associated with the Musha-Fasham Fault.



- Compression
- Dilatation
- ⊗ Pole of nodal plane

Fig. (7-4b). Composite fault plane solution of group two of the earthquakes associated with the Musha-Fasham Fault, showing an alternative nodal plane.

the fault. In fact, on geological grounds it is highly unlikely that either of the second pair of planes represents the fault, since no fault in that area has the necessary strike. The Musha-Fasham Fault in that area with which this group of epicenters seems to be associated, strikes  $N 100^{\circ} E$ , which is in excellent agreement with the uncertain plane in Figure (7-4 a), consequently identified with the fault. Thus the mechanism, as in the first group, is sinistral strike-slip, with some degree of reverse movement. In this case the stress axes of compression and tension found for the first solution (Figure 7-4 a) are  $N 55^{\circ} E$ , and  $N 145^{\circ} E$  plunging  $5^{\circ} SW$  and  $17^{\circ} SE$  respectively.

Shirokava (1962 and 1967) using data from the Seismicity of the Earth (Gutenberg and Richter, 1954), the Bulletin of Seismic Stations of the USSR, and the BCIS\* Bulletin, for the period 1904 to 1960, made a thorough study of the tectonics of the Mediterranean-Asian region. Even though the early epicentral locations by Gutenberg and Richter (1954) were not accurate enough to enable definite conclusions to be reached about the active belts and tectonics of the region, the result from the fault plane solutions by Shirokava for the northern part of Iran shows excellent agreement with that of the tectonic structures. Her mechanism solutions for the events in the Tehran region are indicative of a thrust component as well as strike-slip displacement.

---

\* Bureau Central International de Seismologie, Strasbourg, France.

Nowroozi (1971) studied the seismotectonics of the Persian Plateau and its surrounding areas and showed that the direction of the relative movement on the Musha-Fasham (Shahrud Fault) is left-lateral. On the basis of the re-located epicenters between 1950 and 1965, he concluded that the southern margin of the Caspian Sea along the Alborz Mountains behaves as an active zone, joining the Anatolian Fault in the west to the NW-SE Zagros Mountains bordering the Persian Gulf.

Ambraseys (1963) showed from field observations that displacements resulting from the great Buyin-Zahra earthquake of September 1, 1962, were 51 cm left-lateral and 76 cm vertical respectively. In chapter two there was shown, from the satellite photograph interpretation, the possibility of the eastwards continuation of the Buyin-Zahra Fault to join the faults forming the southern boundary of the Alborz, so that here is indirect field confirmation of at least some left-lateral movement on these faults.

Berberian (1971), in a report on the structural analysis of the Buyin-Zahra Fault concluded that the stresses responsible imply a sinistral sense for the recent movements on it.

Wellman (1966), by mapping the fault patterns of Iran and the neighbouring countries, from aerial photographs, showed that the major active fault of the southern boundary of the Alborz Mountains is of wrench type. He concluded that the relative motion between the Persian and south Caspian Plates is indicative of a large left-lateral fault. Wellman's suggestion was particularly supported by the horizontal dis-

placement (left-lateral) component of the Buyin-Zahra earthquake (see above).

McKenzie (1972) discussed the reasons for small lateral movement in this region. He pointed out that since the errors in focal depth determinations are of the order of 50 Km (especially for earthquakes before 1950) and the crustal velocity structure was not known in the area, even a large component of strike-slip movement would not be apparent in the fault plane solutions for the earthquakes in this region.

A detailed study of the satellite photographs (see chapter two) revealed clearly left-lateral movement along the Buyin-Zahra Fault, which is thought to be the continuation of the North-Tehran Fault (see Figure 2-4).

The striking coincidence of the compression axes inferred from the composite fault plane solutions given here with the direction of movement of the Arabian Plate relative to the Eurasian Plate, NE, (McKenzie 1970, and 1972), also with the compression axes found by Mohajer-Ashjai (1975) in Eastern Central Iran, the excellent agreement with the compressive direction resulting from the circular diagram of azimuthal distribution of faults (see chapter two), and consistency of diagrams (Figures 7-3 and 7-4 a) is believed to attest to the validity of the composite fault plane solution and the regional nature of the stresses producing the earthquakes.

It should be noted that the possible fault planes deduced from the mechanisms of the microearthquakes are aligned along the strike of the fault trace and the geological structures and that the direction of the principal stress axes

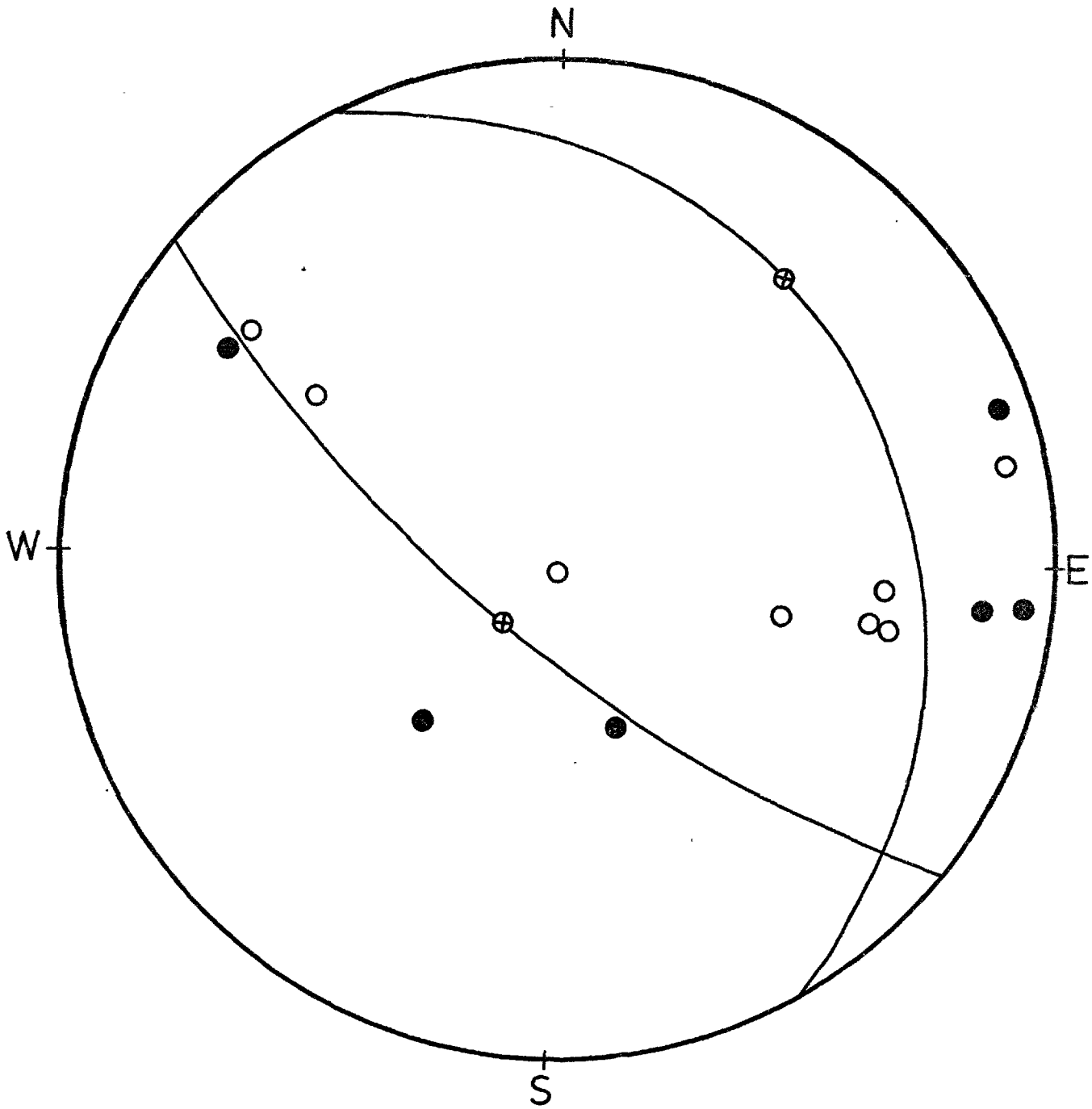
relative to the tectonic axes clearly indicate that the processes responsible for the earthquake activity in the region can be governed by regional tectonics.

Thus the seismological observations show that, whatever may have been true in the past, the Musha-Fasham Fault is now behaving as a strike-slip fault with some degree of thrust movement.

Figure (7-5) depicts the polarity diagram made up from the first motions of the microearthquakes which occurred on the newly discovered Rey-Lineation. The resulting composite fault plane solution shows two well defined planes. One strikes  $N 148^{\circ} E$  and dips at  $20^{\circ}$  in the direction  $N 58^{\circ} E$ , the other strikes  $N 129^{\circ}$  and dips at  $70^{\circ}$  in the direction  $N 141^{\circ} W$ . As there is no surface feature associated with this lineation, it is not immediately obvious which of the planes represents the plane of the fault. However, as the former is more in agreement with the strike of the line of microearthquake epicenters and some historical events (see Figure 5-7), and regarding the general direction of the compressive axis (NE-SW), it might be safe to choose the former as the fault plane. In this case, the mechanism is a shallow thrust with the north-eastern side overriding.

The difficulty of detecting shallow thrust faults, as compared with normal and strike-slip, in recent alluvial deposits from topographic evidence probably explains why this fault has been undetected until now. Such a situation is not unique in Iran; the 1971 San Fernando earthquake in California also demonstrates this point. It is interesting





- Compression
- Dilatation
- ⊗ Pole of nodal plane

Fig. (7-5). Composite fault plane solution of the micro-earthquakes occurring on the proposed Rey Lineation.

also that much of the region to the south-west of this proposed fault is topographically depressed (see chapter two), reflecting the nature of the movement, good proof for the existence of the Qom-Ardakan Depression (Seismotectonic Map of Iran, 1973).

#### 7.4 Profile Across the Musha-Fasham Fault

Figure (7-6) shows the projection of all the located microearthquakes in the Tehran survey onto a plane perpendicular to the strike of the Musha-Fasham Fault. The profile indicates a very pronounced grouping of hypocenters around depths of 2 and 18 Km respectively within the crust (see also Figure 5-8), which corresponds with the boundaries of layers in the crustal velocity model used in locating the microearthquakes. These two horizontal bands are separated by a thickness of rather less intensive activity. It seems that the majority of the microearthquakes in this region, which are associated with the Musha-Fasham Fault, lie on a plane dipping steeply towards the north-east.

An alternative way of demonstrating the concentration of activity within distinct bands is to convert magnitude to energy, using the Gutenberg and Richter (1956) formula:

$$\text{Log } E = 11.4 + 1.5 M.$$

The result of this conversion is shown in Figure (7-7). As can be seen, two anomalous energy bands are clearly present around depths of 2-3 and 17-18 kilometers. These two zones

Fig. (7-6). Projection of all the located microearthquakes onto a plane perpendicular to the strike of the Musha-Fasham Fault, alongside the crustal velocity model used. Note the pronounced grouping of events at two distinct depths. F: Fault; NABF: North Alborz Boundary Fault; NFT: North-Tehran Fault; MFF: Musha-Fasham Fault. Numbers refer to the earthquakes listed in table (5-3).

Crustal Velocity	
P(Km/Sec)	S(Km/Sec)
3.45	2.00

585      3.40

6.70      3.90

8.00      4.70

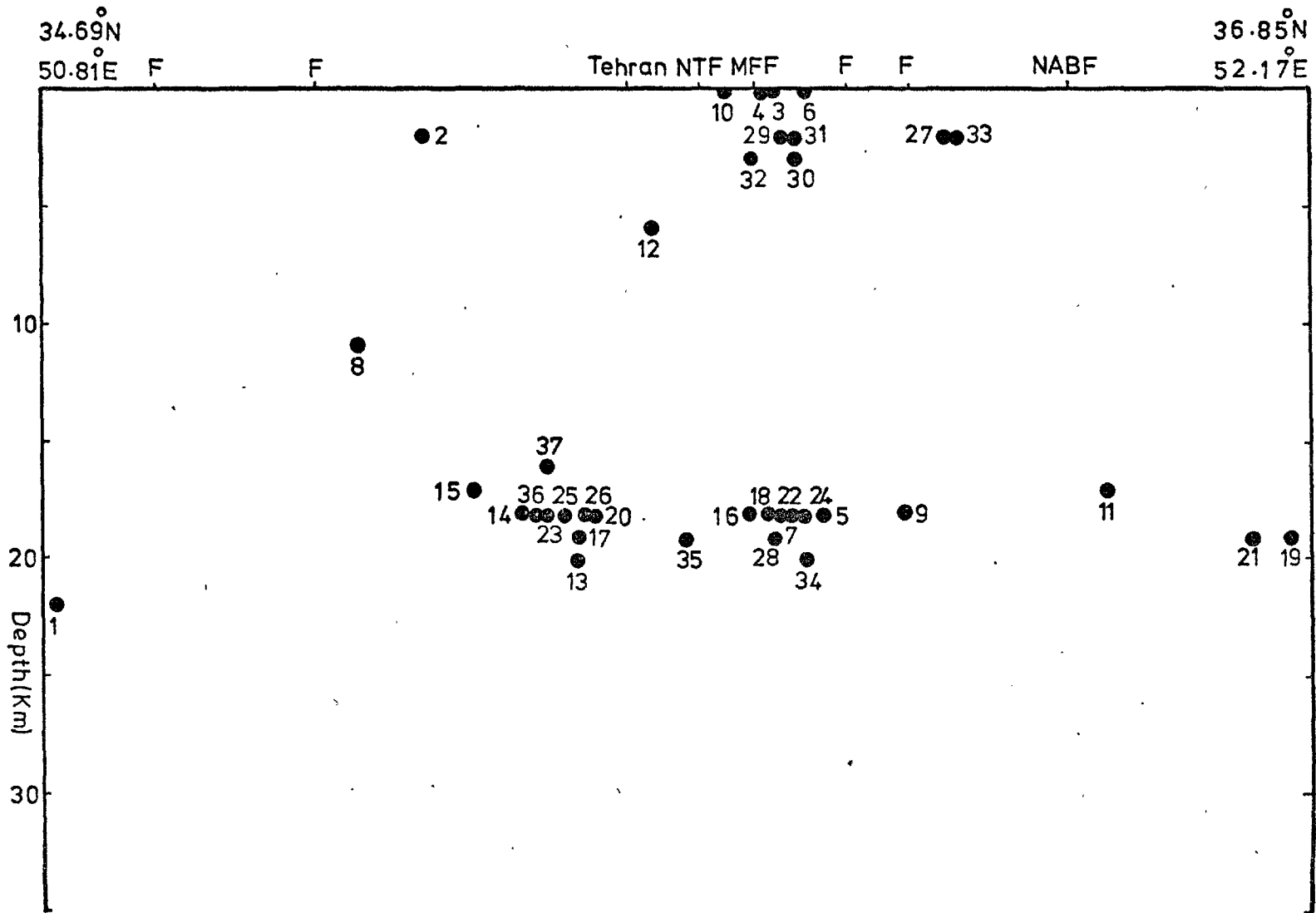


Fig. (7-6).

Fig. (7-7). Energy release of located microearthquakes versus depth, showing the concentration of activity at two particular depths.

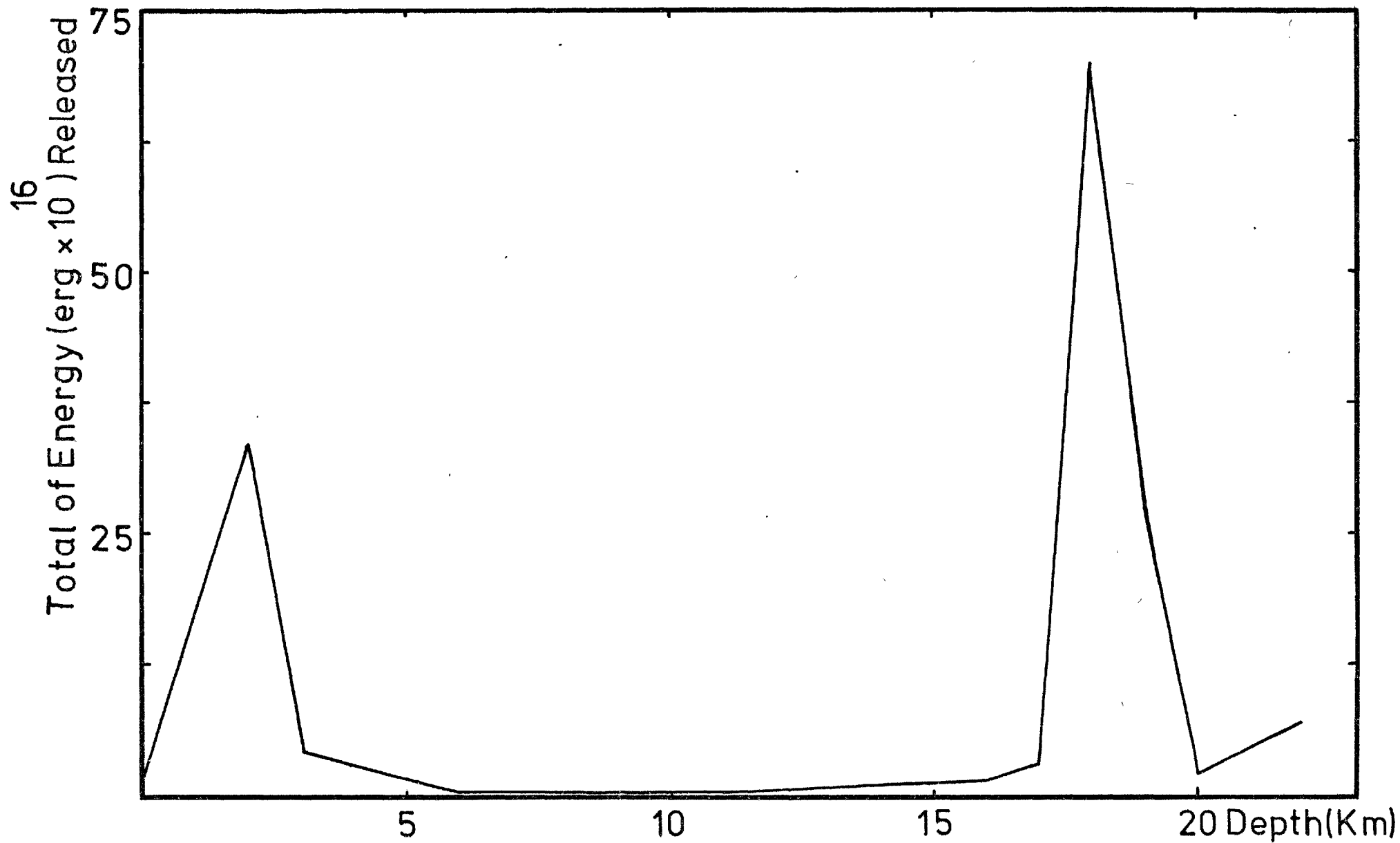


Fig. (7-7).

could be indicative of stress concentration around these two boundaries.

This situation is not unique to the region studied. Similar results have been found from microearthquakes and aftershock sequence studies in other parts of the world. Eaton et al., (1970) made a detailed study of more than 600 aftershocks of the Parkfield-Cholame earthquake of July 27, 1966 and concluded that the majority of events originated from distinct depths (Figure 7-8). The upper band consisted of earthquakes at depth 3-4 km and the lower band was a source of events at depth 8-9 km.

In studying the seismicity of northern and central California, Bolt and Miller (1971) showed that the focal depths of earthquakes in this region did not exceed 16 km, and about 50 percent of events occurred at a depth of less than 5 km.

A study of the energy released by more than 1000 shocks in the Uzbekistan, USSR, (Shemyakin and Shcheglov, 1974) showed that most of the energy was dissipated at depths of 5 and between 12 and 15 km. According to them also, the depth of the upper band in the case of the Matsushiro swarm of Japan ranged from 4 to 6 kilometers. Similarly Gedny and Berg (1969) showed that the depths of earthquakes at Fairbanks, Alaska, ranged from near-surface to 25 km, but most occurred between 9 and 16 km.

Shemyakin and Shcheglov (1974) calculated the energy released by the aftershocks of the Parkfield earthquake (Figure 7-9) and showed that the distribution of energy

Fig. (7-8). Number of events versus depths of aftershock activity of the Parkfield-Cholame earthquake of July 27, 1966, showing the origination of most of the activity around depths 3-4 and 8-9 km. Numerals on the figure show the magnitude of events (after Eaton et al., 1970).



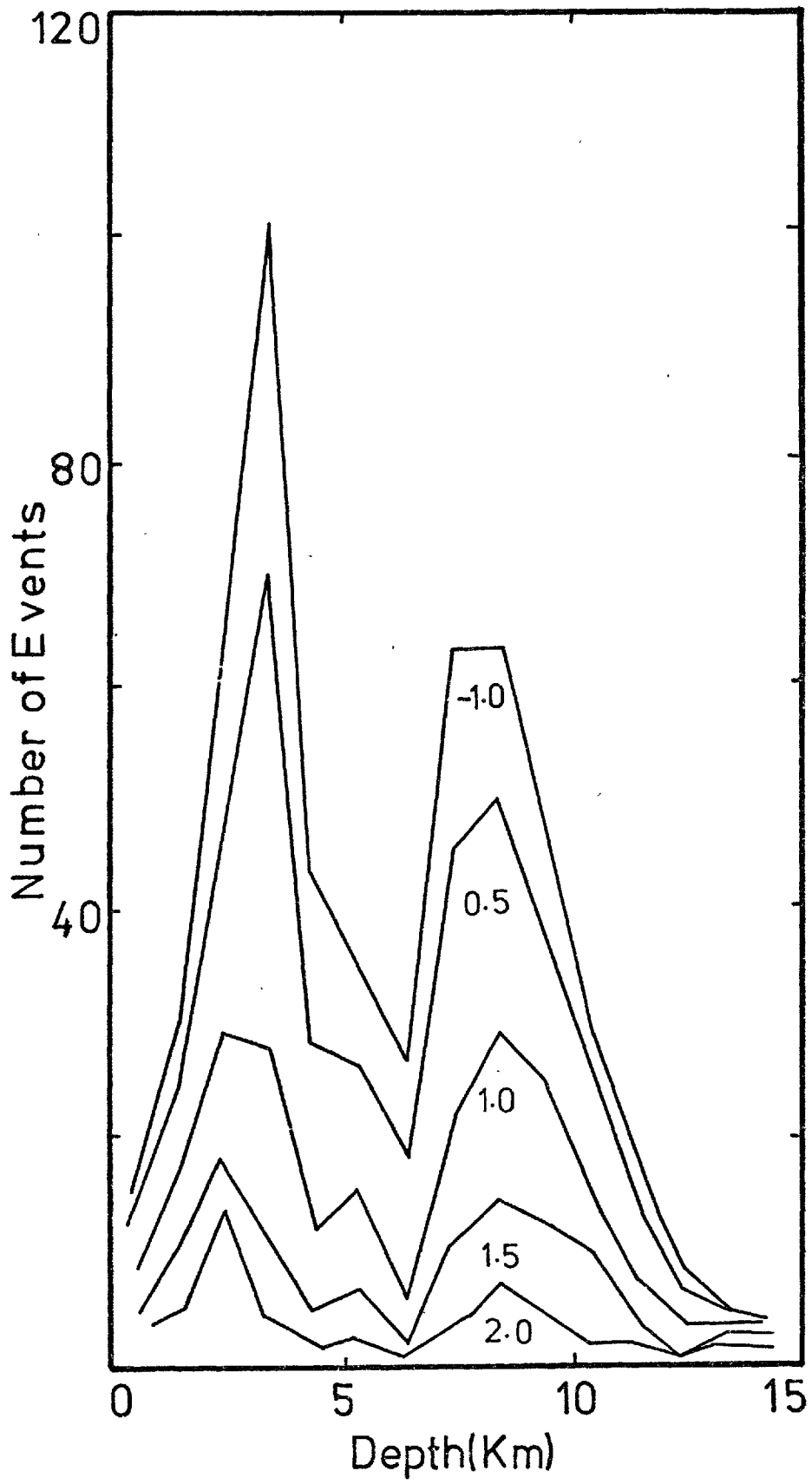


Fig. (7-8).

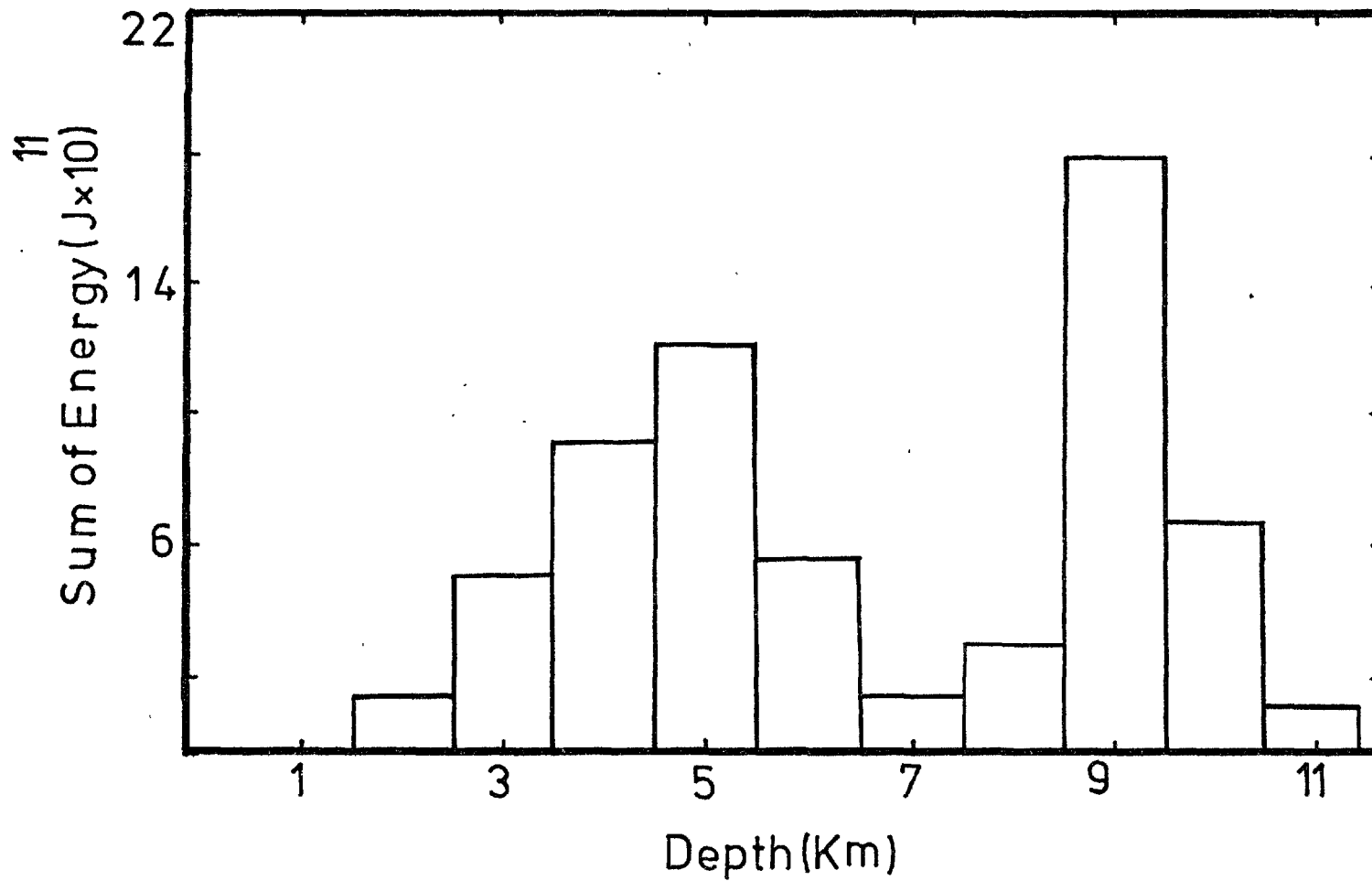


Fig. (7-9). Energy released of the aftershock sequence of the Parkfield-Cholame earthquake, indicating of concentration of energy at two specified depths (after Shemyakin and Shcheglov, 1974).

released at two particular depths, between 3 and 5 km and between 8 and 11 km respectively.

From the above investigations it might be concluded that the concentration of seismic activity at two distinct depths is typical of shallow-focus earthquakes, and that their presence strongly suggests the existence of characteristic physical boundaries.

According to laboratory studies undertaken by Shemyakin and Shcheglov (1974), when a specimen undergoes compression the elastic parameters of the sample increase as the pressure increases, up to 1 Kb. During the compression, first, due to closing of pores, the elastic constants of a rock increase and, secondly, any solution contained in its pores may be forcefully expelled, "lubricating" its surface and leading, in a crustal situation, to an earthquake. Depending on geological factors, the depth at which the necessary pressure would be reached is around 5 km, which corresponds to the depth range of the upper spatial energy anomaly in the seismicity. The depth in the case of the Tehran region is typically 2-3 Km.

They have shown also that the concentration of seismic activity in the lower band could be attributed to the physical properties of the materials at the lower depth. A lowering of the friction coefficient, giving consequently greater mobility to the medium, could be one reason for the high activity at this depth.

Similarly, on the basis of dislocation theory, Rybicki (1971) developed a mathematical model showing the existence of two boundaries generating crustal earthquakes (Figure 7-10).

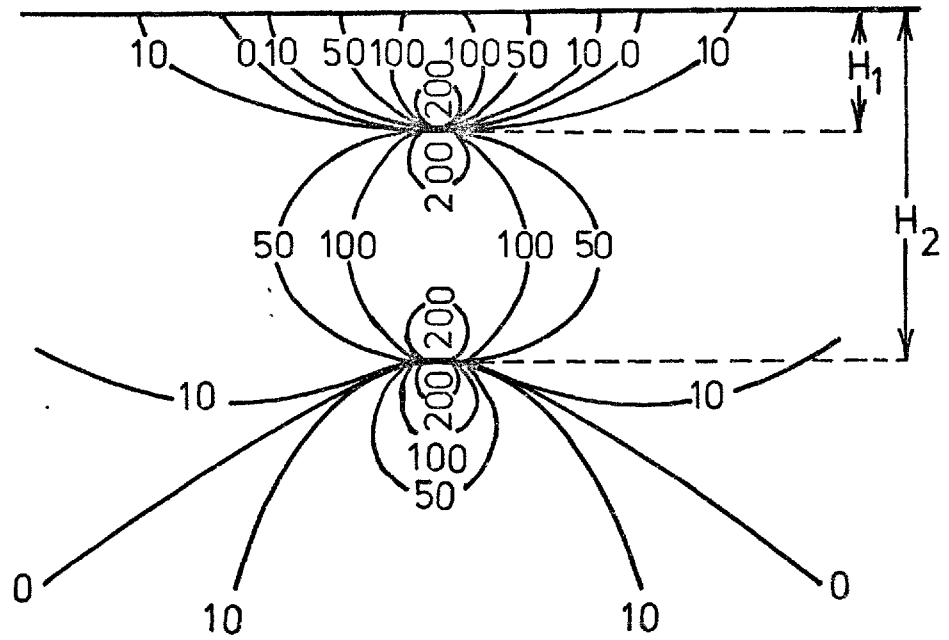


Fig. (7-10). Contour lines representing shear stress changes for the model of the 1966 Parkfield-Cholame earthquake at depths  $H_1 = 3$  and  $H_2 = 9$  km. Contour values are in unit of  $10^5 \text{ dyn/cm}^2$  (after Rybicki, 1971).

The model, which was applied to the 1966 Parkfield-Cholame earthquake, showed good agreement between the calculated residual stress field and the distribution of the aftershock sequence.

#### 7.5 Regional Strain Release, Tectonics and Seismicity of the Tehran Region

The occurrence of more than 100 moderate to destructive earthquakes in the last fifty years from July, 1926 to October, 1973, as well as the microearthquakes recorded in the Tehran survey in late 1974, provided an opportunity for investigation of the strain release characteristics, tectonics and seismicity of the region.

During recent decades, a number of techniques have been introduced and developed for describing quantitatively the strain release associated with tectonic movements, and the seismic activity level, in a particular region.

However, Benioff (1949) seems to have been the first to propose an empirical relation between the square root of the energy of an earthquake, on a given fault, and that of the strain which triggers the earthquake. He used this relation (1951, 1955) to construct global strain accumulation and release curves, using major earthquakes. As a result, he found that earthquakes of magnitude 8.0 and greater cannot be treated as independent events, and that they have some inter-relation through the world-wide stress system. On a smaller scale, applying the technique to the aftershock sequence, from July to December, 1952, St. Amant (1956) showed

conclusively the concentration of activity at each end of the White Wolf Fault, responsible for the 1952 Kern County earthquake.

To investigate the seismicity of northern California and West Nevada, Niazi (1964) calculated the strain release, using 1,500 local earthquakes of magnitude two and over, recorded from January 1956 to December 1960 at Berkeley seismographic station, in one-year intervals. He showed that the region underwent striking variations of seismic activity. In particular he found that, except for one section, the San-Andreas Fault trace was relatively active throughout the above investigation. The quiet segment, between  $38^{\circ}$  and  $39^{\circ}$  N, was the section which showed the maximum displacement at the time of 1906 San-Andreas earthquake.

To evaluate the relationship between seismic activity and the geological structure of southern California, Allen et al., (1965) used a slightly different procedure. They represented strain release, on maps, in terms of the number,  $N_3$ , of magnitude 3 earthquakes that an earthquake of any other magnitude  $M$  is equivalent to, using the relation:

$$\text{Log}_{10} N_3 = 0.75(M-3.0) \text{ (after Allen et al., 1965).}$$

Using historical events since 1836, as well as instrumental earthquakes up to 1961, Ryall et al., (1966) constructed a seismicity map of the western United States, based on Benioff's formula.

Results of the strain release calculation for the whole Persian Plateau, and Hindu Kush, by Niazi and Basford (1968) showed excellent correlation of seismic zones with geological structure.

#### 7.5.1 Method of Analysis

To construct seismicity maps of the Tehran region, the energy and strain of all earthquakes occurring between July 1926 and October 1973 were calculated and summed. For this, the relation:

$$F = \frac{1}{A T} \sum \sum E^{\frac{1}{2}} dA dT \quad (\text{after St. Amand 1956})$$

was used.  $F$  is the so called "tectonic flux"  $A$  and  $T$  are area and time respectively, and  $E^{\frac{1}{2}}$  is the strain released by the individual earthquakes (Benioff 1949 and 1951).

The integration of the above expression is done by summation of the calculated energy of the earthquakes in a selected unit of time and area, using the empirical formula given by Gutenberg and Richter (1956):

$$\text{Log } E = 11.4 + 1.5 M$$

where  $M$  is the magnitude and  $E$  the energy, in ergs. Any other expression relating energy and magnitude could be used, since minor changes in the coefficients do not change the energy extensively or the seismicity picture of the region.

The method of plotting strain release used here as an indicator of seismicity and tectonics has several advantages when compared with the technique of showing the activity by various symbols for different classes of earthquake magnitude and depth. These advantages could be summarized as follows:

- a. To some extent, inaccuracies involving the epicentral locations are eliminated by normalising the strain release over an area in a particular time span.
- b. It shows significantly the continuity and discontinuity of the tectonic processes, as well as migration of activity.
- c. Strain release maps exhibit a better correlation of tectonic activity with geological features.

The earthquakes used in compiling the strain release maps (table 5-2) are taken from the catalogues of relocated events given by Nabavi (1972) and Nowroozi (1971), and from the USCGS, ISS, BCIS, and Moscow Seismological Bulletin. An arbitrary magnitude of 4.0 has been assigned to those earthquakes for which a value has not been published, since this seems to be the lower threshold for events to be recorded by the distant seismograph stations around Iran. These earthquakes are marked by asterisks in table (5-2).

In processing the data, the unit of time has been chosen as a ten-year interval, of which there are five from 1926 to



1975, while that of area has been taken to be fifteen-minute geographic quadrangles.

### 7.5.2 Strain Release Maps

Figures (7-11) to (7-14) depict the logarithm to the base ten of the normalised tectonic flux in  $(\text{erg})^{\frac{1}{2}}$  for the years 1926 to 1975 in steps of ten years.

The dynamic representations of the seismic activity in ten-year intervals shown in Figure (7-11) are indicative of variation, migration, and quiet periods in the region.

The tectonic flux represented in Figure (7-11A), which shows clearly the concentration of activity eastwards from longitude  $53^{\circ}$  E, can be divided into two parts, south and north of  $35.5^{\circ}$  N respectively. The activity of the first region started with a shock of magnitude 6.5 on July, 1926, which was followed by eight moderate to strong aftershocks, the largest of which had a magnitude of 5.75 - 6. The trend of this tectonic flux is nearly in an ENE to NE direction, and it seems that activity in this zone developed within two years.

The largest shock in the second region, of magnitude 5.75, occurred on 12, April 1935. This shock, which was preceded by six foreshocks and followed by three aftershocks, was the first known earthquake to have occurred in this area. The overall trend of this high strain release area is almost NE-SW, well aligned with that of the neighbouring Alborz. A further important feature of this period, is the absence

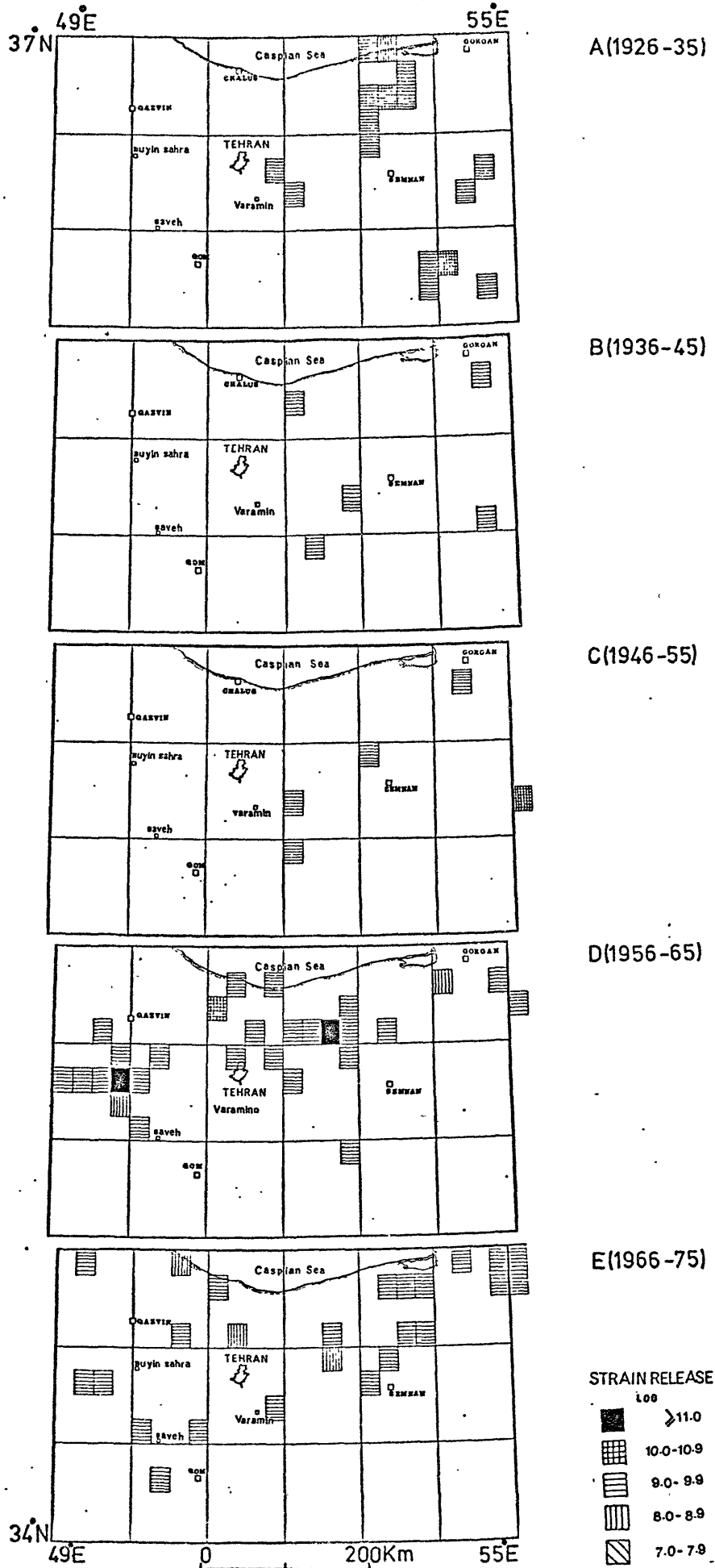


Fig. (7-11). Strain release maps for the years 1926 to 1975, in step of 10 years.

of activity west of longitude  $53^{\circ}$  E.

Even though some scattered activity occurred in the southern part of the Tehran region in the two decades from 1936 to 1955, Figures (7-11B) and (7-11C) show that the region was relatively quiet during this period.

With the occurrence of a destructive shock of magnitude 7.4 on 2 July, 1957 a sequence of activity started to the north of Tehran itself during the period 1956-1965. As a result, an elongated zone of high tectonic flux, whose trend follows a general E-W direction north of Tehran, and extends over about two hundred km, developed within two years. The activity spread further down towards the west of the capital of Iran, with the occurrence of the catastrophic earthquake of September 1, 1962, of magnitude 7.3. The general trend of this high strain zone is parallel to that of the North-Tehran Fault (Figure 7-11D). One very peculiar feature of the tectonics of this period is the migration of the activity from east of longitude  $53^{\circ}$  E to west of it, and its relatively very low level. But scattered activity could still be observed to the south of the city at this period.

The strain release pattern from 1966 to 1975 is shown in Figure (7-11E). Although the tectonic flux at this period is rather dispersed, apparently most of the seismic activity is associated with re-activation to the east of longitude  $53^{\circ}$  E of an area whose overall trend is NE-SW. Also, higher activity in the southern part of the city of Tehran is noticeable in this period.

Figure (7-12) is produced from the strain released by the microearthquakes recorded in the Tehran survey. The tectonic flux pattern shows the concentration of activity in the southern part of the Alborz Mountains, namely on the Musha-Fasham Fault and the newly proposed Rey-Lineation, which links the activity with the region in the west.

Figure (7-13) which is constructed by superposition of Figures (7-11A,B,C,D and E) and (7-12) may be considered as the seismicity map of the Tehran region based on the available data from 1926 to 1975. Close inspection of Figure (7-13) reveals some significant feature:

1. The correlation of the activity of the region in general with that of the Alborz-Mountains trend, which might be indicative of regional adjustment since the Alpidic Orogeny of the Tertiary Period. The activity seems to be mostly associated with the Musha-Fasham Fault.
2. A quite active segment of the Alborz trend around  $36^{\circ}$  N,  $52.5^{\circ}$  E is of particular interest. This is the place where the NE trending zone of Alborz Mountains changes to a NW direction.
3. In the last half-century, destructive earthquakes have occurred in the Alborz Ranges, three of them of magnitude 6 or greater. It is interesting to note that this high level of activity, which starts in the eastern part of the Alborz Mountains, ends sharply at longitude  $51^{\circ}$  E and leaves the NW trend of the mountains with particularly little

Fig. (7-12). Map showing the pattern of strain release by microearthquakes, indicating the concentration of activity on the southern flank of the Alborz Mountains.

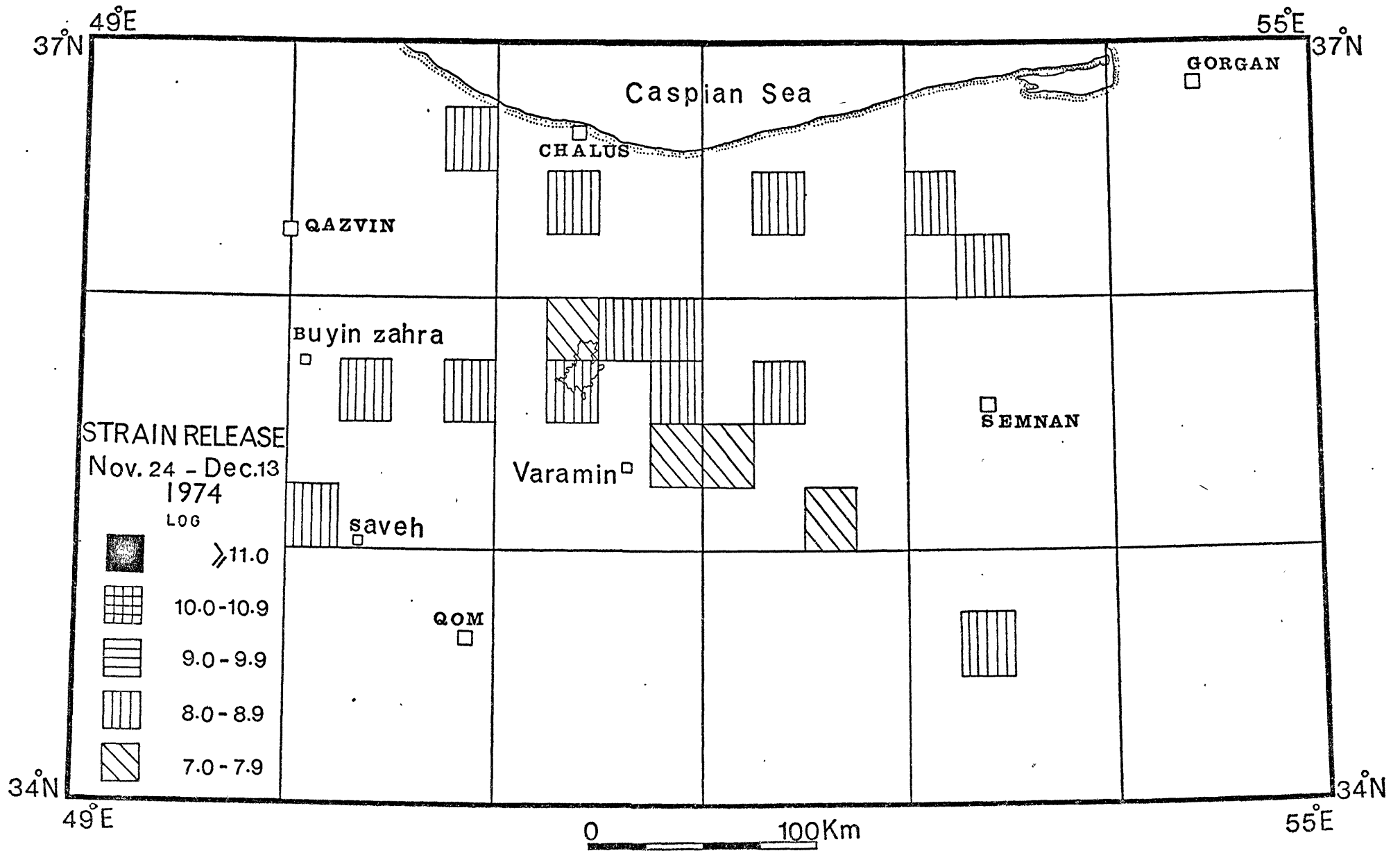


Fig. (7-12).

Fig. (7-13). Seismotectonic map of North-Central Iran (Tehran region) from 1926 to 1975, including the micro-earthquake data.

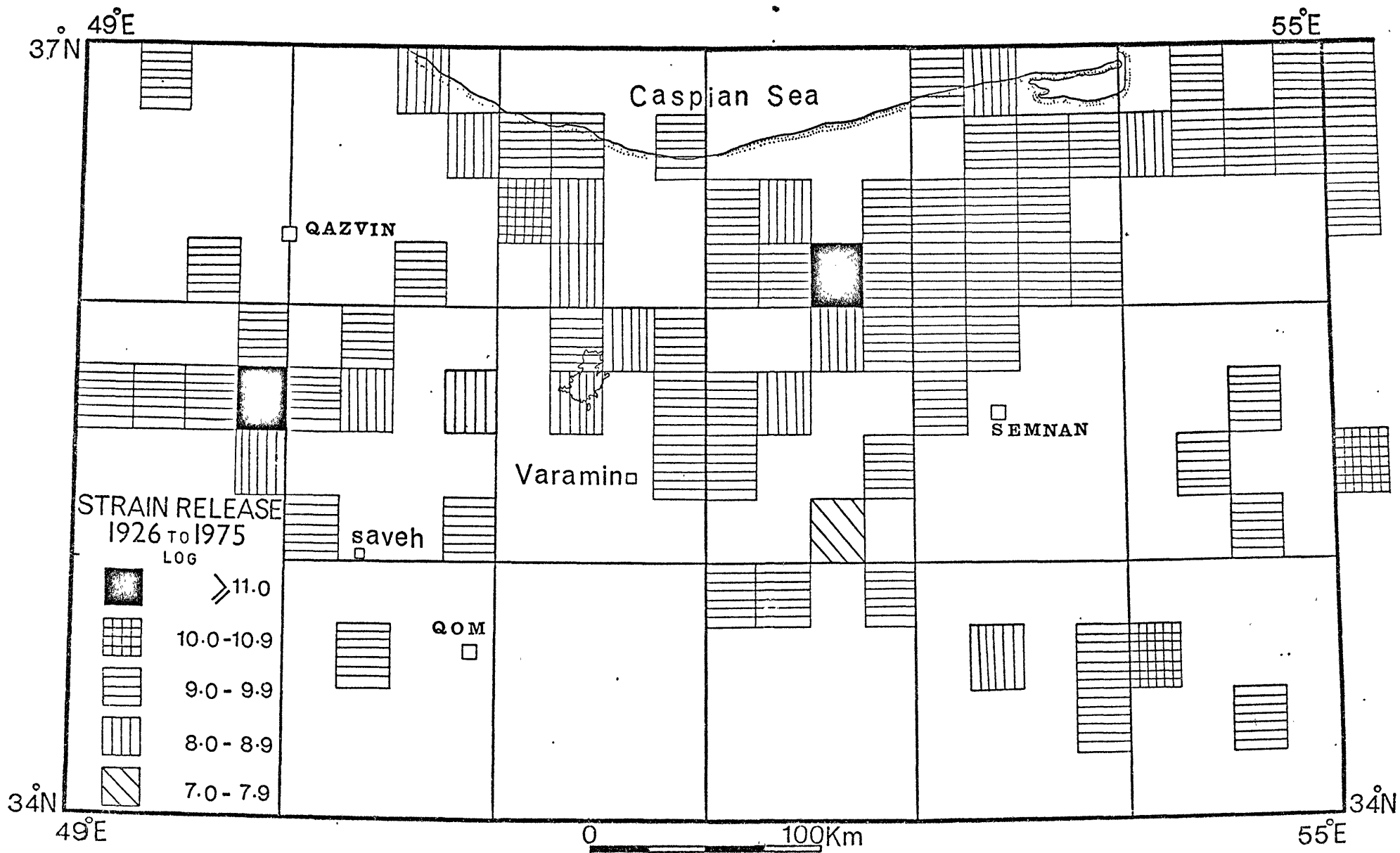


Fig. (7-13).



activity.

4. It seems that the seismic activity to the south of the city of Tehran which started early in the 20th century is continuing, and the area shows even more activity at the present time.

To show better the locations of the high concentrations of seismicity apparent in Figure (7-13), the data is presented in the form of a contour map in Figure (7-14). In this, a contour scale value of 7 or 8 represents the effect of one or more earthquakes and higher contour values mean more strain released. The normalizing effect of the integration of  $E^{\frac{1}{2}}$  will show a more even distribution of tectonic flux as the number of earthquakes increases.

Of particular interest is the continuous high concentration of activity around  $35^{\circ}$  N,  $52.5^{\circ}$  E, since 1926. The maximum strain release calculated for this zone is 9.8, and the dashed curves are postulated tectonic flux. It is suggested that this particularly highly active seismic zone, which happens to be the end of the newly discovered Rey-Lineation, could be a potential source of future activity.

Plotting the cumulative strain released against time from 1926, Figure (7-15), suggests the presence of successively active and quiet periods. Each quiet period seems to last between 10 and 15 years, the active ones about 2 to 5 years. The overall strain release for this region can be determined as  $0.8 \times 10^{10} \text{ (erg)}^{\frac{1}{2}} \text{ year}^{-1}$ , which is equivalent to one earthquake of magnitude between 5 and 6 each year.

Fig. (7-14). Contours of equal strain release. Note the trend of activity on the north of Tehran, which is parallel to that of the Alborz-Mountains, and the concentration of activity on the west and south of Tehran on both ends of the proposed Rey Lineation. Dashed contours signify a region of potential future major earthquakes.

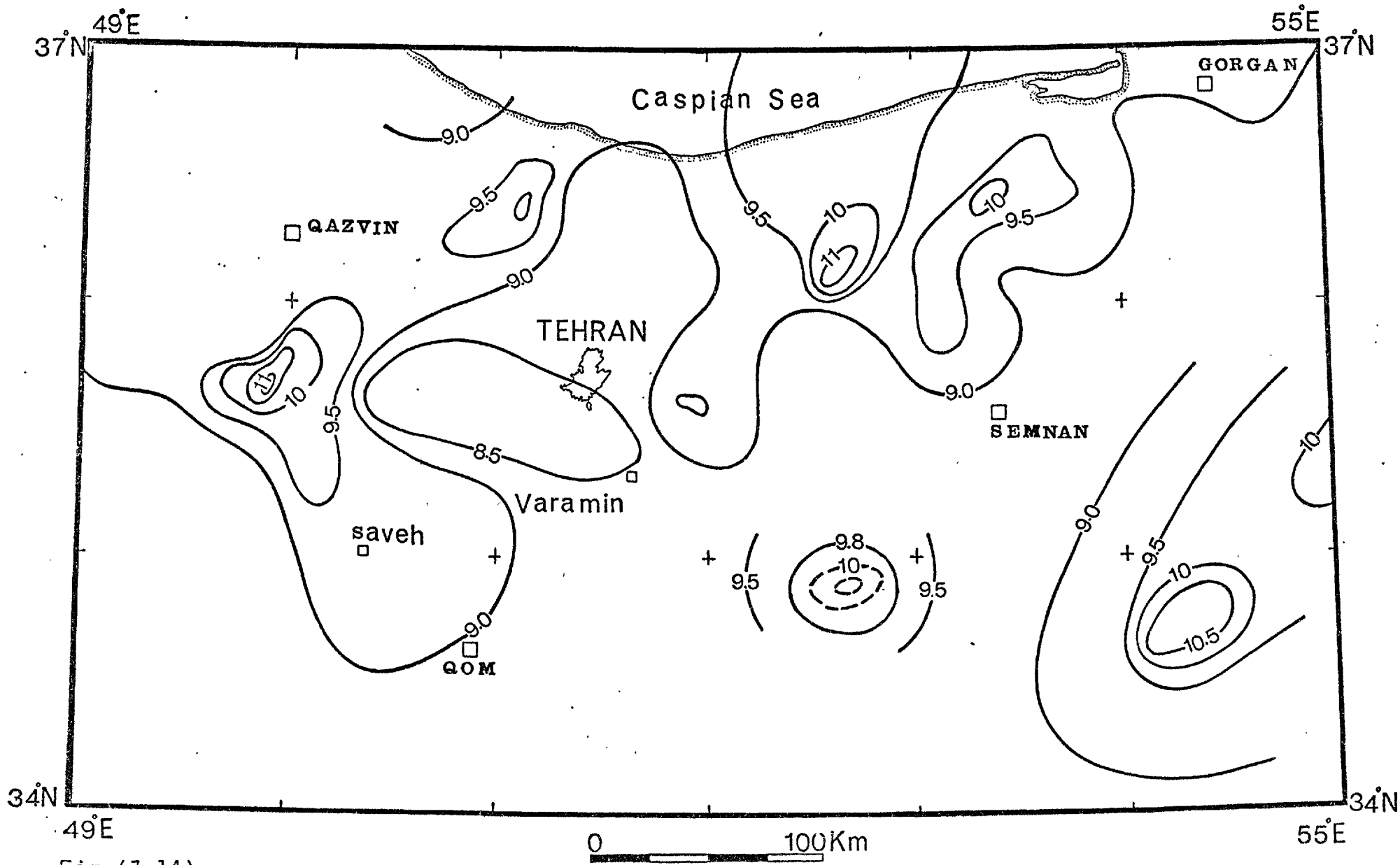


Fig. (7-14).

Fig. (7-15). Cumulative strain release versus time from 1926 up to the present time. The successively active and quiescent periods, and continuous activity after 1962, is noticeable.

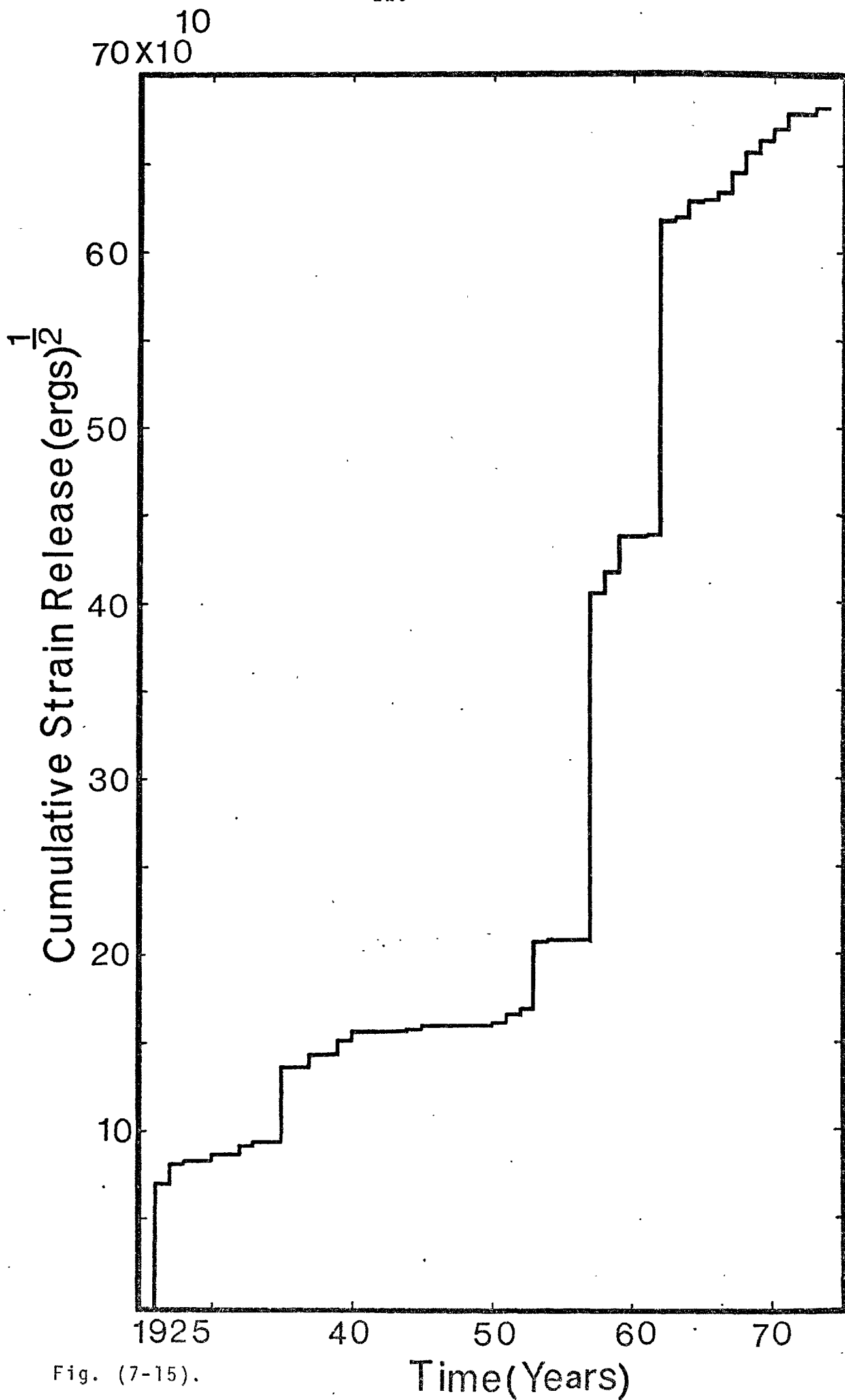


Fig. (7-15).

To compare the present activity of the region with that of historic time, attention has been given to the time distribution of historical events, from 280 to 1926, discussed in chapter five. To estimate the tectonic flux for the historical earthquakes which occurred between 280 and 1926, magnitude 7 was arbitrary assigned to each earthquake, on the assumption that the destruction caused by lower magnitudes would have been too local to achieve general notice. This magnitude seems to be a reasonable threshold for those devastating earthquakes. Converting this magnitude to strain release (see section 7.5) and considering that about 50 earthquakes occurred in 1650 years, the average tectonic flux will be about  $0.4 \times 10^{10} \text{ (erg)}^{\frac{1}{2}} \text{ year}^{-1}$ , equivalent to an earthquake of magnitude 5 each year.

Comparing the strain released by historical events with that by instrumental earthquakes shows not only the continuity of the activity since 1926, but also reveals a higher level of seismicity for the region. This implication, which was also deduced from the microearthquake survey, is further enhanced by the occurrence of small to moderate earthquakes since 1926, and might provide warning of accumulation of strain, and future activity. Moreover, the mean length of a quiet period obtained here (10-15 years) is the same as was determined in chapter four, where it was found that the return period for a moderate sized event is 10 to 12 years.

## CHAPTER VIII

## CONCLUSIONS AND SUGGESTIONS FOR FUTURE RESEARCH

8.1 Conclusions

Perhaps one of the most significant implications of micro-earthquake data is its capability of providing a measure of the seismic activity of a region in a relatively short period of time, because of the high rate of occurrence and wide distribution of microearthquakes in time and space. Micro-earthquake records are a valuable supplement to those of larger earthquakes, and geodetic surveys, and provide great help in understanding seismicity and tectonic processes.

The seismicity and tectonics of the North-Central Persian Plateau, particularly the Tehran region, has been investigated in the light of detailed microearthquake studies, by interpretation of satellite photographs and by construction of a strain release map based on earthquakes recorded from 1926 up to the present time, and on field observations. In addition, attention has been given to the implications of the historical events which have occurred in the region since 280 AD. The main conclusions reached from this investigation are summarized as follows.

1. The microearthquake survey of part of North-Central Iran around the city of Tehran suggests that the region, considering the occurrence of more than 21 events per day, is under high stress. This micro-

earthquake activity contrasts with the distribution of larger events which have been, since the inception of instrumental records, occurring almost entirely on the northern flank of the Alborz Mountains much further from Tehran. It is suggested that this imbalance of activity on the southern flank indicates the reactivation of some of the faults there, particularly the Musha-Fasham Fault.

2. A high rate of microearthquake activity was also located on the hitherto unappreciated lineation, hereafter called the Rey Lineation, stretching from west of Tehran to the south east of the city, with a total length of some two hundred kilometers. At its nearest approach, this lineation passes within thirty kilometers of the city, and it is proposed that it represents a buried fault whose past activity has been responsible for historically recorded destruction in the area.
3. The slope of the linear portion of the recurrence curve (b-value) calculated from the recorded microearthquakes, 0.79, and that from USCGS records of larger earthquakes between 1961 and 1973 was determined as 0.86. The fact that the calculated b-values from completely different sets of data show closely comparable values might be indicative of mechanical homogeneity through the region. The average b-value obtained from Eastern-Central Iran was 0.5 (mohajer Ashjai, 1975).



By comparing the b-values and the normalised number of magnitude 4 earthquakes, 0.53 for the Tehran region and 0.33 for Eastern-Central Iran, it is clear that the Tehran region is more active, seismically, than Eastern-Central Iran.

4. Because of unpredictability of the magnitude, number, and epicentral locations of future earthquakes affecting construction sites, a seismic intensity risk curve was produced for the Tehran region. It is suggested that the region can expect ground movement of intensity 7 every twelve years, though high intensities can be considered likely in time intervals of about three hundred and fifty years, which is in good agreement with assessments of historical activity.
5. It is shown that the located events of the micro-earthquakes recorded in the Tehran region are mostly associated with the Musha-Fasham Fault and the Rey Lineation. Lack of activity on the North-Tehran Fault might be a result of less seismicity on it, or possibly that it is creeping.
6. Reactivation of the Tehran region at the present time could be deduced from historical events. The time distribution of the historical earthquakes from 280 AD up to present time shows conclusively high activity of the region between 800 and 1000 AD, and the comparative quietness until the 18th century, when the high seismicity which has continued up to

the present time, again commenced.

7. Velocity-depth variation studies for the Tehran region suggest the existence of velocity reversals in the region. It is found that the velocity decreases at 6 Km depth and then abruptly increases at the "Forsch Discontinuity", at a depth of 11 Km.
8. Regarding earthquake prediction, it is concluded that changes in the ratio of longitudinal to transverse wave velocities,  $V_p/V_s$ , in the epicentral region of microearthquakes of small to moderate magnitude do occur in the Tehran region. The premonitory changes in seismic velocities in the region, which measure up to 14 percent, may give additional support to the results of similar investigations in other parts of the world.  
It is shown that the time duration of the anomaly changes with the magnitude of the earthquake. The relation  $\text{Log } t = 0.7 M - 1.4$ , derived between the anomaly time and the magnitude of the resulting earthquake for the region, has the remarkable justice that there is a longer warning time for the greater disaster. Therefore, it is suggested that this method may furnish a practical way of predicting future activity, at least of a certain class of magnitudes.
9. The station distribution for the Tehran study was designed to provide good coverage for the composite

fault plane solutions, from which it was hoped to deduce the regional stress pattern. The results show dominantly left-lateral strike-slip movement on the Musha-Fasham Fault. It is concluded from these results that the stress pattern in this region is controlled by a  $N 50^{\circ} - 60^{\circ} E$  compression, in good agreement with the strike of the general compressive axis found from the azimuthal distribution of the main faults of the area,  $N 35^{\circ} - 40^{\circ} E$ .

In the case of the Rey Lincation, the resulting composite fault plane solution is indicative of shallow thrusting. The difficulty of seeing shallow thrust faults in Recent alluvial deposits probably explains why this fault has been undetected until now. Another striking feature which warrants special attention is the depressed region on the south-west side of this proposed fault, which might reflect the nature of the movement, a perfectly good reason for the existence of the Qom-Ardakan Depression.

In summary, it should be pointed out that the possible fault planes deduced from the mechanisms of the microearthquakes are aligned along the strike of the fault traces and geological structures, and that the directions of the principal axes of stress relative to the tectonic axes clearly indicate that the processes responsible for the earthquakes activity in the region are governed by regional tectonics.

10. On the basis of dislocation theory, as well as laboratory experiments, it has been shown that crustal earthquakes, depending on the geological features of a region, occur dominantly at depths of around 5 and 16 Km. Projecting the located microearthquake hypocenters onto a plane perpendicular to the general direction of the strike of the Musha-Fasham Fault, it is shown conclusively that the hypocentral depths in the Tehran region cluster at between 2 and 3 and between 17 and 18 Km.
11. The time required to construct a tectonic map of a region, since it is directly related to the rate of strain release, has been a matter of controversy among seismologists. This time has to be long enough to show a distinct pattern of the seismicity and yet short enough to exhibit changes in regional activity. This period might be chosen as the time span during which significant changes in seismic activity could be inferred. Using the fifty years of instrumentally recorded events, which seems to be long enough to show changes of activity, a tectonic map of the Tehran region has been constructed, and the following conclusions reached.
  - a. The activity of the region in general correlates well with the Alborz Mountains trend, which might be indicative of continuing regional adjustment since the Alpidic Orogeny of the Tertiary Period.

- b. There is a noticeable continuous activity around  $36^{\circ}$  N and  $52.5^{\circ}$  E, where the NE trending zone of the Alborz Mountains changes to an E-W direction.
- c. One interesting feature of the tectonic map of the Tehran region is the lack of activity in the western part of the Alborz Mountains around  $51^{\circ}$  E.
- d. The continuous activity in the southern part of the Alborz which began early this century, and the strain release map derived from the microearthquake results, implies a resurgence of activity in that part of the region which seems to be mostly associated with the Musha-Fasham Fault.
- e. Comparing the result of the strain release study with that of the time-distribution of historical events supports the idea of reactivation of the region, and provides warning of the accumulation of strain, particularly since 1962.

## 8.2 Suggestions for Future Studies

Microearthquakes may be used, since they can provide a good deal of information in a relatively short period of time, to delineate the seismicity and the tectonics of a region. It seems that this survey has begun the task of understanding the present day activity of the southern Alborz and the Tehran region and it is certainly the beginning. It is hoped that the suggestions and ideas discussed here will be used as a foundation for future investigations.

A comprehensive program of investigation, using seismograph, strain meter, tiltmeter, magnetometer, etc., as initiated in California might well be considered for the area. However, if only the monitoring of local activity, using portable, and more permanent, seismographs could be extended, this will be a big step forward.

ACKNOWLEDGEMENTS

The author would like to extend his obligations to those contributors without which the investigation described would not have been accomplished.

I am specially indebted to Professor R.G. Mason whose supervisions, critical suggestions, and comments led to several important additions and improvements of this thesis.

Special acknowledgement should be made to the Jondi Shapour University, Ahwaz Iran, which provided much of the financial assistance, whence the author was on leave of absence.

I thank the Geological Survey of Iran which furnished the local transportation and technical assistance, and Messrs Nabavi and M. Berberian in particular, and the Centre for Curriculum Planning and Faculty Development of the Iranian Ministry of Science and Higher Education whose financial support was vital for completion of this work.

Special acknowledgements are extended to Professor N.N. Ambraseys, for his fruitful discussions and encouragements without which this research would not have been pursued.

The field work expenses were met out of a research grant from the U.K. Natural Environmental Research Council, who also provided the Geostore tape recorders.

Thanks are due to Dr. J.L. Brander for his reviewing the text and his contribution by assisting me with part of the field work, Geophysical Institute of Tehran University who kindly provided the USCGS data used, and the Dames and

Moore Inc., particularly Drs. D.J. Leeds and D. Papastamatiou, for permission to use the instrumental records of events in North-Central Iran.

Finally, my deep appreciations are due to my family, particularly my parents for their collaboration during the course of this study. Special thanks are due to my wife Shirin for her tolerance and typing the first draft of the manuscript, and to Miss M. Chock for final typing.



List of other contributions of the Author

- Hedayati, A. and T. Hirasawa, 1966. Mechanism of the Hindu-Kush earthquake of Jan. 28, 1964, derived from S-wave data: The use of pP-phase for the focal mechanism determination. Bull. Earthq. Res. Ins. Tokyo Univ. 44, 1419-1434.
- Sobuti, M., M.S. Nabavi, A. Eslami, A. Hedayati, Kh. Moftakhar, and M. Peyman, 1969. Report on the great Dasht-e-Bayaz earthquake of August 31, and September 1, 1968. Ins. Geophy. Tehran Univ., Pub. No. 46.
- Hedayati, A., J.L. Brander, and M. Berberian, 1975. A micro-earthquake survey of the Tehran region (abstract). Tehran Symposium of the Geodynamics of South-West Asia. 8-15 September 1975, Tehran, Iran.
- Hedayati, A., 1976. A composite fault plane solution for the Glenalmond earthquake series of February 1970-March 1972. Ins. Geophy. Tehran Univ. Iran (in press).
- Hedayati, A., J.L. Brander, and M. Berberian, 1976. Micro-earthquake survey of the Tehran region, Iran. Bull. Seism. Soc. Am. October Issue (in press).
- Hedayati, A., J.L. Brander, and R.G. Mason, 1976. Instances of precursory crustal velocity ratio changes in Iran (in preparation).

## REFERENCES

- Abdalian, S. 1962. The great Buyin-Zahra earthquake. Inst. Geophys. Tehran Univ. Pub. No. 15.
- Adams, W.M. 1958. A study of earthquake mechanism using s-wave data. Bull. Seism. Soc. Am. 48, 201-219.
- Afshar, H.K. 1966. The seismicity of North-Central Iran. Inst. Geophys. Tehran Univ. Pub. No. 34.
- Aggarwal, Y.P., L.R. Sykes and M.L. Sbar, 1972. Prediction of earthquakes. EOS. Trans. Amer. Geophys. Union 53, 1041.
- Aggarwal, Y.P., L.R. Sykes, J. Armbruster and M.L. Sbar, 1973. Premonitory changes in seismic velocity and prediction of earthquakes. Nature 241, 101-104.
- Aggarwal, Y.P., L.R. Sykes, D.E. Simon and P.G. Richards, 1975. Spatial and temporal variation of  $t_s/t_p$  in P-wave residuals at Blue Mountain Lake, New York: Application to earthquake prediction. J. Geophys. Res. 80, 718-732.
- Aki, K. 1966. Generation and propagation of G-waves from the Niigata earthquake of June 16, 1964, Part 2: Estimation of earthquake moment, release energy and stress strain drop from the G-wave spectrum. Bull. Earthq. Res. Inst. 44, 73-88.
- Allen, C.R., P. St. Amand, C.F. Richter and J.M. Nordquist, 1965. Relationship between seismicity and geologic structure in the Southern California region. Bull. Seism. Soci. Am. 55, 753-797.
- Ambraseys, N.N. 1961. On the seismicity of south west Asia. Revue pour l'etude des Calmités (Geneva) 37, 18-30.
- Ambraseys, N.N. 1963. The Buyin-Zahra (Iran) earthquake of September 1962: A field report. Bull. Seism. Soc. Am. 53, 704-740.
- Ambraseys, N.N. 1966. The seismicity of North-Central Iran. Inst. Geophys. Tehran Univ. Pub. No. 34.
- Ambraseys, N.N. 1968. Early earthquakes in North-Central Iran. Bull. Seism. Soc. Am. 58, 485-496.
- Ambraseys, N.N. and J.S. Tchalenko, 1969. The Dasht-e-Bayaz (Iran) earthquake of August 31, 1968: A field report. Bull. Seism. Soc. Am. 59, 1751-1792.
- Ambraseys, N.N. 1971. Value of historical records of earthquakes. Nature, 232, 375-379.
- Ambraseys, N.N. 1974. Historical seismicity of North-Central Iran. Geol. Surv. Iran. 29, 47-95.
- Arnold, E.P., B.A. Bolt, G.E. Clawson, E.R. Engdahl, H.W. Freedman, D.W. Gordon, A.L. Hales, J.L. Lobdell, O. Nuttli, C. Romney, J. Taggart, W. Tucker and E. Herrin (chairman),

1968. Seismological tables for P-phases. Bull. Seism. Soc. Am., 58, 1193-1241.
- Asada, T. 1957. Observations of nearby microearthquakes with ultra sensitive seismometers. J. Phys. Earth. 5, 83-113.
- Asada, T. 1958. Observations of nearby microearthquakes with ultra sensitive seismometers at Matsushira, Japan. J. Phys. Earth. 6, 23-33.
- Assereto, R. 1966. Geological map of Upper Djadjud and Lar Valleys (1:50,000), with explanatory notes. Inst. Geol. Univ. Milano, Serie G. Pub. No. 232, 86 pp.
- Assereto, R. 1972. Geological maps of the Central Alborz (1:100,000). Geol. Surv. Iran.
- Barazangi, M. and J. Dorman, 1969. World seismicity maps compiled from ESA, Coast and Geodetic Survey, epicenter data, 1961-1967. Bull. Seism. Soc. Am. 59, 369-380.
- Bassir, M. (1971). In genievrego logische baugrum duntersu chungen in der region gross - Tehran, Iran: Dissertasion, Rbeinisch-Westfälische Tech. Hochsch., Aachen, 109 pp.
- Bayer, K.C., L.E. Hevckroth and R.A. Karim, 1969. An investigation of the Dasht-e-Bayaz earthquake of August 31, 1969. Bull. Seism. Soc. Am. 59, 1793-1822.
- Benioff, H. 1949. Seismic evidence for the fault origin of oceanic deeps. Bull. Geol. Soc. Am. 60, 1837-1857.
- Benioff, H. 1951. Gelobal strain accumulation and release as revealed by great earthquakes. Bull. Geol. Soc. Am. 62, 331-338
- Benioff, H. 1955. Seismic evidence for crustal structure and tectonic activity Bull. Geol. Soc. Am. Special Paper 62, 61-74.
- Berberian, M. 1971. Preliminary report on structural analysis of Ipack active fault. Geol. Surv. Iran. Inter. Repo.
- Berberian, M. 1973. Seismicity map of Iran. 1,2,500,000 Geol.Surv.Iran.
- Berry, M.J. and G.F. West, 1966. An interpretation of the first-arrival data of the Lake Superior experiment by the time-term method. Bull. Seism. Soc. Am. 56, 141-171.
- Berry, M.J. 1972. Low velocity channel with earth's crust? Comm. Earth. Sci. Geophys. 3, 59-68.
- Bisztricsany, E.A. 1958. A new method for the determination of the magnitude of earthquakes. Geofiz. Kozlemen, 7, No. 2, 69-96.
- Bolt, B.A. 1960. The revision of the earthquakes epicenters, focal depth and origin time using a high-speed computer. Geophys. J. 3, 433-440.
- Bolt, B.A. and R.D. Miller, 1971. Seismicity of northern and central California, 1965-1969. Bull. Seism. Soc. Am. 61, 1831-1947.

- Borovik, N., L. Misharina and A. Teskov, 1971. On the possibility of strong earthquakes in Pribaykalia in the future. *Izv. Acad. Sc. USSR. Phys. Solid Earth. Engl. transl.* 2, 21.
- Brown, R. 1973. Precursory changes in  $V_p/V_s$  before strike-slip events. *Proc. Conf. Tecto. Prob. San-Andreas Fault System, Stanford Univ. Pub.* 13, 463-472.
- Byerly, P. 1926. The Montana earthquake of June 28, 1925. *Bull. Seism. Soc. Am.* 16, 209-265.
- Byerly, P. 1928. The nature of the first motion in the Chilean earthquake of November 11, 1922. *Am. J. Sci., 5th Ser.* 16, 232-236.
- Caputo, M., V.I. Keilis, T.L. Kronrod, G.M. Malchan, C.F. Panza, A. Piva, V.M. Podgaetskaja and D. Postpischp, 1974. The estimation of seismic risk for central Italy. *Ann. Geof.* 27, N. 1-2, 349-365.
- Chinnery, M.A. 1966a. Secondary faulting. Theoretical aspects. *Can. J. Earth Sci.* 2, 163-174.
- Chinnery, M.A. 1966b. Secondary faulting. Geological aspects. *Can. J. Earth Sci.* 3, 175-190.
- Cornell, C.A. 1968. Engineering seismic risk analysis. *Bull. Seism. Soc. Am.* 58, 1583-1606.
- Cornell, C.A. 1973. Seismic risk analysis based on a quadratic magnitude frequency law. *Bull. Seism. Soc. Am.* 63, 1999-2006.
- Crampin, S. 1969. Aftershocks of the Dasht-e-Bayaz, Iran earthquake of August, 1968. *Bull. Seism. Soc. Am.* 59, 1843-1861.
- Crampin, S. 1970. A method for the location of near seismic events using travel times along ray paths. *Geophys. J.R. ast. Soc.* 21, 535-539.
- Crampin, S. and P.L. Willmore, 1973. Small earthquakes observed within local seismometer networks. *Phil. Trans. R. Soc. Lon.* 274, 383-387.
- Crosson, R.S. 1972. Small earthquakes, structure and tectonics of the Puget Sound region. *Bull. Seism. Soc. Am.* 62, 1133-1171.
- Eaton, J.P. 1969. HYPOLAR - a computer program for determining hypocenters of local earthquakes in the earth consisting of uniform flat layers over a half space. U.S. Geol. Sur. open file report.
- Eaton, J.P., M.E. O'Neill and J.N. Murdock, 1970. Aftershocks of the 1966 Parkfield-Cholame, California earthquake: A detailed study. *Bull. Seism. Soc. Am.* 60, 1151-1197.
- Engdahl, E.R. and R.H. Gunst, 1966. Use of a high speed computer for the preliminary determination of earthquake hypocenters. *Bull. Seism. Soc. Am.* 56, 325-336.
- Englanc, M. 1968. Contribution a la geologie, geomorphologie, hydrologie de la region de Teheran (Iran). C.E.R.H., Montpellier, France, 365 pp.

- Esteva, L. and E. Rosenbueth, 1964. Spectra of earthquake at moderate and large distances. Soc. Mex. de Ing. Sismica, Mexico II, 1-18.
- Evernden, J.F. 1970. Study of regional seismicity and associated problems. Bull. Seism. Soc. Am. 60, 393-446.
- Ewing, M. and B. Heezen, 1956. Some problems of the Antarctic submarine geology, in Anarctica, in the International Year. Geophys. Monograph 1 edited by P. Fox, pg. 75-81. Am. Geophys. Uni. Washington D.C..
- Fedotov, S.A., A. Bagdasarova, I.K. and R. Tarakanov, 1969. Earthquake and the deep structure of south Kurile Island Arc. Akad. Nauk. USSR. Engl. transl. Nat. Inf. Servic. Springfield; va. 1971.
- Filson, J. and T.V. McEvelly, 1967. Love wave spectra and the mechanism of the 1966 Parkfield sequence. Bull. Seism. Soc. Am. 57, 1245-1257.
- Flinn, E.A. 1960. Local earthquake location with an electronic computer. Bull. Seism. Soc. Am. 50, 467-470.
- Fuchs, K. and G. Muller, 1971. Computation of synthetic seismogram with the reflectivity method of comparison with observation. Geophys. J.R. ast. Soc. 23, 417-433.
- Gansser, A. 1969. The large earthquakes of Iran and their geological frame. Eclog. Geol. Heb. 62, 443-466.
- Gardner, J.K. and L. Knopoff, 1974. Is the sequence of earthquakes in southern California with aftershocks removed Poissonian? Bull. Seism. Soc. Am. 64, 1363-1367.
- Gedney, L. and E. Berg, 1969. The Fairbanks earthquakes of July 21, 1967; aftershock distribution, focal mechanisms, and crustal parameters. Bull. Seism. Soc. Am. 59, 73-100.
- Gutenberg, B. 1950. Structure of the earth's crust in the continent. Science, 111, 29.
- Gutenberg, B. and C.F. Richter, 1954. Seismicity of the earth and associated phenomena, 2nd. 310 pp. Princeton Univ. Press, Princeton N.J..
- Gutenberg, B. and C.F. Richter, 1956. Magnitude and energy of earthquakes. Ann. Geof. 9, 1-15.
- Gupta, I.N. 1972. Seismic velocities in rocks subjected to axial loading up to shear fracture. EOS. Trans. Am. Geophys. Uni., 53, 513.
- Hadley, D. and J. Combs, 1974. Microearthquake distribution and mechanism of faulting in the Fontana-San Bernardino area of southern California. Bull. Seism. Soc. Am. 64, 1477-1499.
- Hasegawa, T., H. Hasegawa and R. Hori, 1975. Premonitory variation in seismic velocity related to the south eastern Akita earthquake of 1970. J. Phys. Earth 23, 189-203.

- Healy, J.H., W.H.K., Lee, L.C. Pakiser, C.B. Raleigh and M.D. Wood, 1972. Prospect for earthquake prediction and control. *Tectonophysics*, 14 (314): 319-332.
- Hedayati, A. and Hirasawa, T. 1966. Mechanism of the Hindu Kush earthquake of Jan. 28, 1964, derived from s-wave data: the use of pP-phase for the focal mechanism determination. *Bull. Earthq. Res. Inst.* 44, 1419-1434.
- Hedayati, A., J.L. Brander and M. Berberian, 1975. A microearthquake survey of the Tehran region. *Tehran Symposium of the Geodynamic of the South West Asia*, 8-11 Sept. 1975 (abstract).
- Hedayati, A. 1976. A composite fault plane solution for the Glenalmond earthquake series of February 1970-March 1972. *J. Earth and Space Phys. Inst. Geophys. Tehran. Univ.* (in press).
- Hedayati, A., J.L. Brander and M. Berberian, 1976. Microearthquake survey of Tehran region, Iran. *Bull. Seism. Soc. Am.* October 1976 (in press).
- Honda, H. 1962. Earthquake mechanism and seismic waves. *Geophys. Notes. Tokyo Uni.* 15, Supplement, 1-97.
- Howell, B.F. 1973. Average regional seismic hazard (ARSHI) in the United States. *Geology, seismicity and environmental impact* (special publication). Association of engineering geologists, 277-285.
- Isack, B., J. Oliver and L.R. Sykes, 1968. Seismology and the new global tectonics. *J. Geophys. Res.* 73, 5855-5899.
- Ishimoto, M. and K. Iida, 1939. Observation sur les seismes enregistres par microsismographe construit derniereement. *Bull. Earth. Res. Inst.* 17, 443-478 (in Japanese with French abstract)
- Iwao, S. and A. Hushmandzadeh, 1971. Stratigraphy and petrology of the low-grade regionally metamorphosed rocks of the Eocenen formation in Alborz range, north of Tehran, Iran. *J. Jap. Assoc. Min. Pet. Econ. Geol.* 65(6), 265-285.
- James, D.E., I.S. Sacks, E.L. Lazo and P.G. Aparicio, 1969. On locating local earthquakes using small networks. *Bull. Seism. Soc. Am.* 59, 1201-1212.
- Jeffreys, H. and K.E. Bullen, 1940. *Seismological tables.* Bri. Ass. Adva. Sci. London.
- Kaila, K.L., N.M. Rao and H. Narain, 1974. Seismotectonic maps of south west Asia region comprising eastern Turkey, Caucasus, Persian Plateau, Afghanistan and Hindu Kush. *Bull. Seism. Soc. Am.* 64, 657-669.
- Kelleher, J. and J. Savino, 1975. Distribution of seismicity before large strike-slip and thrust type earthquakes. *J. Geophys. Res.* 80, 260-271.
- Kisslinger, C. 1974. Earthquake prediction: variation in physical properties such as electrical conductivity and elevation of benchmarks may foretell not just the place

but also the time and magnitude of an earthquake.  
*Phys. Today*, March 1974, 36-42.

- Kisslinger, C., and E.R. Englahl, 1974. A test of the Semenov prediction technique in the central Aleutian Islands. *Tectonophysics*, 23, 273-246.
- Knopoff, L. 1964. The statistics of earthquakes in southern California. *Bull. Seism. Soc. Am.* 54, 1871-1873.
- Kosminskaya, I.P., N.N. Puzyrev and A.S. Alckseyev, 1971. Explosion seismology: its past, present and future. *Tectonophysics*, 13, 309-323.
- Langenkamp, D.F. and J. Combs, 1974. Microearthquake study of the Elsimore fault zone, southern California. *Bull. Seism. Soc. Am.* 64, 187-203.
- Le Pichon, X. 1968. Sea-floor spreading and continental drift. *J. Geophys. Res.* 73, 3661-3697.
- Lee, W.H., R.E. Benneth and K.L. Meagher, 1972. A method of estimating the magnitude of local earthquakes from signal duration. U.S. Geol. Surv. open file report.
- Lomnitz, C. 1966. Statistical prediction of earthquakes. *Rev. Geophys.* 4, 377-393.
- McKenzie, D.P. and R.L. Parker, 1967. The North Pacific: An example of tectonics on a shere. *Nature*, 216, 1276-1279.
- McKenzie, D.P. 1970. Plate tectonics of the Mediterranean region. *Nature*. 226, 239-243.
- McKenzie, D.P. 1972. Active tectonics of the Mediterranean region. *Geophys. J.R. ast. Soc.* 30, 109-185.
- McEvelly, T.V. and L.R. Johnson, 1973. Earthquake of strike-slip type in Central California: Evidence on the question of dilatancy. *Science* 182, 581-584.
- Milne, W.G. and A.G. Davenport, 1969. Distribution of earthquake risk in Canada. *Bull. Seism. Soc. Am.* 59, 729-754.
- Moazami-Gudarzi, K., J.H. Javaheri, M.A. Karimkhani and K. Rajaie, 1972a. Seismic zoning of the Iranian Plateau, Part I-Shiraz. *J. Earth Space Phys.* 1, No. 2, 13-16 (in Persian).
- Moazami-Gudarzi, K., J.H. Javaheri, H. Eban and K. Rajaie, 1972b. Seismic zoning of the Iranian Plateau. Part II-Birjand. *J. Earth Space Phys.* 1, No. 2, 17-18 (in Persian).
- Mohajer-Ashjai, A. 1975. Recent and contemporary crustal deformation in Eastern Iran. Ph.D. Thesis, London Univ.
- Mogi, K. 1962a. Study of elastic shocks caused by a fracture of heterogeneous materials and its relation to earthquake phenomena. *Bull. Earthq. Res. Inst.* 40, 125-173.
- Mogi, K. 1969a. Some features of recent seismic activity in and

- near Japan, activity before and after great earthquakes. Bull. Earthq. Res. Inst. 47, 395-417.
- Mohr, P.A. 1972. ERTS-1 imagery of eastern Africa: A first look at the geological structure of selected areas. Research in Space and Science. SAO, special report, No. 347.
- Mohr, P.A. 1973. Structural geology of the African rift system. Summary of new data from ERTS-1 imagery. Presented at the third ERTS-1 Symposium, Washington D.C. Dec. 73.
- Mohr, P.A. 1974. Mapping of the major structures of the African rift system. Research in Space and Science. SAO, special report, No. 361.
- Morgan, W.J. 1968. Rises, trenches, great faults and crustal blocks. J. Geophys. Res. 73, 1959-1982.
- Müller, S. and M. Landisman, 1966. Seismic studies of the earth's crust in Continent I: evidence for a low velocity zone in the upper part of the lithosphere. Geophys. J.R. ast. Soc. 10, 525-538.
- Nabavi, M.S. 1969. Le Seisme de Macou, dans la Province d'Azarbaydjan (29, Avril, 1968). Inst. Geophys. Univ. Teheran. Pub. No. 51.
- Nabavi, M.S. 1972. The seismicity of Iran. M. Phil. Thesis, Univ. Lond.
- Niazi, M. 1964. Seismicity of Northern California and Western Nevada. Bull. Seism. Soc. Am. 54, 845-850.
- Niazi, M. and J.R. Basford, 1968. Seismicity of the Iranian Plateau and Hindu Kush region. Bull. Seism. Soc. Am. 58, 417-426.
- Niazi, M. 1969. Source dynamics of the Dasht-e-Bayaz earthquake of August 31, 1968. Bull. Seism. Soc. Am. 59, 1843-1861.
- NIOC, National Iranian Oil Company, 1959. Geological map of Iran with explanatory notes. 1:2,500,000.
- Nordquist, J.M. 1962. A special purpose program for earthquake location with an electronic computer. Bull. Seism. Soc. Am. 52, 431-437.
- Nowroozi, A.A. 1971. Seismotectonics of the Persian Plateau, Eastern Turkey, Caucasus, and Hindu Kush. Bull. Seism. Soc. Am. 61, 317-341.
- Nowroozi, A.A. 1972. Focal mechanism of earthquakes in Persia, West Pakistan and Afghanistan and plate tectonics of the Middle East. Bull. Seism. Soc. Am. 62, 823-850.
- Nur, A. and G. Simmons, 1969. The effect of the saturation on velocity in low porosity rocks. Earth Planet. Sci. Lett. 7, 183-193.
- Nur, A. 1972. Dilatancy, pore fluids, and premonitory variations of ts/tp travel times. Bull. Seism. Soc. Am. 62, 1217-1222.



- Ohtake, M. 1973. Change in the  $V_p/V_s$  ratio related with occurrence of some shallow earthquakes in Japan. *J. Phys. Earth*, 21, 173-184.
- Oliver, J., A.R. James, N. Brune and D.B. Slemmons, 1966. Micro-earthquake activity recorded by portable seismographs of high sensitivity. *Bull. Seism. Soc. Am.* 56, 899-924.
- Real, C.R. and T.L. Teng, 1974. Local Richter magnitude and total signal duration in southern California. *Bull. Seism. Soc. Am.* 63, 1809-1927.
- Reid, H.F. 1910. The mechanisms of earthquakes in the California earthquakes of April 18, 1906. Report of the State earthquake commission 2; Carnegie Institute of Washington D.C..
- Richter, C.F. 1935. An instrumental earthquake scale. *Bull. Seism. Soc. Am.* 25, 1-32.
- Richter, C.F. 1958. *Elementary Seismology*. Freeman and Company, San Francisco.
- Richter, C.F. 1959. Seismic regionalization. *Bull. Seism. Soc. Am.* 49, 123-162.
- Rieben, E.H. 1953. Note preliminaire sur les terrains alluviaux de Teheran et particulierement due territoire de Shemran. *Bull. Lab. Geol. Min. Geophys. et Mus. Geol. Uni. la Usanne*, 105, 1-12.
- Rieben, E.H. 1955. The geology of the Tehran Plane. *Amer. J. Sci.* 253, 617-639.
- Rieben, E.H. 1966. Geological observations on alluvial deposits in northern Iran. *Geol. Surv. Iran Rep.* 9, 39 pp.
- Rikitatke, T. 1975. Earthquake precursors. *Bull. Seism. Soc. Am.* 65, 1133-1162.
- Riviere, A. 1936. Contribution a l'etude geologique de l'Anti Elborz. *Rev. Geogr. Phys. Geol. Dyn.* 7, 277-298.
- Ryall, A., D.B. Slemmons and L.O. Gedney, 1966. Seismicity tectonics, and surface faulting in the western United States during historic time. *Bull. Seism. Soc. Am.* 56, 1105-1135.
- Rybicki, K. 1971. The elastic residual field of a very long strike-slip fault in the presence of a discontinuity. *Bull. Seism. Soc. Am.* 61, 79-92.
- Rybicki, K. 1973. Analysis of the aftershocks on the basis of dislocation theory. *Physics. Earth Planet Int.* 7, 409-422.
- Rykovnov, L.N., V.V. Sedov, L.A. Savrina and V. Ju. Bourmin, 1972. Study of the microearthquakes in the rift zones of East Africa. *Tectonophysics.* 15(1/2), 123-130.
- Sadovsky, M., I. Nersesov, S. Nigmatallaev, L. Latyna, A. Lukk, A. Semenov, I. Simbireva and V. Ulomov, 1972. The processes proceeding strong earthquakes in some regions of middle Asia. *Tectonophysics*, 14, 295-307.
- Sanford, A.R. and C.R. Holmes, 1962. Microearthquakes near Socorro, New Mexico. *J. Geophys. Res.* 67, 4449-4459.

- Scholz, C.H. 1968a. Microfracturing and inelastic deformation of rock in compression. *J. Geophys. Res.* 73, 1417-1432.
- Scholz, C.H. 1968b. The frequency-magnitude relation of microfaulting in rock and its relation to earthquakes. *Bull. Seism. Soc. Am.* 58, 399-415.
- Scholz, C.H., M. Wyss and S.W. Smith, 1969. Seismic and aseismic slip on San-Andreas fault. *J. Geophys. Res.* 74, 2049-2069.
- Scholz, C.H., L.R. Sykes and Y.P. Aggarwal, 1973. Earthquake Prediction: A physical basis. *Science*, 181, 803-810.
- Seeber, L., M. Barazangi and A.A. Nowroozi, 1970. Microearthquake, seismicity and tectonics of Coastal Northern California. *Bull. Seism. Soc. Am.* 60, 1669-1699.
- Semenov, A.N. 1969. Variation of the travel time of transverse and longitudinal waves before violent earthquakes. *Izv. Acad. Sci. USSR Phys. Solid Earth, Engl. transl.* 4, 245-248.
- Shemyakin, Ye. I. and V.I. Shcheglov, 1974. A study of the movement mechanism during crustal earthquakes. *Izv. Earth Phys. Engl. transl.* 12, 22-31.
- Shirokava, E.I. 1962. Stress effective in earthquake foci in the Caucasus and adjacent districts. *Izv. Acad. Sci. USSR, Ser. Geophys.* 10, 809-815.
- Shirokava, E.I. 1967. General features in the orientation of principal stress in earthquake foci in the Mediterranean-Asian seismic belt. *Izv. Acad. Sci. USSR, Ser. Geophys.* 1, 12-22.
- Singh, S. and A.R. Sanford, 1972. Statistical analysis of microearthquakes near Socorro, New Mexico. *Bull. Seism. Soc. Am.* 62, 917-926.
- Shlien, S. and M.N. Toksöz, 1970. A clustering model for earthquake occurrences. *Bull. Seism. Soc. Am.* 60, 1765-1787.
- Sobuti, M., M.S. Nabavi, A. Eslami, A. Hedayati, Kh. Moftakhar and M. Peyman, 1969. The great Dasht-e-Bayaz earthquake of August 31, and September 1, 1968. *Inst. Geophys. Tehran Univ. Pub. No.* 46.
- Solovev, S.L. 1965. Seismicity of Sakhalin. *Bull. Earthq. Res. Inst.* 43, 95-102.
- St. Amand, D. 1956. Two proposed measures of seismicity. *Bull. Seism. Soc. Am.* 46, 41-45.
- Stauder, W. 1960. The Alaska earthquake of July 10, 1958: seismic studies. *Bull. Seism. Soc. Am.* 50, 293-322.
- Steinhart, J.S. and R.P. Meyer, 1961. Explosion Studies of Continental Structure. *Carnegie Inst. Wash. Pub.* 622.
- Steinhart, J.S. 1964. Lake Superior seismic experiment: shots and travel-times. *J. Geophys. Res.* 69, 5335-5352.

- Stöcklin, J. 1968. Structural history and tectonics of Iran: A review Bull. Amer. Asso. Petro. Geol. 52, 1229-1258.
- Stöcklin, J. and M.H. Nabavi, 1971. Tectonic map of Iran. 1:2,500,000. Geol. Surv. Iran.
- Stöcklin, J. 1974. Northern Iran: Alborz Mountains. Mesozoic-Cenozoic Orogenic Belt. Data for orogenic studies. Edited by A.M. Spencer.
- Sutton, G.H. and E. Berg, 1958. Direction of faulting from first-motion studies. Bull. Seism. Soc. Am. 48, 117-128.
- Suyehiro, S. 1966. Difference between aftershocks and foreshocks in the relationship of magnitude to frequency of occurrence for the great Chilean earthquake of 1960. Bull. Seism. Soc. Am. 56, 185-200.
- Suzuki, A. 1959. A statistical study on the occurrence of small earthquakes. Sci. Rept. Tohoku, Univ. Geophys. Ser. 11, 10-54.
- Takin, M. 1972. Iranian geology and continental drift in the Middle East. Nature, 235, 147-150.
- Tchalenko, J.S., M. Berberian, H. Iranmanesh, M. Bailly and M. Arsovsky, 1974. Tectonic framework of the Tehran region. Geol. Serv. Iran, 29, 7-46.
- Tchalenko, J.S. 1974. Outline of seismotectonic province of North-Central Iran. Geol. Surv. Iran, 29, 117-126.
- Tectonic map of Iran, 1971. 1:2,500,000. Geol. Surv. Iran.
- Tehran University Report, 1962. The great Buyin-Zahra earthquake of September 1, 1962. Inst. Geophys. Tehran Univ. Pub. No. 15
- The Institute of Geophysics of Tehran University, 1966. The seismicity of North-Central Iran. Pub. No. 34.
- Trimble, A.B. and R.B. Smith, 1975. Seismicity and contemporary tectonics of the Hebgen Lake-Yellowstone Park region. J. Geophys. Res. 80, 733-741.
- Tsubokawa, I., Y. Ogawa and T. Hayashi, 1964. Crustal movement before and after Niigata earthquake. J. Geod. Soc. Japan. 10, 165-171.
- Tsubokawa, I. 1969. On relation between duration of crustal movement and magnitude of earthquake expected. J. Geod. Soc. Japan, 15, 75-88 (in Japanese with English abstract).
- Tsumura, K. 1967. Determination of earthquake magnitude from total duration of oscillation. Bull. Earthq. Res. Inst. 15, 7-18.
- Udias, A. and J. Rice, 1975. Statistical analysis of earthquake activity near San-Andreas geological observatory, Hollister, California. Bull. Seism. Soc. Am. 65, 809-827.

- Unger, J. 1969. The microearthquake activity of Mt. Rainier, Washington. Ph.D. Thesis, Dartmouth College, 1969.
- Utsu, T. 1961. A statistical study on the occurrence of after-shocks. *Geophys. Mag.* 30, 521-605.
- Vita-Finzi, C. 1969. Late alluvial chronology in Iran. *Geol. Rundschau*, 58(3), 951-973.
- Wellman, H.W. 1966. Active wrench faults of Iran, Afghanistan and Pakistan. *Geol. Rundschau*, 55, 716-735.
- Whitcomb, J.H., J.D. Garmany and D.L. Anderson, 1973. Earthquake prediction: variation of seismic velocities before the San Fransisco earthquake. *Science* 180, 632-635.